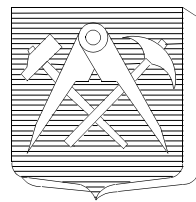


FACULTE POLYTECHNIQUE DE MONS



DOCTORATE THESIS

COMPUTER-AIDED KINEMATICS AND DYNAMICS OF MULTIBODY SYSTEMS WITH CONTACT JOINTS

by

Deming WANG

Members of Examining Committee:

Dr. Ir. **D. LAMBLIN**, FPMs, President
Prof. **P. DRAZETIC**, UVHC, Valenciennes
Prof. **J-C SAMIN**, UCL, Louvain
Prof. **A. PILATTE**, FPMs, Dean
Prof. **S. BOUCHER**, FPMs, Rector
Prof. **C. CONTI**, FPMs, Supervisor
Dr. Ir. **R.TARGOWSKI**, FPMs

September, 1996

Laboratory of Theoretical Mechanics, Dynamics and Vibrations
31 Boulevard Dolez B-7000, Mons, Belgium

ACKNOWLEDGMENT

Special recognition goes to Professor C. Conti whose help, interest, patience and teaching are greatly appreciated and invaluable, without which this dissertation could not have been accomplished. Recognition also goes to Drs. P. Dehombreux and O. Verlinden for their helpful comments, questions and interest. The moral support, generous help and encouragement of Prof. S.Boucher are greatly appreciated.

I thank my committee members Dr. Ir D. Lamblin, Prof. P. Drazetic. Prof. J-C Samin, Prof. A. Pilatte, Dr. R.Targowski, for reviewing and serving on my dissertation committee.

Financial support is greatly appreciated, which was provided by Mons Polytechnic University through graduate scholarships.

TABLE OF CONTENTS

Contents	Page
ACKNOWLEDGMENT	1
LIST OF FIGURES	7
LIST OF TABLES	11
LIST OF NOMENCLATURE	13

CHAPTER 1 - INTRODUCTION

1.1 Background and objective of the thesis	17
1.2 Survey of literature	
1.2.1 Changing contacts and multibody systems	21
1.2.2 Impact and multibody systems	22
1.3 Contents of the thesis	24

CHAPTER 2 - KINEMATIC ANALYSIS

2.1 Introduction	27
2.2 Basic principles of the kinematic approach	27
2.2.1 Influence of the choice of coordinates on kinematic and dynamic simulation	27
2.2.2 Topology analysis	29
2.2.2.1 Basis of the topological analysis	30
2.2.2.2 Numerical methodology of detection of independent loops	34
2.2.2.3 Simplified topological analysis method	38
2.2.3 Basic strategy of a computer aided kinematics using relative coordinates	40
2.2.3.1 Reference frames and relative joint variables	40
2.2.3.2 Setting of the constraint equations and position analysis	41
2.2.4 Velocity analysis	47
2.2.4.1 Expression of the velocity of a point P	47
2.2.4.2 Influence coefficients	51
2.3 Kinematic properties for articulated joints	55
2.3.1 Reference frames	55
2.3.2 Relative joint coordinates	55
2.3.3 Joints and derivative matrices	55
2.4 Kinematic properties for contact joint	58
2.4.1 Reference frames	59
2.4.2 Relative joint coordinates	61
2.4.3 Joint and derivative matrix	66
2.5 Detection strategy of changing contact joints	76
2.5.1 Switching function for discontinuous problems	76

2.5.2	Transition between curve elements	77
2.5.3	Addition of constraint due to interference	82
2.6	Illustrative example: kinematics of a crank-slider connected to a four-bar linkage mechanism	85

CHAPTER 3 - DYNAMIC ANALYSIS

3.1	Introduction	91
3.2	Basic principles of dynamic simulation using canonical equation	93
3.3	Setting of the motion equations using independent coordinates	97
3.3.1	Choice of a set of independent coordinates	97
3.3.2.	Motion equations using canonical formulation and independent coordinates	98
3.4	Numerical integration	101
3.5	Contact joints	103
3.5.1	Continuous method	103
3.5.1.1	Impact procedure	103
3.5.1.2	Example of contact model	108
3.5.2	Piecewise method	110
3.5.3	Comparison of two impact analysis methods	113
3.5.3.1	Example of application of the continuous method	113
3.5.3.2	Example of application of the piecewise method	117
3.5.3.3	Comparison of the two methods	117
3.6	Changing contact joints in dynamic simulation	119
3.6.1	Addition of contact joint	119
3.6.2	Deletion of contact joint due to the insufficient contact force	120
3.6.2.1	Procedure of calculation of the contact force	121
3.6.2.2	Calculation of the mass matrix derivatives with respect to the added degree of freedom in virtual motion	122
3.6.2.3	Expression of the static and dynamic parts of the contact force	127
3.6.3	Illustrative example of deletion/addition of a contact joint	129
3.7	Illustrative example: dynamics of a crank-slider connected to a four bar linkage mechanism	133

CHAPTER 4 - DESCRIPTION OF THE SOFTWARE AND EXAMPLES

4.1	Introduction	141
4.2	Description of the ACDMC software	141
4.3	Cam-follower mechanism with a profile composed by a succession of polynomial curvilinear	145
4.4	Cam-follower mechanism with a profile composed by a series of geometric elements	150
4.5	Trigger mechanism of an automatic machine-gun	159

CHAPTER 5 - CONCLUSION	167
-------------------------------------	-----

REFERENCES	169
-------------------------	-----

APPENDICES

APPENDIX A	Constraint transformation matrices and linear derivative operators	173
APPENDIX B	Generalized mass matrix and it's derivatives	183
APPENDIX C	Position, velocity, acceleration and static analysis of a cam-follower mechanism	187
APPENDIX D	Structure of the data used by the ACDMC software and examples of input files	195

LIST OF FIGURES

Figure	Page
1.1-1 Trigger mechanism of an automatic machine-gun	19
1.1-2 Trigger mechanism: block stage	20
1.3-1 Test mechanisms used in this thesis	26
2.2.1-1 Coordinate choices in the case of a four-bar mechanism	29
2.2.2-1 Particular arrangements leading to open loop	31
2.2.2-2 Topology of the trigger mechanism	32
2.2.2-3 Oriented mechanical network associated to the trigger mechanism	33
2.2.2-4 Tree structure of the trigger mechanism	35
2.2.2-5 Mechanical network of the trigger mechanism	37
2.2.2-6 Flowchart of topology analysis	39
2.2.3-1 Reference frames of associated to a kinematic chain	40
2.2.3-2 Coordinate transformation between two coordinate frames	41
2.2.3-3 Mechanism with multi-loops	44
2.2.4-1 Point p on link k of a kinematic loop	48
2.3-1 Local coordinate frames associated to articulated joints	56
2.4-1 Cam-follower mechanism with a “line-arc” contact joint	58
2.4.1-1 Particular coordinate frames associated to each curve element	60
2.4.1-1 Expression of contact element i	62
2.4.2-2 Coordinate frames and joint variables of contact surfaces when the contact surfaces are used as PCP	63
2.4.2-3 Cam-follower mechanism	64
2.4.2-4 Example of relative curvilinear coordinates of a cam	64
2.4.2-5 Evolution of the relative curvilinear coordinates in the function of the angular rotation (kinematic simulation)	65
2.4.2-6 Changes of the contact model by transition between consecutive curve elements (cam - follower mechanism)	65
2.4.3-1 “Arc- line” contact joint	66
2.4.3-2 Arc contacting element	68
2.4.3-3 Line segment contacting element	70
2.4.3-4 Polynomial contacting element	72
2.5.2-1 Transition between consecutive contact elements	79
2.5.2-2 Contact break due to a geometrically impossible configuration (The Newton-Raphson procedure is divergent)	81
2.5.3-1 Definition of a “virtual” contact joint	83
2.6-1 Crank-slider connected to a four-bar linkage through a contact joint (In this initial position, the contact is not active)	85
2.6-2 Crank-slider connected to a four-bar linkage through a contact joint (The contact is active)	86
2.6-3 Topology analysis of the mechanism of Fig. 2.6-1	88

2.6-4	Motion of link L7: kinematic simulation with $\omega=5$ rad/sec and $\theta=0, \beta=0$ (initial position)	89
2.6-5	Switching functions, piloting the changes of the contact joint	89
2.6-6	Different configurations of the mechanism of Fig. 2.6-1	90
3.1-1	Deletion of contact due to insufficient contact force and addition due to interference	91
3.5.1-1	Impact between bodies <i>i</i> and <i>j</i>	104
3.5.1-2	Contact joint used for impact analysis (similar to a virtual contact joint)	105
3.5.1-3	Hertz contact force model	109
3.5.3-1	A two pendulum apparatus	114
3.5.3-2	Position, velocity, and acceleration of point A of pendulum 1 in x-direction	114
3.5.3-3	Hertz contact model - indentation versus time	115
3.5.3-4	Hertz contact model - force versus time	115
3.5.3-5	Hertz contact model - force versus indentation	116
3.5.3-6	Hertz contact model - indentation velocity versus time	116
3.5.3-7	Velocity comparison of point A of pendulum 1 in x-direction by using different impact models ($e=0.8$)	117
3.6.2-1	Virtual displacement in contact joint k	122
3.6.3-1	Cam mechanism with flat-faced follower	130
3.6.3-2	Contact force between the cam and follower with a cam velocity of 1.5 rad/sec	130
3.6.3-3	Contact force between the cam and follower with a cam velocity of 1.9 rad/sec	131
3.6.3-4	Output motion of the cam mechanism in different velocity	131
3.6.3-5	Configuration of the cam-follower mechanism (cam velocity=1.9 rad/sec)	132
3.7-1	Contact forces in the joint C45 when input speed, $\omega=-5$ (rad/sec)	134
3.7-2	Contact forces in the joint C45 when input speed, $\omega=-8$ (rad/sec)	134
3.7-3	Switching functions, piloting the changes of contact joint ($e=0, \omega=-8$ rad/sec)	135
3.7-4	Motion of L7: dynamic simulation with $e=0$ and $\omega=-8$ (rad/sec)	135
3.7-5	Switching functions, piloting the changes of contact joint ($e=0.2, \omega=-8$ rad/sec)	138
3.7-6	Motion of L7: dynamic simulation with $e=0.2$ and $\omega=-8$ (rad/sec)	139
4.2-1	Main functions of ACDMC software	142
4.2-2	Screen appearance of ACDMC software	143
4.2-3	Flowchart of ACDMC software	144
4.3-1	Simple cam mechanism	145
4.3-2	Profile of the cam	146
4.3-3	Position analysis of the cam mechanism	148
4.3-4	Velocity analysis of the cam mechanism	148
4.3-5	Acceleration analysis of the cam mechanism	149
4.3-6	Contact force analysis of the cam mechanism	149
4.4-1	Cam-follower mechanism with a profile composed by a series of geometric elements	150

4.4-2	Relative curvilinear coordinate and the mark of different contact elements for a cam with complex contact surfaces	151
4.4-3	Contacting position analysis of the cam-follower mechanism of Fig. 4.4-1	152
4.4-4	Position analysis of the cam-follower mechanism of Fig. 4.4-1	153
4.4-5	Velocity analysis of the cam-follower mechanism of Fig. 4.4-1	153
4.4-6	Acceleration analysis of the cam-follower mechanism of Fig. 4.4-1	154
4.4-7	Contact force evolution of the cam-follower mechanism of Fig. 4.4-1 ($K=1.5 \text{ N/cm}$)	154
4.4-8	Contact force evolution of the cam-follower mechanism of Fig. 4.4-1 ($k=0.35\text{N/cm}$)	156
4.4-9	Evolution of the contacting position	156
4.4-10	Evolution of the follower position	157
4.4-11	Evolution of the follower velocity	157
4.4-12	Evolution of the follower acceleration	158
4.4-13	Dynamic simulation of the cam-follower mechanism of Fig. 4.4-1 ($K=0.35\text{N/cm}$)	158
4.5-1	Automatic machine-gun	160
4.5-2	Topology of the trigger mechanism	161
4.5-3	The trigger mechanism: initial position - blocking stage	161
4.5-4	The trigger mechanism: firing stage	162
4.5-5	The trigger mechanism: stopping stage	162
4.5-6	Successive topologies of the trigger mechanism	163
4.5-7	Positions of the trigger mechanism for different successive topologies	163
4.5-8	Relative coordinates concerning the sear and tripping lever	164
4.5-9	Relative coordinates, piloting the change of contact between the sear and tripping lever	164
4.5-10	Changes of contact model between the sear and tripping lever	165
A.2-1	Point as a contact element	179
A.2-2	Circle as a contact element	181
C.1-1	Cam-follower mechanism with an “arc-arc” contact joint	187
C.2-1	Cam-follower mechanism with a “point-arc” contact joint	189
C.3-1	Cam-follower mechanism with a “line-arc” contact joint	192

LIST OF TABLES

Table	Page
2.2.2-1 Fundamental entities of topology graph associated to a mechanical systems	30
2.4-1 Types of contact joints	59
3.7.1 Different phases of the simulation for mechanism of Fig. 2.6-1 (e=0)	136
3.7.2 Departing velocities after impact	136
3.7.3 Different phases of the simulation for mechanism of Fig. 2.6-1 (e=0.2)	137
4.3-1 Profile of the Cam	147
4.4-1 Comparison of simulation results	155

LIST OF NOMENCLATURE

i, j, k, a, b	: Order number
N_b	: Number of moving bodies
N_{li}	: Number of links
N_c	: Number of constraint equations
N_{lo}	: Number of constraint loops
N_g	: Number of generalized coordinates
N_{ca}	: Number of cartesian coordinates
N_{cr}	: Number of real contact joints
N_{cv}	: Number of virtual contact joints
N_a	: Number of articulated contact joints
DOF	: Number of degrees of freedom
m	: Number of joint variables (or relative coordinates) in a mechanical system
n	: Number of joints in a constraint loop
$_ \{ \}$: Vector notation
$[]$: Matrix
$[]^T$: Translate matrix
$[]^{-1}$: Inverse matrix
$L''i''$: Name of link i
$R''ij''$: Revolute joint connecting link i and link j
$P''ij''$: Prismatic joint connecting link i and link j
$C''ij''$: Contact joint which connects link i and link j
Γ	: Incidence Matrix
d_i	: Degree of link i
Π	: Oriented loop matrix
Π_l	: Oriented loop matrix with l independent loops
t_j	: Number of joint variables in joint j
q_j	: Joint variables in the joint j,
\underline{q}	: Relative coordinate vector,
f	: Independent Generalized coordinate vector
\underline{d}	: Dependent coordinate vector
\underline{p}	: Generalized momentum vector
\underline{R}_p	: Absolute homogeneous coordinate vector of point P
\underline{r}_k^p	: Relative homogeneous coordinate vector of point P in frame k
x_0, y_0, z_0	: Fixed frame,
x_i, y_i, z_i	: Local frame attached to link i (located at the mass center point)
x_k^-, y_k^-, z_k^-	: Local frame of the preceding pair of joint k
x_k^+, y_k^+, z_k^+	: Local frame of the following pair of joint k
x_k, y_k, z_k	: Common normal frame of contact point of the preceding pair of joint k
x_k, y_k, z_k	: Common normal frame of contact point of the following pair of joint k
A_{ij}	: Interlink transformation matrix from the body reference frame i to body reference frame j
A_{ij}^*	: Interlink transformation matrix from the body reference frame i to body

	reference frame j (with estimated values of joint variables)
T_{ij}	: Shape transformation matrix between the body reference frame i to the joint reference frame j
Φ	: Set of constraint equations
φ_k	: Joint transformation matrix from the preceding pair k^- to the following pair k^+
φ_k^*	: Joint transformation matrix from the preceding pair k^- to the following pair k^+ (with estimated values of joint variables)
E_d	: Transformation matrix describe the virtual displacement in the normal direction of the contact joint
δq_{ji}	: Residual difference between estimated and real values
I	: 4*4 unit matrix
α_{aji}	: Constant which is used to determine the relationship between joint variables and relative coordinates
Q_{ji}	: Joint linear derivative operator matrix
B_{ji}	: Linear derivative operator matrix of joint variables
B_{ji}^*	: Linear derivative operator matrix of joint variables (with estimated values of joint variables)
Λ_{ka}	: Linear derivative operator matrix of relative coordinates
R_{cji}	: Joint second order linear derivative operator matrix,
γ_{kba}	: System second order linear derivative operator matrix of a joint variable
$[\Omega_k]$: System second order linear derivative operator matrix of relative coordinates
$[C]$: Jacobian matrix
L	: Lagrangian function
L^*	: Lagrangian function for constrained mechanical systems
$[K]$: Influence coefficient matrix between relative coordinates and generalized coordinates
G_I	: Interference switching function vector
G_F	: Contact force switching function vector
G_T	: Transition switching function vector
G_V	: Relative velocity switching function vector
ε	: Tolerance value
T	: Kinetic energy
V	: Potential energy
H	: Hamilton function
J_k	: Inertia tensor (4 x 4) matrix of body k
$[M]$: Generalized mass matrix
F_a	: Generalized applied force vector
F_c	: Generalized conservative force vector
F_k	: Generalized contact force vector of joint k
F_{kn}	: Normal contact force
F_{kt}	: Tangent contact force
Δ	: Virtual displacement

For impact analysis

k : Elastic parameter of material

D	: Damping parameter of material
μ	: Hysteresis damping factor
δ	: Contact indentation
e	: Coefficient of restitution
π_k	: impulse of contact joint k
Π_k	: Generalized impulse vector
Ψ_k	: Vector giving the partial derivative of virtual displacement with respect to independent variables

CHAPTER ONE - INTRODUCTION

1.1 Background and objectives of the thesis

Contact joint is pervasive in modern mechanisms. The most common, gear and cam pairs, appear in all types of mechanisms. Contact joints are typically cheaper, more compact and more robust than actuators. They are more versatile than articulated joints because they can realize multiple functions and operating modes through contact changes. They play a central role in mechanism design, specially in precision mechanisms. They serve as path function, and motion generators in mechanisms, such as copiers, cameras, sewing machines or sear mechanisms. A survey of 2500 mechanisms in Atrobolevski's engineering encyclopaedia shows that more than 60% contain contact joints and about 1 to 5 involve intermittent contacts. [1]

Such mechanisms exhibit kinematic functions, which can be altered by manufacturing variations in relation to the nominal shapes and configurations of their parts. When the design has flaws, such as interference or jamming, the designer must determine the causes and deduce shape and position modifications that yield the desired results.

The necessary tool which would help the designer to overcome those difficulties is based on a **kinematic tolerance analysis** which study the variation of the kinematic functions due to the manufacturing variations.

A kinematic tolerance analysis has to be based on a reliable **kinematic analysis tool** which derives the displacements, velocities and accelerations of the parts for given driving motions. A computer-aided kinematic analysis is not simple at all in the case of mechanisms including contact joints because the software must determine which part features interact at each stage of the work cycle. He must compute the effects of the interaction and identify the contact changes. The main difficulties lie in the large number of potential contacts and in the discontinuities induced by contact changes.

A kinematic simulation can only detect discontinuities concerning geometric and kinematic properties, specially:

- the transition between consecutive curve elements,
- the interference between bodies which in a kinematic simulation, is assumed to lead to an active contact once interference occurs.

The deletion of an existing contact point however requires the calculation of the contact force. A **quasi static or dynamic simulation** is therefore necessary in order to detect the deletion of a contact due to an insufficient contact force. Otherwise an interference between bodies in a dynamic simulation requires an **impact analysis** which can be a deciding factor in the creation of a new active contact.

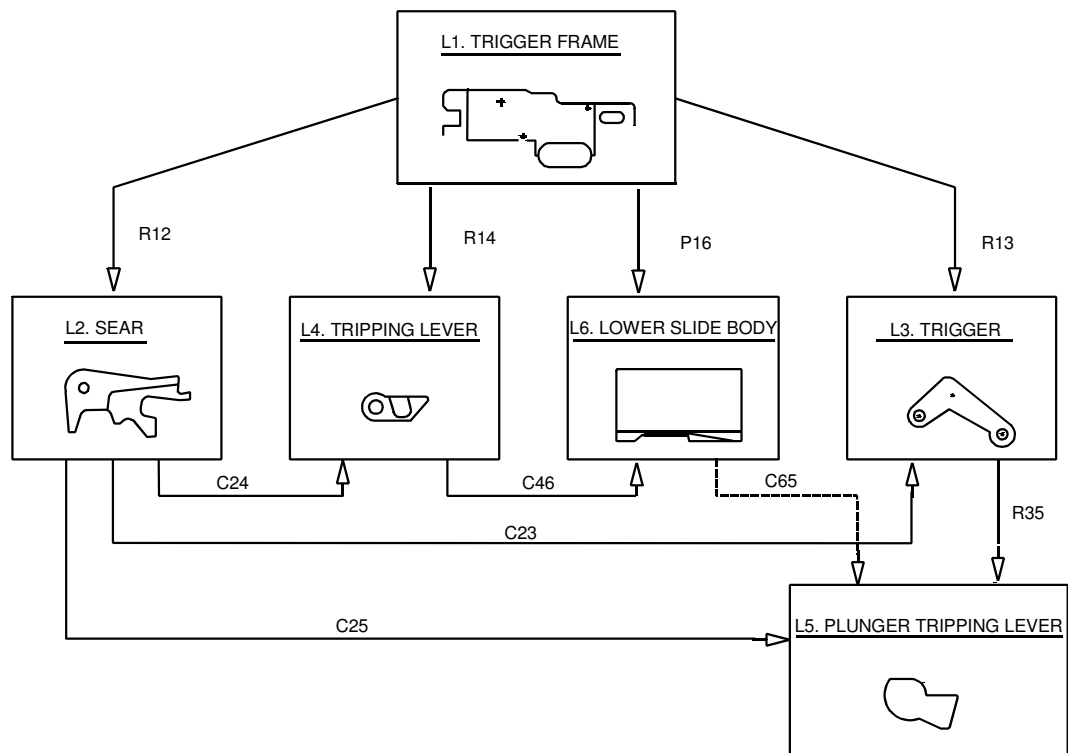
Fig. 1.1-1 illustrates the typical case of a “sear and trigger” mechanism of a machine-gun. The central part of the mechanism is the lower slide body (L6), which can be animated by a translational motion along the DE axis, and which has to be blocked in the stopping fire position (Fig. 1.1-2), and to move freely in the automatic fire position. To ensure this blocking and to remove it, a series of four links can be animated with respect to the body trigger frame (L1). This last one contains two axes at points A and B: the sear (L2) rotates around the A-axis, the trigger (L3) and the tripping lever (L4) around the B-axis. Moreover, the trigger contains a C axis about which the plunger tripping lever (L5) can rotate. This sear and trigger mechanism contains a series of intermittent contact joints, the contacting curves being composed of the juxtaposition of simple geometric elements.

This industrial mechanism is typical of the **particular contacting elements** which will be considered in this thesis:

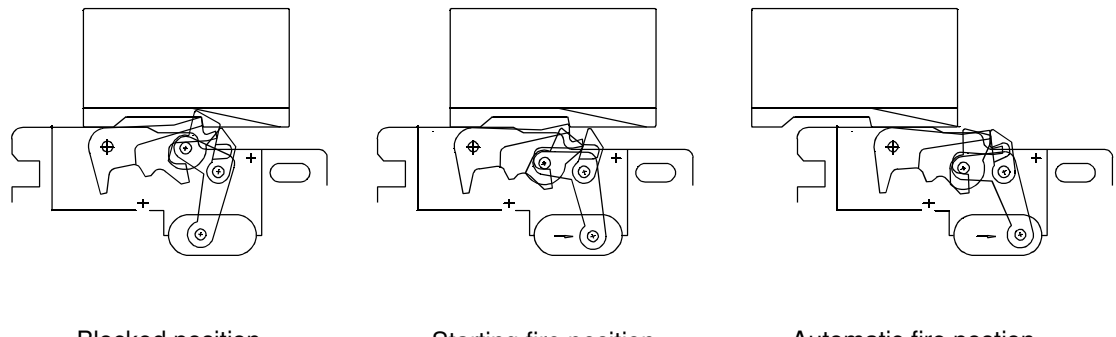
- the contacting curves are formed by a series of juxtaposed simple geometric elements such as line segments, circle arcs, circles, points or curves defined by a polynomial profile,
- a planar contact joint works under sliding conditions, and is characterized by two degrees-of-freedom,
- the contacting curves are not permanently active during motion and the topology changes are not intuitively predictable.

Current computer-aided simulation programs offer limited support for mechanisms with such changing contact joints [4,5]. Recent mechanical engineering researches generally address the kinematic and dynamic analysis of multibody systems which consist of assemblies of parts permanently connected by joints. The joints can be formed either by lower pairs representing surface contacts, such as hinges and screws, or by higher pairs representing point and line contacts, such as cams and gears. Efficient analysis programs have been developed for lower pair mechanisms, but it generally provides little support for reasoning about higher pairs. They generally do not automate contact constraint formulation, except for special cases such as gear involutes and cam profiles which are permanently in contact. Little developments have been done on contact changes or contact interactions.

It is precisely the purpose of this thesis to develop the principle of a unified approach for a computer-aided kinematic and dynamic simulation of mechanisms with changing contact joints.



(a) Topology structure



(b) Typical stages during the fire cycle

Fig. 1.1-1: Trigger mechanism of an automatic machine-gun

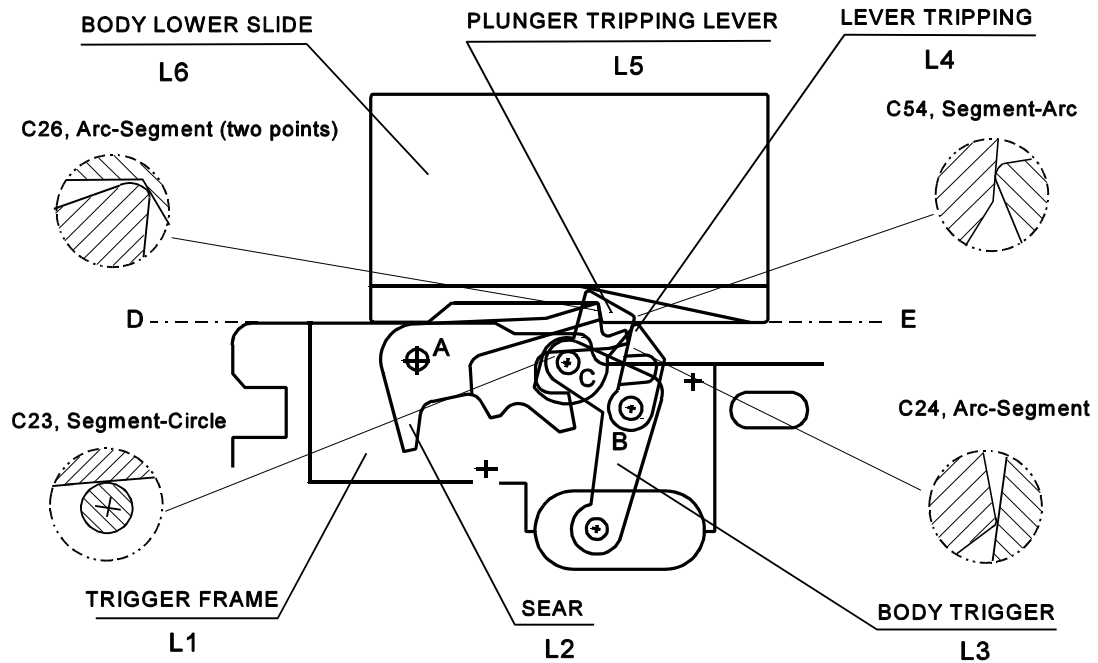


Fig. 1.1-2: Trigger mechanism: blocked position

1.2 Survey of literature

1.2.1 Changing contact joints and multibody systems

The area of computer aided kinematics and dynamics of mechanical systems with changing contact joints has attracted more and more attention in recent years. Joskowicz [6-7] proposes a kinematic tolerance analysis method for the design of such mechanisms. A new kinematic model based on a kinematic tolerance space is developed, that generalizes the configuration space representation of nominal kinematics function. Kinematic tolerance space captures quantitative and qualitative variations in kinematic function due to variations in part shape and part configuration.

Conti and Corron [8] develop a unified numerical approach for investigation of the kinematic behaviour of spatial mechanisms with classical lower pair, and contact joints with simple geometric contacting curves. Intermittent contacts and detection of interferences have been considered. This approach has been applied to the kinematic analysis of complex mechanisms, where special cautions have to be taken to tolerancing.

Dubowsky, Deck and Costello [9] present a dynamic model for links coupled with clearance. They develop an impact pair method which uses the concept of an equivalent spring-mass-damper system to model impact. The calculated relative contact displacement compared with the clearance pilots the existence or the deletion of the contact.

Lee and Wang [10] use the same idea to analyse intermittent motion mechanisms. The concept of changing topology, as a function of the reaction force at the contact point between bodies has been used by F.Y. Chen [11] in the case of a cam follower mechanism.

Chang and Shabana [12] develop a pieced interval analysis scheme that accounts for the change in the spatial system topology due to the changes in the connectivity between bodies. In order to guarantee a smooth transition from one topology to another, a set of spatial interface conditions or compatibility conditions have been formulated.

Crossley and al. [13] state the importance of the sudden changes of topologies, which result in discontinuities on the differential equation formulations. Major inaccuracies occur when crossing those boundaries which require the reduction of the step size.

Winfrey, Anderson, and Gnilka [14] present an analysis strategy for computer use, which includes the effect of intermittent separation and impact between members. The user is required to indicate all the possible topologies that the system may exhibit during the simulation. Using a similar concept, Wehage and Haug [15-16] present a general analysis strategy for the dynamic analysis of systems with discontinuous constraints. The logical events and variables, which indicate the possible changes in the system constraints, must however be supplied by the user, who must anticipate all the possible connectivity changes.

Ganter and Uicker [17] use a “swept solid” concept to detect collisions between bodies. This method represents the space volumetrically swept out by the motion of a given body along

a given trajectory. A swept solid is created for each body in the given environment. Using the swept solids created for each body, calculations can be performed to determine if these swept solids intersect. If the original bodies will collide while traversing the given trajectories, then their swept solids will statically interfere. This method is applied to perform a work space analysis of robots. It is however not adequate to simulate the motion after collision.

Gilmore[18,19] uses a geometric boundary (shape) representation of the bodies to predict and detect the changes in constraints and reformulate the dynamic equations of motion. The topology changes of the systems are characterized by addition, deletion and modification of contact between bodies. The method employs the concepts of "point to line" contact to establish the kinematic constraints force closure, a "ray firing" technique as well as the information provided by the rigid body boundary descriptions (the state variables) characterize the kinematic constraint changes. Since the method automatically predicts and detects constraint changes, it can simulate mechanical systems with unpredictable or unforeseen changes in topology. Cartesian coordinates are used to set the constraint equations which only deals with "point-line" contact joints.

Han [20,21] extends the Gilmore's approach for mechanical systems with changing topology, which takes into account arc boundaries and frictional contact. A rule-based approach adapted to the prediction and detection of kinematic constraint changes between bodies with arc and line boundaries is presented. Stick/slip friction is treated as well as pure rolling and slipping rolling. The efficiency of the rule-based simulation algorithm as a design tool is demonstrated through the design and experimental validation of parts feeder.

1.2.1 Impact and multibody systems

The scientific literatures [22, 23] mostly deal with impacts concerning systems of particles or systems of rigid bodies without kinematic joints.

Two different analysis methods can be applied to impact problems. One method considers the impact in a micro-sense: the motion is not discontinuous and the contact forces act on the bodies in a continuous manner. This analysis method is referred to as the "**continuous analysis method**". Another method is to consider the impact in a macro-sense: the duration of the contact between the two colliding bodies is considered as sufficiently small to ensure that the impact occurs instantaneously. The analysis referred to as the "**piecewise analysis method**" distinguishes two time intervals: before and after impact, the impact being described by the velocity jumps.

Most of the computational methods are based on the **continuous analysis method**. The most current model uses a spring-damper element (Kelvin-Voigt model) [24], which does not however represent the physical characteristics of the energy transfer process. The best-known contact force model was derived by Hertz [25]. Based on the theory of elasticity, he formulates a force-displacement law at the interface of two contacting solid spheres. A large number of studies have been performed since then to extend the model used by Hertz to the contact between any other two surfaces.

In the case of an impact within a constrained mechanical system, Kecs and Teodorescu [26] apply the mathematical theory of distribution for the dynamic analysis of the impact phase. They treat the discontinuities in the equations of motion with the use of “heaviside step functions” and obtain analytical solutions in terms of these functions. This underlying distribution theory is also employed by Ehle and Haug [27]: the discontinuities of the excitation functions are smoothed to provide a set of ordinary differential equations of motion for all times including the time of impact. Huang, Haug and Andrews [28] incorporate this idea in the design sensitivity analysis of mechanisms subjected to intermittent motion.

Khulief and Shabana [29,30] use a “logical” spring-damper element representing the Kelvin-Voigt model in the analysis of impact between two rigid bodies. Both the stiffness and the damping coefficient are estimated from the energy-balance relations and the impulse-momentum equations for different coefficients of restitutions. The logical spring-damper is active during the duration of impact. The numerical technique incorporates logical event predictors. These ones are geometric conditions used during the numerical integration process to locate the occurrence of an impact before it is encountered. This prepares the integration routine beforehand to handle the short-lived contact force variations. Wu and Haug [31,32] propose a substructure synthesis method to account for contact impact effects in mechanical systems.

Friction has been taken into account by Keller [33], who evaluates the impulse due to the application of the friction force by calculating the slip velocity between two colliding bodies from their equations of motion. He applies the law of friction to calculate the friction force. The integral of friction force during the small period of impact yields the frictional impulse. His analysis however is restricted to the collisions between particles or free bodies. Han and Gilmore [34] further analyse the contact impact with friction problems, such as reverse sliding or sticking which may occur at different times throughout the impact.

The **piecewise analysis method** in the literature has mostly been used for systems containing particles or unconstrained bodies. A set of momentum balance-impulse equations in terms of the coefficient of restitution are solved at the time of impact to evaluate the velocities of the system right after impact. Wehage [35] develops a set of momentum balance-impulse equations for impact within a constrained mechanical system, whose solution yields the velocity jumps of all the bodies in the system after impact. Pereira and Nikravesh [36] use the same concept, and include the dry friction.

Lankarani [37-39] extends Khulief’s method and employs a logical spring-damper element to study the relationship between the parameter of restitution and relative velocity and material of collided bodies. His research results show that when the damping of the material is small, the analysis result of a piecewise method is in agreement with the result coming from a continuous method.

1.3 Content of the thesis

The following **assumptions** have been made in this thesis:

- 1) the mechanisms considered in this dissertation comprise:
 - rigid bodies,
 - classical force elements such as weightless springs and dampers,
 - classical lower pair joints,
 - planar contact joints, whose shape can be represented by a set of successive geometric elements such as points, line segments, circle arcs, circles and polynomial shape curves,
- 2) impact between rigid bodies occurs with a low relative velocity during a very small time interval, so that a piecewise impact analysis can be employed,
- 3) when active, contact joints are sliding and involve 2 degrees of freedom.

The **main choices** at the basis of this thesis concern:

- 1) the use of relative coordinates to describe in a unified way the properties of either lower-pair or higher pair joints: relative coordinates appear to us to have a more physical meaning because the configuration of the multibody system is directly described by the joint behaviour, which is very useful to detect the changes of contact models (Section 2.2),
- 2) the definition of an original set of relative coordinates associated to each contact joint: curvilinear coordinates have been defined with their integer part associated to the current active contact element, and their decimal part describing the exact location of the contact point (Section 2.4),
- 3) the use of a "virtual contact joint" concept: the deletion of an existing contact joint reduces to the change from an active contact with 2-DOF to a virtual contact with 3 DOF, which suppresses the necessity to perform a new topological analysis. The addition of a new contact is made by the reverse operation (Section 2.5),
- 4) the setting of the equations of motion by the Hamilton canonical formulation: this formulation has been adapted to develop a minimal set of dynamic equations, a set of independent coordinates being chosen among the primary relative joint coordinates. This formulation is well suited to a piecewise method which is used for the determination of the velocity jumps of the bodies after impact (Sections 3.2 and 3.3),
- 5) the use of a set of switching functions, which are at the basis of the strategies developed to detect the modifications of constraints during motion: the transition between consecutive contact elements, the addition of constraints due to boundary interference and the break of constraints due to insufficient closing forces (Sections 2.5 and 3.6),

Based on those choices, the ACDMC software(Analyse Cinematique et Dynamique Mécanismes avec liaisons de Contact) has been developed, and applied to a series of test mechanisms represented in Fig. (1.3-1).

The content of the **three main chapters** that constitute this thesis is as follows:

--- Chapter 2 is dedicated to the **kinematic analysis** of mechanical systems with changing contact joints. Some basic principles of a unified computer-aided kinematic approach are presented, specially the choice of the coordinate system, the basis of a topology analysis when using relative coordinates, and the strategy which has to be used for computer-aided kinematics in relative coordinates. The kinematic properties are described for articulated joints, and then transposed to the case of contact joints. The strategies of detection of the change of contact joints are then developed particularly in the case of the transition between consecutive elements (contact point sliding out of the boundaries of the consecutive curve elements) and the addition of constraints due to interference. An illustrative example is described concerning a crank-slider mechanism connected through a contact joint to a four-bar linkage mechanism.

--- The **dynamic analysis** for constraint mechanical systems is developed in Chapter 3. The basis of a dynamic simulation using canonical equations is first described, as well as the setting of the motion equations in independent coordinates. The independent variables are automatically selected from the relative coordinates by a Gaussian elimination technique with total pivoting. The motion equations are then solved by a Runge-Kutta numerical integration to yield the time response of the system. Two basic aspects of the dynamical simulation of multibody systems with changing contact joints, impact between bodies and contact force calculation are then emphasized. Two kinds of impact analysis methods, the continuous and piecewise methods are discoursed. The closure forces of contact joints are calculated by using the principle of virtual work, which treats each constraint individually. Finally some strategies of detection of changing contact joints are developed in the case of deletion of constraints due to insufficient closing forces. The same illustrative example as the one used in the kinematic part is presented.

--- Chapter 4 presents a brief description of the ACDMC software developed in this thesis, and describes **three illustrative examples**:

- the first example compares in the case of a simple cam-follower mechanism (with a polynomial shape) the obtained results with those calculated with the ADAMS software,
- the second one illustrates the case of a cam-follower mechanism, with a cam composed by a series of arc, points and line elements,
- the third one illustrates the results obtained in the particular case of the trigger-sear mechanism in an automatic gun.

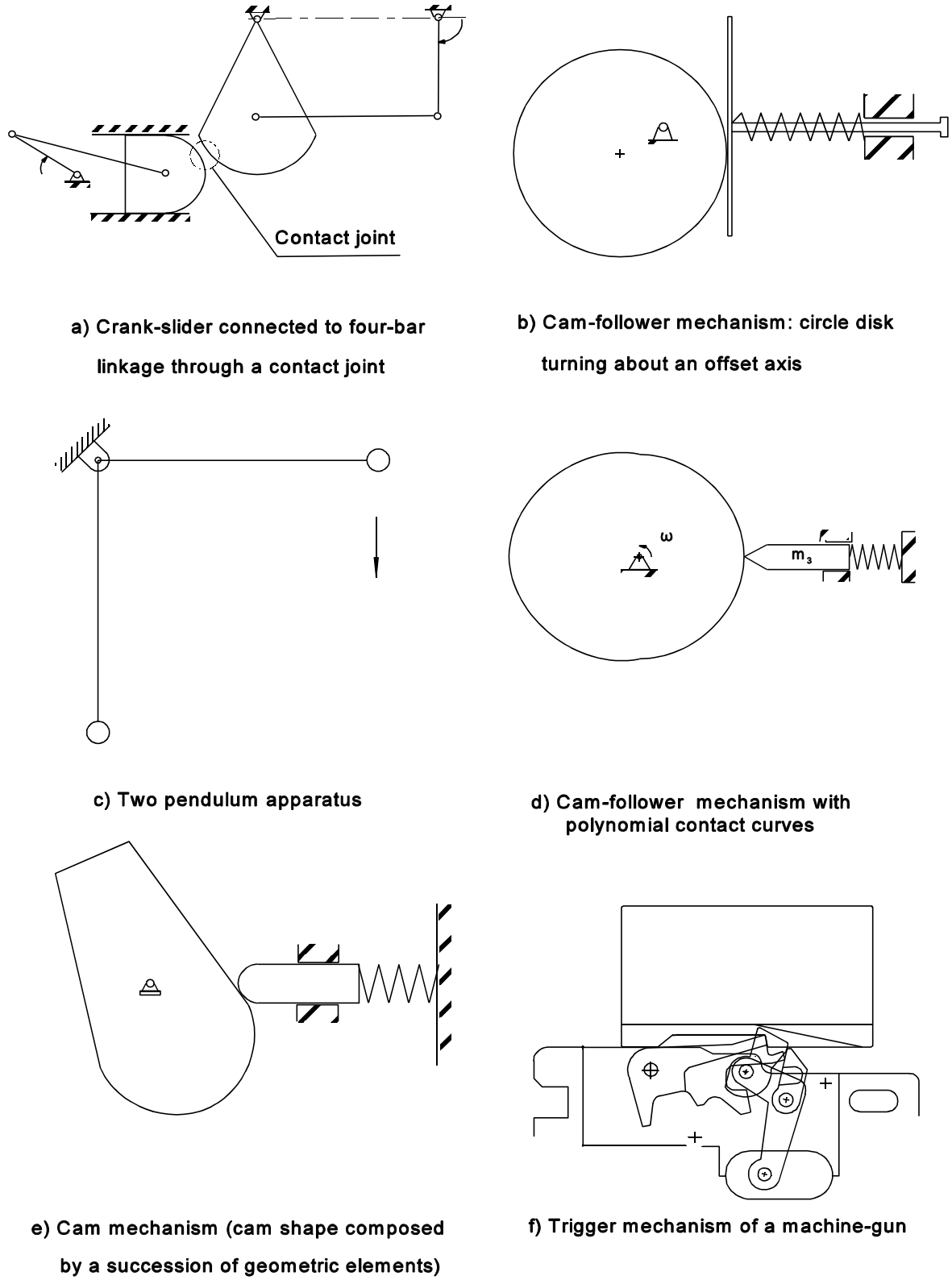


Fig. 1.3-1: Test mechanisms used in this thesis

CHAPTER 2 KINEMATIC ANALYSIS

2.1 Introduction

The purpose of a kinematic analysis tool is to derive the displacements, velocities and accelerations of the parts of the multibody system, for given driving motions. In the case of mechanisms including contact joints, it is necessary to determine which part features interact at each stage of the motion: the contact changes must be identified as well as the consecutive modifications to the system.

This chapter will describe the procedure adopted to perform a kinematic simulation: it is based on the choice of relative coordinates and the use of 4×4 transformation matrix concept. Either lower-pair or higher-pair joints are treated in a unified way by using a set of relative coordinates associated to each contact joint. The closure of the loops detected by a topology analysis leads to the setting of the constraint equations at the basis of the kinematic behaviour.

The changes of contact joints based on geometric and kinematic properties are detected, principally the transition between consecutive elements and the addition of a new contact due to interference between bodies. These changes of contact are managed by means of the use of a virtual joint concept, which avoids the systematic recourse to a topological analysis as well as the definition of a set of switching functions which monitor the changes during motion.

2.2 Basic principles of the kinematic approach

2.2.1 Influence of the choice of coordinates on kinematic and dynamic simulation

When using cartesian coordinates, the configuration of a mechanical system is identified by a set of absolute coordinates associated to each moving link; generally, they correspond to the translation coordinates of the centre of mass, associated to three coordinates, such as the Euler or Bryant angles, to describe the orientation of each link. In order to avoid indeterminate positions consecutive to the use of the Euler or Bryant angles, the Euler parameters can also be used. This choice which is strongly widespread, presents the advantage to induce a systematic formulation of the equations of motion, well adapted to a computer aided analysis. The main drawback of a cartesian approach is that the number of coordinates describing the system is rather important ($6 \times N_b$ or $7 \times N_b$ in a spatial case, if N_b is the number of moving bodies). Moreover, these coordinates are constrained by the joints limiting the motion between links. A set of constraint equations have to be added to the motion equations ($6N_b - \text{DOF}$ constraint equations, if DOF is the number of degrees of freedom). Cartesian co-

ordinates yield a system of algebraic differential equations whose size will be specially important when the number of links increases and the number of degrees of freedom becomes small.

Relative coordinates describe the configuration of a mechanical system by means of the coordinates associated to each joint. In the case of a closed loop topology, these coordinates are not independent but are constrained by a series of constraint equations consecutive to the existence of closed topological loops. The number of coordinates is usually less important than in the case of cartesian coordinates but the formulation of the constraint equations requires a topological analysis in order to detect the kinematic loops of the system. The setting of the equations of motion is generally less direct owing to the dependence of the mass matrix with the configuration of the system. Relative coordinates yield a system of algebraic differential equations whose size will increase if the number of joints and the number of closed loops of the system increases.

Generalized coordinates correspond to the case of a number of coordinates which equals the number of degrees of freedom of the system. The dynamic behaviour is expressed by a minimal set of differential equations but their setting is not direct. The expression of the equations of motion in generalized coordinates requires an explicit kinematic model which is not always possible to establish directly [47]. An indirect way to express the equations of motion in generalized coordinates is to transform the equations of motion obtained with either cartesian or relative coordinates by choosing a set of independent coordinates. The constraint equations are then solved in order to express the dependent coordinates in function of the independent ones. One of the main advantages when using generalized coordinates is that the set of differential equations is easier to integrate as the algebraic differential systems resulting from the use of either cartesian or relative coordinates. Fig. 2.2.1-1 illustrates those choices in the case of a four-bar mechanism.

In the case of this thesis, kinematics is the basic analysis governing the behaviour of the considered mechanisms such as the trigger mechanism. The use of relative coordinates appears to us to **have a more physical meaning** because relative coordinates are directly connected with the joint action: as it will be described in section 2.5, the definition of the switching functions required to pilot the discontinuities associated to the change of contact joints is facilitated by the use of relative coordinates.

One of the main drawbacks of this choice is that **it requires a topological analysis** in order to identify the independent loops of the system. This drawback can however be reduced by use of the “virtual contact joint” concept (presented in section 2.2.2): it also has the advantage to consider in a unified way either articulated or contact joints.

As it will be seen in section 3.5, in order to minimize the integration problem consecutive to the algebraic differential system at the basis of the dynamic behaviour, a transformation based on the choice of an independent set of coordinates will be done, combined with the use of a Hamilton formulation well suited to the resolution of the impact problem consecutive to the formation of new contact joints.

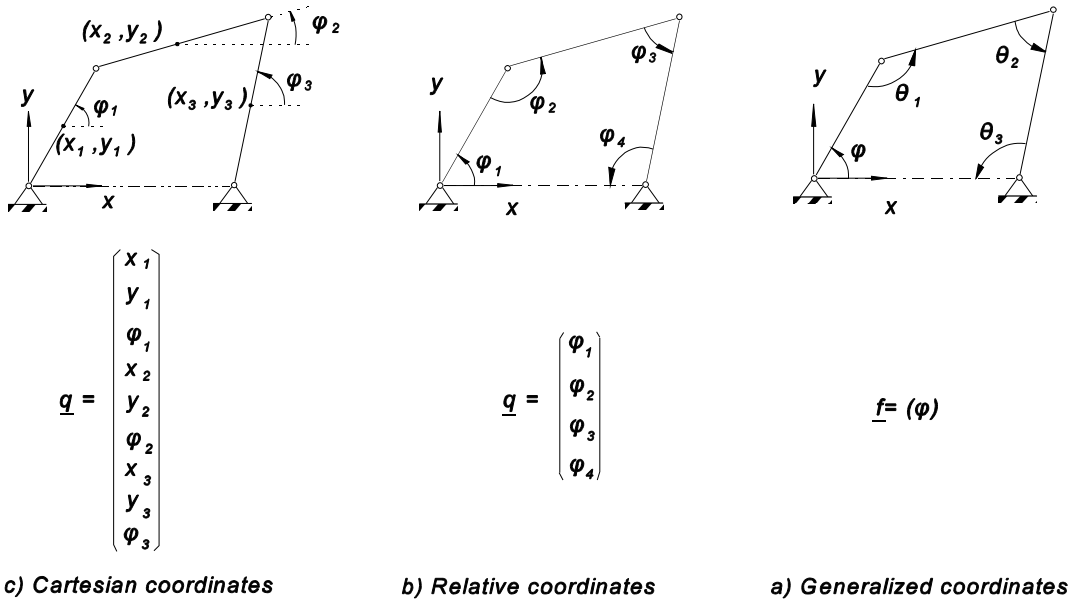


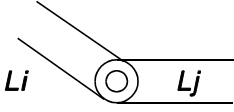
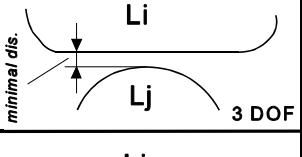
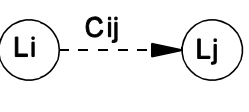
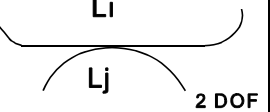
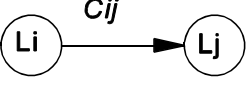
Fig. 2.2.1-1: Coordinate choices in the case of a four-bar mechanism

2.2.2 Topological analysis

The topological characteristics of a mechanical system can be described by a set of properties such as the total number of bodies, the number and types of joints between bodies, the arrangement order between links and joints, which induces the existence of independent closed loops. Those characteristics are resumed by a network, which is represented by a topology graph, where each link is symbolized by a vertex and each joint between links by a line. The conventional notations used in this dissertation to represent the fundamental entities of the topology graph are illustrated in table 2.2.2-1. The following three fundamental entities are used:

- rigid links, referenced by the letter L and an integer associated to the link,
- articulated joints, referenced by a letter associated with the joint functionality (R: revolute, S: spherical, P: prismatic, ...) and by two integers associated to the concerned links,
- contact joints, referenced by the letter C and the two integers associated to the concerned links. A contact joint can be considered either in active (solid line) or virtual state (dotted line).

**Table 2.2.2-1: Fundamental entities of topology graph
associated to a mechanical system**

Entity		<i>Physical Model</i>	<i>Topological Model</i>
<i>Rigid link</i>			
<i>Articulated joint</i>			
<i>Changing contact joint</i>	<i>Virtual contact</i>		
	<i>Active contact</i>		

A joint can be active or not during motion. When a new contact appears or disappears, it generally concerns some predefined links of the mechanism. For this reason we have chosen to use the concept of “virtual” contact to predefine the connection between links that during motion can interfere or loose contact.

The creation of new closed kinematic loops or the deletion of existent ones is consecutive to the emergence or breaking of contact joints. The virtual contact joint concept presents the advantage that the breaking of a contact or the formation of a new one does not change the mechanical network. As it will be seen in section 2.5, when not active, a virtual contact will require three parameters; when the contact is active, only two parameters are required. The mechanical network keeps unchanged but constraint equations have to be modified. Appropriate switching functions have also to be defined to pilot the transformation from virtual to active or from active to virtual contact.

2.2.2.1 Basis of the topological analysis

Topological analysis methods are derived from the graph theory [41,43], applied to detect the independent closed loops in a network. It uses a series of mathematical tools well adapted to describe the networks at the basis of the graph theory: the concepts of connected network, oriented network, incidence matrix and oriented loop matrix.

A **connected network** is a network which cannot be grouped into two sub-networks

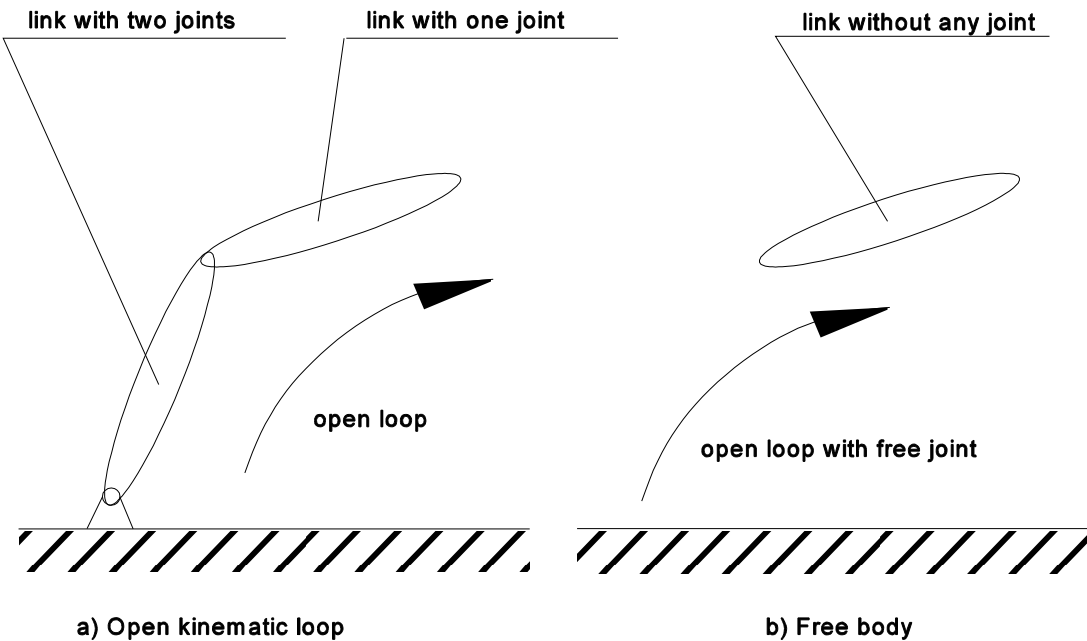


Fig. 2.2.2-1: Particular arrangements leading to open loop

by only removing one link. Each link of a mechanical system has at least two joints connected with other links. Two exceptions have however to be handled:

-- **Exception 1:** when a body only has one joint connected with another body, it will form

an open kinematic loop (see Fig. 2.2.2-1a),

-- **Exception 2:** if a body has not any joint contacted with another body, the body is free.

A free joint is then added to connect the free body to the ground, the body being considered as belonging to an open kinematic loop (2.2.2-1a).

An **oriented network** is a network where the orientation of the joints is specified. If the orientation of a constraint j is chosen (arbitrarily) as directed from links i to j , then the constraint is said to be negatively incident with link i and positively incident with link j . The topology of the trigger mechanism of the machine-gun in its initial position described in section 1.2 is illustrated in Fig. 2.2.2-2. Its oriented mechanical network is shown in Fig. 2.2.2-3.

The **incidence matrix** serves to represent the connection between links and joints: each row of the incidence matrix represents a link, each column represents a constraint and the entries define the incidence between corresponding columns and rows. For a mechanical network having N_{li} links and N_c constraints, the incidence matrix Γ is a $(N_{li} \times N_c)$ matrix

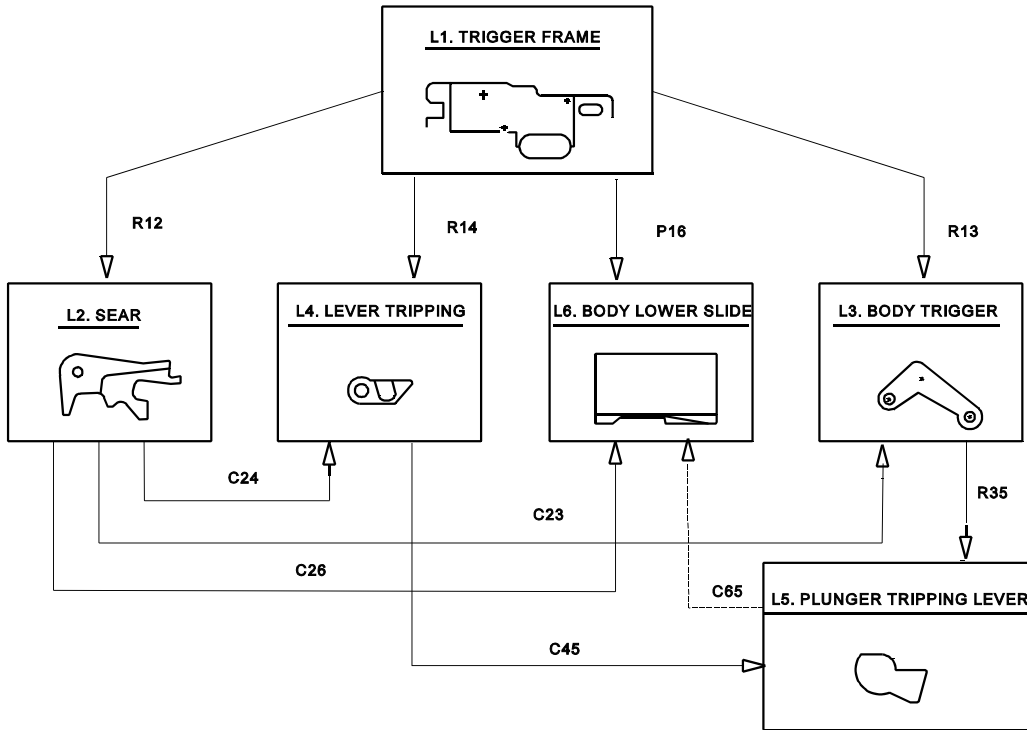


Fig. 2.2.2-2: Topology of the trigger mechanism

whose components γ_{ij} are defined by:

$$\gamma_{ij} = \begin{cases} +1 & \text{if constraint } j \text{ is positively incident with link } i, \\ -1 & \text{if constraint } j \text{ is negatively incident with link } i, \\ 0 & \text{if constraint } j \text{ is not incident with link } i. \end{cases} \quad (2.2.2-1)$$

For the oriented network of the trigger mechanism in Fig. 2.2.2-2, the incidence matrix is the following one:

$$\Gamma = \begin{matrix} & R12 & R13 & R14 & P16 & R35 & C23 & C45 & C56 & C26 & C24 \\ R12 & -1 & -1 & -1 & -1 & 0 & 0 & 0 & 0 & 0 & 0 & L1 \\ R13 & 1 & 0 & 0 & 0 & 0 & -1 & 0 & 0 & -1 & -1 & L2 \\ P16 & 0 & 1 & 0 & 0 & -1 & 1 & 0 & 0 & 0 & 0 & L3 \\ R35 & 0 & 0 & 1 & 0 & 0 & 0 & -1 & 0 & 0 & 1 & L4 \\ C23 & 0 & 0 & 0 & 0 & 1 & 0 & 1 & -1 & 0 & 0 & L5 \\ C45 & 0 & 0 & 0 & 1 & 0 & 0 & 0 & 1 & 1 & 0 & L6 \end{matrix} \quad (2.2.2-2)$$

The **degree of a link** d_i is the number of constraints incident with this link i . It can be easily obtained by summing the absolute values of the elements of the corresponding row of the incidence matrix:

$$d_i = \sum_{j=1}^c |\gamma_{ij}| \quad i=1,2,\dots,N_{li} \quad (2.2.2-3)$$

For a mechanical network, each link must be connected to at least two others: d_i is therefore larger than and equal to two. If the number of degrees of freedom of a link is less than two, the link will form an open loop.

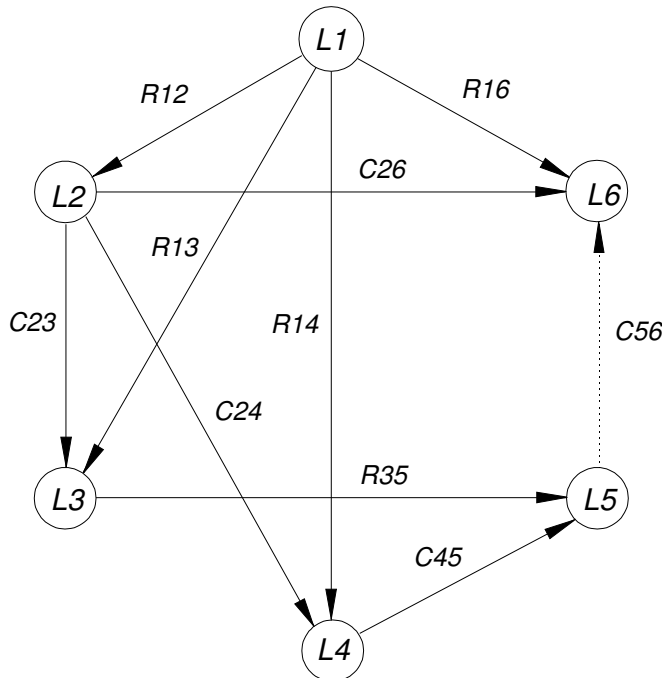


Fig. 2.2.2-3: Oriented mechanical network associated to the trigger mechanism.

The **oriented loop matrix** is a matrix Π , describing the components of an oriented loop of the mechanical system: each row corresponds to a loop and each column to the constraints contained in the corresponding loop. The components π_{ij} are defined as follows:

- +1 if constraint j is contained in a loop i , and if the orientation of constraint j and the conventional orientation of a loop i are the same,
 - $\pi_{ij} =$ if constraint j is contained in a loop i , and if the orientation of constraint j and the conventional orientation of a loop i are opposite,
 - 0 if constraint j is not contained in a loop i .
- (2.2.2-4)

For the trigger mechanism of Fig. 2.2.2-2, the oriented loop matrix has the following expression:

	<i>R12</i>	<i>R13</i>	<i>R14</i>	<i>P16</i>	<i>R35</i>	<i>C23</i>	<i>C45</i>	<i>C56</i>	<i>C26</i>	<i>C24</i>	
	1	-1	0	0	0	1	0	0	0	0	<i>Loop1</i>
	1	0	-1	0	0	0	0	0	0	1	<i>Loop2</i>
$\Pi =$	0	1	0	-1	1	0	0	1	0	0	<i>Loop3</i>
	0	1	-1	0	1	0	-1	0	0	0	<i>Loop4</i>
	1	0	0	-1	0	0	0	0	1	0	<i>Loop5</i>
	0	1	0	-1	1	0	-1	0	1	0	<i>Loop6</i>

In this example, it can be seen that the loops are not each other independent. It can be seen indeed that, for example:

$$\text{Loop6} = \text{Loop5} + \text{Loop4} \quad (2.2.2-7)$$

A methodology has then to be developed in order to detect the independent loops of the multibody system.

2.2.2.2 Numerical methodology of detection of independent loops

A series of concepts are necessary in order to define a numerical methodology of detection of independent loops, principally the concepts of tree graph, tree root and node, tree branch and chord.

A tree graph is a sub-graph of the graph of the mechanical network defined by the following rule: if any one of its lines is removed, it falls into two separate pieces; in practice, in a tree graph, each vertex pair is connected by a unique simple chain. If a particular vertex is used as the basic point connected to the other edges and vertices, forming a tree structure, the vertex is considered as the tree root. Any vertex in a graph can become a tree root. The others are considered as the tree nodes. The connections between a tree root and nodes are considered as tree branches. The removed lines from a connected graph to form a tree are considered as the chords.

Let's recall two basic theorems at the basis of the methodology [39]:

-- The incidence matrix of a connected network of N_{li} links has rank $N_{li} - 1$, which means

that a link in the connected network can form all closed loops. If the link moves out, the connected network does not exist and the determinant of an incidence matrix is

not equal to zero.

-- When the columns of the incidence matrix Γ (link-joint matrix) and the oriented loop

matrix Π (loop-joint matrix) are ordered consistently, these two matrices are orthogonal, which physically means that every link used in a loop corresponds to two

joints; the sum of the elements of a row in the incidence matrix is then equal to zero:

$$\Gamma \Pi^T = [0] \quad (2.2.2-8)$$

A) Partitioning of the incidence matrix Γ :

If a network is connected, then theorem 1 insures the incidence matrix Γ can be partitioned as follows:

$$\Gamma = \begin{bmatrix} \Gamma_{11} & \Gamma_{12} \\ \Gamma_{21} & \Gamma_{22} \end{bmatrix} \quad (2.2.2-9)$$

where Γ_{11} is a nonsingular square submatrix of order ($N_{li} - 1$) and Γ_{21}, Γ_{22} consist of only a single row submatrix. Some rows and columns' interchanges may be required to achieve the nonsingular submatrix Γ_{11} . For the trigger mechanism, after rearrangement, the incidence matrix can be expressed as:

$$\Gamma = \begin{array}{cccccccccc} R12 & R13 & R14 & P16 & R35 & C23 & C45 & C56 & C26 & C24 \\ \hline 1 & 0 & 0 & 0 & 0 & -1 & 0 & 0 & -1 & -1 \\ 0 & 1 & 0 & 0 & -1 & 1 & 0 & 0 & 0 & 0 \\ 0 & 0 & 1 & 0 & 0 & 0 & -1 & 0 & 0 & 1 \\ 0 & 0 & 0 & 1 & 0 & 0 & 0 & 1 & 1 & 0 \\ 0 & 0 & 0 & 0 & 1 & 0 & 1 & -1 & 0 & 0 \\ -1 & -1 & -1 & -1 & 0 & 0 & 0 & 0 & 0 & 0 \end{array} \quad L2 \quad L3 \quad L4 \quad L6 \quad L5 \quad L1 \quad (2.2.2-10)$$

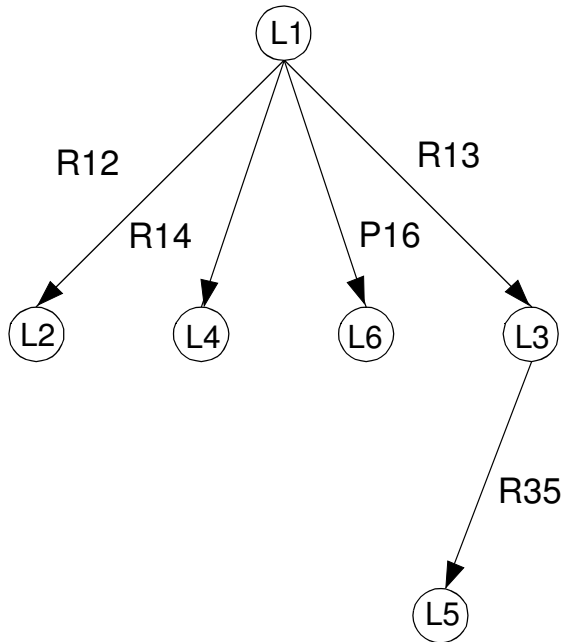


Fig. 2.2.2-4: Tree structure of the trigger mechanism

Let's note here the significance of this partitioning. The new mechanical network represented by the submatrices Γ_{11} and Γ_{21} taken together, has the same number of links as the original one, but certain of the constraints are disconnected. As shown in Fig. 2.2.2-2, it is clear from this figure that precisely the necessary number of constraints was disconnected so that the network remains connected but no longer contains any loop. The Γ_{11} matrix in Equ. (2.2.2-10) forms a tree, fixed body L1 being the tree root (see Fig. 2.2.2-4).

Each disconnected constraint can therefore, be reconnected in turn and a unique constraint loop will be successively formed. Since each of these loops contains at least one constraint (the connected constraint) which appears in not any other one, these loops can be considered as independent. Since $N_c - (N_{li} - 1)$ constraints were disconnected in forming the tree, this procedure shows that there exists at least $N_{lo} = N_c - N_{li} + 1$ independent loops in the mechanical system.

B) Partitioning of the oriented loop matrix Π :

By supposing that N_{lo} constraint loops have been formed by the preceding procedure, the oriented loop matrix Π can be partitioned as follows:

$$\Pi = [\Pi_l \quad -I] \quad (2.2.2-13)$$

where I is a ($N_{lo} \times N_{lo}$) identity matrix and the rows of Π_l correspond to the unique oriented chains through the tree.

The algorithm for determining the chains in Π_l based on theorem 2 leads to the following expression concerning the product of the partitioned loop and incidence matrices:

$$\begin{bmatrix} \Gamma_{11} & \Gamma_{12} \\ \Gamma_{21} & \Gamma_{22} \end{bmatrix} \begin{bmatrix} \Pi_l^T \\ -I \end{bmatrix} = [0] \quad (2.2.2-14)$$

The expansion of the top row leads to:

$$\Gamma_{11}\Pi_l^T - \Gamma_{12} = [0] \quad (2.2.2-15)$$

Since Γ_{11} is a nonsingular submatrix, the equation can be readily solved for the unknown portion of the oriented loop matrix:

$$\Pi = [(\Gamma_{11}^{-1}\Gamma_{12})^T, -I] \quad (2.2.2-16)$$

Using this procedure on the trigger mechanism example, Equation (2.2.2-9) gives:

$$\Gamma_{11}^{-1} = \begin{bmatrix} 1 & 0 & 0 & 0 & 0 \\ 0 & 1 & 0 & 0 & 1 \\ 0 & 0 & 1 & 0 & 0 \\ 0 & 0 & 0 & 1 & 0 \\ 0 & 0 & 0 & 0 & 1 \end{bmatrix} \quad (2.2.2-17)$$

and

$$\Gamma_{11}^{-1}\Gamma_{12} = \Pi_l^T = \begin{bmatrix} -1 & 0 & 0 & -1 & -1 \\ 1 & 1 & -1 & 0 & 0 \\ 0 & -1 & 0 & 0 & 1 \\ 0 & 0 & 1 & 1 & 0 \\ 0 & 1 & -1 & 0 & 0 \end{bmatrix} \quad (2.2.2-18)$$

The independent loops are then obtained from matrix Π :

$$\Pi = \begin{bmatrix} R12 & R13 & R14 & P16 & R35 & C23 & C45 & C56 & C26 & C24 \\ -1 & 1 & 0 & 0 & 0 & -1 & 0 & 0 & 0 & 0 \\ 0 & 1 & -1 & 0 & 1 & 0 & -1 & 0 & 0 & 0 \\ 0 & -1 & 0 & 1 & -1 & 0 & 0 & -1 & 0 & 0 \\ -1 & 0 & 0 & 1 & 0 & 0 & 0 & 0 & -1 & 0 \\ -1 & 0 & 1 & 0 & 0 & 0 & 0 & 0 & 0 & -1 \end{bmatrix} \quad (2.2.2-19)$$

As shown by the first five rows in Equ. (2.2.2-6), loops 1 to 5 appear as an independent set of oriented loops (" - loop" means the opposite direction of the conventional one has to be considered for the loop) for the trigger mechanism.

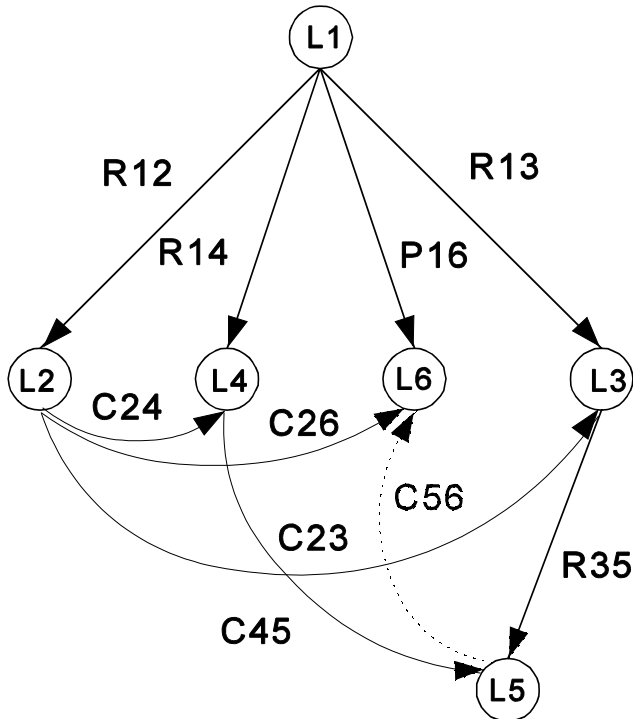


Fig. 2.2.2-5: Mechanical network of the trigger mechanism

If the graph of the mechanical system is constructed using these results, the mechanical network of Fig. 2.2.2-5 is formed from the tree of Fig. 2.2.2-4. **The joints added to form the closed loops are precisely the chords, each chord determining an independent closed loop.** This important conclusion will be used in the next section to develop a simplified topology analysis. The topology analysis result concerning this example gives the following independent constrained loops:

Constraint loops:

- loop 1: 1-2-3-1,
- loop 2: 1-2-4-1,
- loop 3: 1-3-5-6-1,
- loop 4: 1-3-5-4-1.
- loop 5: 1-2-6-1.

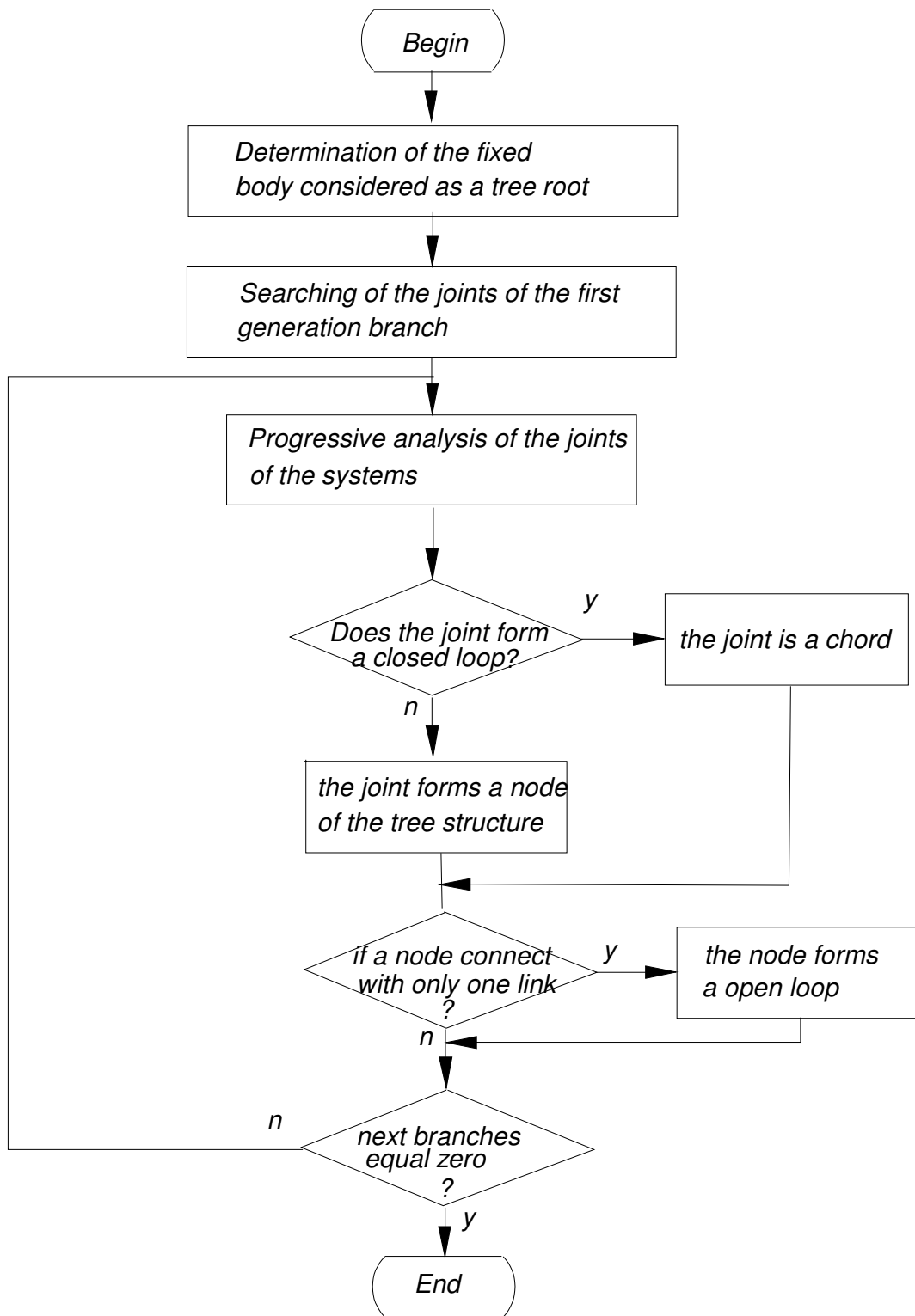
In the particular case of the starting shot position, loop 3 is a virtual constraint loop, because links L5 and L6 do not interfere in this position.

2.2.2.3 Simplified topology analysis method

From the above graph theory, the independent loops of a mechanical system can be obtained by Equ. (2.2.2-16) with the calculation of the incidence and oriented loop matrices, Γ_{11} and Γ_{12} being a partitioning of the incidence matrix of the network. If Γ_{11} is a nonsingular square submatrix, it constructs a tree structure of the network, and Γ_{12} describes the chords of the network, each chord determining an independent loop. In this thesis, a direct searching method has been defined: the Γ_{11} and Γ_{12} matrix can be obtained by a progressive analysis of the tree structure, and the progressive detection of the chords by taking advantage of the structure of the database used in the software to describe the arrangement between links and joints.

The following rules have been applied:

- Step one: Determination of the fixed body considered as the tree root.
- Step two: Searching of the relevant joints connecting the fixed body with the other links of the mechanism. They will form the first generation branches of the tree.
- Step three: Determination of the next generation branches by adding the other links of the mechanism. If the addition of a link and the corresponding joints forms a closed loop, the joint is considered as a chord, which will form an independent closed loop. If the addition of a link and the corresponding joint does not close a loop, the joint will form a new branch and the link will form a new node of the tree structure.
- Step four: If a node is connected to a unique branch (only one joint connected to the link), the node is considered as an element of an open loop.
- Step five: When the next generation branch is equal to zero, the tree has been completely constructed and the topology analysis is finished.

**Fig. 2.2.2-6: Flowchart of the topology analysis**

2.2.3 Basic strategy of a computer aided kinematics using relative coordinates

To determine the motion of a rigid body i , it is necessary to specify the spatial location of the origin and the angular orientation of the $x_iy_iz_i$ coordinate frame fixed to each body. The description of the functionalities of each joint is also required, specially:

- first, the setting of the reference frames associated to both part of each joint,
- secondly, the definition of the joint parameters describing the state of the joints,
- thirdly, the setting of the constraints between the joints' parameters due to the functionality of each joint.

2.2.3.1 Reference frames and relative joint variables

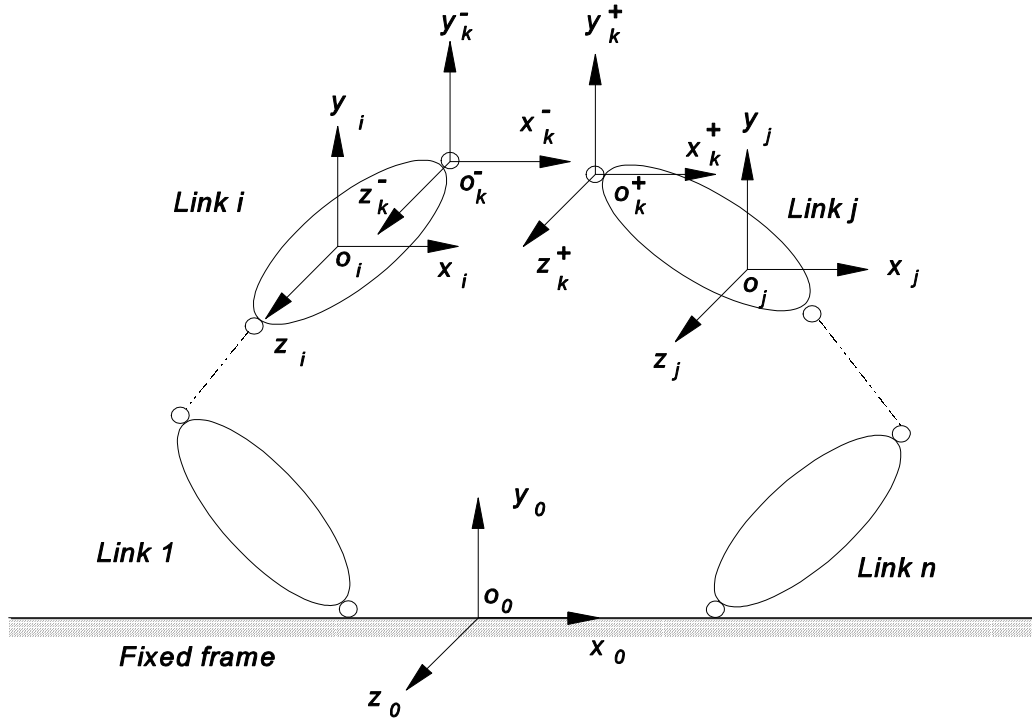


Fig. 2.2.3-1: Reference frames associated to a kinematic chain

In order to realize the above purposes, two kinds of particular reference frames are attached to each body:

- a **body reference frame**, which could be arbitrarily chosen if only kinematics has to be performed, but which will be located at the centre of mass of the considered body to facilitate further dynamic simulation (frame $x_iy_iz_i$ on body i and frame $x_jy_jz_j$ on body j in Fig. 2.2.3-1); this frame will also be used for the specification of moments and products of inertia, attachment points for springs and dampers, points of applications for forces.

-- **joint reference frames**, which are located at each side of a joint and which will be used to express the constraint relationships involved by the existence of the joint (frames $x_k^+y_k^+z_k^+$ and $x_k^-y_k^-y_k^-$ on bodies i and j in Fig. 2.2.3-1).

It should be noted that the constraints which will describe the functionalities of a joint are dependent of the locations and orientations of the joint reference frames. Section 2.3 and Section 2.4 describe the main conventional choices which have been taken in this thesis respectively in the case of articulated and contact joints.

2.2.3.2 Setting of the constraint equations and position analysis

The setting of the constraint equations is based on the use of the transformation matrix concept and requires the definition of particular transformation matrices such as shape matrix, joint matrix and interlink matrix.

a) Transformation matrix concept

Transformation matrix is a well-known concept which is used to describe the relative position of two reference frames. If one considers a point P , the homogeneous coordinates r_i^P of point P in frame i is equal to the product of the transformation matrix T_{ij} relating frames i and j , by the homogeneous coordinates r_j^P of P in frame j (Fig. 2.2.3-2):

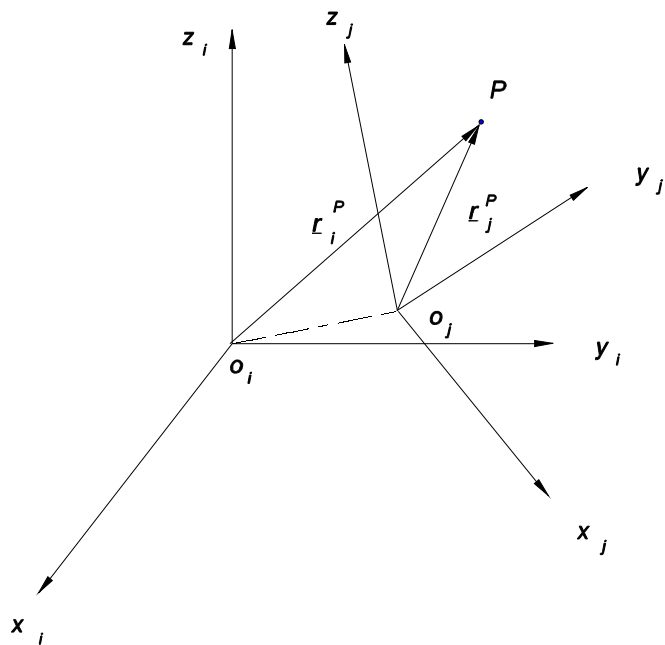


Fig. 2.2.3-2: Coordinate transformation between two coordinate frames

$$\underline{x}_i^P = T_{ij} \underline{x}_j^P \quad (2.2.3-1)$$

The transformation matrix T_{ij} has the three following important properties:

- It is composed as follows:

$$T_{ij} = \begin{pmatrix} \{\underline{x}_j\}_i & \{\underline{y}_j\}_i & \{\underline{z}_j\}_i & \{O_i O_j\}_i \\ 0 & 0 & 0 & 1 \end{pmatrix} \quad (2.2.3-2)$$

the first three columns containing the projections on frame i of the unit vectors of frame j, and the last column describing the vector which locates the origin O_j of frame j in the reference frame i.

- If an intermediate frame k is considered, the transformation matrix T_{ij} from coordinate frames i to j is equal to the product of two successive transformation matrices, respectively from frames i to k and from frame k to j:

$$T_{ij} = T_{ik} T_{kj} \quad (2.2.3-3)$$

- The transformation matrix T_{ij} from coordinate frames i to j is equal to the inverse transformation matrix from coordinate frame j to i:

$$T_{ij} = T_{ji}^{-1} \quad (2.2.3-4)$$

b) Definition of shape matrix T_{ij} , joint matrix ϕ_k and interlink matrix A_{ij}

Let's take for example the case illustrated in Fig. 2.2.3-1 of two links i and j of a kinematic chain, connected by the joint k.

The transformation matrix T_{ik} between the body reference frame $x_i y_i z_i$ and the joint reference frame $x_k^- y_k^- z_k^-$ describes the necessary information to locate the position of joint k with respect to link i:

$$\begin{pmatrix} x_i \\ y_i \\ z_j \\ 1 \end{pmatrix} = T_{ik} \begin{pmatrix} x_k^- \\ y_k^- \\ z_k^- \\ 1 \end{pmatrix} \quad (2.2.3-5)$$

T_{ik} is a constant **shape transformation matrix**, which expresses the position of the joint. The shape transformation matrix T_{jk} can be defined in the same way between the body reference frame $x_j y_j z_j$ and the joint reference frame $x_k^+ y_k^+ z_k^+$.

Each joint is completely defined by the functional relationship describing the characteristics of the relative motion that is permitted between the two constrained links. It entails the representation of the relative motion in the form of a joint matrix ϕ_k corresponding to the linear

transformation between coordinate frames k^- attached to link i and k^+ attached to link j (Fig. 2.2.3-1). The elements of the matrix representing this linear transformation are functions of the determined constraint variables (the number of variables ranging theoretically from zero (blocked) to six (free body), usually from one to five, depending on the particular constraint). The relative position between the two coordinate frames in the joint is described by the following equation:

$$\begin{pmatrix} \mathbf{x}_k^- \\ \mathbf{y}_k^- \\ \mathbf{z}_k^- \\ 1 \end{pmatrix} = \varphi_k(\underline{\alpha}_k) \begin{pmatrix} \mathbf{x}_k^+ \\ \mathbf{y}_k^+ \\ \mathbf{z}_k^+ \\ 1 \end{pmatrix} \quad (2.2.3-6)$$

where φ_k is the (4×4) **joint transformation matrix** corresponding to the k^{th} joint and $\underline{\alpha}_k$ is a vector including the t_k variables of the k^{th} joint:

$$\underline{\alpha}_k = (\alpha_{k1}, \alpha_{k2}, \dots, \alpha_{k, t_k})^T \quad 1 \leq t_k \leq 5. \quad (2.2.3-7)$$

The relationship between links i and j which are constrained by joint k can be described by:

$$\begin{pmatrix} \mathbf{x}_i \\ \mathbf{y}_i \\ \mathbf{z}_i \\ 1 \end{pmatrix} = T_{i,k} \varphi_k(\underline{\alpha}_k) T_{kj} \begin{pmatrix} \mathbf{x}_j \\ \mathbf{y}_j \\ \mathbf{z}_j \\ 1 \end{pmatrix} = A_{ij} \begin{pmatrix} \mathbf{x}_j \\ \mathbf{y}_j \\ \mathbf{z}_j \\ 1 \end{pmatrix} \quad (2.2.3-8)$$

where the **interlink matrix** A_{ij} provides the relative position of link j with respect to link i, this information including both the kinematic shapes of the links and the functionality of the joint:

$$A_{ij} = T_{ik} \varphi_k(\underline{\alpha}_j) T_{kj}. \quad (2.2.3-9)$$

c) Expression of the geometrical constraint equations

The topology analysis gives the independent loops of the mechanical system. For a mechanism with N_{lo} closed constraint loops (see Fig.2.2.3-3), using the successive (4×4) shape and joint matrices, the N_{lo} following matrix equations can be gotten:

$$\begin{aligned} \Phi_1 &= (A_{01} T_{11} \varphi_1(\underline{\alpha}_1) T_{12} T_{22} \varphi_2(\underline{\alpha}_2) T_{23} T_{33} \varphi_3(\underline{\alpha}_3) \dots \varphi_n(\underline{\alpha}_n) T_{n1} A_{10})_1 = I \\ \Phi_2 &= (A_{01} T_{11} \varphi_1(\underline{\alpha}_1) T_{12} T_{22} \varphi_2(\underline{\alpha}_2) T_{23} T_{33} \varphi_3(\underline{\alpha}_3) \dots \varphi_n(\underline{\alpha}_n) T_{n1} A_{10})_2 = I \\ &\dots \\ \Phi_{N_{lo}} &= (A_{01} T_{11} \varphi_1(\underline{\alpha}_1) T_{12} T_{22} \varphi_2(\underline{\alpha}_2) T_{23} T_{33} \varphi_3(\underline{\alpha}_3) \dots \varphi_n(\underline{\alpha}_n) T_{n1} A_{10})_{N_{lo}} = I \end{aligned} \quad (2.2.3-10)$$

where I is the 4×4 unit matrix. Matrix A_{01} is defined as the transformation matrix between the basic reference frame Ro and the first link reference frame of a loop. If both reference frames are coincident, it is equal to the unit matrix I.

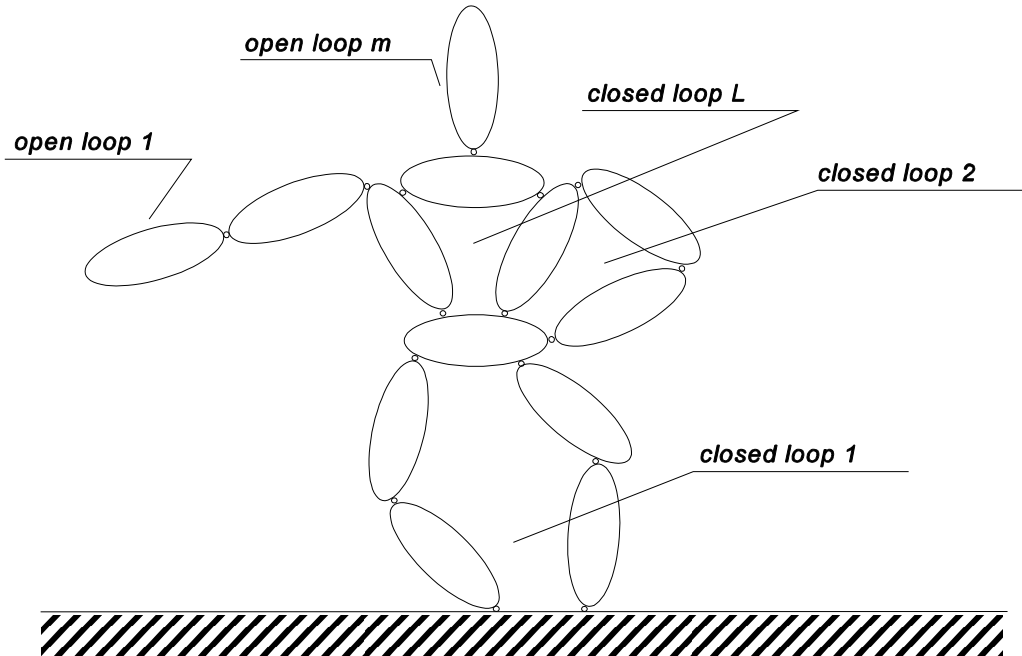


Fig. 2.2.3-3: Mechanism with multi-loops

d) Newton-Raphson solving procedure

The calculation of a position from the above constraint implicit matrix equation with relative coordinates can be obtained by the classical Newton-Raphson method, which needs a starting estimated set of values of the joint coordinates.

If the values q_{ji}^* are the estimated values of the real joint coordinates q_{ji} , solution of the matrix equation, the following relationship can be written:

$$q_{ji} = q_{ji}^* + \delta q_{ji} \quad (2.2.3-11)$$

δq_{ji} representing the residual difference between estimated and real values.

If φ_j^* is the matrix associated to joint j with the estimated set of values, it is possible to linearize the matrix around these estimated values, by developing the joint matrix in Taylor series, limited to the first order:

$$\varphi_j = \varphi_j^* + \sum_{i=1}^{t_j} \left(\left(\frac{\partial \varphi_j}{\partial q_{ji}} \right)_{q_{ji}^*} \delta q_{ji} \right) \quad (2.2.3-12)$$

t_j being the number of relative coordinates associated to joint j.

For a constraint transformation matrix φ_j , the derivation versus the coordinate q_{ji} can be obtained by using a matrix Q_{ji} , such that:

$$\left(\frac{\partial \varphi_j}{\partial q_{ji}} \right)_{q_{ji}^*} = Q_{ji} \varphi_j^* \quad i=1, 2, \dots, 5. \quad (2.2.3-13)$$

The matrix Q_{ji} is a **linear derivative operator** of a joint variable that depends on the kind of joint and is usually function of the relative coordinates of the joint. The following equation provides a straightforward method to calculate the Q_{ji} matrix:

$$Q_{ji} = \left(\frac{\partial \varphi_j}{\partial q_{ji}} \right) \left(\varphi_j(q_j) \right)^{-1} \quad i=1, 2, \dots, 5. \quad (2.2.3-14)$$

The derivative operator matrices Q_{ji} for the particular joints used in this thesis are listed in Appendix A. The Equ. (2.2.3-12) can be rewritten as:

$$\varphi_j = (I + \sum_{i=1}^{t_j} (Q_{ji} \delta q_{ji}) \varphi_j^*) \quad (2.2.3-15)$$

By replacing each matrix φ_j by the corresponding linerized development, the general closing equation becomes:

$$\begin{aligned} & A_{01} T_{01} \varphi_1^* T_{12} T_{22} \varphi_2^* T_{23} T_{33} \dots \varphi_n^* T_{nn} A_{n0} \\ & + A_{01} T_{01} \left(\sum_{i=1}^{t_1} Q_{1i} \delta q_{1i} \right) \varphi_1^* T_{12} T_{22} \varphi_2^* T_{23} T_{33} \dots \varphi_n^* T_{nn} A_{n0} \\ & + A_{01} T_{11} \varphi_1^* T_{12} T_{22} \left(\sum_{i=1}^{t_2} Q_{2i} \delta q_{2i} \right) \varphi_2^* T_{23} T_{33} \dots \varphi_n^* T_{nn} A_{n0} \\ & + \dots \dots + \\ & + A_{01} T_{11} \varphi_1^* T_{12} T_{22} \varphi_2^* T_{23} T_{33} \dots \left(\sum_{i=1}^{t_n} Q_{ni} \delta q_{ni} \right) \varphi_n^* T_{nn} A_{n0} \\ & = I \end{aligned} \quad (2.2.3-16)$$

The first term is the matrix transformation of the reference frames to itself when the loop is described with the estimated values of the parameters. This term will be noted I^* because it will tend to the unit matrix I , when the parameters tend to their respective solution.

If A_{oj}^* represents the absolute estimated position of the coordinates frame attached to link j :

$$(A_{oj}^*) = A_{01} T_{11} \varphi_1^* T_{12} T_{22} \varphi_2^* T_{23} \dots T_{jj} \quad (2.2.3-17)$$

and using the following evident relation:

$$(A_{oj}^*)^{-1}(A_{oj}^*) = I \quad (2.2.3-18)$$

Equ. 2.2.3-16 can be turned into:

$$\begin{aligned} I^* + \sum_{i=1}^{t_1} (A_{01}^* T_{11} Q_{1i} T_{11}^{-1} A_{01}^{*-1}) I^* \delta q_{1i} + \sum_{i=1}^{t_2} (A_{02}^* T_{22} Q_{2i} T_{22}^{-1} A_{02}^{*-1}) I^* \delta q_{2i} + \\ \dots + \sum_{i=1}^{t_n} (A_{0n}^* T_{nn} Q_{ni} T_{nn}^{-1} A_{0n}^{*-1}) I^* \delta q_{ni} = I \end{aligned} \quad (2.2.3-19)$$

or

$$\sum_{i=1}^{t_1} B_{1i}^* \delta q_{1i} + \sum_{i=1}^{t_2} B_{2i}^* \delta q_{2i} + \dots + \sum_{i=1}^{t_n} B_{ni}^* \delta q_{ni} = I^{*-1} - I \quad (2.2.3-20)$$

where

$$B_{ji}^* = A_{oj}^* T_{jj} Q_{ji} T_{jj}^{-1} A_{oj}^{*-1} \quad (2.2.3-21)$$

Owing to the antisymmetric form of the B_{ji}^* matrix, this matrix equation can equally be transformed into six algebraic independent equations. If α_{kl} are the elements of the matrix $I^{*-1} - I$, the equation can be written in the following explicit form:

$$\begin{bmatrix} B_{11}^*(1,2) & B_{12}^*(1,2) & \dots & B_{21}^*(1,2) & B_{22}^*(1,2) & \dots & B_{nt_n}^*(1,2) \\ B_{11}^*(1,3) & B_{12}^*(1,3) & \dots & B_{21}^*(1,3) & B_{22}^*(1,3) & \dots & B_{nt_n}^*(1,3) \\ B_{11}^*(2,3) & B_{12}^*(2,3) & \dots & B_{21}^*(2,3) & B_{22}^*(2,3) & \dots & B_{nt_n}^*(2,3) \\ B_{11}^*(1,4) & B_{12}^*(1,4) & \dots & B_{21}^*(1,4) & B_{22}^*(1,4) & \dots & B_{nt_n}^*(1,4) \\ B_{11}^*(2,4) & B_{12}^*(2,4) & \dots & B_{21}^*(2,4) & B_{22}^*(2,4) & \dots & B_{nt_n}^*(2,4) \\ B_{11}^*(3,4) & B_{12}^*(3,4) & \dots & B_{21}^*(3,4) & B_{22}^*(3,4) & \dots & B_{nt_n}^*(3,4) \end{bmatrix} \begin{bmatrix} \delta q_{11} \\ \delta q_{12} \\ \vdots \\ \delta q_{21} \\ \delta q_{22} \\ \vdots \\ \delta q_{nt_n} \end{bmatrix} = \begin{bmatrix} \alpha_{11} \\ \alpha_{12} \\ \alpha_{13} \\ \alpha_{23} \\ \alpha_{14} \\ \alpha_{24} \\ \alpha_{34} \end{bmatrix} \quad (2.2.3-22)$$

If all the N_{lo} loops are treated, the following global linear system is obtained:

$$[C]_{(6N_{lo}*m)} [\delta q]_{(m*1)} = [R]_{(6N_{lo}*1)} \quad (2.2.3-23)$$

each of the N_{lo} loops corresponding to six equations, each of them containing some of the m joint coordinates δq_{ji} . If N_r is the rank of the $[C]$ matrix, only one submatrix of rank N_r can be diagonalized with $N_r \leq m$ and $N_r \leq 6N_{lo}$. Generally, $m - N_r$ residues can be fixed arbitrarily, and the remaining can be calculated. The calculated residues can be added to the previous estimated values of the joint coordinates, and the results will be used as starting estimated values in an iterative process which will converge to the solution, if each residue tends to zero; this is the case if a solution exists and if the initial estimates were not so far from the real solution.

In order to have a simple notation, denote the unknown correction of q_{ji} by δ_k ($k=1, 2, \dots, m$) where it is understood that $\delta_{q_{ji}}$ have one-to-one correspondence with δ_k :

$$[C]_{(6N_{lo} \times m)} [\delta]_{(m \times 1)} = [R]_{(6N_{lo} \times 1)} \quad (2.2.3-24)$$

If Newton-Raphson method is used to solve these constraint equations, the correction terms of the independent variables must be zero.

In practice, let's suppose the last DOF variables $\underline{\delta}_2$ in the $\underline{\delta}$ vector (and hence the corresponding columns in the [C] matrix) relate to the specified independent constraint variables. This can always be achieved by simple interchange of the columns in the [C] matrix, without affecting the relative locations of the elements of the [R] vector. The (m-DOF) remaining correction terms will be found by a Newton-Raphson iterative process. The rearranging of matrix [C] results in the following partitioned form:

$$\begin{bmatrix} C_{11} & C_{12} \\ C_{21} & C_{22} \end{bmatrix} \begin{Bmatrix} \underline{\delta}_1 \\ \underline{\delta}_2 \end{Bmatrix} = \begin{Bmatrix} \underline{R}_1 \\ \underline{R}_2 \end{Bmatrix} \quad (2.2.3-25)$$

where

$[C_{11}] = (N_r \times N_r)$ nonsingular matrix;

$[C_{12}] = (N_r \times \text{DOF})$ matrix;

$[C_{21}] = (\text{DOF} \times N_r)$ matrix;

$[C_{22}] = (\text{DOF} \times \text{DOF})$ matrix.

The solution of equation (2.2.3-25) can now be obtained by:

$$\underline{\delta}_1 = [C_{11}]^{-1} \underline{R}_1 - [C_{12}] \underline{\delta}_2 \quad (2.2.3-26)$$

As the DOF elements of the $\underline{\delta}_2$ vector, the corrections $\underline{\delta}_1$ are expressed by:

$$\underline{\delta}_1 = [C_{11}]^{-1} \underline{R}_1 \quad (2.2.3-27)$$

They will be added to the corresponding constraint variables q_{ji} and the iteration process can be continued until the norm of $\underline{\delta}_1$ becomes less than a predetermined tolerance, ε_1 . Thus, the initial position is assumed to be properly determined when:

$$||\underline{\delta}_1|| < \varepsilon_1 \quad (2.2.3-28)$$

2.2.4 Velocity analysis

2.2.4.1 Expression of the velocity of a point P

Considering a point P on link k of a mechanical system (see Fig. 2.2.4-1), the local coordinates of this particle in the correspondent link reference frame are represented by vector r_k^P . The absolute vector \underline{R}_P of this particle in the global coordinate frame is given by:

$$\underline{R}_P = A_{ok}(\underline{q}_1, \underline{q}_2, \dots, \underline{q}_{k-1}) \underline{x}_k^P \quad (2.2.4-1)$$

where A_{ok} is the interlink transformation matrix between the global coordinate frame and link k. It can be expressed by the following matrix products:

$$A_{ok} = A_{01} T_{11} \varphi_1(\underline{q}_1) T_{12} T_{22} \varphi_2(\underline{q}_2) \dots \varphi_{k-1}(\underline{q}_{k-1}) T_{k-1,k} \quad (2.2.4-2)$$

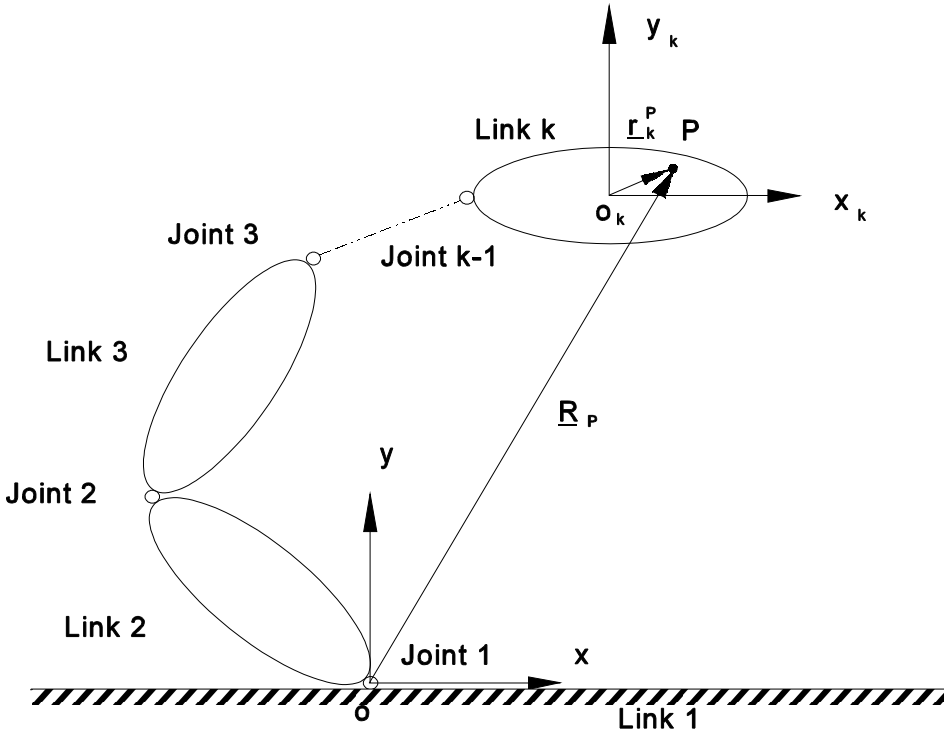


Fig. 2.2.4-1: Point P on link k of a kinematic loop

Let's arrange the order of the joint variables to form a relative coordinate vector $\{\underline{q}'\}$:

$$\{\underline{q}'\}_{1*m}^T = (\underline{q}_{11}, \underline{q}_{12}, \dots, \underline{q}_{1,t_1}, \dots, \underline{q}_{n,1}, \underline{q}_{n,2}, \dots, \underline{q}_{n,t_n}) \quad (2.2.4-3)$$

where n is the number of joints of the system and m is the total number of relative variables concerning all the joints with:

$$m = \sum_{j=1}^n t_j \quad (2.2.4-4)$$

where t_j is the number of constraint variables in joint j. The ath element of a vector $\{\underline{q}'\}$ is given by:

$$\underline{q}'_a = \sum_{j=1}^n \sum_{i=1}^{t_j} \alpha_{aji} \underline{q}_{ji} \quad (2.2.4-5)$$

where α_{aji} is a constant, defined by:

$$\begin{aligned} \alpha_{aji} &= 1, & \text{if } a = \sum_{n=1}^j t_n + i \\ \alpha_{aji} &= 0, & \text{other cases} \end{aligned} \quad (2.2.4-6)$$

The absolute position vector of a point is then expressed by:

$$\underline{\underline{R}}_P = \mathbf{A}_{ok}(\underline{\underline{q}}') \underline{\underline{x}}_k^P \quad (2.2.4-7)$$

Differentiating Equation (2.2.4-1), the velocity of point P on link k is given by:

$$\frac{d\dot{\underline{x}}_P}{dt} = (\dot{x}, \dot{y}, \dot{z}, 0)^T = \frac{dA_{o1}}{dt} \underline{x}_k^P + A_{o1} \frac{d\underline{x}_k^P}{dt} \quad (2.2.4-8)$$

Owing to the hypothesis of a non flexible link adopted in this thesis, the differentiation of vector r_k^P is equal to zero, and

$$\frac{dR}{dt} = \frac{dA_{ok}}{dt} r_k^P \quad (2.2.4-9)$$

The differentiation of A_{eq} versus time can be deduced from equation (2.2.4-2), and leads to:

$$\begin{aligned}
\frac{dA_{ok}}{dt} &= \frac{d}{dt} (T_{01} T_{11} \varphi_1(\underline{q}_1) T_{12} T_{22} \varphi_2(\underline{q}_2) T_3 \dots \varphi_{k-1}(\underline{q}_{k-1}) T_{k-1,k}) \\
&= T_{01} T_{11} \sum_{i=1}^{t_1} \frac{\partial \varphi_1(\underline{q}_1)}{\partial q_{1i}} \dot{q}_{1i} T_{12} T_{22} \varphi_2(\underline{q}_2) T_{23} \dots \varphi_{k-1}(\underline{q}_{k-1}) T_{k-1,k} \\
&\quad + T_{01} T_{11} \varphi_1(\underline{q}_1) T_{12} T_{22} \sum_{i=1}^{t_2} \frac{\partial \varphi_2(\underline{q}_2)}{\partial q_{2i}} \dot{q}_{2i} T_{23} \dots \varphi_{k-1}(\underline{q}_{k-1}) T_{k-1,k} \\
&\quad + \dots \dots \dots \dots \dots \dots \dots \\
&\quad + T_{01} T_{11} \varphi_1(\underline{q}_1) T_{12} T_{22} \varphi_2(\underline{q}_2) T_{23} \dots \sum_{i=1}^{t_{k-1}} \frac{\partial \varphi_{k-1}(\underline{q}_{k-1})}{\partial q_{k-1,i}} \dot{q}_{k-1,i} T_{k-1,k}
\end{aligned} \tag{2.2.4-10}$$

Using the derivative operators' matrices, the equation can be reconstructed as:

$$\begin{aligned} \frac{dA_{ok}}{dt} = & \sum_{i=1}^{t_1} [T_{01} T_{11} Q_{1i} \dot{q}_{1i} T_{01}^{-1} T_{01} \varphi_1(\underline{q}_1) T_{12} T_{22} \varphi_2(\underline{q}_2) T_{23} \dots \varphi_{k-1}(\underline{q}_{k-1}) T_{k-1,k}] \\ & + \sum_{i=1}^{t_2} [T_{01} T_{11} \varphi_1(\underline{q}_1) T_{12} T_{22} Q_{2i} \dot{q}_{2i} (T_{01} \varphi_1(\underline{q}_2) T_{12} T_{22})^{-1} (T_{01} \varphi_1(\underline{q}_1) T_{12} T_{22}) \\ & \quad \varphi_2(\underline{q}_2) T_{23} \dots \varphi_{k-1}(\underline{q}_{k-1}) T_{k-1,k}] \end{aligned}$$

$$+ \sum_{i=1}^{t_{k-1}} [(T_{01}T_{11}\varphi_1(\underline{q}_1)T_{12}T_{22}\varphi_2(\underline{q}_2)T_{23}\dots)Q_{k-1,i}\dot{q}_{k-1,i}(T_{01}\varphi_1(\underline{q}_1)T_{12}T_{22}\varphi_2(\underline{q}_2)T_{23}\dots)^{-1}(T_{01}\varphi_1(\underline{q}_1)T_{12}T_{22}\varphi_2(\underline{q}_2)T_{23}\dots)\varphi_{k-1}(\underline{q}_{k-1})T_{k-1,k}] \quad (2.2.4-11)$$

From the equation (2.2.3-9) and (2.2.3-18), equation (2.2.4-11) can be rewritten as:

$$\begin{aligned} \frac{dA_{ok}}{dt} = & \sum_{i=1}^{t_1} (A_{01}T_{11}Q_{1i}T_{11}^{-1}A_{01}^{-1})A_{0k}\dot{q}_{1i} + \sum_{i=1}^{t_2} (A_{02}T_{22}Q_{2i}T_{22}^{-1}A_{02}^{-1})A_{0k}\dot{q}_{2i} \\ & + \dots + \sum_{i=1}^{t_{k-1}} (A_{0,k-1}T_{k-1,k-1}Q_{k-1,i}T_{k-1,k-1}^{-1}A_{0,k-1}^{-1})A_{0k}\dot{q}_{k-1} \end{aligned} \quad (2.2.4-12)$$

or

$$\frac{dA_{ok}}{dt} = (\sum_{i=1}^{t_1} B_{1i}\dot{q}_{1i} + \sum_{i=1}^{t_2} B_{2i}\dot{q}_{2i} + \dots + \sum_{i=1}^{t_{k-1}} B_{k-1,i}\dot{q}_{k-1,i})A_{ok} \quad (2.2.4-13)$$

where

$$B_{ji} = A_{oj}T_{jj}Q_{ji}T_{jj}^{-1}A_{oj}^{-1} \quad (2.2.4-14)$$

Introducing equation (2.2.4-13) into equation (2.2.4-9), the absolute velocity of point P is determined by:

$$\frac{dR_P}{dt} = (\sum_{i=1}^{t_1} B_{1i}\dot{q}_{1i} + \sum_{i=1}^{t_2} B_{2i}\dot{q}_{2i} + \dots + \sum_{i=1}^{t_{k-1}} B_{k-1,i}\dot{q}_{k-1,i})A_{ok}\underline{r}_k^P \quad (2.2.4-15)$$

Based on the definition of relative coordinates and equation (2.2.4-5), the following equation can be defined as:

$$\sum_{j=1}^{k-1} \sum_{i=1}^{t_j} B_{ji}\dot{q}_{ji} = \sum_{a=1}^m \Lambda_{ka}\dot{q}'_a \quad (2.2.4-16)$$

where k is the ordinal number of the links in the considered kinematic loop and n is the total number of relative coordinates of the mechanical system. The Λ_{ka} is referred as the **coefficient matrix of relative velocity** of link k, and is expressed by:

$$\begin{aligned} \Lambda_{ka} = & \sum_{j=1}^{k-1} \sum_{i=1}^{t_j} \alpha_{aji} B_{ji} \quad (\alpha = 1, 2, \dots, \sum_{j=1}^{k-1} t_j) \\ \Lambda_{ka} = & 0 \quad (\sum_{j=1}^{k-1} t_j < \alpha \leq m) \end{aligned} \quad (2.2.4-17)$$

where coefficients α_{aji} in the equation are the same as the ones in Equation (2.2.4-6).

From Equation (2.2.4-16), Equation (2.2.4-13) can be rewritten as:

$$\frac{dA_{ok}}{dt} = \sum_{a=1}^m \Lambda_{ka}\dot{q}'_a A_{ok} \quad (2.2.4-18)$$

or

$$\frac{dA_{ok}}{dt} = \{\Lambda_k\}^T \{\dot{q}'\} A_{ok} \quad (2.2.4-19)$$

Finally, the velocity of point P on link k can be expressed by:

$$\frac{dR_p}{dt} = \sum_{a=1}^m \Lambda_{ka} \dot{q}_a' A_{ok} \underline{x}_k^P \quad (2.2.4-20)$$

or

$$\frac{dR_p}{dt} = \{\Lambda_k\}^t \{\dot{q}'\} A_{ok} \underline{x}_k^P \quad (2.2.4-21)$$

If the velocities of all relative coordinates are known, the velocity of the point P can be obtained by this last equation. In kinematic analysis, only DOF independent velocities are given, the other relative velocities being function of the independent ones. The concept of influence coefficient will be introduced in order to obtain a more direct relation between dependent and independent velocities.

2.2.4.2 Influence coefficients

If DOF is the number of degrees of freedom of the system, a set of DOF independent coordinates can be defined and noted by f_i ($i=1,2,\dots,DOF$). The relative coordinates q'_j ($j=1,2,\dots, m$, where m is the number of joint variables) can be expressed as a function of these variables:

$$q'_j = q'_j(f_1, f_2, \dots, f_{DOF}) \quad (2.2.4-22)$$

Differentiating this last equation with respect to time t , the relationship between relative and independent velocity coordinates becomes:

$$\dot{q}'_j = \frac{\partial q'_j}{\partial f_1} \dot{f}_1 + \frac{\partial q'_j}{\partial f_2} \dot{f}_2 + \dots + \frac{\partial q'_j}{\partial f_{DOF}} \dot{f}_{DOF} \quad (2.2.4-23)$$

or, more concisely:

$$\underline{\dot{q}'} = [K] \underline{\dot{f}} \quad (2.2.4-24)$$

where $[K]$ is the matrix of **influence coefficients**, the element k_{ji} being defined by:

$$k_{ji} = \frac{\partial q'_j}{\partial f_i} \quad (2.2.4-25)$$

In the preceding section, the topology analysis identifies the N_{lo} independent kinematical loops of the mechanical system. For a mechanism with N_{lo} closed constraint loops (see Fig.2.2.3-2), the N_{lo} matrix equations are obtained (see Equ. 2.2.3-10):

$$\begin{aligned}\Phi_1 &= (A_{01} T_{11} \varphi_1(\underline{q}_1) T_{12} T_{22} \varphi_2(\underline{q}_2) T_{23} \dots \varphi_n(\underline{q}_n) T_{n1} A_{10})_1 = I \\ \Phi_2 &= (A_{01} T_{11} \varphi_1(\underline{q}_1) T_{12} T_{22} \varphi_2(\underline{q}_2) T_{23} \dots \varphi_n(\underline{q}_n) T_{n1} A_{10})_2 = I \quad (2.2.4-26) \\ &\dots \\ \Phi_{N_{lo}} &= (A_{01} T_{11} \varphi_1(\underline{q}_1) T_{12} T_{22} \varphi_2(\underline{q}_2) T_{23} \dots \varphi_n(\underline{q}_n) T_{n1} A_{10})_{N_{lo}} = I\end{aligned}$$

For the sake of simplicity, one single loop is considered here. By differentiating the matrix loop equations with respect to time t , the following matrix equation is obtained:

$$\begin{aligned}\frac{d\Phi_1}{dt} &= \sum_{i=1}^{t_1} A_{01} T_{11} \frac{\partial \varphi_1}{\partial q_{1i}} T_{12} T_{22} \varphi_2 T_{23} \dots \varphi_n T_{n1} A_{10} \dot{q}_{1i} \\ &+ \sum_{i=1}^{t_2} A_{01} T_{11} \varphi_1 T_{12} T_{22} \frac{\partial \varphi_2}{\partial q_{2i}} \dots \varphi_n T_{n1} A_{10} \dot{q}_{2i} \\ &+ \dots \\ &+ \sum_{i=1}^{t_n} A_{01} T_{11} \varphi_1 T_{12} T_{22} \varphi_2 T_{23} \dots \frac{\partial \varphi_n}{\partial q_{ni}} T_{n1} A_{10} \dot{q}_{ni} \\ &= [0] \quad (2.2.4-27)\end{aligned}$$

where t_n is the number of joint variables in joint n . Using joint linear derivative operator Q_{ji} (defined in Equ. 2.2.3-13), the general term corresponding to joint j in Equ. (2.2.4-27) can be rewritten as:

$$\begin{aligned}&\sum_{i=1}^{t_j} A_{01} T_{11} \varphi_1 T_{12} T_{22} \varphi_2 T_{23} \dots T_{j,j} Q_j \varphi_j T_{j,j+1} \dots \varphi_n T_{n1} A_{10} \dot{q}_{ji} \\ &= \sum_{i=1}^{t_j} A_{0j} T_{jj} Q_{ji} (A_{0j} T_{jj})^{-1} A_{0,j} T_{jj} \varphi_j T_{j,j+1} A_{j+1,0} \dot{q}_{ji} \\ &= \sum_{i=1}^{t_j} B_{ji} \dot{q}_{ji} \quad (2.2.4-28)\end{aligned}$$

where B_{ji} is called the **system linear derivative operator** associated to the considered joint variable, which has been already used in Equ. (2.2.3-21).

The velocity-level constraint equations for a kinematic loop can be rewritten:

$$\sum_{i=1}^{t_1} (B_{1i})_2 \dot{q}_{1i} + \sum_{i=1}^{t_2} (B_{1i})_2 \dot{q}_{2i} + \dots + \sum_{i=1}^{t_n} (B_{ni})_2 \dot{q}_{ni} = [0] \quad (2.2.4-29)$$

Using Equ. (2.2.4-16), the equation (2.2.4-29) is rewritten as follows:

$$(\Lambda_{n1}) \dot{q}_1' + (\Lambda_{n2}) \dot{q}_2' + \dots + (\Lambda_{nm}) \dot{q}_m' = [0] \quad (2.2.4-30)$$

where

$$\Lambda_{na} = \sum_{j=1}^n \sum_{i=1}^{t_j} \alpha_{aji} B_{ji} \quad (2.2.4-31)$$

where n is the number of joints in the kinematic loop and α_{aji} the constant parameter defined in (2.2.4-6).

Since the 3×3 rotational sub-matrix A_{oj} is always orthogonal and the rotational sub-matrix of Q_{ji} is always antisymmetric, the matrix $[\Lambda_{na}]_l$ has the following general form:

$$[\Lambda_{na}] = \begin{bmatrix} 0 & \Lambda_{na}(1,2) & \Lambda_{na}(1,3) & \Lambda_{na}(1,4) \\ \Lambda_{na}(2,1) & 0 & \Lambda_{na}(2,3) & \Lambda_{na}(2,4) \\ \Lambda_{na}(3,1) & \Lambda_{na}(3,2) & 0 & \Lambda_{na}(3,4) \\ 0 & 0 & 0 & 1 \end{bmatrix} \quad (2.2.4-32)$$

and

$$\Lambda_{na}(i,j) = -\Lambda_{na}(j,i), \quad j=1,2,3; i=1,2,3 \quad (2.2.4-33)$$

Six simultaneous linear equations are obtained for each loop. One matrix equation in Equation (2.2.4-30) can be reconstructed as:

$$\begin{bmatrix} \Lambda_{n1}(1,2) & \Lambda_{n2}(1,2) & \dots & \Lambda_{nm}(1,2) \\ \Lambda_{n1}(1,3) & \Lambda_{n2}(1,3) & \dots & \Lambda_{nm}(1,3) \\ \Lambda_{n1}(2,3) & \Lambda_{n2}(2,3) & \dots & \Lambda_{nm}(2,3) \\ \Lambda_{n1}(1,4) & \Lambda_{n2}(1,4) & \dots & \Lambda_{nm}(1,4) \\ \Lambda_{n1}(2,4) & \Lambda_{n2}(2,4) & \dots & \Lambda_{nm}(2,4) \\ \Lambda_{n1}(3,4) & \Lambda_{n2}(3,4) & \dots & \Lambda_{nm}(3,4) \end{bmatrix} \begin{Bmatrix} \dot{q}_1' \\ \dot{q}_2' \\ \dots \\ \dot{q}_m' \end{Bmatrix} = \{0\} \quad (2.2.4-34)$$

The solving procedure is then rather similar to the one used for the position analysis (section 2.2.3). If the system has N_{lo} independent kinematic loops, $6 \times N_{lo}$ algebraic equations are obtained, which written in compact form gives:

$$[C] \underline{\dot{q}}' = \underline{0} \quad (2.2.4-35)$$

The matrix $[C]$ is the $N_{co} \times m$ Jacobian matrix of the constraints, N_{co} is the number of constraint equations (equal to $6 \times N_{lo}$ for an arbitrary spatial mechanical system), and m is the number of relative coordinates. The elements of $[C]$, c_{ij} , are only functions of positions \underline{q}' , and $\underline{\dot{q}}'$ is the column vector of relative coordinate velocities. If the rank of a matrix $[C]$ is N_r , then there are $(m-N_r)$ unknown elements in $\underline{\dot{q}}'$ which can be arbitrarily fixed and the others will be uniquely

determined by the constraint equation. In kinematic terms, the number of degrees of freedom (DOF) of the system is:

$$DOF = m - N_r \quad (2.2.4-36)$$

A set of DOF independent relative coordinates can be selected and form the vector \underline{f} of the primary variables. The velocity constraint equation (2.2.4-35) can be rearranged and rewritten as:

$$\begin{bmatrix} C_{11} & C_{12} \\ C_{21} & C_{22} \end{bmatrix} \begin{Bmatrix} \dot{\underline{d}} \\ \dot{\underline{f}} \end{Bmatrix} = \{0\} \quad (2.2.4-37)$$

where C_{11} is a nonsingular square matrix with order N_r . The relative coordinates $\underline{f}(f_1, f_2, \dots, f_{DOF})$ are used as generalized coordinates or independent coordinates, and the remaining relative coordinates are considered as secondary variables $\underline{d}(d_1, d_2, \dots, d_{m-DOF})$. Equation (2.2.4-37) can be inverted to give the secondary velocities $\dot{\underline{d}}$ in terms of the primary velocities $\dot{\underline{f}}$ by:

$$\dot{\underline{d}} = [C_{11}]^{-1} [C_{12}] \dot{\underline{f}} \quad (2.2.4-38)$$

The velocities of the relative coordinates can be calculated from a set of independent coordinates by:

$$\{\dot{\underline{q}}\} = \begin{Bmatrix} \dot{\underline{d}} \\ \dot{\underline{f}} \end{Bmatrix} = \begin{bmatrix} C_{11}^{-1} C_{12} \\ I \end{bmatrix} \{\dot{\underline{f}}\} \quad (2.2.4-39)$$

or

$$\{\dot{\underline{q}}\} = [K] \{\dot{\underline{f}}\} \quad (2.2.4-40)$$

where the linear influence coefficients matrix $[K]$ is expressed by:

$$[K] = \begin{bmatrix} C_{11}^{-1} C_{12} \\ I \end{bmatrix} \quad (2.2.4-41)$$

2.3 Kinematic properties for articulated joints

As it has been described in the preceding section, a kinematic simulation with relative coordinates needs the description of particular reference frames on each considered joint, the definition of relative coordinates describing the state of the joint, as well as the setting of joint and derivative matrices. This approach will be illustrated, in the simple classical case of revolute and prismatic joints. Others articulated joint elements illustrated in Fig. (2.3-1) have been considered in this thesis (cylindric, screw, spheric, universal joint, planar, pure-roll joint, free joint). The detail of their kinematics properties is described in Appendix A.

2.3.1 Reference frames

In a revolute joint (fig. 2.3-1a), the following conventions are imposed on the choice of x_k^- , y_k^- , z_k^- and x_k^+ , y_k^+ , z_k^+ : the z_k^- and z_k^+ axes are selected along the common revolute axis, with an identical arbitrary positive direction, the origins of the two coordinate systems being coincident.

For a prismatic joint (Fig. 2.3-1b), the choice of the coordinate axes respects the following conventions: the z_k^- and z_k^+ axes are placed along the axis of the prismatic joint with an identical positive direction, the x_k^- and x_k^+ axes being each other parallel.

2.3.2 Relative joint coordinates

In a 1 DOF revolute joint, the relative coordinate is defined by the angle q_{k1} measured from the positive x_k^- axis to the positive x_k^+ axis. The angle is considered positive when measured counterclockwise about the z_k^-, z_k^+ axis.

In a prismatic joint, the relative joint coordinate is defined by q_{k1} corresponding to the distance from x_k^- to x_k^+ measured along z_k^-, z_k^+ .

2.3.3 Joint and derivative matrices

In a revolute joint, the axes z_k^- and z_k^+ have been selected along the revolute axis, the relative motion can be considered as a x-y planar motion, the origin of the coordinate frame remaining unchanged. It leads to the following transformation matrix from x_k^-, y_k^-, z_k^- preceding to the x_k^+, y_k^+, z_k^+ following frames:

$$\varphi_k(q_{k1}) = \begin{bmatrix} \cos q_{k1} & -\sin q_{k1} & 0 & 0 \\ \sin q_{k1} & \cos q_{k1} & 0 & 0 \\ 0 & 0 & 1 & 0 \\ 0 & 0 & 0 & 1 \end{bmatrix} \quad (2.3.3-1)$$

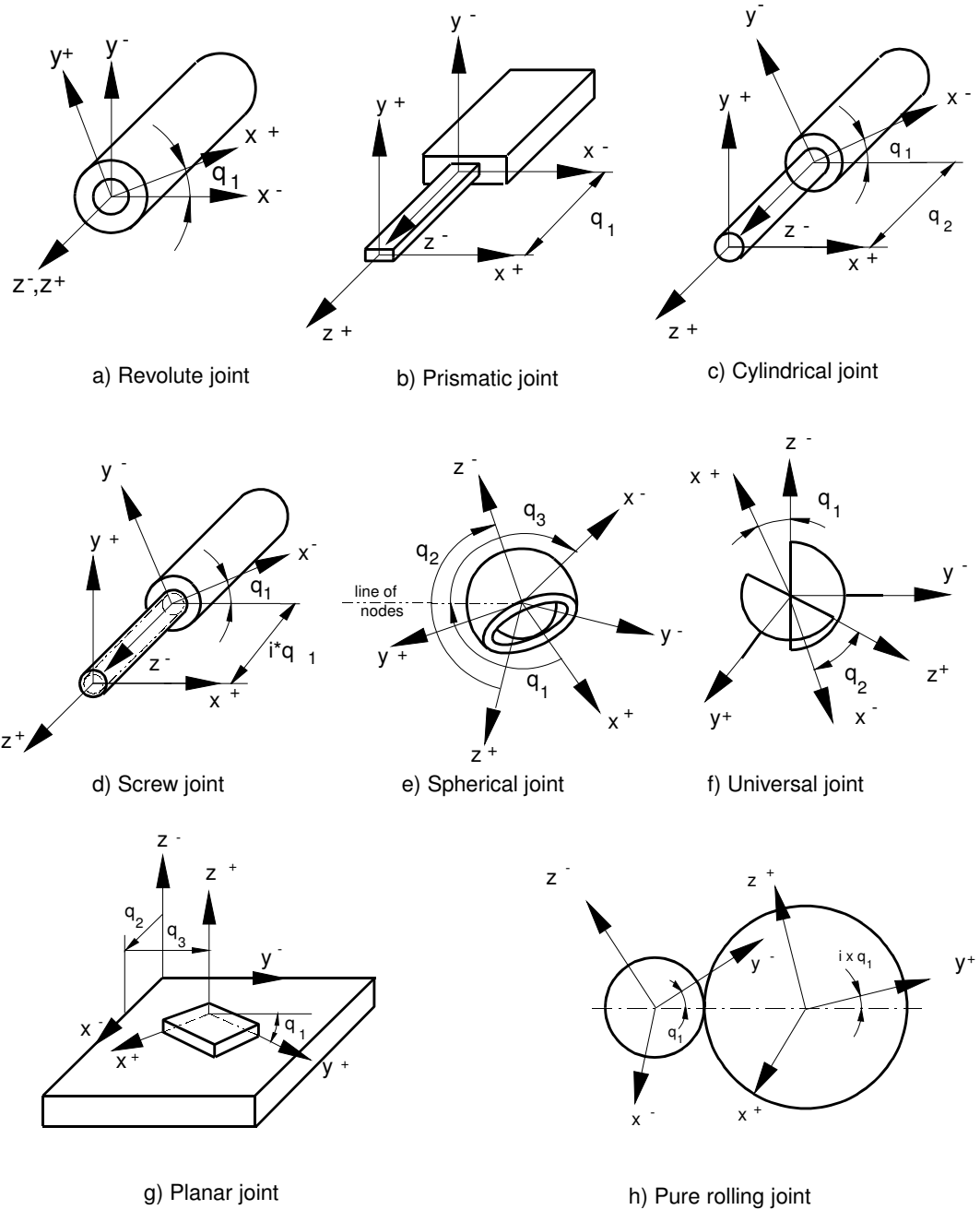


Fig. 2.3-1: Local coordinate frames associated to articulated joints

The associated derivative operator obtained by equation (2.2.5-12) gives:

$$Q_{k1} = \frac{\partial \varphi_k(q_{k1})}{\partial q_{k1}} (\varphi_k(q_{k1}))^{-1} = \begin{vmatrix} 0 & -1 & 0 & 0 \\ 1 & 0 & 0 & 0 \\ 0 & 0 & 0 & 0 \\ 0 & 0 & 0 & 0 \end{vmatrix} \quad (2.3.3-2)$$

In a prismatic joint, the z_k^- and z_k^+ axes have been defined along the prismatic constraint axis. The relative motion between the two bodies is a displacement along the z axis. The planar transformation matrix from the x_k^-, y_k^-, z_k^- preceding frame to the x_k^+, y_k^+, z_k^+ following frame gives

$$\varphi_k(q_{k1}) = \varphi_k(q_{k1}) = \begin{vmatrix} 1 & 0 & 0 & 0 \\ 0 & 1 & 0 & 0 \\ 0 & 0 & 1 & q_{k1} \\ 0 & 0 & 0 & 1 \end{vmatrix} \quad (2.3.3-3)$$

The associated derivative operator is expressed by:

$$Q_{k1} = \frac{\partial \varphi_k(q_{k1})}{\partial q_{k1}} (\varphi_k(q_{k1}))^{-1} = \begin{vmatrix} 0 & 0 & 0 & 0 \\ 0 & 0 & 0 & 1 \\ 0 & 0 & 0 & 0 \\ 0 & 0 & 0 & 0 \end{vmatrix} \quad (2.3.3-4)$$

2.4 Kinematic properties for contact joints

One of the advantages of the procedure adapted in this thesis is to propose a unified method either for contact or lower-pair joints. A similar procedure has therefore been applied for contact joints. Each contact joint requires the attachment of particular coordinate frames to the joint, as well as the definition of relative coordinates describing the configuration of the contact joints, the functionality being expressed by joint and derivative matrices.

As it has been said in the introductory part, this thesis mainly concerns mechanisms with cams that exhibit a profile, which can be described by a succession of simple geometric curves. We have therefore considered that a contact could concern five types of curve elements corresponding to a point, a line, an arc, a circle or a polynomial line. In theory, we can consider that a point element and a line element are two special cases of an arc element when radius is infinitely high or infinitely small. However, both limit cases have been considered, in order to take into account of the exact geometrical properties if necessary.

When active, a contact joint involves the participation of two curve elements, which will be identified as a preceding contact pair (PCP) and a following contact pair (FCP), as it can be seen in Fig. 2.4-1, in the case of a line-arc contact.

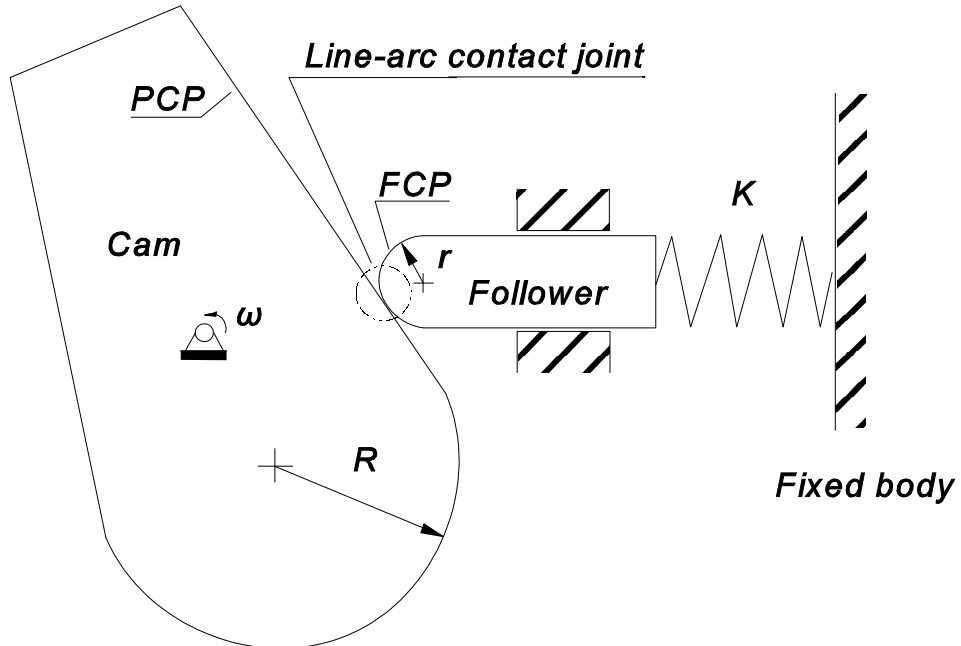


Fig. 2.4-1: Cam-follower mechanism with a "line-arc" contact joint

The different combinations between the considered elements theoretically lead to 25 types of contact joints (see Table 2.4-1). Two types of contact joints have however been excluded

because the possibility of such a combination is instantaneous. When a “point-point” contact or “line-line” contact happens, the contact is instantaneously modified to another contact type.

Table 2.4-1: Types of contact joints

	point	line	arc	circle	polynomial
point	***	point-line	point-arc	point-circle	point-poly.
line	line-point	***	line-arc	line-circle	line-poly.
arc	arc-point	arc-line	arc-arc	arc-circle	arc-poly.
circle	circle-point	circle-line	circle-arc	circle-circle	circle-poly.
polynomial	poly.-point	poly.-line	poly.-arc	poly.-circle	poly.-poly.

Note: “***” means that the contact joint type will not be considered.

2.4.1 Reference Frames

The setting of joint reference frames can be done arbitrarily, but has been chosen to lead to simple joint transformation matrices. Fig. 2.4.1-1 illustrates the different coordinate frames, the notation x_k^-, y_k^-, z_k^- being used if the element is a preceding contact part (PCP), or x_k^+, y_k^+, z_k^+ if the element is a following contact part (FCP).

-- Point

The origin of the particular coordinate frame coincides with the point. The Z axis is perpendicular to the plane of motion, with an arbitrary chosen direction. The Y axis is a tangent to the previous geometrical element. The X axis completes a right-handed Cartesian system X,Y,Z (see Fig. 2.4.1-2a).

-- Arc

The origin of the joint coordinate frame is located on the centre of the arc. The Z axis is perpendicular to the plane of motion. The Y axis is defined from the centre of the arc to the initial point of the arc. The X axis completes a right-handed Cartesian system X,Y,Z (see Fig. 2.4.1-2b).

-- Line

The origin of the joint coordinate frame is located on the initial point of the line. The Z axis is perpendicular to the plane of motion. The X axis is taken from the initial point to the end of the line. The Y axis completes a right-handed Cartesian system X,Y,Z (see Fig. 2.4.1-2c).

-- Circle

The origin of the particular coordinate frame is located on the centre of the circle. The Z axis is perpendicular to the plane of motion. The Y axis is defined from the centre of the circle to an arbitrary chosen initial point of the circle. The X axis completes a right-handed Cartesian system X,Y,Z (see Fig. 2.4.1-2d).

-- Polynomial curve

The origin of the particular coordinate frame is located on the origin of a polar system coordinate. The Z axis is perpendicular to the plane of motion, the sense being arbitrarily chosen. An initial point of the curve is selected and forms the Y axis. The X axis completes a right-handed cartesian system X,Y,Z (see Fig. 2.4.1-2e). The form of the curve is given by a polynomial equation relating the radius r to the angle θ :

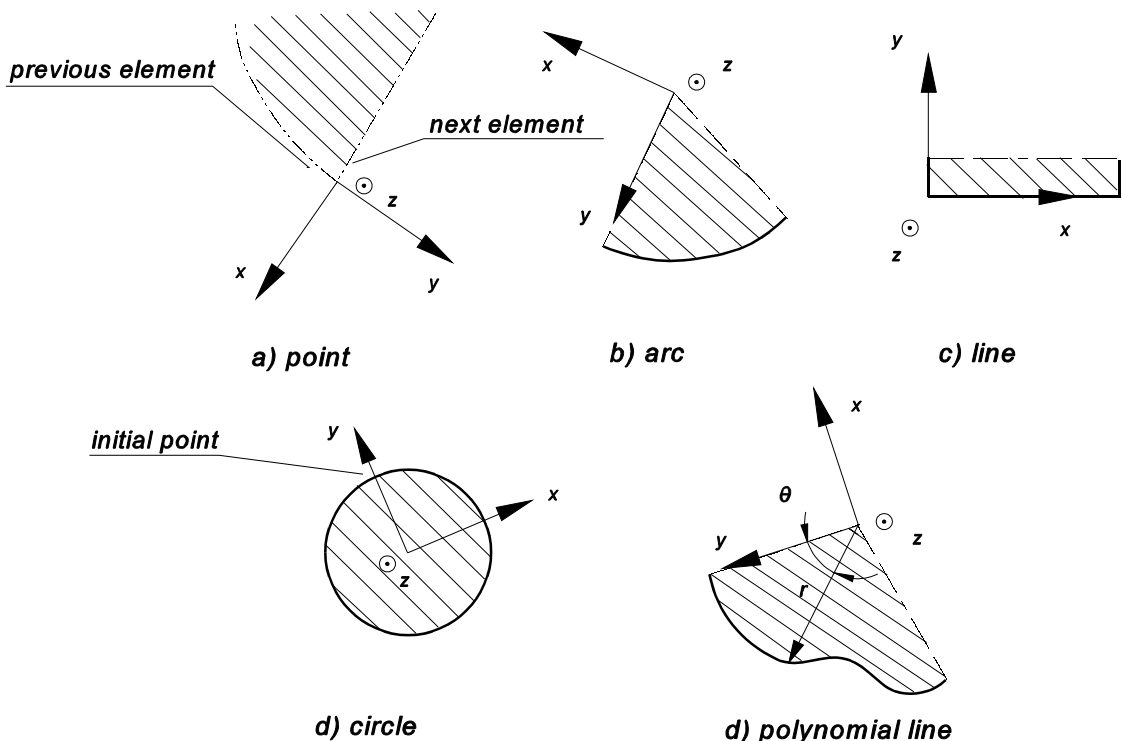


Fig. 2.4.1-1: Particular coordinate frames associated to each curve element

$$r = \sum_i c_i \theta^i \quad (2.4.1-1)$$

2.4.2 Relative joint coordinates

As far as the definition of the joint coordinates is concerned, owing to the slipping conditions between contacting curves, **an active contact can be considered as a joint with 2 degrees of freedom.** It is therefore described by two relative coordinates q_{k1} and q_{k2} . Each contact joint coordinate is made up of two parts:

- an integer part, defining the curve element containing the contact point. For this reason, each transition between the elements of a contacting curve is numbered in an iterative way, in such a positive direction that the link on the left is, relatively to this direction,
- a decimal part, which specifies the exact position of the contact point, this position being expressed in coordinates reduced in the interval [0,1) and respecting the proportionality with the complete variation for the entire current element.

If a current contact point k is located on a contact element described by the range (i_{k-1}, i_k) , the decimal part of the joint is defined as follows:

$$q_{kj} = (i_k - 1) + \frac{v - v_{\min}}{v_{\max} - v_{\min}} \quad (2.4.2-1)$$

The index j refers to the order of the joint coordinate, j=1 if the contact pair is used as PCP(Preceding Contact Pair), and j=2 if it's used as FCP(Following Contact Pair). The parameter v is the geometric parameter which locates the exact point of the contact, v_{\min} and v_{\max} being the values of these geometric parameters corresponding respectively to the lower and upper limits of the contact element (Fig. 2.4.2-1). Fig. 2.4.2-2 illustrates the different definition adopted for this decimal part in the case of a Preceding Contact Pair.

In the case of an arc element, the parameter v is the angle θ_{k1} between the y axis and the radius which locates the exact position of the contact point. One has:

$$v_{\min} = 0 \text{ and } v_{\max} = \beta_{k1}$$

β_{k1} being total angle of the arc, and

$$q_{k1} = (i_k - 1) + \frac{\theta_{k1}}{\beta_{k1}} \quad (2.4.2-2)$$

The circle and polynomial shape elements are treated in a similar way, β_{k1} being equal to 360° for a circle element.

In the case of a line element, the parameter v is the distance s_{k1} between the y axis and the contact point, and

$$q_{k1} = (i_k - 1) + \frac{s_{k1}}{L_{k1}} \quad (2.4.2-3)$$

L_{kl} being the length of the line element.

For a point element, the parameter v is the angle θ_{kl} formed by the x axis with its initial position. As the two extreme positions correspond to:

$$v_{\min} = -90^\circ \text{ and } v_{\max} = 90^\circ - \beta_{kl}$$

β_{kl} being the angle between the two tangent lines to the previous and following elements.

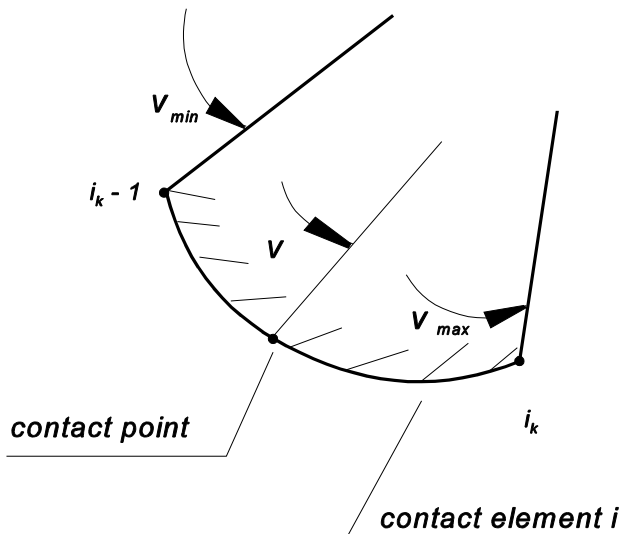
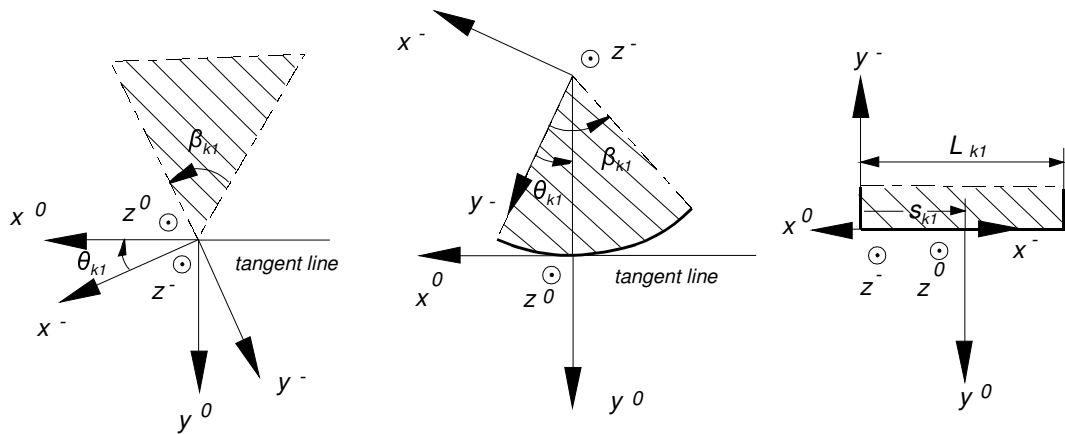


Fig2.4.2-1: Expression of contact element i

Fig. 2.4.2-2 illustrates the basic example of a typical cam S2 that rotates around the oz axis. This cam is in contact with a follower S3, animated by a translational horizontal motion.

The range of values corresponding to the relative curvilinear coordinate associated to the cam is described in Fig. (2.4.2-3). When the contact concerns the first basic geometric element of the cam S2 (arc), the coordinates on the cam S2 are comprised between 0 and 1. When it concerns the fourth element (point), it will be comprised between 3 and 4. During motion, the contact surface of the follower remains an arc, the curvilinear coordinate being comprised between 0 and 1. To illustrate the use of such coordinates, Fig. (2.4.2-4) shows the results obtained by a kinematic analysis; it gives the evolution of the curvilinear coordinates of the cam during motion, when the cam performs one complete revolution. Fig. 2.4.2-5 illustrates the changes of contact model by transition between consecutive curve elements.



$$q_{k1} = (i_k - 1) + \frac{\theta_{k1} + 90}{180^\circ - \beta_{k1}}$$

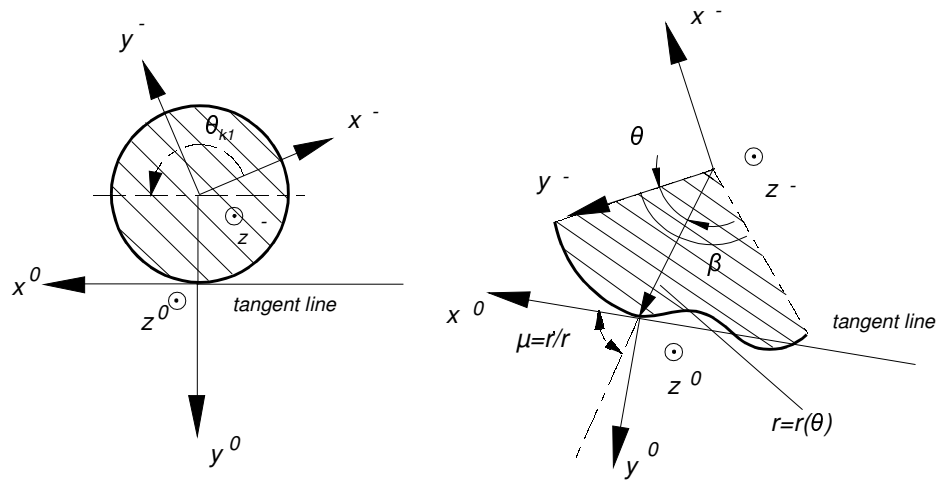
$$q_{k\bar{1}} = (i_k - 1) + \frac{\theta_{k1}}{\beta_{k1}}$$

$$q_{k\bar{1}} = (i_k - 1) + \frac{s_{k1}}{L_{k1}}$$

a) point

b) arc

c) line



$$q_{k1} = (i_k - 1) + \frac{\theta_{k1}}{360^\circ}$$

$$q_{k\bar{1}} = (i_k - 1) + \frac{\theta_{k1}}{\beta_{k1}}$$

d) circle

e) polynomial line

Fig. 2.4.2-2: Coordinate frames and joint variables of contact surfaces when the contact surfaces are used as PCP.

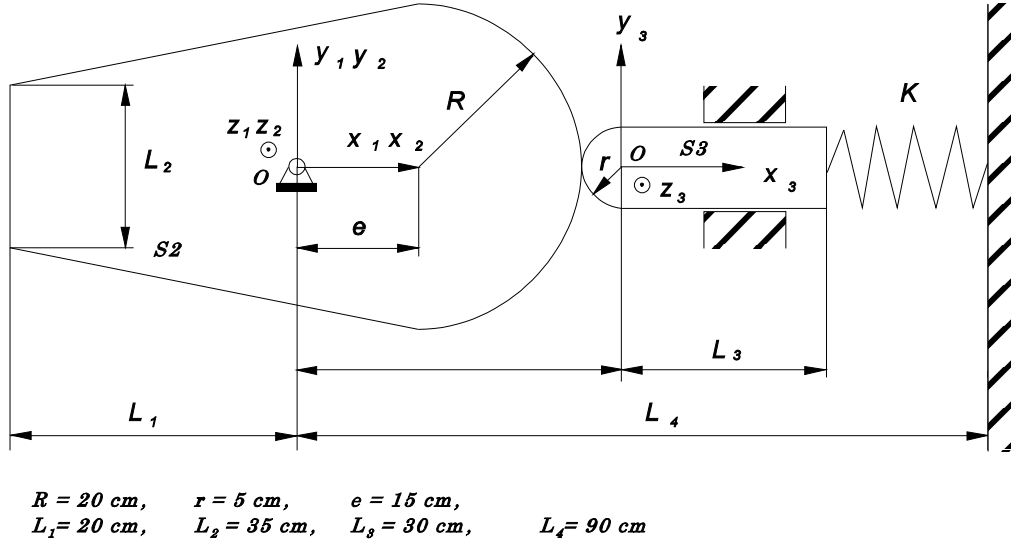
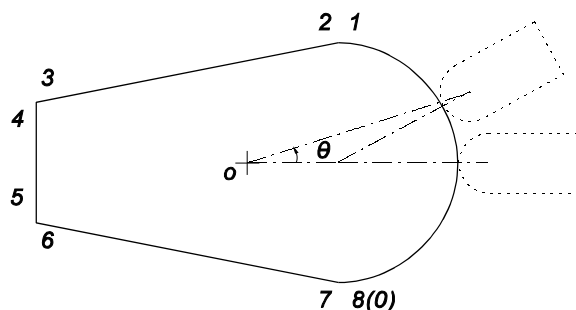


Fig. 2.4.2-3: Cam-follower mechanism



coordinates value	elements
0 - 1	arc
1 - 2	point
2 - 3	line
3 - 4	point
4 - 5	line
5 - 6	point
6 - 7	line
7 - 8	point

Fig. 2.4.2-4: Example of relative curvilinear coordinates of a cam

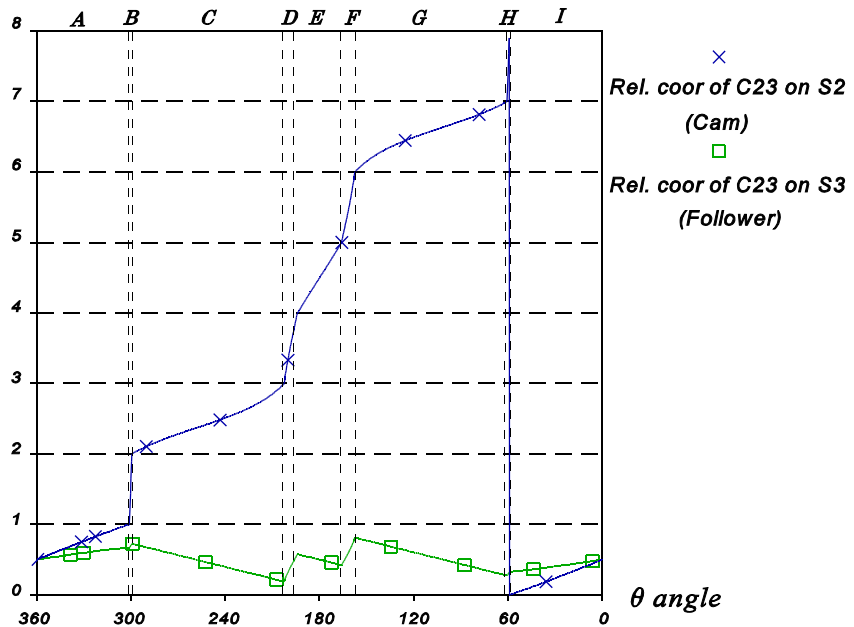


Fig. 2.4.2-5: Evolution of the relative curvilinear coordinates in function of the angular rotation (kinematic simulation)

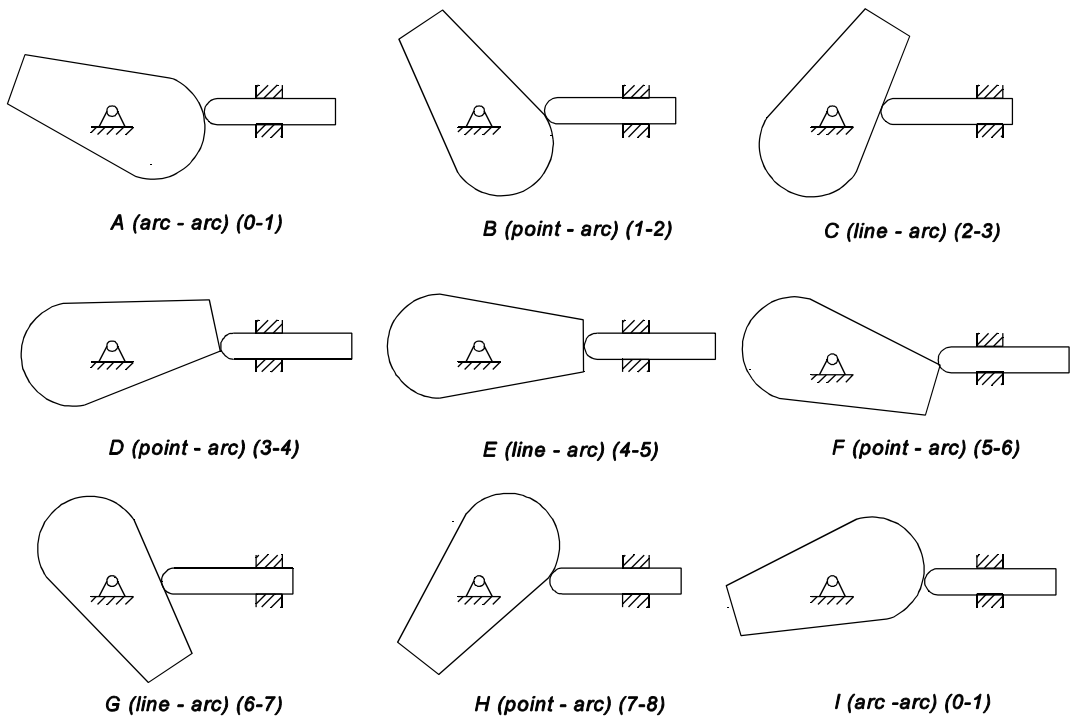


Fig. 2.4.2-6 Changes of the contact model by transition between consecutive curve elements (cam-follower mechanism)

2.4.3 Joint and derivative matrix

When active, each contact joint concerns two different curve elements, which according to an arbitrary conventional direction can be separated into a preceding contact pair (PCP) and a following contact pair (FCP). The setting of a joint transformation matrix between reference frames x_k^-, y_k^-, z_k^- (PCP) and $x_k^+ y_k^+ z_k^+$ (FCP) can be performed by considering an intermediate frame ($x_k^0 y_k^0 z_k^0$):

- the origin of this frame is located at the contact joint,
- the axis x_k^0 is perpendicular to the plane of motion and has the same positive direction as the z_k^- axis of the frame describing the contacting curves,
- the axis y_k^0 is parallel to the common normal direction at the contact point and is directed from the PCP to FCP,
- the axis x_k^0 completes the right-handed cartesian frame.

The complete joint transformation matrix can be obtained by the product of a preceding joint transformation matrix by a following joint transformation matrix.

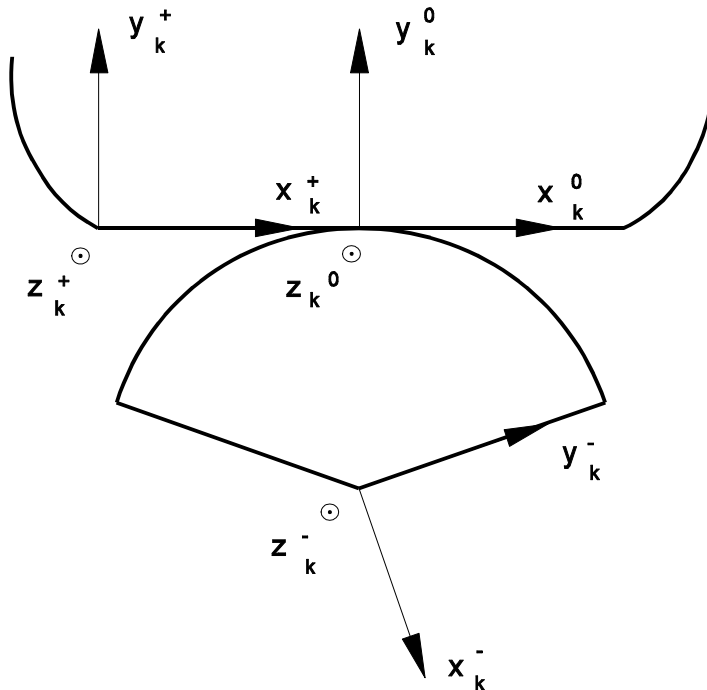


Fig. 2.4.3-1: Arc-line contact joint

Let's take for example the case of an arc-segment contact joint as shown in Fig. 2.4.3-1. The transformation matrix is comprised of two parts: an "arc" preceding transformation from the arc coordinate frame x_k^-, y_k^-, z_k^- to the common contact frame x_k^0, y_k^0, z_k^0 ; a "line" following transformation matrix from the common contact frame x_k^0, y_k^0, z_k^0 to the line coordinate frame x_k^+, y_k^+, z_k^+ .

The transformation matrix can be gotten by the product of the preceding $\varphi_p(q_{k1})$ by the following $\varphi_f(q_{k2})$ matrices:

$$\Phi(q_{k1}, q_{k2}) = \varphi_{kp}(q_{k1}) * \varphi_{kf}(q_{k2}) \quad (2.4.3-1)$$

As it was the case for articulated joints, the corresponding linear derivative operator of joint variables Q_{ji} is obtained by using Equ. (2.2.5-11):

$$\begin{aligned} Q_{k1} &= \frac{\partial \varphi_{kp}(q_{k1})}{\partial q_{k1}} \varphi_{kf}(q_{k2})(\varphi_{kp}(q_{k1})\varphi_{kf}(q_{k2}))^{-1} \\ &= \frac{\partial \varphi_{kp}(q_{k1})}{\partial q_{k1}} \varphi_{kp}^{-1}(q_{k1}) \end{aligned} \quad (2.4.3-2)$$

and

$$\begin{aligned} Q_{k2} &= \varphi_{kp}(q_{k1}) \frac{\partial \varphi_{kf}(q_{k2})}{\partial q_{k2}} (\varphi_{kp}(q_{k1})\varphi_{kf}(q_{k2}))^{-1} \\ &= \varphi_{kp}(q_{k1}) \frac{\partial \varphi_{kf}(q_{k2})}{\partial q_{k2}} \varphi_{kf}^{-1}(q_{k2}) \varphi_{kp}^{-1}(q_{k1}) \\ &= \varphi_{kp}(q_{k1}) Q'_{k2} \varphi_{kp}^{-1}(q_{k1}) \end{aligned} \quad (2.4.3-3)$$

where

$$Q'_{k2} = \frac{\partial \varphi_{kf}(q_{k2})}{\partial q_{k2}} \varphi_{kf}^{-1}(q_{k2}) \quad (2.4.3-4)$$

Both preceding and following joint transformation matrices have to be defined for each considered elements. The details of these matrices are described in appendix A. The case of an arc, a line and a polynomial element will be illustrated here.

-- Arc element

In this case, the joint variable has been defined by:

$$q_{k1} = (i_k - 1) + \frac{\theta_{k1}}{\beta_{k1}} \quad (2.4.3-5)$$

where i_k is the conventional integer associated to the order of the contact element.

When the arc element is used as a preceding contacting pair, the transformation from the arc coordinate frame x_k^-, y_k^-, z_k^- to the intermediate frame x_k^0, y_k^0, z_k^0 can be considered as a planar x-y rotation of angle θ_{k1} about the z_k axis, with the following matrix transformation:

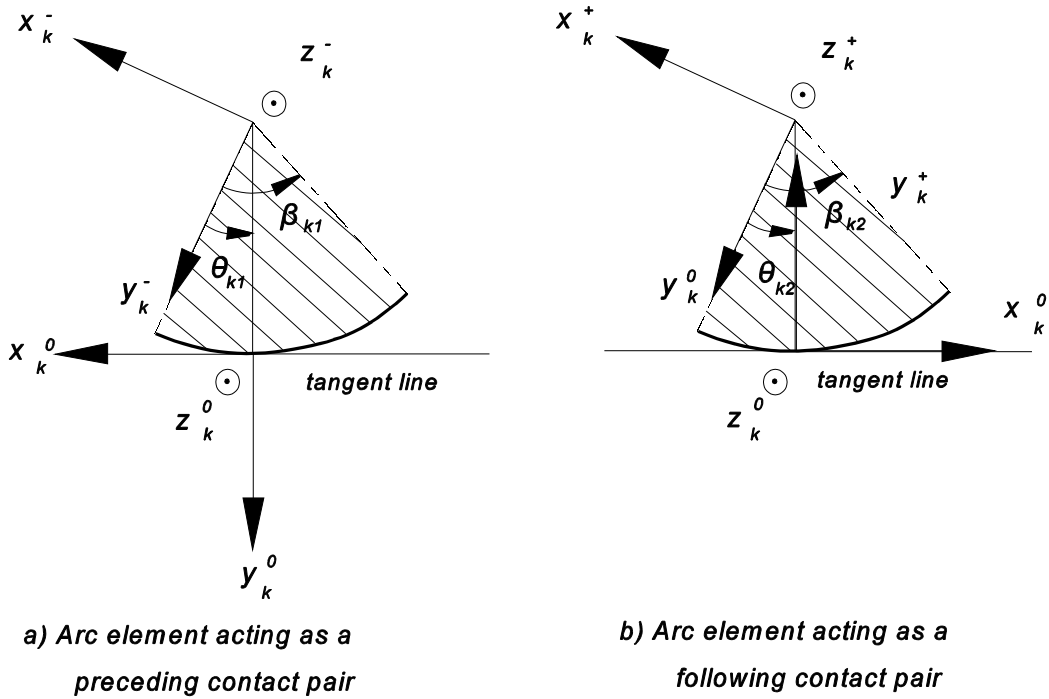


Fig. 2.4.3-2: Arc contacting element

$$(\varphi_k)_p = \begin{bmatrix} \cos\theta_{kl} & -\sin\theta_{kl} & 0 & -R_{kl}\sin\theta_{kl} \\ \sin\theta_{kl} & \cos\theta_{kl} & 0 & R_{kl}\cos\theta_{kl} \\ 0 & 0 & 1 & 0 \\ 0 & 0 & 0 & 1 \end{bmatrix} \quad (2.4.3-6)$$

where R_{kl} is the radius of the arc, θ_{kl} being related to the curvilinear coordinate q_{kl} by:

$$\theta_{kl} = (q_{kl} - i_{kl} + 1)\beta_{kl} \quad (2.4.3-7)$$

β_{kl} being the arc angle. The derivation of this transformation matrix yields:

$$\frac{\partial \varphi_{kp}}{\partial q_{kl}} = \frac{\partial \varphi_{kp}}{\partial \theta_{kl}} \beta_{kl} = \begin{bmatrix} -\sin\theta_{kl} & -\cos\theta_{kl} & 0 & -R_{kl}\cos\theta_{kl} \\ \cos\theta_{kl} & \sin\theta_{kl} & 0 & -R_{kl}\sin\theta_{kl} \\ 0 & 0 & 0 & 0 \\ 0 & 0 & 0 & 0 \end{bmatrix} \beta_{kl} \quad (2.4.3-8)$$

and its inversion:

$$\varphi_{kp}^{-1} = \begin{bmatrix} \cos\theta_{kl} & \sin\theta_{kl} & 0 & 0 \\ -\sin\theta_{kl} & \cos\theta_{kl} & 0 & -R_{kl} \\ 0 & 0 & 1 & 0 \\ 0 & 0 & 0 & 1 \end{bmatrix} \quad (2.4.3-9)$$

The corresponding derivative matrix is then expressed by:

$$Q_{kl} = \begin{bmatrix} 0 & -1 & 0 & 0 \\ 1 & 0 & 0 & 0 \\ 0 & 0 & 0 & 0 \\ 0 & 0 & 0 & 0 \end{bmatrix} \beta_{kl} \quad (2.4.3-10)$$

When an arc element acts as a following contacting pair, the transformation from the intermediate frame, x_k^0, y_k^0, z_k^0 to the arc coordinate frame, x_k^+, y_k^+, z_k^+ , can be considered as a planar x-y rotation of angle $180-\theta_{k2}$ about the z_k axis, with the following matrix transformation:

$$\varphi_{kf} = \begin{bmatrix} -\cos\theta_{k2} & -\sin\theta_{k2} & 0 & 0 \\ \sin\theta_{k2} & -\cos\theta_{k2} & 0 & R_{k2} \\ 0 & 0 & 1 & 0 \\ 0 & 0 & 0 & 1 \end{bmatrix} \quad (2.4.3-11)$$

where R_{k2} is the arc radius, and θ_{k2} is related to the curvilinear coordinate q_{k2} by:

$$\theta_{k2} = (q_{k2} - i_{k2} + 1)\beta_{k2} \quad (2.4.3-12)$$

The derivation of the transformation matrix gives:

$$\frac{\partial \varphi_{kf}}{\partial q_{k2}} = \frac{\partial \varphi_{kf}}{\partial \theta_{k2}} \beta_{k2} = \begin{bmatrix} \sin\theta_{k2} & -\cos\theta_{k2} & 0 & 0 \\ \cos\theta_{k2} & \sin\theta_{k2} & 0 & 0 \\ 0 & 0 & 0 & 0 \\ 0 & 0 & 0 & 0 \end{bmatrix} \beta_{k2} \quad (2.4.3-13)$$

and its inversion:

$$\varphi_{kf}^{-1} = \begin{bmatrix} -\cos\theta_{k2} & \sin\theta_{k2} & 0 & -R_{k2}\sin\theta_{k2} \\ -\sin\theta_{k2} & -\cos\theta_{k2} & 0 & R_{k2}\cos\theta_{k2} \\ 0 & 0 & 1 & 0 \\ 0 & 0 & 0 & 1 \end{bmatrix} \quad (2.4.3-14)$$

leading to the derivative matrix of the following contact pair Q'_{k2} :

$$Q'_{k2} = \frac{\partial \varphi_{kf}}{\partial q_{k2}} \varphi_{kf}^{-1} = \begin{bmatrix} 0 & 1 & 0 & 0 \\ -1 & 0 & 0 & 0 \\ 0 & 0 & 0 & 0 \\ 0 & 0 & 0 & 0 \end{bmatrix} \beta_{k2} \quad (2.4.3-15)$$

-- Line element

When a segment element acts as a preceding contacting pair (see Fig. 2.4.3-3a), the preceding joint transformation matrix from x_k^-, y_k^-, z_k^- to x_k^0, y_k^0, z_k^0 is given by:

$$\varphi_{kp} = \begin{bmatrix} -1 & 0 & 0 & s_{k1} \\ 0 & -1 & 0 & 0 \\ 0 & 0 & 1 & 0 \\ 0 & 0 & 0 & 1 \end{bmatrix} \quad (2.4.3-16)$$

where the joint variable s_{k1} is deduced from the relative curvilinear coordinate q_{k1} by:

$$s_{k1} = (q_{k1} - i_{k1})L_{k1} \quad (2.4.3-17)$$

L_{k1} being the length of the line element in the preceding pair.

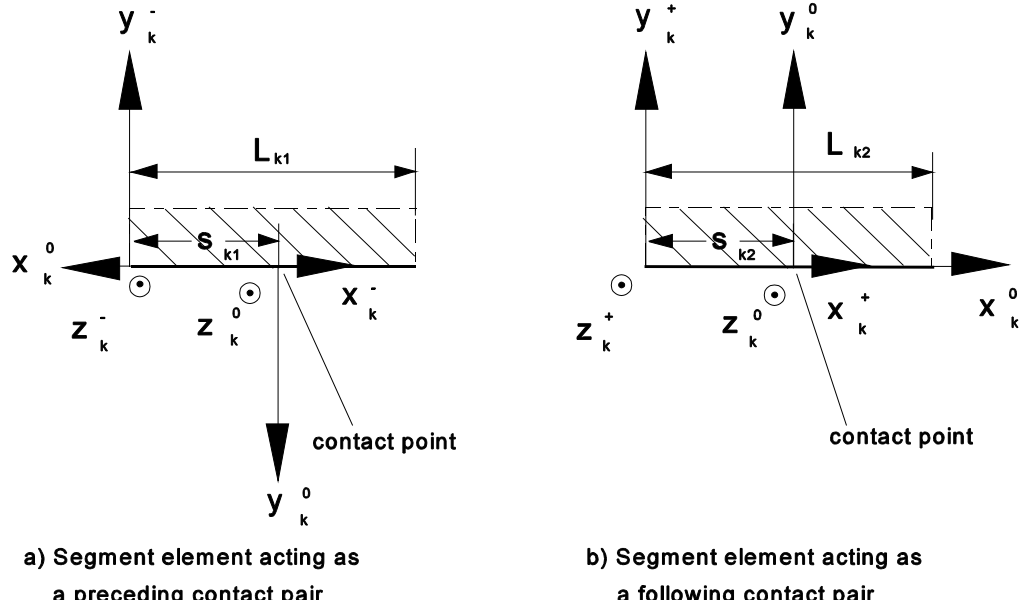


Fig. 2.4.3-3: Line contacting element

The differentiation of the transformation matrix gives:

$$\frac{\partial \varphi_{kp}}{\partial q_{kl}} = \frac{\partial \varphi_{kp}}{\partial s_{kl}} L_{kl} = \begin{bmatrix} 0 & 0 & 0 & 1 \\ 0 & 0 & 0 & 0 \\ 0 & 0 & 0 & 0 \\ 0 & 0 & 0 & 0 \end{bmatrix} L_{kl} \quad (2.4.3-18)$$

and its inversion:

$$\varphi_{kp}^{-1} = \begin{bmatrix} -1 & 0 & 0 & -s_{kl} \\ 0 & -1 & 0 & 0 \\ 0 & 0 & 1 & 0 \\ 0 & 0 & 0 & 1 \end{bmatrix} \quad (2.4.3-19)$$

The derivative matrix is then expressed by:

$$Q_{kl} = \begin{bmatrix} 0 & 0 & 0 & 1 \\ 0 & 0 & 0 & 0 \\ 0 & 0 & 0 & 0 \\ 0 & 0 & 0 & 0 \end{bmatrix} L_{kl} \quad (2.4.3-20)$$

When the segment element acts as a following contacting pair (see Fig. 2.5-7a), the transformation matrix from x_k^0, y_k^0, z_k^0 to x_k^+, y_k^+, z_k^+ is expressed by:

$$\varphi_{kf} = \begin{bmatrix} 1 & 0 & 0 & -s_{k2} \\ 0 & 1 & 0 & 0 \\ 0 & 0 & 1 & 0 \\ 0 & 0 & 0 & 1 \end{bmatrix} \quad (2.4.3-21)$$

where the joint variable s_{k2} is expressed from the relative curvilinear coordinate q_{j2} by:

$$s_{k2} = (q_{k2} - i_{k2} + 1)L_{k2} \quad (2.4.3-22)$$

The derivation of the transformation matrix yields:

$$\frac{\partial \varphi_{kf}}{\partial q_{k2}} = \frac{\partial \varphi_{kf}}{\partial s_{k2}} L_{k2} = \begin{bmatrix} 0 & 0 & 0 & 1 \\ 0 & 0 & 0 & 0 \\ 0 & 0 & 0 & 0 \\ 0 & 0 & 0 & 0 \end{bmatrix} L_{k2} \quad (2.4.3-23)$$

and its inversion:

$$\varphi_{k2}^{-1} = \begin{bmatrix} 1 & 0 & 0 & s_{k2} \\ 0 & 1 & 0 & 0 \\ 0 & 0 & 1 & 0 \\ 0 & 0 & 0 & 1 \end{bmatrix} \quad (2.4.3-24)$$

The derivative matrix in this case becomes:

$$Q_{k2} = \frac{\partial \varphi_{k2}}{\partial q_{k2}} \varphi_{k2}^{-1} = \begin{bmatrix} 0 & 0 & 0 & -1 \\ 0 & 0 & 0 & 0 \\ 0 & 0 & 0 & 0 \\ 0 & 0 & 0 & 0 \end{bmatrix} L_{k2} \quad (2.4.3-25)$$

-- Polynomial element

The form of a polynomial element is described in polar coordinates. It is expressed by taking as origin the conventional frame attached to the polynomial curve:

$$r(\theta) = C_0 + C_1 \theta + C_2 \theta^2 + \dots + C_n \theta^n \quad (2.4.3-26)$$

where, C's are constant coefficients.

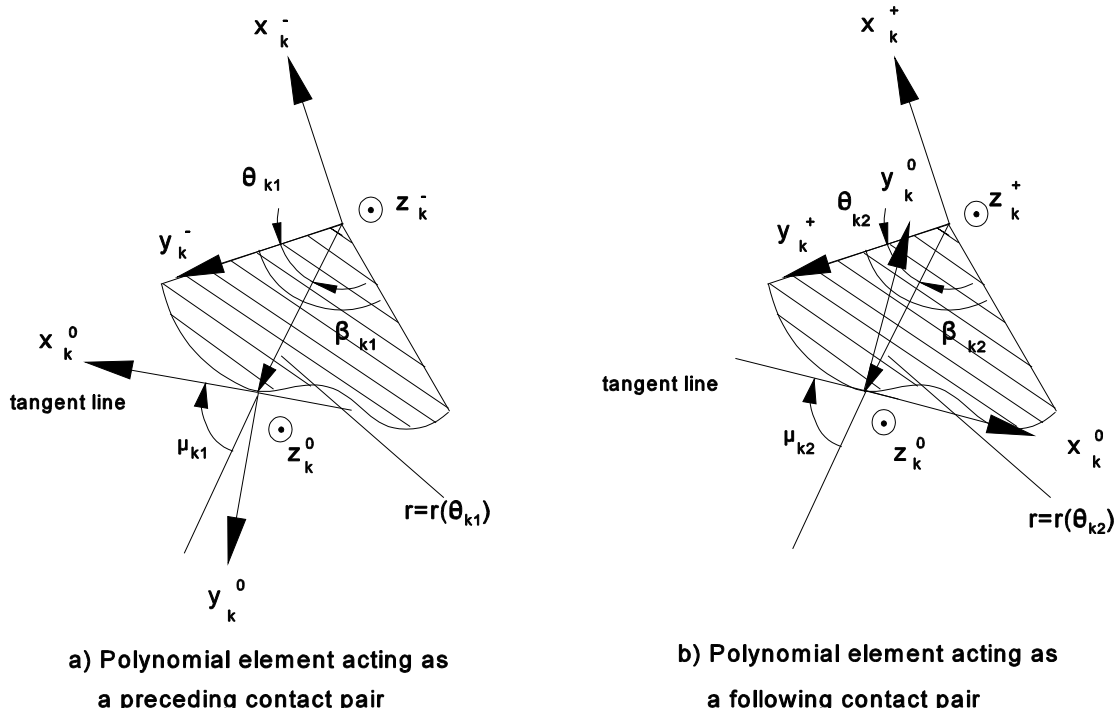


Fig. 2.4.3-4: Polynomial contacting element

The local coordinate frame of a polynomial element has been defined in section 2.3. In order to get the tangent direction, the equations are written in cartesian coordinates:

$$\begin{aligned} x &= -r(\theta)\sin\theta \\ y &= r(\theta)\cos\theta \end{aligned} \quad (2.4.3-27)$$

The differentiation of these equations gives:

$$\begin{aligned}x'_\theta &= -r'(\theta)\sin\theta - r(\theta)\cos\theta \\y'_\theta &= r'(\theta)\cos\theta - r(\theta)\sin\theta\end{aligned}\quad (2.4.3-28)$$

where

$$r'(\theta) = \sum_{i=0}^n iC_i\theta^{i-1} \quad (2.4.3-29)$$

The tangent angle at a point of the line is defined by:

$$\mu = \tan^{-1} \frac{y'}{x'} \quad (2.4.3-30)$$

When a polynomial element acts as a preceding element (see Fig.2.4.3-4a), the preceding transformation matrix is expressed by:

$$\Phi_{kp} = \begin{bmatrix} -\sin(\theta_{kl} - \mu_{kl}) & -\cos(\theta_{kl} - \mu_{kl}) & 0 & -r_{kl}(\theta_{kl})\sin\theta_{kl} \\ \cos(\theta_{kl} - \mu_{kl}) & -\sin(\theta_{kl} - \mu_{kl}) & 0 & r_{kl}(\theta_{kl})\cos\theta_{kl} \\ 0 & 0 & 1 & 0 \\ 0 & 0 & 0 & 1 \end{bmatrix} \quad (2.4.3-31)$$

where r_{kl} and μ_{kl} are functions of θ_{kl} which can be obtained by Equ. (2.4.3-26) and (2.4.3-30). The joint variable θ_{kl} is derived from the relative curvilinear coordinate q_{kl} by:

$$\theta_{kl} = (q_{kl} - i_{kl} + 1)\beta_{kl} \quad (2.4.3-32)$$

The differentiation of the transformation matrix gives:

$$\begin{aligned}\frac{\partial \Phi_{kp}}{\partial q_{kl}} &= \frac{\partial \Phi_{kp}}{\partial \theta_{kl}} \beta_{kl} \\&= \begin{bmatrix} -\cos(\theta_{kl} - \mu_{kl})(1 - \frac{\partial \mu_{kl}}{\partial \theta_{kl}}) & \sin(\theta_{kl} - \mu_{kl})(1 - \frac{\partial \mu_{kl}}{\partial \theta_{kl}}) & 0 & x'_{kl} \\ -\sin(\theta_{kl} - \mu_{kl})(1 - \frac{\partial \mu_{kl}}{\partial \theta_{kl}}) & -\cos(\theta_{kl} - \mu_{kl})(1 - \frac{\partial \mu_{kl}}{\partial \theta_{kl}}) & 0 & y'_{kl} \\ 0 & 0 & 0 & 0 \\ 0 & 0 & 0 & 0 \end{bmatrix} \beta_{kl} \quad (2.4.3-33)\end{aligned}$$

where x'_{kl}, y'_{kl} is obtained from Equ. (2.4.3-28):

$$\frac{\partial \mu_{kl}}{\partial \theta_{kl}} = (\cos \mu_{kl})^2 \frac{y''_{kl} x'_{kl} - y'_{kl} x''_{kl}}{x'^{k2}_{kl}} \quad (2.4.3-34)$$

The inversion of the transformation matrix is:

$$\varphi_{kl}^{-1} = \begin{bmatrix} -\sin(\theta_{kl} - \mu_{kl}) & \cos(\theta_{kl} - \mu_{kl}) & 0 & -r_{kl} \cos \mu_{kl} \\ -\cos(\theta_{kl} - \mu_{kl}) & -\sin(\theta_{kl} - \mu_{kl}) & 0 & -r_{kl} \sin \mu_{kl} \\ 0 & 0 & 1 & 0 \\ 0 & 0 & 0 & 1 \end{bmatrix} \quad (2.4.3-35)$$

leading to the derivative matrix of the preceding contact pair expressed by:

$$Q_{kl} = \frac{\partial \varphi_{kp}}{\partial q_{kl}} \varphi_{kl}^{-1}$$

$$= \begin{bmatrix} 0 & \left(1 - \frac{\partial \mu_{kl}}{\partial \theta_{kl}}\right) 0 & r_{kl} \left(1 - \frac{\partial \mu_{kl}}{\partial \theta_{kl}}\right) \cos \theta_{kl} + x'_{kl} \\ \left(1 - \frac{\partial \mu_{kl}}{\partial \theta_{kl}}\right) 0 & 0 & -r_{kl} \left(1 - \frac{\partial \mu_{kl}}{\partial \theta_{kl}}\right) \sin \theta_{kl} + y'_{kl} \beta_{kl} \\ 0 & 0 & 0 \\ 0 & 0 & 0 \end{bmatrix} \quad (2.4.3-36)$$

When a polynomial element acts as a following joint element (see Fig.2.4.3-4b), the transformation matrix is defined by:

$$(\varphi_k)_f = \begin{bmatrix} -\sin(\mu_{k2} + \theta_{k2}) & \cos(\mu_{k2} + \theta_{k2}) & 0 & -r_{k2} \sin \mu_{k2} \\ -\cos(\mu_{k2} + \theta_{k2}) & -\sin(\mu_{k2} + \theta_{k2}) & 0 & r_{k2} \cos \mu_{k2} \\ 0 & 0 & 1 & 0 \\ 0 & 0 & 0 & 1 \end{bmatrix} \quad (2.4.3-37)$$

where r_{k2} and μ_{k2} are the functions of θ_{k2} which can be obtained by Equ. (2.4.3-26) and (2.4.3-30). The joint variable θ_{k2} is deduced from the relative curvilinear coordinate q_{k2} by:

$$\theta_{k2} = (q_{k2} - i_{k2} + 1)\beta_{k2} \quad (2.4.3-38)$$

The derivation of the transformation matrix leads to:

$$\frac{\partial \varphi_{kf}}{\partial q_{k2}} = \frac{\partial \varphi_{kf}}{\partial \theta_{k2}} \beta_{k2}$$

$$= \begin{bmatrix} -\cos(\mu_{k2} + \theta_{k2})(1 + \frac{\partial \mu_{k2}}{\partial \theta_{k2}}) & -\sin(\mu_{k2} + \theta_{k2})(1 + \frac{\partial \mu_{k2}}{\partial \theta_{k2}}) & 0 & x'_{k2} \\ \sin(\mu_{k2} + \theta_{k2})(1 + \frac{\partial \mu_{k2}}{\partial \theta_{k2}}) & -\cos(\mu_{k2} + \theta_{k2})(1 + \frac{\partial \mu_{k2}}{\partial \theta_{k2}}) & 0 & y'_{k2} \\ 0 & 0 & 0 & 0 \\ 0 & 0 & 0 & 0 \end{bmatrix} \beta_{k2} \quad (2.4.3-39)$$

where x'_{k2}, y'_{k2} can be obtained from Equ. (2.4.3-28):

$$\frac{\partial \mu_{k2}}{\partial \theta_{k2}} = (\cos \mu_{k2})^2 \frac{y''_{k2} x'_{k2} - y'_{k2} x''_{k2}}{x'^2_{k2}} \quad (2.4.3-40)$$

The inversion of the transformation matrix is:

$$\varphi_{kf}^{-1} = \begin{bmatrix} -\sin(\mu_{k2} + \theta_{k2}) & \cos(\mu_{k2} + \theta_{k2}) & 0 & -r_{k2} \sin \theta_{k2} \\ \cos(\mu_{k2} + \theta_{k2}) & -\sin(\mu_{k2} + \theta_{k2}) & 0 & r_{k2} \cos \theta_{k2} \\ 0 & 0 & 1 & 0 \\ 0 & 0 & 0 & 1 \end{bmatrix} \quad (2.4.3-41)$$

The derivative matrix Q'_{k2} is then expressed by:

$$Q'_{k2} = \frac{\partial \varphi_{kf}}{\partial q_{k2}} \varphi_{kf}^{-1} = \begin{bmatrix} 0 & (1 + \frac{\partial \mu_{k2}}{\partial \theta_{k2}}) & 0 & r_{k2} \sin \mu_{k2} (1 + \frac{\partial \mu_{k2}}{\partial \theta_{k2}}) + x'_{k2} \\ (1 + \frac{\partial \mu_{k2}}{\partial \theta_{k2}}) & 0 & 0 & -r_{k2} \cos \mu_{k2} (1 + \frac{\partial \mu_{k2}}{\partial \theta_{k2}}) + y'_{k2} \\ 0 & 0 & 0 & 0 \\ 0 & 0 & 0 & 0 \end{bmatrix} \beta_{k2} \quad (2.4.3-42)$$

2.5 Detection strategy of changing contact joints

This section will develop the strategy used to detect the change of contact joints due to kinematic factors. When a kinematic simulation is performed, the discontinuities that can be detected only concern geometric properties, specially:

- 1) the transition between curve elements (points, lines, arcs and etc.), the active contact point going from a curve element to the next one,
- 2) the interference between bodies which in a kinematic simulation is assumed to lead to an active contact once interference occurs.

In a kinematic simulation, it is assumed that the normal force is strong enough to maintain the contact. This normal force will however be calculated and monitored in the dynamic simulation, which will be discoursed in Chapter 3.

As it has been described in section 2.2.3, the kinematic simulation of a constrained mechanical system requires the solving of a set of nonlinear constraint algebraic equations (Newton-Raphson method). For a mechanical system with a changing topology, the constraint equations can be discontinuous during motion. In practice, the following steps have to be followed:

- 1) detection of a discontinuity,
- 2) localization of the exact discontinuity point,
- 3) change of the constraint equations.

Mathematically, the concept of switching functions has been used to facilitate the detection of the discontinuities during motion.

2.5.1 Switching function for discontinuous problems

In order to localize the points of discontinuity during motion, a switching function associated to each discontinuity is used. It has the two following purposes:

- 1) state if a discontinuity has occurred in the last step of the numerical resolution procedure by testing the sign of the switching function,
- 2) localize the exact time when the discontinuity occurs: this time occurs when the switching function vanishes, or in practice becomes less than a given tolerance.

If t^* expresses the exact time of a discontinuity i , a switching function G_i can be set up:

$$G_i(t^*)=0 \quad (2.5.1-1)$$

In practice, after each step of the numerical calculating routine, it is tested if in the last calculating step $[t_n, t_{n+1}]$ one of the defined switching functions changes its sign. If a sign changes,

the procedure of localization of the switching point is started.

The localization of this switching point involves the solution of a one-dimensional root finding problem. The exact value of the root must be iteratively calculated by numerical methods due to the high nonlinearities of systems. Among the many numerical available methods, we have chosen a bisection method.

When the sign of a switching function changes in the last step Δt , the localization of the switching point is started. Using the interval's midpoint to replace a sup-limit or a sub-limit of a new interval which depends on the sign of the switching functions. After k iterations the bounds containing the root decreases down to $\Delta t / 2^k$.

If the switching function is less than a given tolerance ε , after k iterations:

$$|G_i(t^*)| < \varepsilon \quad (2.5.1-2)$$

the switching point is localized.

2.5.2 Transition between curve elements

The contacts considered in this thesis concern geometric curve elements such as points, line segments, circle arcs, circles and polynomials. During motion, the active contact point passes from a geometric element to an adjacent one (see Fig. 2.5.2-1). This transition induces a change of active curve element, which induces modifications to the constraint equations.

The switching function is directly calculated from the relative coordinates used to describe the state of a contact joint. If we take the example of a contact joint k between an arc and line elements (see Fig. 2.5.2-1a), the relative curvilinear coordinates q_{k1} and q_{k2} of the contact joint must match up the physical range of validity of the current contact model. If the contact is active between an arc (i_c, i_c+1) and a line segment (j_d, j_d+1), the current curvilinear coordinates have a physical sense between i_c and i_c+1 for the arc, and j_d and j_d+1 for the segment:

$$i_c < q_{k1} < i_c + 1 \quad (2.5.2-1)$$

$$j_d < q_{k2} < j_d + 1 \quad (2.5.2-2)$$

The constraint equations expressing the closure of the loop containing the contact joint k is expressed by:

$$A_{01} T_{11} \varphi_1(q_1) T_{12} T_{22} \varphi_2(q_2) T_{23} \dots T_{nI} A_{1,0} = I \quad (2.5.2-3)$$

which can be written as:

$$A_{0,k} T_{k,k} \varphi_k(q_k) T_{k,k+1} A_{k+1,0} = I \quad (2.5.2-4)$$

taking into account the definition of the interlink A_{ok} matrix (section 2.2). The matrix $\varphi_k(q_k)$ is

the transformation matrix corresponding to an "arc-line" contact joint:

$$\varphi_k(q_k) = \begin{bmatrix} \cos q_{k1} & -\sin q_{k1} & 0 & -q_{k2} \cos q_{k1} - R_{ic} \sin q_{k1} \\ \sin q_{k1} & \cos q_{k1} & 0 & -q_{k2} \sin q_{k1} + R_{ic} \cos q_{k1} \\ 0 & 0 & 1 & 0 \\ 0 & 0 & 0 & 1 \end{bmatrix} \quad (2.5.2-5)$$

During motion, when q_{k2} reaches the integer value j_d , the active contact will pass from a line element to a point element. The integer value of a relative curvilinear coordinate acts as a physical limit. If at a calculation step, a curvilinear coordinate reaches the upper integer value, it means that the contacting point comes outside the physical interval (Fig. 2.5.2-1b). When one of the conditions (Equations 2.5.2-1 and 2.5.2-2) is not satisfied, a constraint modification occurs. The last step of the numerical process is suppressed and the procedure to determine the transition point is started. In the case of Fig. 2.5.2-1b, a new "arc-point" contact is formed: the curvilinear coordinate q_{k1} becomes active between i_c and i_c+1 (arc), and q_{k2} between j_d-1 and j_d (point):

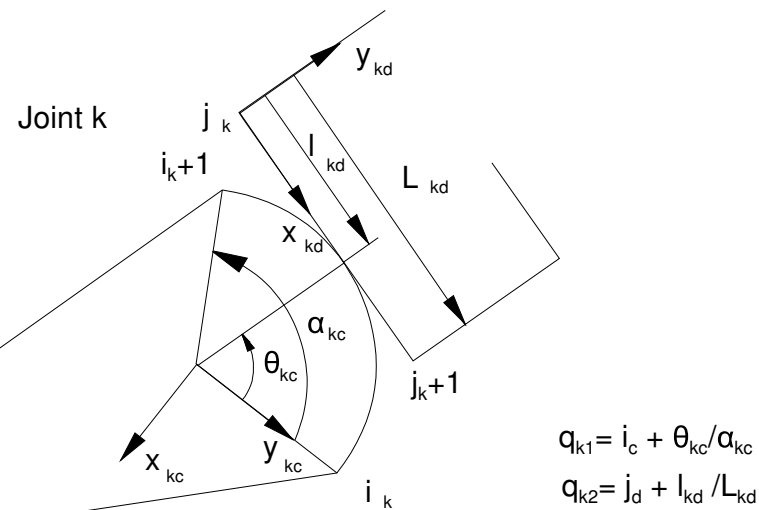
$$i_c < q_{k1} < i_c + 1 \quad (2.5.2-6)$$

$$j_d - 1 < q_{k2} < j_d \quad (2.5.2-7)$$

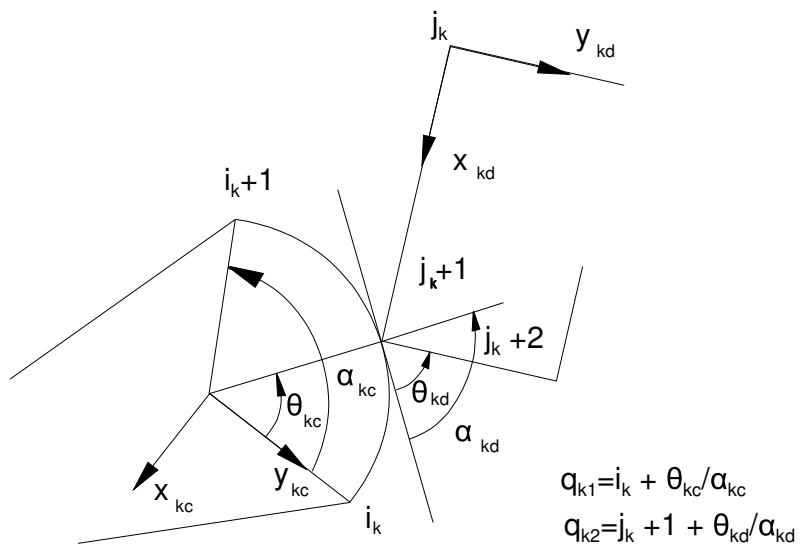
The $\varphi_k(q_k)$ in Equation (2.5.2-4) must then be changed into the transformation matrix corresponding to the "arc-point" contact:

$$\varphi_k(q_k) = \begin{bmatrix} \cos(q_{k1} - q_{k2}) & -\sin(q_{k1} - q_{k2}) & 0 & -R_{kl} \sin q_{k1} \\ \sin(q_{k1} - q_{k2}) & \cos(q_{k1} - q_{k2}) & 0 & R_{kl} \cos q_{k1} \\ 0 & 0 & 1 & 0 \\ 0 & 0 & 0 & 1 \end{bmatrix} \quad (2.5.2-8)$$

The discontinuous change of the contact joint matrix can be determined by monitoring the relative curvilinear coordinates. The following two switching functions G_{T1} &nd G_{T2} monitor the transitions between successive elements. They are defined for each curvilinear coordinate q_{kj} ($j=1,2$) of a contact joint:



a) "Arc-line" contact joint



b) "Arc-point" contact joint

Fig. 2.5.2-1: Transition between consecutive contact elements

$$G_{T1} = q_{kl} - i_c \quad (2.5.2-9)$$

$$G_{T2} = q_{kl} - (i_c + 1) \quad (2.5.2-10)$$

When a transition occurs, the contact model of the contact joint will change, resulting in a set of new constraint equations. If the Newton-Raphson process of the constraint equations is convergent, the contact joint is still active after passing through the transition.

If the Newton-Raphson procedure remains divergent with the new set of constraint equations, it can mean that the new transition is geometrically impossible, and that the contact joint cannot remain active. This is the only case where a kinematic simulation will lead to the deletion of an active constraint, the indicator of a geometrically impossible simulation being the fact that during motion, the Newton-Raphson procedure diverges.

Fig. 2.5.2-2 illustrates this case between link L6 (lower slide body) and link L2 (sear) of the trigger mechanism. During the starting firing phase, the contact point D between both bodies evolves up to point E. Due to particular form of the sear L2 and owing to the translational motion of the slider L6, after transition point, the contact can no longer be active, for it would cause a geometrically impossible configuration. The contact must therefore be deleted to continue the simulation.

In practice, the deletion of a constraint is made by transforming the 2 DOF- active joint to a 3 DOF- virtual joint, as it can be seen in the dynamic part, where the deletion of constraints will be decided from the determination of insufficient contact forces.

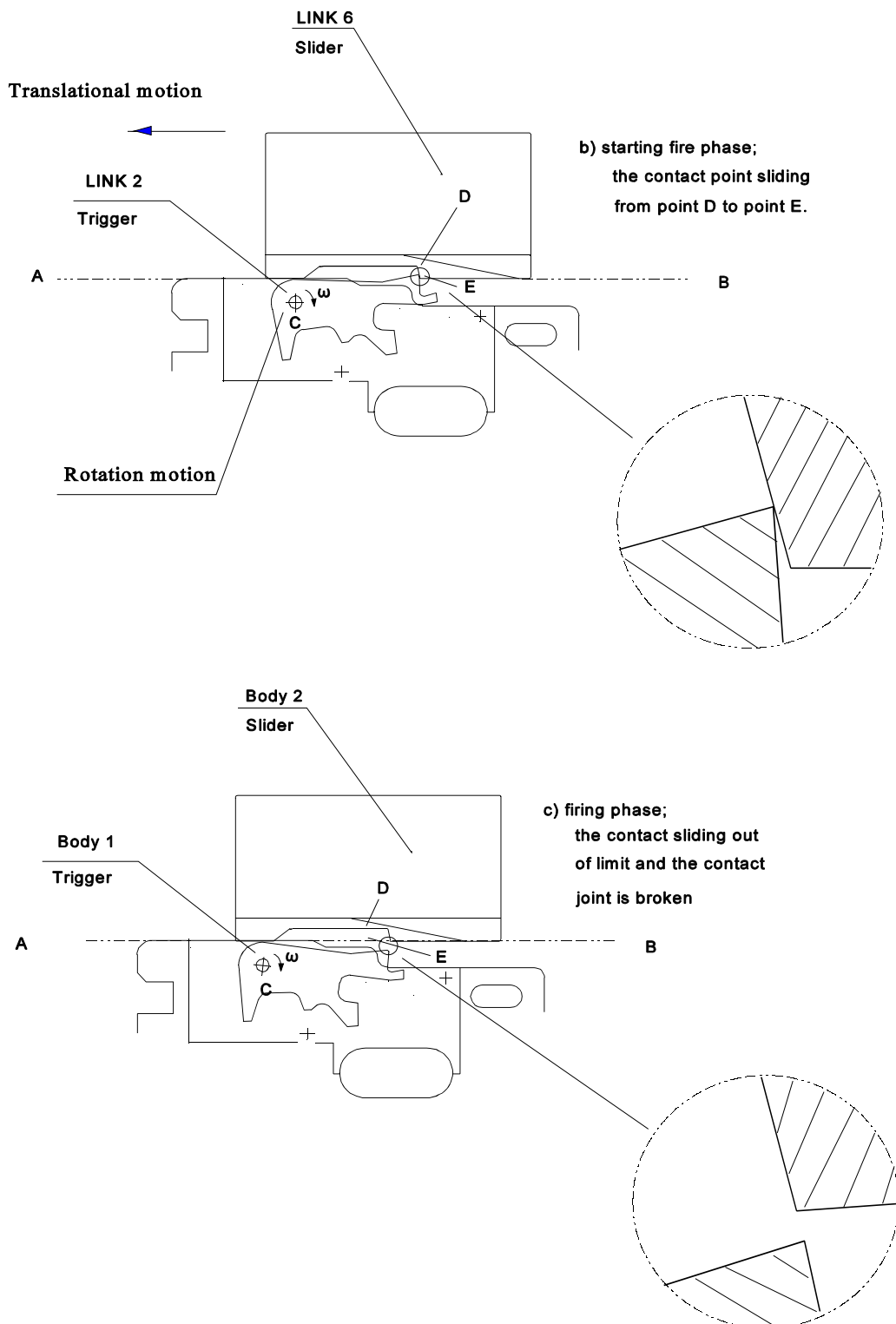


Fig. 2.5.2-3: Contact break due to transition between two contacting surfaces of the trigger mechanism

2.5.3 Addition of constraints due to interference

When an interference occurs between two bodies of a mechanical system, a new contact can be formed between them. In a kinematic simulation, we will consider that the contact is directly active once it happens. A strategy has to be used to determine when an interference takes place between bodies. This strategy is based on the determination of the minimal relative distance between the simple geometric elements which can each other interfere. When the distance between the two bodies vanishes and the relative velocity associated to the minimal distance is negative, an interference occurs.

In this dissertation, the concept of a "virtual" contact joint has been defined. When two bodies can interfere, a "virtual" contact joint is defined by describing the potential relation between the two curve elements which can interfere. Three relative coordinates are used to describe a virtual contact joint. In the case of an arc-segment virtual contact (Fig. 2.5.3-1), the three following variables are used.

$$\{\underline{q}_k\} = \begin{Bmatrix} q_{k1} \\ q_{k2} \\ q_{k3} \end{Bmatrix} = \begin{Bmatrix} i_c + \frac{l_{ic}}{L_{ic}} \\ j_d + \frac{\theta_{jd}}{\alpha_{jd}} \\ d_{min} \end{Bmatrix} \quad (2.5.3-1)$$

where q_{k3} is the minimal distance between the two geometric elements, measured on the common normal between both elements, q_{k1} and q_{k2} are the relative coordinates defined on both curve elements by locating the position of the intersection point with the common normal line.

When a virtual contact joint is defined, an extra constraint loop is formed leading to a constraint matrix equation:

$$A_{0k} T_{kk} \varphi'_k(\underline{q}_k) T_{k,k+1} A_{k+1,0} = I \quad (2.5.3-2)$$

where $\varphi'_k(\underline{q}_k)$ is the transformation matrix of the virtual contact joint.

The contact joints considered in this thesis being characterized by a planar motion, the equation (2.5.3-2) leads to three independent constraint equations. The addition of a virtual contact joint does however not change the number of degrees of freedom of the system.

During motion, the three dependent joint variables q_{k1}, q_{k2}, q_{k3} in the virtual contact joint are directly obtained. When the minimal distance q_{k3} equals zero and the velocity \dot{q}_{k3} associated to the minimal distance is negative, an interference is detected between two bodies:

$$q_{k3} = 0 \quad (2.5.3-3)$$

$$\dot{q}_{k3} < 0 \quad (2.5.3-4)$$

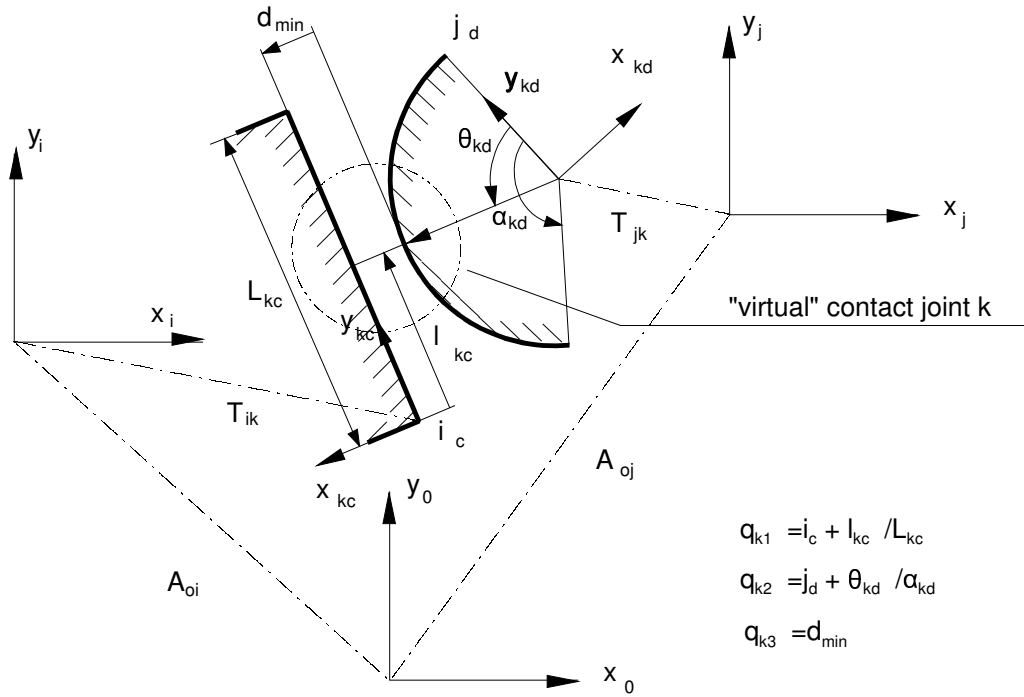


Fig. 2.5.3-1: Definition of a virtual contact joint

The minimal distance and the velocity associated to the minimal distance can be easily calculated by using the constraint matrix equation and velocity constraint matrix equations.

When a new contact joint is formed, the coordinates q_{k1}, q_{k2} become the relative coordinates involved in the new contact joint; the formation of a new contact induces therefore the change from a virtual contact to a real one.

The switching function G_{II} associated to the interference between two curve elements is defined by:

$$G_{I1}(t) = q_{k3}(t) = 0 \quad (2.5.3-5)$$

associated with

$$G_{I2}(t) = \dot{q}_{k3}(t) < 0$$

The switching point is located with precision by using a bisection method. When the sign of G_{II} changes, G_{I2} being positive, the virtual contact joint changes into a real contact joint and the corresponding transformation matrix (defined in Section 2.4) changes from $\varphi_p(q_{k1}) \varphi_D(q_{k3}) \varphi_f(q_{k2})$ to $\varphi_p(q_{k1}) \varphi_f(q_{k2})$ with

$$\varphi_D(q_{k3}) = \begin{vmatrix} 1 & 0 & 0 & 0 \\ 0 & 1 & 0 & q_{k3} \\ 0 & 0 & 1 & 0 \\ 0 & 0 & 0 & 1 \end{vmatrix}_{q_{k3}=0} = \mathcal{I} \quad (2.5.3-7)$$

The contact joint is changed from virtual into real contact, the relative variable q_{k3} being removed.

2.6 Illustrative example: kinematics of a crank-slider connected to a four-bar linkage mechanism

A mechanism with a changing contact joint is taken as a basic example to describe the application of the kinematic and dynamic simulation methods developed in this thesis. This mechanism is composed by two simple classical sub-mechanisms: a crank-slider mechanism and a four-bar linkage (see Fig. 2.6-1). The two mechanisms can interfere by means of a contact between links L4 and L5. In its initial position, the four-bar linkage is at rest. When the crank of the crank-slide mechanism, L2, rotates in a clockwise direction, the slider L4 interferes with link L5 of the four-bar linkage. The output motion of the mechanism will be described by the rotation angle β of link L7. A virtual contact joint is employed to describe the possible interference between the two parts of the mechanisms. When the contact is active, it means that links L5 and L6 are in contact through a joint described by 2 relative contact coordinates (see Fig. 2.6-2). When the contact is not active, it will induce to "virtual" contact with 3 relative coordinates.

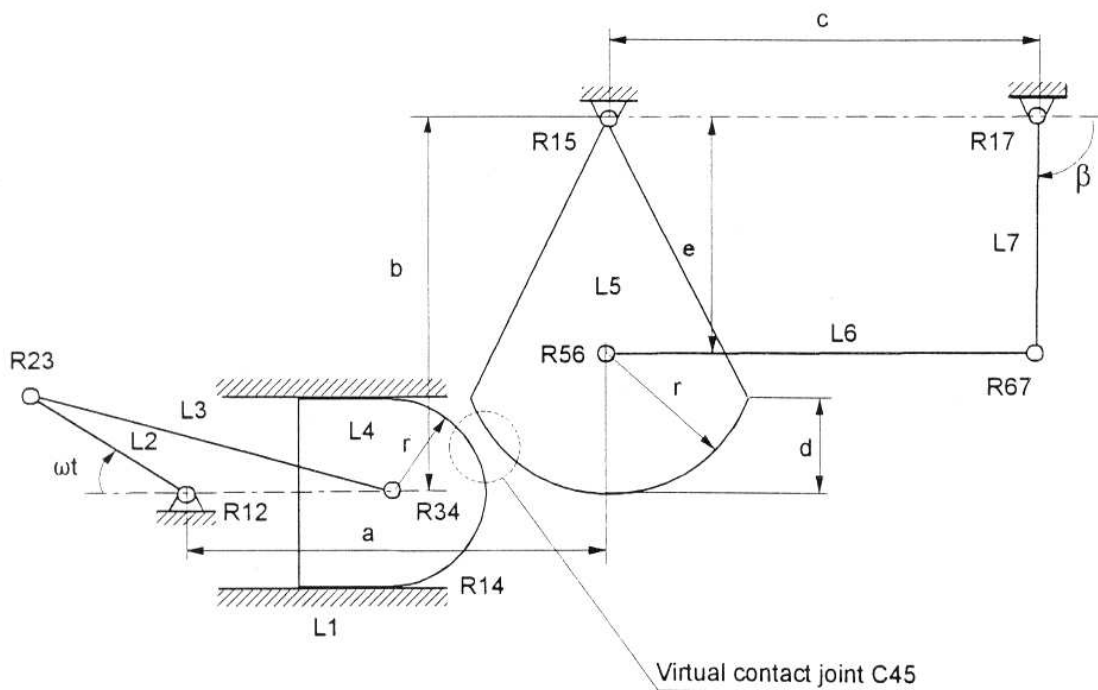


Fig. 2.6-1: Crank-slider connected to a four-bar linkage through a contact joint (in this initial position, the contact is not active)

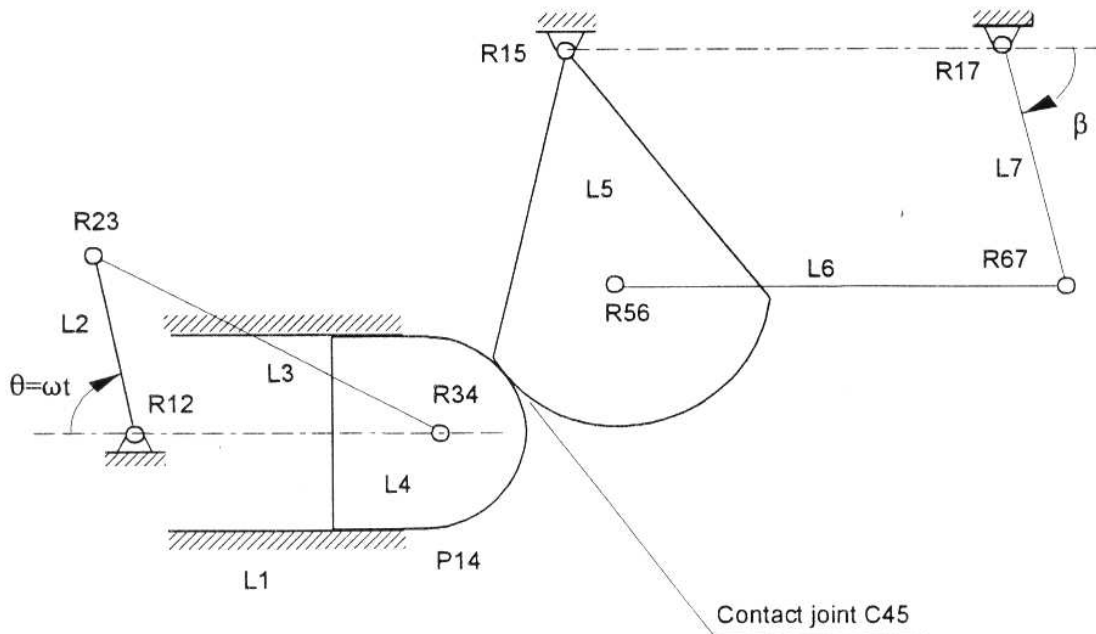


Fig. 2.6-2: Crank-slider connected to a four-bar linkage through a contact joint (the contact is active)

The geometrical dimensions of the mechanism are the following ones:

Dimensions of the links:

$$\begin{array}{lll} L_2 = 2 \text{ (m)}, & L_3 = 4 \text{ (m)}, & L_6 = 4 \text{ (m)}, \\ r_1 = 1 \text{ (m)}, & r_2 = 1.5 \text{ (m)}, & d = 1 \text{ (m)}, \\ & & L_7 = 2.5 \text{ (m)}, \\ & & e = 2.5 \text{ (m)}. \end{array}$$

Position of the fixed joint:

$$a = 4.5 \text{ (m)}, \quad b = 4 \text{ (m)}, \quad c = 4 \text{ (m)}.$$

If a kinematic simulation is performed, it is then assumed that the contact joint will remain active once interference happens. The changes of contact between the two simple mechanisms are detected by the two following switching functions:

- addition of a contact joint due to interference between two bodies, detected by the interference switching functions G_I ,
- transition of contact joints due to contact surface changing from one basic geometric element to another one, detected by the switching functions G_T .

The mechanism contains six moving links (L_2, L_3, \dots, L_7) and eight articulated joints ($R_{12}, R_{23}, R_{34}, P_{14}, R_{15}, R_{56}, R_{17}$).

If the contact between L4 and L5 is not active, there are two independent kinematical loops corresponding to the two simple basic mechanisms:

$$\begin{aligned} \text{Crank-slider mechanism: Loop 1, } & 1 - 2 - 4 - 4 - 1 \\ \text{Four-bar mechanism : Loop 2, } & 1 - 5 - 6 - 7 - 1 \end{aligned}$$

The two closed kinematic loops induce six constraint equations (for planar motion). If N_a expresses the total number of variables describing the articulated joints and N_{lo} the number of closed kinematic loops, the number of degrees of freedom DOF is:

$$DOF = N_a - 3 * N_{lo} = 2 \quad (4.5-1)$$

where $N_a = 8$, $N_{lo} = 2$.

In order to detect the possible interference between the two basic mechanisms, a virtual contact joint is added between L4 and L5 (see Fig. 4.5-1), forming a virtual kinematical loop:

$$\text{virtual closed kinematic loop: Loop 3, } 1 - 4 - 5 - 1$$

Fig. 2.6-3b illustrates the topology of the mechanism.

The addition of the virtual pair does not change the number of degrees of freedom: there are three independent kinematic loops in the mechanism. Because a virtual contact joint induces three variable parameters and one kinematic loop, if N_{cv} expresses the number of virtual contact joints, the number of degrees of freedom DOF remains unchanged:

$$\begin{aligned} DOF = N_a + 3 * N_{cv} - 3 * N_{lo} &= 2 \\ \text{where } N_a = 8, N_{cv} = 1 \text{ and } N_{lo} = 3. \end{aligned}$$

If the contact between links L4 and L5 is active, the number of loops remains unchanged but the number of degrees of freedom will change from 2 to 1. If N_{cr} expressed the number of real contact joints, the number of degrees of freedom DOF is in this case:

$$\begin{aligned} DOF = N_a + 2 * N_{cr} - 3 * N_{lo} &= 1 \\ \text{where } N_a = 8, N_{cr} = 1 \text{ and } N_{lo} = 3. \end{aligned}$$

The kinematic loops are automatically detected by the topology analysis method developed in Section 2.2. A tree structure whose root is the fixed link L1 is formed (see Fig. 2.6-3a). The links connected with L1 (L2, L4, L5, L7) are successively added to form the tree structure by considering the joint R12, P14, R15, R17. When we consider link L3, the R13 joint has to be included in the tree structure but the addition of the R34 joint would close a loop: R34 has thus to be considered as a chord. Joint R34 forms thus an independent loop 1-2-3-4-1. The same procedure is used to detect the two other chords C45 and R67 which form respectively the closed loop 1-4-5-1 and 1-5-6-7-1 (2.6-3b).

The kinematic simulation results corresponding to the output link L7 of the mechanism are shown in Fig. 2.6-4, the angular velocity ω of the crank L2 being constant ($\omega = 5 \text{ rad/sec}$).

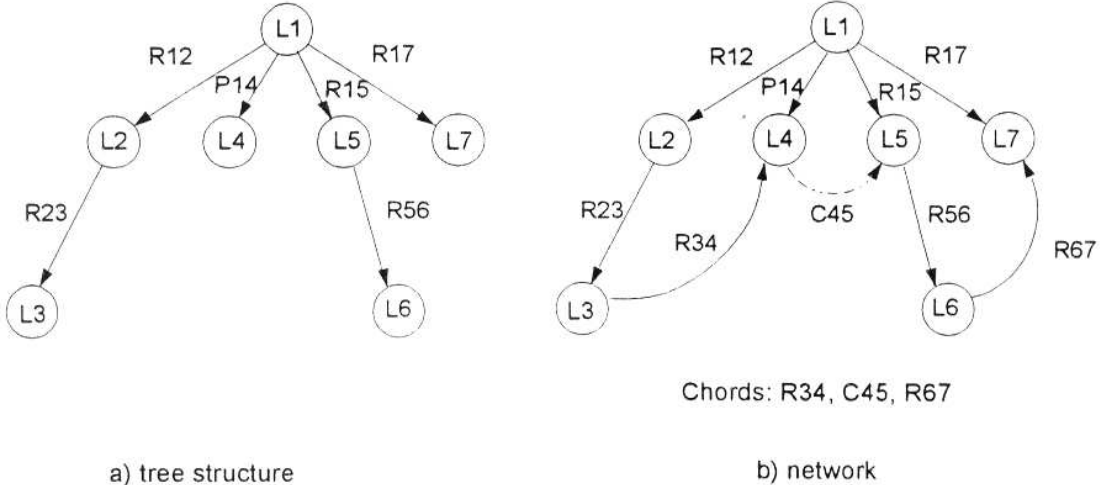


Fig. 2.6-3: Topology analysis of the mechanism of Fig. 2.6-1.

The different discontinuities occur at different time (t_1, t_2, \dots, t_5) and are uniquely caused by the changing contact joint between links L4 and L5. They are accurately determined by the set of switching functions, shown in Fig. 2.6-5. The interference switch G_{II} calculates the minimal distance between bodies 4 and 5: the variable q_{k3} associated to the virtual contact joint (which measures that minimal distance) vanishes at time t_1 when contact happens. In a kinematic simulation, the contact becomes active and the virtual contact joint is changed into a real one. Switches G_{T1} and G_{T2} concern the relative curvilinear coordinates of the contact joint, which pilot the changes from one basic geometric element to another one. In particular, when it passes through an integer value, the constraint equations of the kinematic simulation must be modified. The switch G_{T1} expresses the relative curvilinear coordinate of the contact joint C45 on link L4 varying from 0 to 1, and the switch G_{T2} , the relative curvilinear coordinate of the contact joint C45 on link 5, which varies from 0 to 3. At the time t_2 , the integer part of the switch G_{T2} changes from 2 to 1, which means the contacting surface changes from an "arc" element to a "point" element: the contact type changes from "arc-arc" to "point-arc". At time t_3, t_4 and t_5 , the same procedure is applied to detect the transition between consecutive curve elements. The different configurations of the system during motion are illustrated in the Fig. (2.6-6).

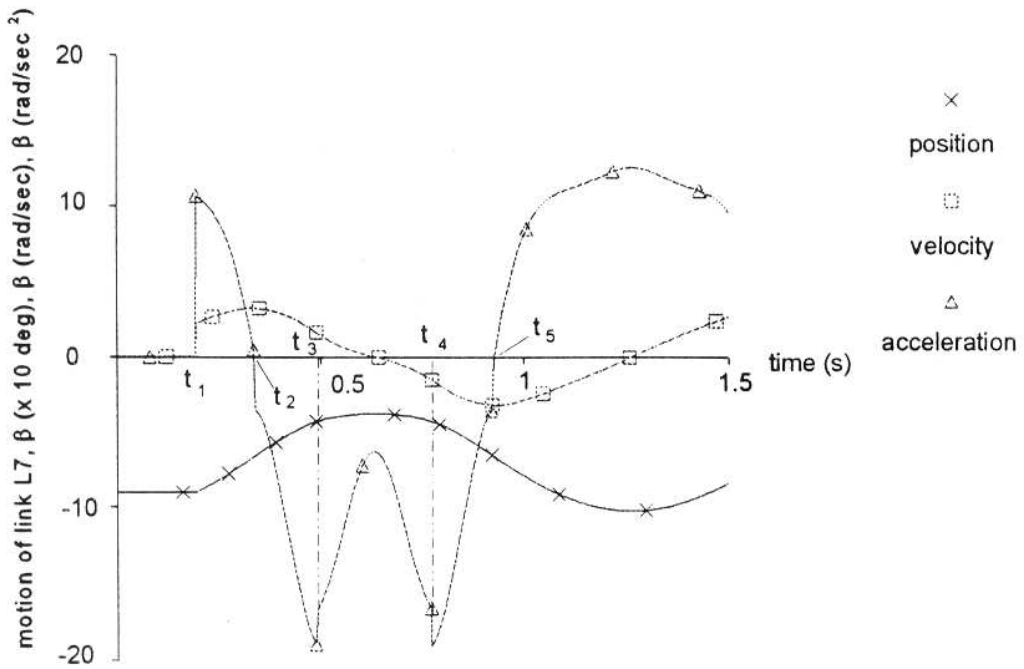


Fig. 2.6-4: Motion of link L7 : kinematic simulation with $\omega = 5 \text{ rad/sec}$ and $\theta = 0, \beta = 0$ (initial position)

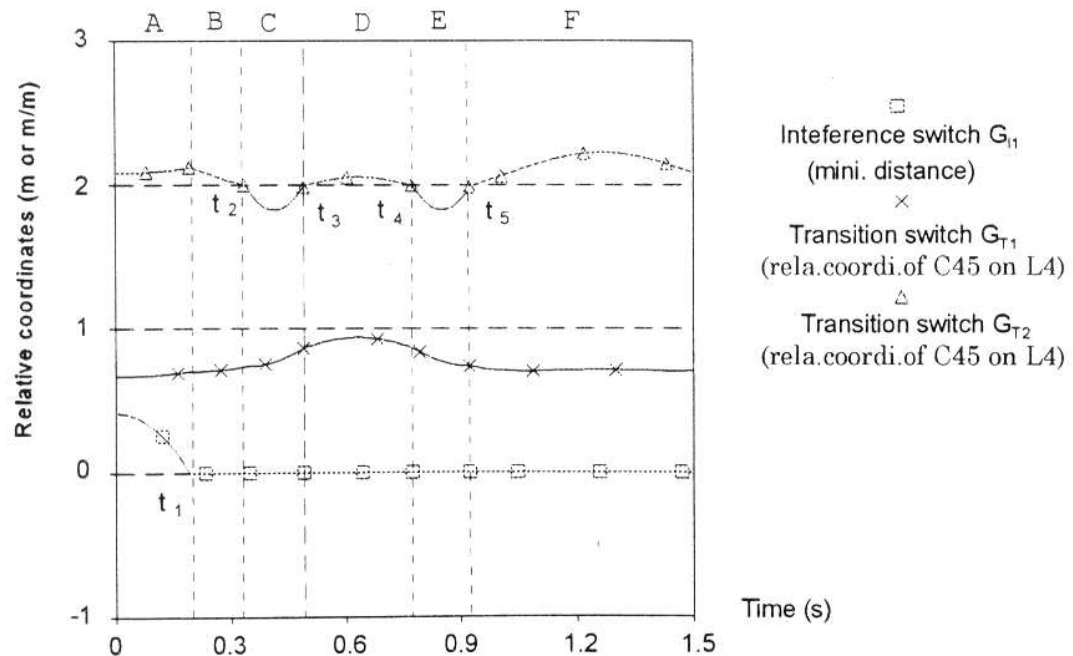


Fig. 2.6-5: Switching functions, piloting the changes of the contact joint

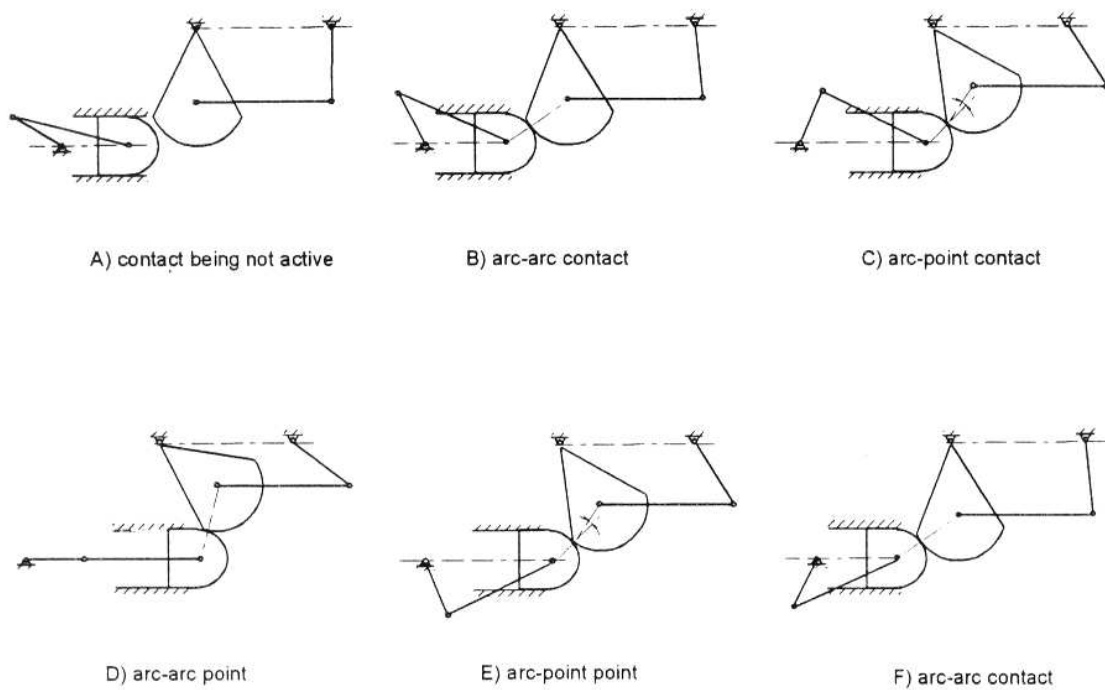


Fig. 2.6-6: Different configurations of the system during motion

CHAPTER 3 - DYNAMIC ANALYSIS

3.1 Introduction

As it has been seen in chapter 2, a kinematic analysis can only detect changes of contact joints due to geometric and kinematic factors, such as addition of constraints due to interferences between bodies, transition between curve elements or deletion of constraints due to a geometrically impossible configuration. A dynamic simulation is nevertheless required for mechanisms containing contact joints, in order to predict the deletion of constraints at a point of contact when the reaction force ceases to be compressive (see fig. 3.1-1).

This chapter will propose a systematic procedure to take into account the changes of contact joints in the motion equation.

1. First, the outline of the dynamic analysis is presented. The Hamilton's formalism is applied to develop the canonical motion equations. This formulation is suitable to solve impact problems because the dynamic equilibrium equations are expressed in terms of generalized position and momentum variables. A coordinate partitioning technique is used to determine a

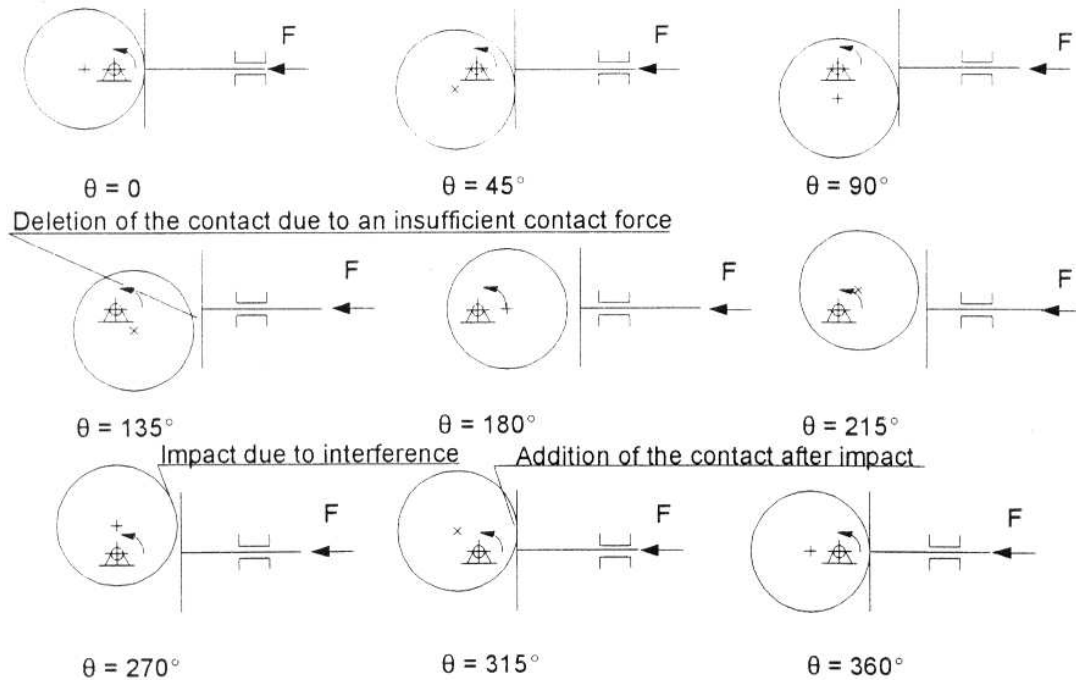


Fig. 3.1-1: Deletion of contact due to insufficient contact force and addition due to interference

set of independent coordinates and to develop a minimal set of motion equations, which are numerically integrated by means of a classical fourth order Runge-Kutta scheme.

2. Two basic aspects of the dynamic simulation of multibody systems with changing contact joints, i.e. contact force calculation and impact between bodies, will be emphasized. The computation of contact forces is required to determine whether an active contact will disappear during motion. The principle of virtual displacements is applied to evaluate the contact forces in active contact joints. Impact phenomena are also considered: they occur in mechanical systems with changing contact joints due to the interference between bodies (see Fig. 3.1-1). Two kinds of impact models could be used: a continuous impact model and a piecewise impact model. After comparing their respective advantages and disadvantages, the piecewise analysis method has been preferred in this thesis.

3. Strategies to detect the changes of contact joints during dynamic simulation are developed in addition to the preceding geometrical switching functions which are here equally applied.

3.2 Basic principles of a dynamic simulation using canonical equations

The canonical equations of motion are derived from the Hamiltonian function characteristic of a multibody system [40]. Although the expression of the canonical equations using the Hamiltonian is detailed in classical mechanics books [41], the fundamental equations are recalled hereafter for clarity.

The Lagrangian function L of a mechanical system is expressed by:

$$L(\dot{q}, \ddot{q}) = T(\dot{q}) - V(q) \quad (3.2-1)$$

where T and V denote respectively the kinetic and the potential energies of the system, \dot{q} is the vector of the N_g generalized coordinates, and \ddot{q} the vector of generalized velocities.

The generalized momentum p of an unconstrained mechanical system is defined by:

$$p = (L_{\dot{q}})^T = \left(\frac{\partial L}{\partial \dot{q}} \right)^T \quad (3.2-2)$$

where $L_{\dot{q}}$ is a conventional notation associated to a $(1 \times N_g)$ matrix whose components are the partial derivatives of L with respect to each component of the vector \dot{q} :

$$L_{\dot{q}} = \frac{\partial L}{\partial \dot{q}} = \left\{ \frac{\partial L}{\partial \dot{q}_1}, \frac{\partial L}{\partial \dot{q}_2}, \dots, \frac{\partial L}{\partial \dot{q}_{N_g}} \right\} \quad (3.2-3)$$

Expressed in a condensed form, it gives:

$$L_{\dot{q}} = \frac{\partial T}{\partial \dot{q}} \quad (3.2-4)$$

In the case of a constrained mechanical system, a new Lagrangian function L^* is introduced by taking into account the kinematic velocity constraint equations:

$$L^* = L - \underline{\lambda}^T \dot{\underline{\Phi}} \quad (3.2-5)$$

where $\underline{\lambda}$ is the $(N_c \times 1)$ vector of the Lagrangian multipliers associated with the momenta of the constraints, and $\dot{\underline{\Phi}}$ is the $(N_c \times 1)$ vector corresponding to the N_c velocity constraint equations, which can be expressed in the following form:

$$\dot{\underline{\Phi}} = \underline{\Phi}_{q_1} \dot{q}_1 + \underline{\Phi}_{q_2} \dot{q}_2 + \dots + \underline{\Phi}_{q_{N_g}} \dot{q}_{N_g} = 0 \quad (3.2-6)$$

or

$$\dot{\underline{\Phi}} = [C] \dot{q} = 0 \quad (3.2-7)$$

where

$$[C] = \{\Phi_{q_1}, \Phi_{q_2}, \dots, \Phi_{q_{N_g}}\}$$

$[C]$ being the Jacobian matrix.

The vector of momenta of a constrained mechanical system \underline{p} is defined as:

$$\underline{p} = (L_{\dot{q}})^T = (T_{\dot{q}} - \underline{\lambda}^T \dot{\Phi}_{\dot{q}})^T = (T_{\dot{q}} - \underline{\lambda}^T [C])^T \quad (3.2-8)$$

the differentiation of $\dot{\Phi}_{\dot{q}}$ with respect to the velocity giving the $[C]$ matrix.

The Hamiltonian function H associated with the Lagrangian L^* is expressed by:

$$H(q, \dot{q}, t) = -L^* + L_{\dot{q}}^* \dot{q} = -L^* + \underline{p}^T \dot{q} \quad (3.2-9)$$

The canonical equations are expressed as a set of $2N_g$ first-order differential equations in terms of the positions q and the momenta \underline{p} . They are derived from the Hamiltonian function H :

$$\dot{q} = H_{\underline{p}}^T \quad (3.2-10)$$

$$\dot{\underline{p}} = E_a - H_q^T \quad (3.2-11)$$

where E_a is the vector of the applied forces.

If the kinetic energy is expressed as a quadratic function of the velocities:

$$T = \frac{1}{2} \dot{q}^T [M] \dot{q} \quad (3.2-13)$$

the partial derivative of the kinetic energy equation with respect to \dot{q} is given by:

$$T_{\dot{q}} = ([M] \dot{q})^T \quad (3.2-14)$$

The first set of the canonical equations can be transformed by using Equ. (3.2-8), leading to:

$$\underline{p} = (([M] \dot{q})^T - \underline{\lambda}^T [C])^T = [M] \dot{q} - [C]^T \underline{\lambda}$$

and

$$\dot{q} = [M]^{-1} (\underline{p} + [C]^T \underline{\lambda})$$

The second set of the canonical equations can be transformed by using equations (3.2-7) and (3.2-8), giving:

$$\dot{\underline{p}} = E_a + (T_{\dot{q}} - V_{\dot{q}} - \underline{\lambda}^T \dot{\Phi}_{\dot{q}})^T \quad (3.2-12)$$

The gradient of the potential energy yields the vector of conservative forces E_c acting on the

system:

$$\underline{E}_c = -V_q^T \quad (3.2-15)$$

Upon substitution of equations (3.2-12) and (3.2-14) into the equations (3.2-11), one obtains:

$$\dot{q} = [M]^{-1}(\underline{p} + [\Phi_q]^T \underline{\lambda}) \quad (3.2-16)$$

$$\dot{p} = \underline{E}_a + \underline{E}_c + \frac{1}{2}(\underline{p}^T + \underline{\lambda}^T [\Phi_q]) [M]^{-1} \left(\frac{\partial [M]}{\partial q} \right)^T [M]^{-1} (\underline{p} + [\Phi_q]^T \underline{\lambda}) - [\dot{\Phi}_q]^T \underline{\lambda} \quad (3.2.17)$$

According to the nature of the coordinates used to describe the configuration of the mechanical system, the motion equations are formulated as listed below:

-- with cartesian (or absolute) coordinates:

$$\dot{q} = [M]^{-1}(\underline{p} + [\Phi_q]^T \underline{\lambda}) \quad (3.2-19)$$

$$\dot{p} = \underline{E}_a + \underline{E}_c - [\dot{\Phi}_q]^T \underline{\lambda} \quad (3.2-20)$$

where $[M]$ is a $N_{ca} \times N_{ca}$ constant mass matrix (For planar systems, $N_{ca} = 3 \times$ number of moving bodies; for spatial systems, $N_{ca} = 6 \times$ number of moving bodies).

-- with relative coordinates:

$$\dot{q} = [M]^{-1}(\underline{p} + [\Phi_q]^T \underline{\lambda}) \quad (3.2-21)$$

$$\dot{p} = \underline{E}_a + \underline{E}_c + \frac{1}{2}(\underline{p}^T + \underline{\lambda}^T [\Phi_q]) [M]^{-1} \left(\frac{\partial [M]}{\partial q} \right)^T [M]^{-1} (\underline{p} + [\Phi_q]^T \underline{\lambda}) - [\dot{\Phi}_q]^T \underline{\lambda} \quad (3.2-22)$$

where $[M]$ is a $m \times m$ position-dependent varying mass matrix ($m =$ number of joint variables).

-- with independent generalized coordinates:

$$\dot{q} = [M]^{-1} \underline{p} \quad (3.2-23)$$

$$\dot{p} = \underline{E}_a + \underline{E}_c + \frac{1}{2} \underline{p}^T [M]^{-1} \left(\frac{\partial [M]}{\partial q} \right)^T [M]^{-1} \underline{p} \quad (3.2.24)$$

where $[M]$ is a DOF \times DOF position-dependent varying mass matrix (DOF = number of generalized coordinates).

As shown in chapter 2, relative coordinates can express conveniently the kinematic properties of mechanical systems with changing contact joints. Nevertheless, in dynamic analysis, the expression and the differentiation of the mass matrix with respect to each relative coordinate is time-consuming. Moreover, the integration of the algebraic differential systems

consecutive to the use of relative coordinates can cause some difficulties, which could be overcome by using an independent set of generalized coordinates.

3.3. Setting of the motion equations using independent coordinates

3.3.1 Choice of a set of independent coordinates

The relationship between relative coordinates \dot{q}' (defined in section 2.2.3) and independent coordinates f is expressed by a linear influence coefficient matrix $[K]$ that we recall here:

$$\dot{q}' = [K]f \quad (3.3.1-1)$$

where:

$$[K] = \begin{Bmatrix} -[C_{11}]^{-1}[C_{12}] \\ [I] \end{Bmatrix} \quad (3.3.1-2)$$

The elements k_{ji} of $[K]$ are the influence coefficients, which depend on the choice of the independent coordinates.

If m is the number of relative coordinates and N_r is the rank of the parameter matrix of velocity constraint equations (Equ. 2.2.4-38), any $m-N_r$ relative coordinates can be selected as independent coordinates f , the rest of the relative coordinates being the dependent variables d . The velocity constraint equations can be rewritten as:

$$\begin{Bmatrix} C_{11} & C_{12} \\ C_{21} & C_{22} \end{Bmatrix} \begin{Bmatrix} \dot{d} \\ \dot{f} \end{Bmatrix} = \{0\} \quad (3.3.1-3)$$

The set of independent variables can be chosen arbitrarily. Nevertheless, a particular attention should be paid during the selection process in order to guarantee a good numerical conditioning of the constraint equations and avoid singular positions appearing during the simulation procedure.

Different methods have been proposed in order to select the set of independent coordinates such as Gaussian elimination technique with total pivoting [45], Singular Value Decomposition (SVD) [46] and QR Decomposition of the jacobian matrix of the constraints [47]. These methods exhibit different efficiency and stability properties (Reference [48] details the comparison). In the dissertation, the Gaussian elimination technique with total pivoting has been used to determine a decomposition of relative coordinates into dependent d and independent parameters f . A $(N_r \times N_r)$ nonsingular sub-matrix $[C_{11}]$ is automatically determined by this technique.

The choice of a Gaussian elimination technique with total pivoting presents the advantage to perform an adequate automatic choice of the independent variables, the selection being based on the nonzero pivot elements.

3.3.2 Motion equations using canonical formulation and independent coordinates

If f denotes the independent variables, the Hamiltonian function is simplified as:

$$H(f, p, t) = T(f, p) + V(f) \quad (3.3.2-1)$$

where p is the vector of the generalized momenta, which is defined by:

$$p = [M]f \quad (3.3.2-2)$$

The kinetic energy is classically expressed as a quadratic function of the velocities:

$$T = \frac{1}{2} \dot{f}^T [M] \dot{f} = \frac{1}{2} p^T [M]^{-1} p \quad (3.3.2-3)$$

where $[M]$ is the generalized mass matrix, which will be derived in the following paragraphs.

If a particle P of mass "dm" is considered on link k , its kinetic energy is expressed by:

$$dT_P = \frac{1}{2} (\dot{x}_P^2 + \dot{y}_P^2 + \dot{z}_P^2) dm \quad (3.3.2-4)$$

which can also be written:

$$dT_P = \frac{1}{2} \text{Tr}[\dot{\underline{R}}_P \dot{\underline{R}}_P^T] dm \quad (3.3.2-5)$$

where "Tr" indicates the trace of a square matrix, \underline{R}_P being the absolute position of the particle.

From Equations (2.2.4-20) and (2.2.4-43), the velocity of the point P on link k is given:

$$\begin{aligned} \frac{d\underline{R}_P}{dt} &= \sum_{a=1}^m \Lambda_{ka} \dot{q}_a' A_{ok} \underline{r}_k^P \\ &= \sum_{i=1}^{DOF} \sum_{a=1}^m \Lambda_{ka} K_{ai} \dot{f}_i A_{ok} \underline{r}_k^P \\ &= \sum_{i=1}^{DOF} \omega_{ki} A_{ok} \underline{r}_k^P \dot{f}_i \end{aligned} \quad (3.3.2-6)$$

where the elements ω_{ki} are the generalized velocity parameters given by:

$$\omega_{ki} = \sum_{a=1}^m \Lambda_{ka} k_{ai} \quad (3.3.2-7)$$

Submitting Equation (3.3.2-6) into Equation (3.3.2-5), the kinetic energy of mass "dm" can be written as:

$$\begin{aligned}
dT_P &= \frac{1}{2} \operatorname{Tr} \left[\sum_{i=1}^{DOF} \dot{f}_i \omega_{ki} A_{0k} \underline{r}_k^P \sum_{j=1}^{DOF} \underline{r}_k^{P^T} A_{0k}^T \omega_{kj}^T \dot{f}_j \right] dm \\
&= \frac{1}{2} \sum_{i=1}^{DOF} \sum_{j=1}^{DOF} \operatorname{Tr} [\omega_{ki} A_{0k} \underline{r}_k^P \underline{r}_k^{P^T} A_{0k}^T \omega_{kj}^T] \dot{f}_i \dot{f}_j dm \quad (3.3.2-8)
\end{aligned}$$

Let's notice that for the given link k , the ω_{ki} and A_{0k} matrices can be numerically evaluated once the instantaneous motion state of the independent constraint variables is known. These matrices are the same for all the particles on link k . Therefore, the total kinetic energy of link k can be found by integrating Equ. (3.3.2-8) over the entirety of the link k :

$$T_k = \frac{1}{2} \sum_{i=1}^{DOF} \sum_{j=1}^{DOF} \operatorname{Tr} [\omega_{ki} A_{0k} \left(\int_{link k} \underline{r}_k^P \underline{r}_k^{P^T} dm \right) A_{0k}^T \omega_{kj}^T] \dot{f}_i \dot{f}_j \quad (3.3.2-9)$$

Similarly, the inertial properties are introduced by means of a (4×4) inertia matrix:

$$J_k = \int_{link k} \underline{r}_k^P \underline{r}_k^{P^T} dm = \begin{bmatrix} \int x^2 dm & \int xy dm & \int xz dm & \int xd dm \\ \int xy dm & \int y^2 dm & \int yz dm & \int yd dm \\ \int xz dm & \int yz dm & \int z^2 dm & \int zd dm \\ \int xd dm & \int yd dm & \int zd dm & \int dm \end{bmatrix}_{link k} \quad (3.3.2-10)$$

Using the mass m_k , the coordinates of the centre of mass, $\bar{x}_k, \bar{y}_k, \bar{z}_k$ and the central inertia moments I_{xx}, I_{yy}, I_{zz} and the central inertia product I_{xy}, I_{xz}, I_{yz} , the (4×4) inertia matrix J_k can be expressed as:

$$J_k = \begin{bmatrix} \frac{1}{2}(-I_{xx} + I_{yy} + I_{zz}) & I_{xy} & I_{xz} & m_k \bar{x}_k \\ I_{xy} & \frac{1}{2}(I_{xx} - I_{yy} + I_{zz}) & I_{yz} & m_k \bar{y}_k \\ I_{xz} & I_{yz} & \frac{1}{2}(I_{xx} + I_{yy} - I_{zz}) & m_k \bar{z}_k \\ m_k \bar{x}_k & m_k \bar{y}_k & m_k \bar{z}_k & m_k \end{bmatrix} \quad (3.3.2-14)$$

Using equation (3.3.2-12), the kinetic energy of link k is expressed by:

$$T_k = \frac{1}{2} \sum_{i=1}^{DOF} \sum_{j=1}^{DOF} \operatorname{Tr} [\omega_{ki} A_{0k} J_k A_{0k}^T \omega_{kj}^T] \dot{f}_i \dot{f}_j \quad (3.3.2-15)$$

The total kinematic energy content of a constrained mechanical system with L links is given by:

$$T = \frac{1}{2} \sum_{k=1}^{N_u} \sum_{i=1}^{DOF} \sum_{j=1}^{DOF} Tr[\omega_{ki} A_{ok} J_k A_{ok}^T \omega_{kj}^T] \dot{f}_i \dot{f}_j \quad (3.3.2-16)$$

which can be expressed as a quadratic form:

$$T = \frac{1}{2} \dot{f}^T [M] f \quad (3.3.2-17)$$

where \dot{f} denotes the DOF x 1 vector of the independent generalized velocities. $[M]$ is the DOF x DOF symmetric mass matrix, whose elements m_{ij} are functions of the geometry of the mechanical system by:

$$m_{ij} = \sum_{k=1}^{N_u} Tr[\omega_{ki} A_{ok} J_k A_{ok}^T \omega_{kj}^T] \quad (3.3.2-18)$$

This generalized mass matrix is used into the canonical motion equations that we recall here (3.2-23) and (3.2-24):

$$\dot{f} = [M]^{-1} p \quad (3.3.2-19)$$

$$\dot{p} = F_a + F_c + \frac{1}{2} p^T ([M]^{-1} (\frac{\partial [M]}{\partial f})^T [M]^{-1}) p \quad (3.3.2-20)$$

The differentiation of the mass matrix with respect to the generalized coordinates f can be computed from the general term:

$$\begin{aligned} \frac{\partial m_{ji}}{\partial f_a} &= \sum_{k=1}^{N_u} Tr[(\gamma_{kia} + \omega_{ki} \omega_{ka}) A_{ok} J_k A_{ok}^T \omega_{kj}^T] \\ &+ \sum_{k=1}^{N_u} Tr[\omega_{ki} A_{ok} J_k A_{ok}^T (\omega_{ka}^T \omega_{kj}^T + \gamma_{kja}^T)] \end{aligned} \quad (3.3.2-21)$$

where

$$\gamma_{kia} = \frac{\partial \omega_{ki}}{\partial f_a} \quad (3.3.2-22)$$

which is derived in Appendix B.

3.4 Numerical Integration

The numerical simulation of the dynamics of a mechanical system requires an integration method to solve the motion equations. In the dissertation, a classical Fourth Order Runge-Kutta numerical method is employed.

This integration scheme is an explicit one that consists of four different stages in which the derivatives have to be evaluated. From the canonical equations (3.2.1-35) and (3.2.1-40), the motion equations can be written as:

$$\dot{f} = [M(f)]^{-1} p \quad (3.4-1)$$

$$\dot{p} = E_a(t, f) + E_c(f) + \frac{1}{2} p^T ([M(f)]^{-1} [\frac{\partial M(f)}{\partial f}]^T [M(f)]^{-1}) p \quad (3.4-2)$$

Using this Runge-Kutta method with a step size h , the solution at step $s+1$, f_{s+1} , p_{s+1} can be calculated from the known values at step s , f_s , p_s :

$$f_{s+1} = f_s + \frac{1}{6} (\underline{c}_1 + 2\underline{c}_2 + 2\underline{c}_3 + \underline{c}_4) \quad (3.4-3)$$

$$p_{s+1} = p_s + \frac{1}{6} (\underline{d}_1 + 2\underline{d}_2 + 2\underline{d}_3 + \underline{d}_4) \quad (3.4-4)$$

where,

$$\underline{c}_1 = h [M(f_s)]^{-1} p_s \quad (3.4-5)$$

$$\underline{d}_1 = h (E_a(t, f_s) + E_c(f_s) + \frac{1}{2} p_s^T ([M(f_s)]^{-1} [\frac{\partial M(f_s)}{\partial f}]^T [M(f_s)]^{-1}) p_s) \quad (3.4-6)$$

$$\underline{c}_2 = h [M(f_s + \frac{1}{2} \underline{c}_1)]^{-1} (p_s + \frac{1}{2} \underline{d}_1) \quad (3.4-7)$$

$$\begin{aligned} \underline{d}_2 &= h (E_a(t_s + \frac{1}{2} h, f_s + \frac{1}{2} \underline{c}_1) + E_c(f_s + \frac{1}{2} \underline{c}_1) + \frac{1}{2} (p_s + \frac{1}{2} \underline{d}_1)^T ([M(f_s + \frac{1}{2} \underline{c}_1)]^{-1} \\ &\quad [\frac{\partial M(f_s + \frac{1}{2} \underline{c}_1)}{\partial f}]^T [M(f_s + \frac{1}{2} \underline{c}_1)]^{-1}) (p_s + \frac{1}{2} \underline{d}_1)) \end{aligned} \quad (3.4-8)$$

$$\underline{c}_3 = h [M(f_s + \frac{1}{2} \underline{c}_2)]^{-1} (p_s + \frac{1}{2} \underline{d}_2) \quad (3.4-9)$$

$$\begin{aligned} \underline{d}_3 &= h(E_c(t_s + \frac{1}{2}h, f_s + \frac{1}{2}\underline{c}_2) + E_c(f_s + \frac{1}{2}\underline{c}_2) + \frac{1}{2}(p_s + \frac{1}{2}\underline{d}_2)^T([M(f_s + \frac{1}{2}\underline{c}_2)]^{-1} \\ &\quad [\frac{\partial M(f_s + \frac{1}{2}\underline{c}_2)}{\partial f}]^T[M(f_s + \frac{1}{2}\underline{c}_2)]^{-1})(p_s + \frac{1}{2}\underline{d}_2)) \end{aligned} \quad (3.4-10)$$

$$\underline{c}_4 = h[M(f_s + \underline{c}_3)]^{-1}(p_s + \underline{d}_3) \quad (3.4-11)$$

$$\begin{aligned} d_4 &= h(E_a(t_s + h, f_s + \underline{c}_3) + E_c(f_s + \underline{c}_3) + \frac{1}{2}(p_s + \underline{d}_3)^T([M(f_s + \underline{c}_3)]^{-1} \\ &\quad [\frac{\partial M(f_s + \underline{c}_3)}{\partial f}]^T[M(f_s + \underline{c}_3)]^{-1})(p_s + \underline{d}_3)) \end{aligned} \quad (3.4-12)$$

The Runge-Kutta method is self-starting and treats every step in a sequence of steps in an identical manner. The integration step size can be adjusted easily and without any additional computational operations (compared with a multistep method, for example).

3.5 Contact joints

When an interference occurs between two different bodies, a new contact force is suddenly applied, which causes impacts and velocity jumps in the mechanical system.

Two different approaches are generally used for impact problems. The first one considers the impact in a micro-sense. This means that the contact force acts on the bodies in a continuous manner and the motion is not discontinuous. This analysis method is referred as a "continuous" analysis method. The canonical equations of motion of the system remain the same as the ones developed in the previous section. The only difference is that a contact force between the colliding bodies must be transformed into its generalized force acting during the period of contact. Since the duration of the contact is usually very small, extra care must however be taken in the numerical integration of the equations of motion over that period.

In the second method of analysis, the impact is considered in a macro-sense. The duration of contact between the two colliding bodies is assumed to be so small that the impact is considered to occur instantaneously. In that case, the analysis is divided into two intervals: before and after impact. The interconnection between the two intervals is provided by the balancing of the system momenta right before and right after impact. This analysis method is referred as the "piecewise" analysis method. To relate the velocities (or momenta) before and after impact, a coefficient of restitution has to be considered. The important features in the numerical treatment of impact problems using the piecewise analysis method are the determination of the exact time of impact and the evaluation of the velocity (or momenta) jumps by solving the momentum balance-impulse equations at that time.

The two analysis methods will be described in the following sections, in order to outline their advantages and drawbacks. In this thesis, the piecewise analysis method has been preferred because it is a "natural" extension of the kinematic simulation which was the main point of the particular mechanisms considered in this thesis. It is also well adapted to the quasi static or dynamic simulation of mechanism containing rigid bodies.

3.5.1 Continuous method

3.5.1.1 Impact procedure

Although the duration of an impact is usually very small, the contact force can be considered as acting in a continuous manner. The magnitude of the contact force depends on the local contact deformation. If the contact impact happens under frictionless condition, the direction of the contact impulse is in the normal direction, and will be noted by F_{kn} (see Fig. 3.5.1-1).

The concept of virtual contact joint can still be used to calculate the contact force: in order to express the force acting between the two contacting bodies, a real contact will be considered as a virtual contact joint, which use the distance between both contact elements as a real degree of freedom.

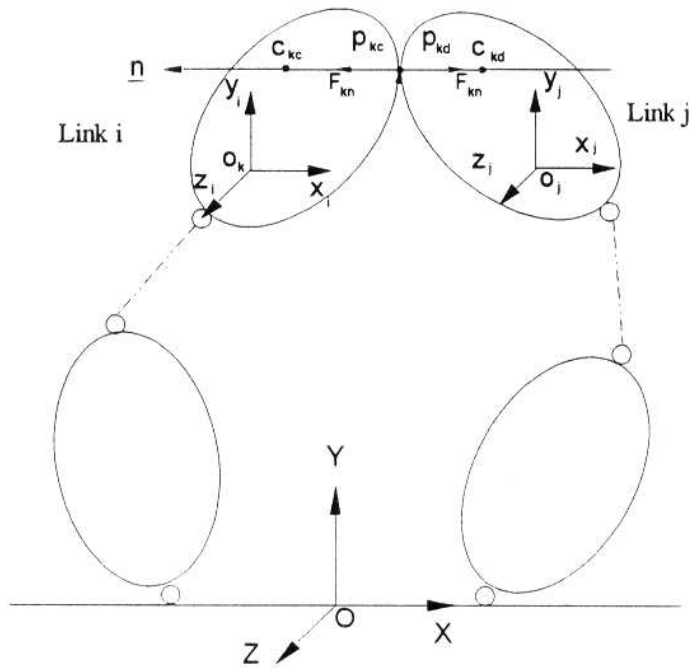


Fig. 3.5.1-1: Impact between bodies i and j

Suppose that two bodies i and j are interfering each others as shown in Fig. (3.5.1-1). The following constraint loop equation can be written:

$$A_{oi} T_{11} \Phi_1 T_{12} T_{22} \dots T_{ik} \Phi_k(q_k) T_{kj} T_{jj} \dots T_{nl} A_{10} = I \quad (3.5.1-1)$$

The contact joint matrix (see Fig. 3.5.1-2) is composed as in the case of a virtual contact by the products of 3 consecutive matrices:

$$\Phi_k(q_k) = \Phi_{kp}(q_{k1}) \Phi_{kd}(q_{k3}) \Phi_{kj}(q_{k2}) \quad (3.5.1-2)$$

where Φ_{kp} and Φ_{kf} describe the relations between respectively x_{kc}, y_{kc}, z_{kc} and x_k, y_k, z_k reference frames, and x'_k, y'_k, z'_k and x_{kd}, y_{kd}, z_{kd} frames. The x_k, y_k, z_k and x'_k, y'_k, z'_k frames are respectively located at the basis of the common normal used to measure the minimal distance q_{k3} between the preceding and following contact pairs. The transformation matrix between these two frames is expressed by Φ_{kd} :

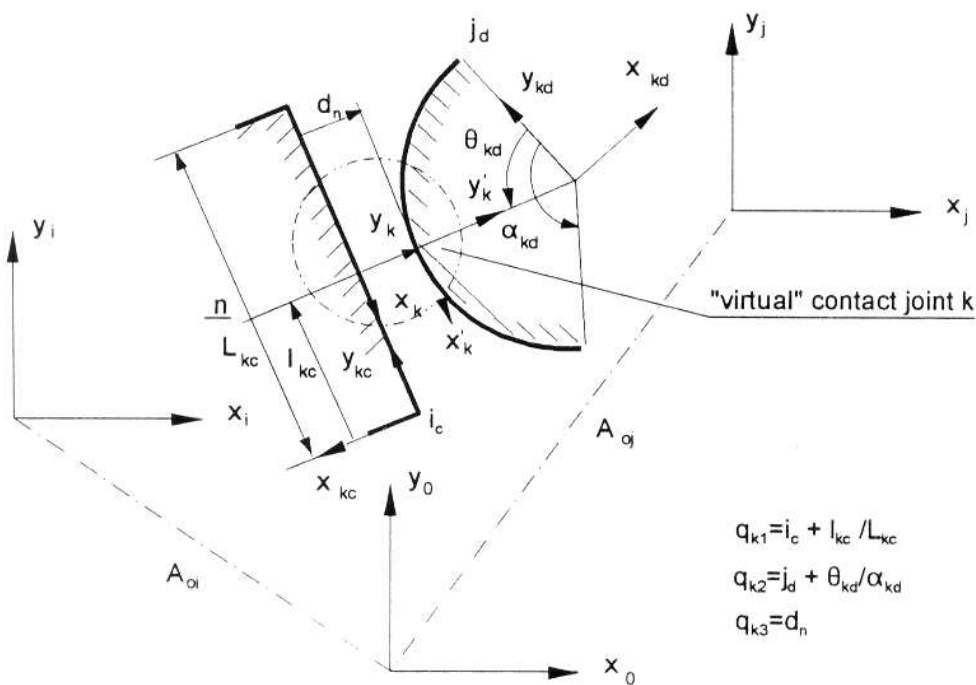


*Fig. 3.5.1-2: Contact joint used for impact analysis
(similar to a virtual contact joint)*

$$\Phi_{kd} = \begin{pmatrix} 1 & 0 & 0 & 0 \\ 0 & 1 & 0 & q_{k3} \\ 0 & 0 & 1 & 0 \\ 0 & 0 & 0 & 1 \end{pmatrix} \quad (3.5.1-3)$$

The parameter q_{k3} is the minimal distance between the two bodies, whose direction is the same as the direction of the impulse when impact occurs without friction. When

$$q_{k3} < 0 \quad (3.5.1-4)$$

the impact procedure can be applied and the magnitude of the contact F_{kn} force at a particular instant is principally expressed in function of q_{k3} and depends on the elastic contact model chosen to model the contact:

$$F_{kn} = F_{kn}(q_{k3}) \quad (3.5.1-5)$$

This force must be transformed into the generalized coordinates of the system according to the principle of virtual work. The work developed by F_{kn} for a small virtual displacement δq_{k3} is given by:

$$\delta w = F_{kn} * \delta q_{k3} \quad (3.5.1-6)$$

The virtual displacement in the normal direction associated to the virtual contact joint can be expressed in function of the generalized coordinates by:

$$\delta q_{k3} = \sum_{i=1}^{DOF} \frac{\partial q_{k3}}{\partial f_i} \delta f_i \quad (3.5.1-7)$$

Equ. (3.5.1-6) can be rewritten as:

$$\delta w = \sum_{i=1}^{DOF} F_{kn} * \frac{\partial q_{k3}}{\partial f_i} \delta f_i \quad (3.5.1-8)$$

or

$$\delta w = \sum_{i=1}^{DOF} F_{ki} \delta f_i \quad (3.5.1-9)$$

where F_{ki} are defined as the generalized force:

$$F_{ki} = F_{kn} \frac{\partial q_{k3}}{\partial f_i} \quad i=1,2,\dots,DOF \quad (3.5.1-10)$$

It can be rewritten in a vector form:

$$E_k = \left(\frac{\partial q_{k3}}{\partial f_1}, \frac{\partial q_{k3}}{\partial f_2}, \dots, \frac{\partial q_{k3}}{\partial f_{DOF}} \right)^T * F_{kn} = \Psi_k F_{kn} \quad (3.5.1-11)$$

where

$$\Psi_k = \left(\frac{\partial q_{k3}}{\partial f_1}, \frac{\partial q_{k3}}{\partial f_2}, \dots, \frac{\partial q_{k3}}{\partial f_{DOF}} \right)^T \quad (3.5.1-12)$$

The elements of Ψ_k can be obtained by the following procedure.

Let's consider the constraint matrix equations of the system:

$$\begin{aligned} \Phi_1 &= (A_{01} T_{11} \phi_1(q_1) T_{12} T_{22} \phi_2(q_2) T_{23} T_{33} \phi_3(q_3) \dots \phi_n(q_n) T_{n1} A_{10})_1 = I \\ \Phi_2 &= (A_{01} T_{11} \phi_1(q_1) T_{12} T_{22} \phi_2(q_2) T_{23} T_{33} \phi_3(q_3) \dots \phi_n(q_n) T_{n1} A_{10})_2 = I \\ &\dots \\ \Phi_{N_{loop}} &= (A_{01} T_{11} \phi_1(q_1) T_{12} T_{22} \phi_2(q_2) T_{23} T_{33} \phi_3(q_3) \dots \phi_n(q_n) T_{n1} A_{10})_{N_{loop}} = I \end{aligned} \quad (3.5.1-13)$$

For the sake of simplicity, one single loop is considered here. By differentiating the matrix loop equations with respect to the independent coordinate f_a , the following matrix equation is obtained:

$$\begin{aligned}
\frac{\partial \Phi_l}{\partial f_a} = & \sum_{i=1}^{l_1} A_{01} T_{11} \frac{\partial \phi_1}{\partial q_{1i}} T_{12} T_{22} \phi_2 T_{23} \dots \phi_n T_{nl} A_{10} \frac{\partial q_{1i}}{\partial f_a} \\
& + \sum_{i=1}^{l_2} A_{01} T_{11} \phi_1 T_{12} T_{22} \frac{\partial \phi_2}{\partial q_{2i}} \dots \phi_n T_{nl} A_{10} \frac{\partial q_{2i}}{\partial f_a} \\
& + \dots \\
& + \sum_{i=1}^{l_m} A_{01} T_{11} \phi_1 T_{12} T_{22} \phi_2 T_{23} \dots \frac{\partial \phi_m}{\partial q_{mi}} T_{ml} A_{10} \frac{\partial q_{mi}}{\partial f_a} \\
= & [0] \tag{3.5.1-14}
\end{aligned}$$

Using joint linear derivative operator Q_{ji} (defined in Equ. 2.2.3-13), and system linear derivative operator of joint variables B_{ji} (defined in Equ. 2.2.3-21), the first partial differentiation constraint equations can be rewritten as:

$$\sum_{i=1}^{l_1} B_{1i} \frac{\partial q_{1i}}{\partial f_a} + \sum_{i=1}^{l_2} B_{1i} \frac{\partial q_{2i}}{\partial f_a} + \dots + \sum_{i=1}^{l_n} B_{ni} \frac{\partial q_{ni}}{\partial f_a} = [0] \tag{3.5.1-15}$$

where

$$B_{ji} = A_{oj} T_{jj} Q_{ji} T_{jj}^{-1} A_{oi} \tag{3.5.1-16}$$

From Equ. (2.2.4-5), the vector \mathbf{q}' of the relative coordinates can be expressed, leading to the equivalent of the equation (2.2.4-8) which can be rewritten as follows:

$$(\Lambda_{nj}) \frac{\partial q'_1}{\partial f_a} + (\Lambda_{n2}) \frac{\partial q'_2}{\partial f_a} + \dots + (\Lambda_{nm}) \frac{\partial q'_m}{\partial f_a} = [0] \tag{3.5.1-17}$$

where

$$\Lambda_{na} = \sum_{j=1}^n \sum_{i=1}^{l_j} \alpha_{aji} B_{ji} \tag{3.5.1-18}$$

n is the number of joints in the considered kinematic loop and α_{aji} are the parameter defined in (2.2.4-6).

In a similar way that the one used to establish the constraint equations in section 2.2.4, the equation (3.5.1-17) is expressed in the following form:

$$\begin{bmatrix} \Lambda_{n1}(1,2) & \Lambda_{n2}(1,2) & \dots & \Lambda_{nm}(1,2) \\ \Lambda_{n1}(1,3) & \Lambda_{n2}(1,3) & \dots & \Lambda_{nm}(1,3) \\ \Lambda_{n1}(2,3) & \Lambda_{n2}(2,3) & \dots & \Lambda_{nm}(2,3) \\ \Lambda_{n1}(1,4) & \Lambda_{n2}(1,4) & \dots & \Lambda_{nm}(1,4) \\ \Lambda_{n1}(2,4) & \Lambda_{n2}(2,4) & \dots & \Lambda_{nm}(2,4) \\ \Lambda_{n1}(3,4) & \Lambda_{n2}(3,4) & \dots & \Lambda_{nm}(3,4) \end{bmatrix} \begin{Bmatrix} \frac{\partial q'_1}{\partial f_a} \\ \frac{\partial q'_2}{\partial f_a} \\ \vdots \\ \frac{\partial q'_m}{\partial f_a} \end{Bmatrix} = \{0\} \quad a=1,2,\dots,DOF \quad (3.5.1-19)$$

or

$$[C] \begin{Bmatrix} \frac{\partial q'}{\partial f_a} \end{Bmatrix} = \{0\} \quad (3.5.1-20)$$

The rank of the jacobian matrix [C] equals:

$$N_r = m - DOF \quad (3.5.1-21)$$

Rearranging this algebraic matrix equations by putting independent variables f in last position, the following set of linear equation can be used:

$$\begin{bmatrix} C_{11} & C_{12} \\ C_{21} & C_{22} \end{bmatrix} \begin{Bmatrix} \frac{\partial d}{\partial f_a} \\ \frac{\partial f}{\partial f_a} \end{Bmatrix} = \{0\} \quad (3.5.1-22)$$

where C_{11} is a nonsingular square matrix with rank N_r , d is the set of dependant coordinates which include the three variables in the virtual contact joints, and f is the set of independent variables. The solution of this equation will give the dependent variable derivatives with respect to the considered independent variables.

The generalized contact force vector can now be obtained by Equ. (3.5.1-11). Appending the generalized interference force E_k into the second Hamilton's canonical equation, the motion equation is obtained:

$$\dot{p} = E_a + E_k + E_c + \frac{1}{2} p^T [M]^{-1} \left(\frac{\partial [M]}{\partial f} \right)^T [M]^{-1} p \quad (3.5.1-23)$$

and has to be integrated over the period of contact.

3.5.1.2 Example of contact model

When two bodies are in contact, deformation takes place in the contact zone and a contact force is resulting. The relationship between the contact force and the relative

deformation has been developed in literatures, among others in [24,25]. Usually, an impact can be divided into two phases: the compression phase and the restitution phase. During the compression phase, the two bodies are deformed in the normal direction to the impact surface, until the relative velocity of two bodies in that direction is reduced to zero. The end of the compression phase corresponds to the instant of maximum approach between the two bodies. The restitution phase starts at this point and lasts until the two bodies separate.

The nonlinear elastic contact force model was among others developed by Hertz [18] for the contact between two surfaces of isotropic materials. In this model, the interference force F_{kn} and the deformation δ were linked by the following relation:

$$F_{kn} = k\delta^n + D\dot{\delta} \quad (3.5.1-24)$$

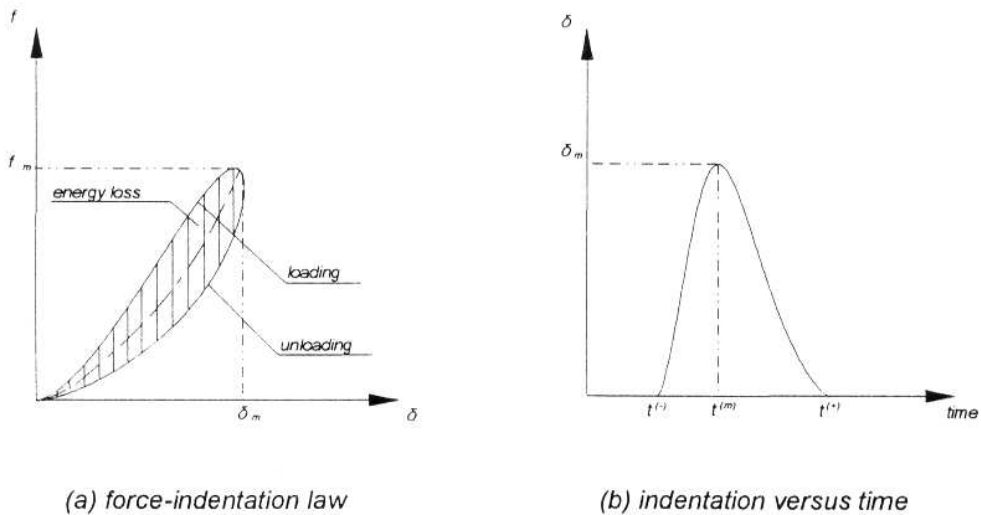


Fig. 3.5.1-3: Hertz Contact force model

The right side of this equation contains two terms: the first term expresses the elastic contribution in the form of a nonlinear relation. The parameters k and n depend on the geometric and the material properties of the two surfaces in contact. The second term expresses the energy loss during impact due to the material damping. A hysteresis damping coefficient was proposed for this model by Hunt and Grossley[47]:

$$D = \mu_D \delta^n \quad (3.5.1-25)$$

where the parameter μ_D is the hysteresis damping factor.

The evolution of the contact force during the compression and the restitution phases of contact is shown in Fig. 3.5.1-3. During the compression period, the contact force follows the loading path. The contact force increases from zero to its maximum value F_{km} where the deformation δ_m is maximum. During the restitution period, the contact force follows the unloading path for which the force and the deformation are both reduced from F_{km} and δ_m to zero. The hatched area in Fig. 3.5.1-3 represents the dissipated energy during impact, and describes the hysteresis loop.

3.5.2 Piecewise method

In the piecewise method, the momentum balance-impulse equations are employed to calculate the velocity jumps due to impact. The basic assumption underlying such analysis is that impact occurs instantaneously. This assumption is justified if the duration of the contact period is small enough such that the configuration of the system can be considered as unchanged during that period.

Integration of motion equations of systems is carried out while checking for the contact between the different components of the system. At the time of impact, the dynamic analysis is stopped and a balancing of the system momenta is performed to obtain the jumps of the velocities (or momenta) of the different bodies. Integration of the system equations of motion is then restarted with the new velocities (or momenta) until the next impact occurs.

The impact occurs during a period $[t^{(-)}, t^{(+)})]$ which is considered small enough such that the generalized coordinates of the system remain the same:

$$\dot{f}^{(-)} = \dot{f}^{(+)} \quad (3.5.2-1)$$

If the motion equations are expressed in the form of independent generalized coordinates, the generalized momentum vector p is defined by:

$$p = [M]\dot{f} \quad (3.5.2-2)$$

The differentiation of this equation with respect to time gives:

$$\dot{p} = [\dot{M}]\dot{f} + [M]\ddot{f} \quad (3.5.2-3)$$

The second term in the right-hand side of this equation equals the generalized forces acting on the system. The equation can be rewritten in the following particular form:

$$\dot{p} = E_a + E_k + E_c + [\dot{M}]\dot{f} \quad (3.5.2-4)$$

where E_a , E_k and E_c are the vectors of the generalized coordinates, associated respectively with the external forces, the contact force due to impact and the conservative forces.

The integration of this equation during the small contact period yields:

$$\Delta p = \int_{t^{(-)}}^{t^{(+)}} (E_a + E_k + E_c + [\dot{M}]\dot{f}) dt \quad (3.5.2-5)$$

Among all the forces acting on the system, only the impulsive force gives a non zero integral value, all the other terms in the equation being finite, and the duration of the period of contact being assumed to be zero.

The vector of the generalized coordinates $\underline{\Pi}_k$ associated to the impulse is given by:

$$\underline{\Pi}_k = \int_{t^{(-)}}^{t^{(+)}} \underline{F}_k dt \quad (3.5.2-6)$$

Using the same principle as in the preceding section (see Equ. 3.5.1-9) and considering the impulse magnitude π_k due to the impulsive force F_{kn} :

$$\pi_k = \int_{t^{(-)}}^{t^{(+)}} F_{kn} dt \quad (3.5.2-7)$$

one obtains:

$$\underline{\Pi}_k = \Psi_k \int_{t^{(-)}}^{t^{(+)}} F_{kn} dt = \Psi_k \pi_k \quad (3.5.2-8)$$

Equ. (3.5.2-5) can be rewritten as:

$$\Delta p = \Psi_k \pi_k \quad (3.5.2-9)$$

leading to the general conclusion that in a constrained mechanical system, if an instantaneous impact occurs, the change of generalized momentum Δp equals the generalized impulse $\underline{\Pi}_k$.

The main physical characteristic describing the contact between two contacting bodies is given by the coefficient of restitution e ; it expresses the relationship between the normal velocities of the two bodies before and after impact. If \underline{n} is the unit vector between the two bodies interfering at point P, the coefficient of restitution e is expressed by:

$$e = -\frac{\underline{n}^T (\dot{\underline{R}}_{pc}^{(+)} - \dot{\underline{R}}_{pd}^{(+)})}{\underline{n}^T (\dot{\underline{R}}_{pc}^{(-)} - \dot{\underline{R}}_{pd}^{(-)})} \quad (3.5.2-10)$$

where $\dot{\underline{R}}_{pc}^{(+)}$ and $\dot{\underline{R}}_{pd}^{(+)}$ are the relative normal velocities of the two bodies at the point P, just

after impact. $\dot{\underline{R}}_{pc}^{(-)}$ and $\dot{\underline{R}}_{pd}^{(-)}$ are the same parameters just before impact.

The concept of virtual contact joint is useful to describe the normal relative velocity, for it is directly expressed by the velocity associated to the variable q_{k3} of the virtual contact joint:

$$e = -\frac{\dot{q}_{k3}^{(+)}}{\dot{q}_{k3}^{(-)}} \quad (3.5.2-11)$$

Those velocities can be expressed as a function of the independent generalized velocities of the mechanical system by (see Equ. 2.2.4-24):

$$\dot{q}_{k3} = \sum_{i=1}^{DOF} \frac{\partial q_{k3}}{\partial f_i} \dot{f}_i = \Psi_k^T \dot{f} \quad (3.5.2-12)$$

where

$$\Psi_k^T = \left(\frac{\partial q_{k3}}{\partial f_1}, \frac{\partial q_{k3}}{\partial f_2}, \dots, \frac{\partial q_{k3}}{\partial f_{DOF}} \right) \quad (3.5.2-13)$$

which leads to the following expression:

$$e = - \frac{\Psi_k^T \dot{f}^{(+)}}{\Psi_k^T \dot{f}^{(-)}} \quad (3.5.2-14)$$

From Equ. (3.3.2-1), the velocities and the momenta are related by:

$$\dot{f} = [M]^{-1} p \quad (3.5.2-15)$$

The substitution of the corresponding momenta before and after impact into Equ. (3.5.2-14) yields:

$$e = - \frac{\Psi_k^T [M]^{-1} p^{(+)}}{\Psi_k^T [M]^{-1} p^{(-)}} \quad (3.5.2-16)$$

which can be rewritten as:

$$\Psi_k^T [M]^{-1} p^{(+)} = -e \Psi_k^T [M]^{-1} p^{(-)}$$

or

$$\Psi_k^T [M]^{-1} \Delta p = -(1+e) \Psi_k^T [M]^{-1} p^{(-)} \quad (3.5.2-17)$$

where

$$\Delta p = p^{(+)} - p^{(-)} \quad (3.5.2-18)$$

From Equ. (3.4.3-7), Δp can be replaced by $\Psi_k \pi_k$, leading to the following form:

$$\pi_k = - \frac{(e+1) \Psi_k^T [M]^{-1} p^{(-)}}{\Psi_k^T [M]^{-1} \Psi_k} \quad (3.5.2-19)$$

Finally, the equation describing the momentum changes can be expressed by:

$$\Delta p = -\Psi_k \frac{(e+1) \Psi_k^T [M]^{-1} p^{(-)}}{\Psi_k^T [M]^{-1} \Psi_k} \quad (3.5.2-20)$$

In conclusion, the procedure for a piecewise analysis comprises the following steps:

- 1) the integration of the canonical equations of motion is carried out until an interference occurs,

- 2) the exact time of contact is localized by using the procedure described in section 2.5.1,
- 3) the components of the vector Ψ_k are calculated.
- 4) the momentum changes are evaluated,
- 5) the integration of the canonical equations is started again with the updated momenta.

3.5.3 Comparison of the two analysis methods

3.5.3.1 Example of application of the continuous method

A simple mechanical system is composed by two colliding pendulums each of them being connected by a pin joint to the ground (Fig. 3.5.3-1). This simple example has been used to illustrate both impact analysis methods.

The initial configuration of the system is shown in Fig. (3.5.3-1) and the following values are used for the Hertz parameters [35].

$$\begin{aligned} K &= 2.3 \times 10^{10} \text{ N/m}^{1.5} \\ n &= 1.5 \\ \mu_D &= 2.5 \times 10^{11} \text{ (Kg/m}^{1.5} \cdot \text{s)} \end{aligned}$$

The simulation performed with the ACDMC computer programs gives the results shown in Fig. (3.5.3-2), which are in good agreement with the results published by [35]. The shapes of the hysteresis loop corresponding to this force model and the solution corresponding to the variations of the indentation with time are shown in Fig. (3.5.3-3) - (3.5.3-6).

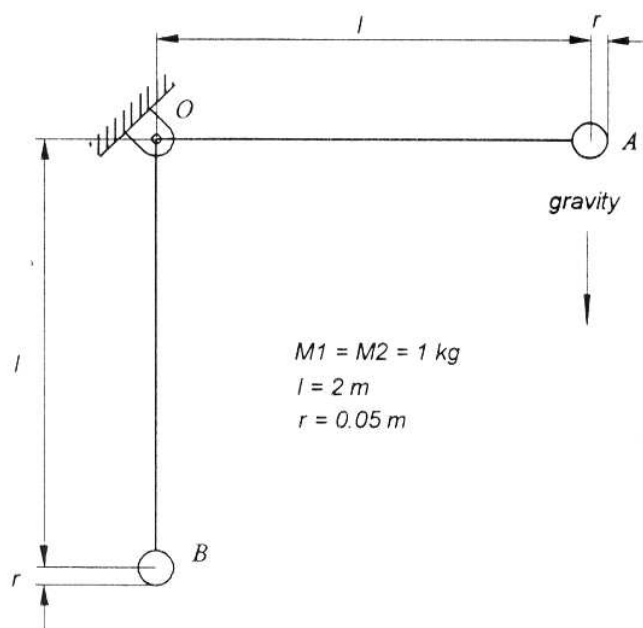


Fig. 3.5.3-1: A two pendulum system

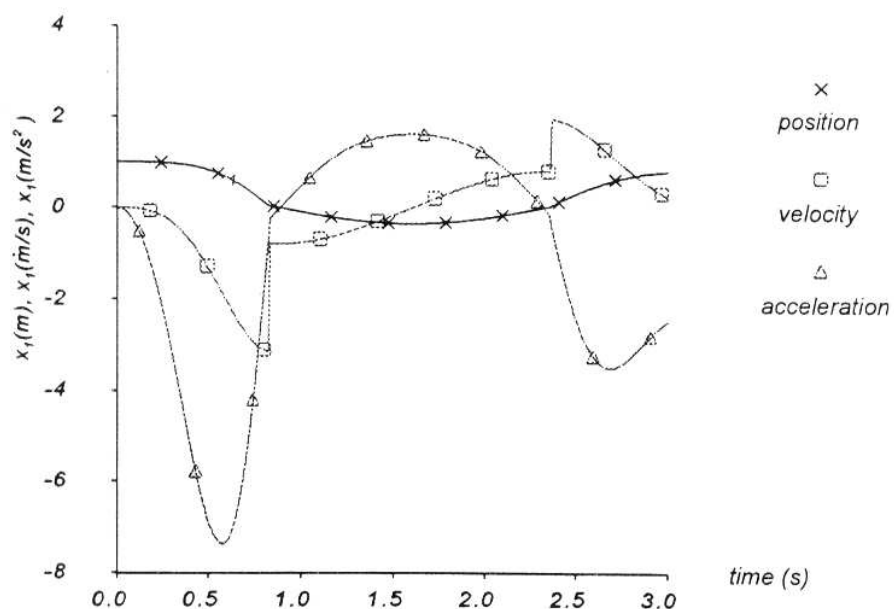


Fig. 3.5.3-2: Position, velocity, and acceleration of point A of pendulum 1 in x -direction

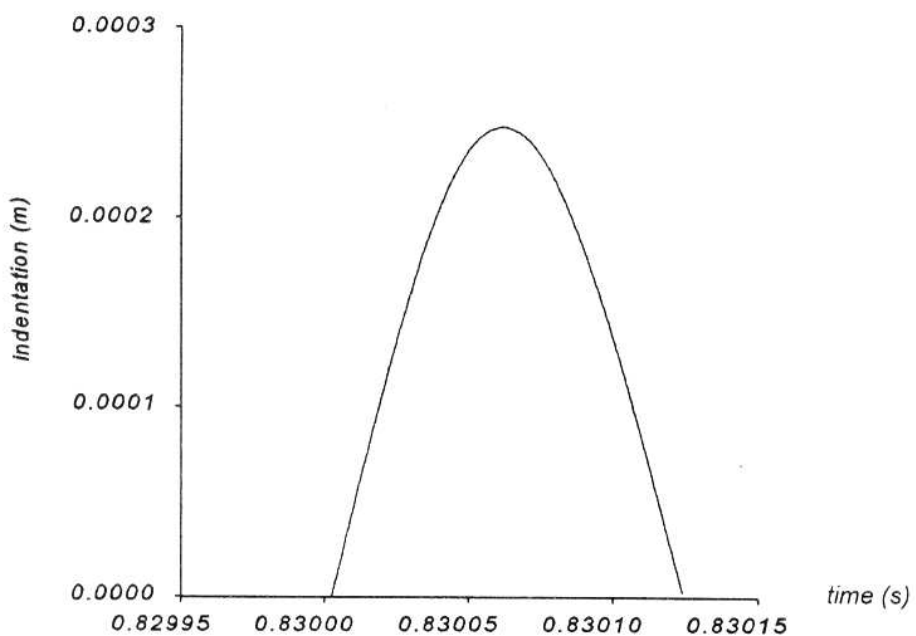


Fig.3.5.3-3: Hertz contact model - indentation versus time

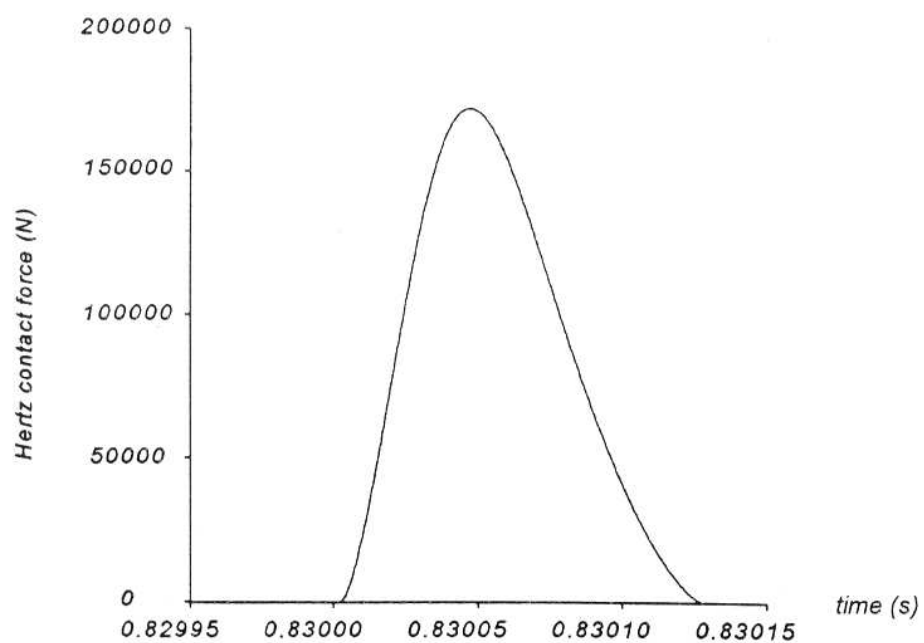


Fig. 3.5.3-4: Hertz contact model - force versus time

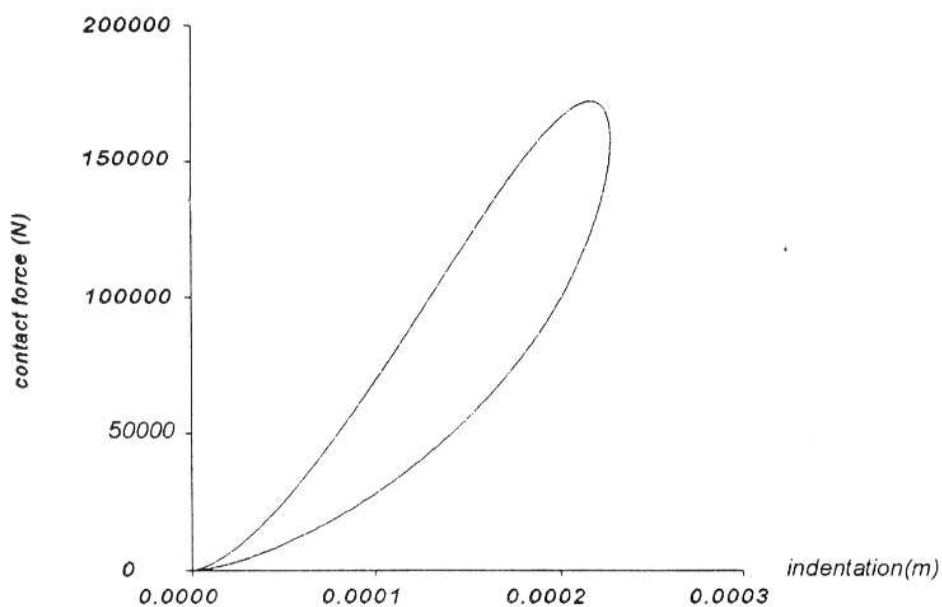


Fig. 3.5.3-5: Hertz contact model - force versus indentation

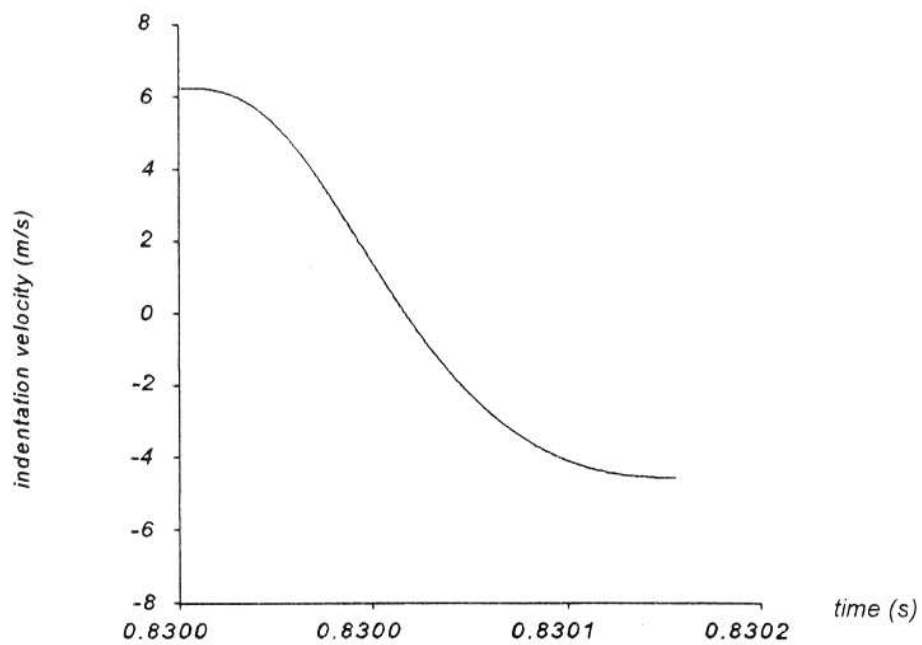


Fig. 3.5.3-6: Hertz contact model - indentation velocity versus time

3.5.3.2 Example of application of the piecewise method

The same system is used to illustrate the results obtained with a piecewise impact analysis method. The coefficient of restitution e has been evaluated by the following relation given by [39]:

$$e = \sqrt{1 - \frac{4 * \delta^{(-)} \mu_D}{3 * k}} \quad (3.5.3-1)$$

where k and μ_D are the stiffness and hysteresis damping factors of the materials. This relationship has been obtained by expressing the loss of energy during impact by two different ways: first, in terms of the coefficient of restitution and secondly, in terms of a hysteresis damping factor. It will be noted that the equivalent restitution coefficient also depends on the impact velocity between the two colliding bodies.

The simulation results obtained from the two analysis methods are shown in Fig. (3.5.3-7), and show a reasonable agreement.

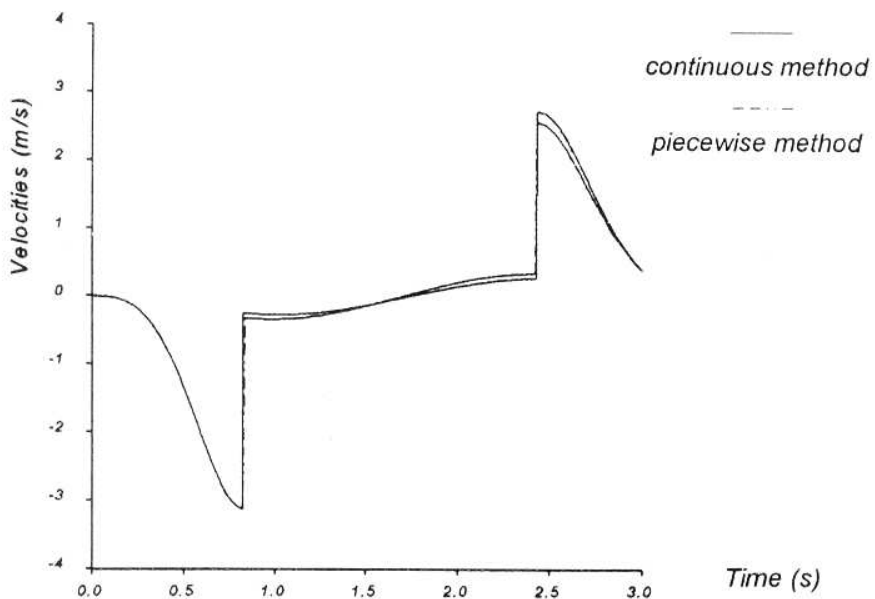


Fig. 3.5.3-7: Comparison of the velocity of point A of pendulum in x-direction ($e=0.8$)

3.5.3.3 Comparison of the two methods

One of the advantages of the continuous analysis method is its easy implementation to an existing code. The contact force is simply added to the motion equations which remain unchanged and which have to be integrated during the period of contact. Another advantage of the continuous analysis is that it can be used when the period of contact cannot be considered as instantaneous. Two factors however limit the application of this analysis method. Numerical integration is complex over the contact period: the period of contact is very small, and the magnitude of the contact force is important. The integration of the whole system equations of motion over the period of contact is a costly procedure due to the small integration steps that must be taken. Another limitation comes from the lack of precision in the knowledge of the material properties (k , n , μ_D).

When compared with the continuous analysis method, the piecewise analysis method does not pose the problem of numerical integration, once the velocity jumps have been calculated. One of the disadvantages is however the assumption of the instantaneous nature of the impact: the duration of impact must be small enough such that the system configuration does not change much during this period. Another disadvantage comes from the knowledge of the coefficient of restitution e and its dependence with the relative velocity. Moreover, the condition at which a contact is formed or not is vague, in case of non purely plastic impact ($e \neq 0$).

In this thesis, the piecewise method has been preferred because it seems to us as the "natural" extension of a kinematic simulation, which was the main objective of the particular mechanisms considered in this thesis. All types of changes of configurations (addition, deletion and transition) can be easily implemented with a piecewise method, well adapted to the simulation of mechanisms composed by a series of rigid bodies.

The case of sliding friction can moreover be considered by taking into account the tangential component of the contact force.

3.6 Changing contact joints in dynamic simulation

In section 2.5, the strategies of detection of the changes of contact joints have been discussed in the case of a kinematic simulation. They merely concern:

- the transition between consecutive elements,
- the detection of interference between bodies.

The deletion of an existing contact joint however requires the calculation of the contact force. A quasistatic or dynamic simulation is therefore necessary in order to detect an insufficient contact force. Otherwise, the addition of contact in a dynamic simulation requires an impact analysis. The procedure describing both addition and deletion of contact while performing a dynamic simulation will be discussed hereafter.

3.6.1 Addition of contact joint

When an impact between two bodies occurs in a mechanical system, the formation of a new contact joint, and the resulting change of topology depends upon the properties of materials and relative contact velocity at the contact point.

In the case of a plastic impact ($e=0$), the elastic energy due to impact compression is dissipated by internal damping and converted into heat energy. After the impact, the two bodies have no relative normal motion at the contact point, and it can be considered that a new high pair joint is directly formed. In the case of an elastic or an elasto-plastic impact, the materials do not totally absorb the elastic energy, which results in a relative normal velocity between the two bodies at the contact point.

Theoretically, after an impact, there is always a relative velocity between the two bodies at the contact point but, in practice, we will consider that if this relative velocity is below a given tolerance, it can be considered that a new contact joint is formed. This tolerance depends on the kind of problem that has to be solved. In practice, in this thesis, when non plastic impacts have been considered ($e \neq 0$), the restitution velocity has been monitored, and compared to a tolerance value.

The use of virtual contact joints makes particularly convenient the addition and deletion of contacts, because:

- an interference is easily detected from the state variable q_{k3} associated to the virtual contact joint,
- if the impact analysis determines that a new contact joint is to be formed, the virtual contact joint is easily converted into a real one,
- if an insufficient contact force is detected in the system, the deletion of the constraint is realized by transforming the real contact to a virtual one.

Let us recall that in a virtual contact joint, there are three dependent variables, q_{k1} , q_{k2} , q_{k3}

(see Fig. 3.5.2-2). If we assume that the impact occurs during a time interval $[t^{(-)}, t^{(+)})$, at time $t^{(-)}$, the variable $q_{k3}^{(-)}$ of the virtual contact joint, corresponding to the normal distance between the bodies, is equal to zero:

$$q_{k3}^{(-)} = 0 \quad (3.6.1-1)$$

and its derivative with respect to time, the normal depart velocity, is negative:

$$\dot{q}_{k3}^{(-)} < 0 \quad (3.6.1-2)$$

As in the case of the kinematic simulation, the interference switching function G_{I1} is defined by Equ. (2.5.3-3) and (2.5.3-4):

$$G_{I1}(t^*) = q_{k3}^{(-)} = 0$$

associated with

$$G_{I2}(t^*) = \dot{q}_{k3}^{(-)} < 0$$

In the case of non plastic impact, the two bodies do no longer interfere each other, so that the relative normal velocity at the contact point $\dot{q}_{k3}^{(+)}$ is positive.

If the departing velocity is under a given tolerance ε :

$$0 < \dot{q}_{k3}^{(+)} < \varepsilon \quad (3.6.1-3)$$

a new contact joint is assumed to be formed, and the virtual contact joint is converted into a real one. The switching function associated with this relative velocity is defined by:

$$G_{I3}(t^*) = \dot{q}_{k3}^{(+)} < \varepsilon \quad (3.6.1-4)$$

3.6.2 Deletion of a contact joint due to insufficient contact force

In real mechanical systems, the contact joints are always unilateral in the sense that they can only transmit compressive forces, coming from the fact that bodies cannot penetrate each other. Inversely, a contact joint is maintained as far as the contact force is compressive but is broken as soon as the contact force becomes tractive.

During the simulation of mechanical systems with contact joints, the contact force of each active contact joint must be monitored so as to detect eventual contact breaks. As soon as the contact force becomes tractive, the joint is considered broken and must be removed from the system by converting it into a virtual one. Of course, the constraint equations have to be reformed after each joint deletion.

If F_{kn} represents the normal reaction force in a contact joint k , assumed positive in the case of a compressive force, the characterization of the unilateral nature of the contact joints is stated analytically by:

$$F_{kn} > 0 \quad k = 1, \dots, \text{number of contact joints} \quad (3.6.2-1)$$

The contact force switching function is then defined by:

$$G_{F1}(t) = F_{kn}(t^*) = 0 \quad (3.6.2-2)$$

In order to detect the exact time of breaking of the contact joint, the zero of this switching function is localized.

3.6.2.1 Procedure of calculation of the contact force

In order to calculate the reaction forces, we have chosen to use the method of virtual work, which presents the following advantages:

- 1) it treats each constraint individually, thus making the method efficient by only calculating the required contact forces,
- 2) it uses the knowledge of the kinematic model which has been developed in the previous section.

Let's recall the principle of virtual work :

"The necessary and sufficient condition for the static equilibrium of a mechanical system which is subject to workless constraints is that zero virtual work be done by the applied forces in moving through an arbitrary virtual displacement satisfying the constraints." [36]

If a mechanical system (shown in Fig. 3.5.2-1) contains a contact joint k between links i and j , the contact force F_k , that link i applies on link j can be considered as a composition by a normal contact force F_{kn} (in the normal direction, \underline{n}), and a potential friction force (in the tangent direction) F_{kt} .

In order to determine the normal contact force F_{kn} , the contact constraint will be released, and the principle of virtual work will be written for a virtual displacement Δ in the normal direction of the contacting surfaces, at the contact point.

The process of evaluating static and dynamic constraint forces consists of simply considering the statics and dynamics of the system with an added degree of freedom in the direction of the constraint. From Hamilton's canonical second equation (3.3.2-20), the motion equation about the virtual displacement is:

$$\dot{\underline{p}} = F_{kn} + F_a + F_c + \frac{1}{2} \left\{ \begin{matrix} p \\ p \end{matrix} \right\}^T [M]^{-1} \left(\frac{\partial [M]}{\partial} \right)^T [M]^{-1} \left\{ \begin{matrix} p \\ p \end{matrix} \right\} \quad (3.6.2-2)$$

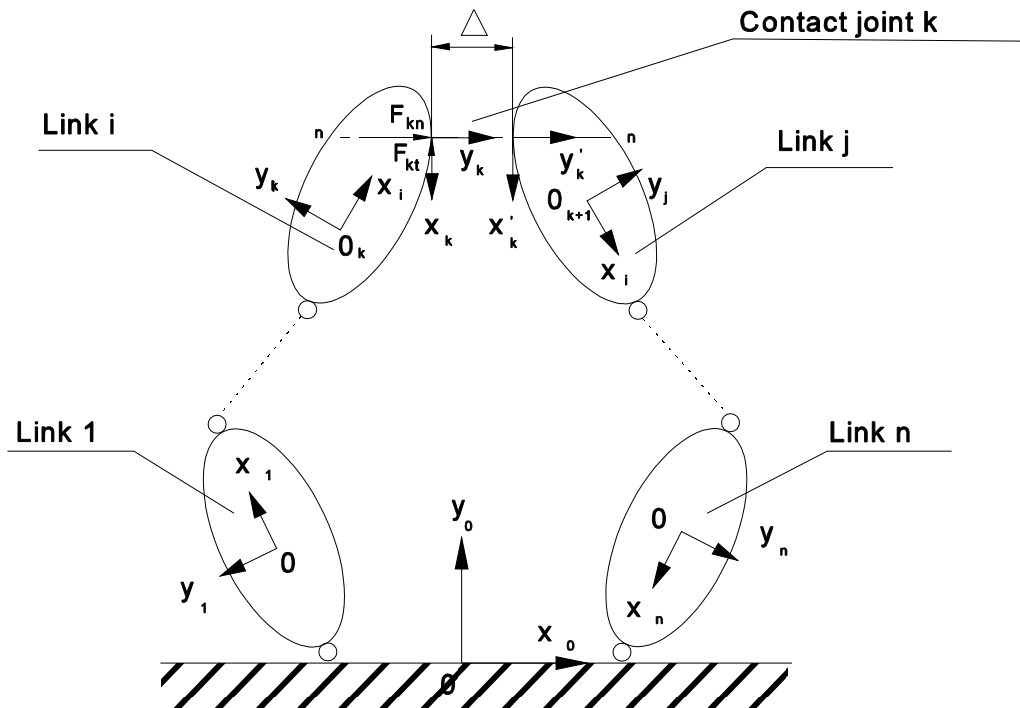


Fig. 3.6.2-1: Virtual displacement in contact joint k

where the external generalized force includes applied generalized forces $F_{a\Delta}$, the normal contact force F_{kn} and the generalized conservative force F_{ct} . $\begin{Bmatrix} p \\ p \end{Bmatrix}$ and M_Δ are respectively the generalized momentum vector and the symmetric mass matrix of the system obtained often the addition of the degree of freedom Δ .

The evaluations of the elements of the mass matrix have to deal with partial derivatives of the contact virtual displacement. The following section will discourse how to get those partial derivatives.

3.6.2.2 Calculation of the mass matrix derivatives with respect to the added degree of freedom in virtual motion

a) Expression of the velocity of a point P

When a virtual displacement is added in a contact joint, the position and motion of the links will change. As explained in Equation (2.2.4-1), the global coordinates of a point P on the link l whose local coordinates are r_l^P , are given by:

$$\underline{R}_p = \underline{A}_{ol} \underline{x}_1^P \quad (3.6.2-4)$$

The interlink matrix \underline{A}_{ol} is composed by a series of matrix multiplications depending on the kinematic loop (from the global coordinate frame to the local coordinate frame of the considered link) and describes the absolute position of link l .

Once a virtual displacement is added, each kinematical loop may comprise or not the contact joint.

When the loop does not comprise the contact joint, the kinematic analysis remains unchanged.

When the loop comprises the contact joint, the position vector equation becomes:

$$\underline{R}_p = \underline{A}_{ol} T_{11} \varphi_1 T_{12} \dots T_{kk} \varphi_k T_{k,k+1} \dots T_{l-1,l-1} \varphi_{l-1} T_{l-1,l} \underline{x}_1^P \quad (3.6.2-5)$$

The joint transformation matrix concerning joint k is redefined by:

$$\varphi_k = (\varphi_k)_p E (\varphi_k)_f \quad (3.6.2-6)$$

where $(\varphi_k)_p$ and $(\varphi_k)_f$ are respectively the preceding and following transformation matrices defined in Section 2.4. The transformation matrix E relative to the virtual displacement in the normal direction of the contact point can be written as:

$$E = I + Q \quad (3.6.2-7a)$$

where Q_Δ is a constant matrix. As the y axis is by convention the normal direction of the contact frame, the matrix Q_Δ is given by:

$$Q = \begin{bmatrix} 0 & 0 & 0 & 0 \\ 0 & 0 & 0 & 1 \\ 0 & 0 & 0 & 0 \\ 0 & 0 & 0 & 0 \end{bmatrix} \quad (3.6.2-7b)$$

Using Equ. (3.6.2-6) and (3.6.2-7), Equ. (3.6.2-5) can be rewritten as:

$$\underline{R}_p = \underline{A}_{ol} T_{11} \varphi_1 T_{12} \dots T_{kk} [\varphi_k + (\varphi_k)_p Q (\varphi_k)_f] T_{k,k+1} \dots T_{l-1,l-1} \varphi_{l-1} T_{l-1,l} \underline{x}_1^P \quad (3.6.2.8)$$

or

$$\underline{R}_p = [I + D_k] \underline{A}_{ol} \underline{x}_k^P \quad (3.6.2-9)$$

where D_k is defined as a derivative operator matrix relative to the virtual displacement Δ in a similar way as for B_{ji} in Equation (2.2.4-14):

$$D_k = \underline{A}_{ok} T_{kk} (\varphi_k)_p Q (\underline{A}_{ok} T_{kk} (\varphi_k)_p)^{-1} \quad (3.6.2-10)$$

The velocity of point P is then expressed by:

$$\frac{d\underline{R}_p}{dt} = \sum_{a=1}^{DOF} \frac{\partial \underline{R}_p}{\partial f_a} \dot{f}_a + \frac{\partial \underline{R}_p}{\partial} . \quad (3.6.2-11)$$

where the first partial differentiation term is given by:

$$\frac{\partial \underline{R}_p}{\partial f_a} = \frac{\partial D_k}{\partial f_a} A_{o1} \underline{r}_p + [I + D_k] \frac{\partial A_{o1}}{\partial f_a} \underline{r}_1^p \quad (3.5.2-12)$$

We know from Equ. (3.3.2-6) that:

$$\frac{\partial A_{ok}}{\partial f_a} = \omega_{ka} A_{ok} \quad (3.6.2-13)$$

On the other hand, as $A_{ok} * A_{ko} = I$, we have:

$$\frac{\partial A_{ko}}{\partial f_a} = -A_{ok}^{-1} \frac{\partial A_{ok}}{\partial f_a} A_{ok}^{-1} = -A_{ok}^{-1} \omega_{ka} \quad (3.6.2-14)$$

It comes therefore from Equ. (3.6.2-10):

$$\begin{aligned} \frac{\partial D_k}{\partial f_a} &= \left(\frac{\partial A_{ok}}{\partial f_a} T_{kk} (\varphi_k)_p + A_{ok} T_{kk} \frac{\partial (\varphi_k)_p}{\partial f_a} \right) Q (\varphi_k)_p^{-1} T_{kk}^{-1} A_{kc} \\ &\quad + A_{ok} T_{kk} Q (\varphi_k)_p \left(\frac{\partial (\varphi_k)_p^{-1}}{\partial f_a} T_{kk}^{-1} A_{ko} + (\varphi_k)_p^{-1} T_{kk}^{-1} \frac{\partial A_{ko}}{\partial f_a} \right) \end{aligned} \quad (3.6.2-15)$$

From Equ. (3.6.2-13), (2.2.3-13) and (2.2.3-21), the equation can be rewritten as:

$$\begin{aligned} \frac{\partial D_k}{\partial f_a} &= \left(\omega_{ka} A_{ok} T_{kk} (\varphi_k)_p + A_{ok} T_{kk} Q_{k1} (\varphi_k)_p \frac{\partial q_{k1}}{\partial f_a} \right) Q (\varphi_k)_p^{-1} T_{kk}^{-1} A_{ko} \\ &\quad + A_{ok} T_{kk} Q (\varphi_k)_p \left(-(\varphi_k)_p^{-1} Q_{k1} \frac{\partial q_{k1}}{\partial f_a} T_{kk}^{-1} A_{ko} - (\varphi_k)_p^{-1} T_{kk}^{-1} A_{ko} \omega_{ka} \right) \\ &= \left(\omega_{ka} + B_{k1} \frac{\partial q_{k1}}{\partial f_a} \right) D_k - D_k \left(\omega_{ka} + B_{k1} \frac{\partial q_{k1}}{\partial f_a} \right) \end{aligned} \quad (3.6.2-16)$$

where

$$B_{k1} = A_{ok} T_{kk} Q_{k1} T_{kk}^{-1} A_{ok}^{-1} \quad (3.6.2-17)$$

The differentiation of position with respect to the independent coordinate f_a is then given by:

$$\frac{\partial \underline{R}_p}{\partial f_a} = \left[\left(\left(\omega_{ka} + B_{k1} \frac{\partial q_{k1}}{\partial f_a} \right) D_k - D_k \left(\omega_{ka} + B_{k1} \frac{\partial q_{k1}}{\partial f_a} \right) D_k \omega_{1a} \right) + (I + D_k) \omega_{1a} \right] A_{o1} \underline{r}_1^p \quad (3.6.2-18)$$

$$= \bar{\omega}_{1a} () A_{o1} \underline{r}_1^p \quad (3.6.2-18)$$

The new derivative operator $\bar{\omega}_{1a}(\)$ is defined by:

$$\bar{\omega}_{1a}(\) = (\omega_{ka} + B_{k1} \frac{\partial q_{k1}}{\partial f_a}) D_k - D_k (\omega_{ka} + B_{k1} \frac{\partial q_{k1}}{\partial f_a}) + D_k \omega_{1a} + \omega_{1a} \quad (3.6.2-19)$$

or

$$\bar{\omega}_{1a}(\) = \varepsilon_{1ka} + \omega_{1a} \quad (3.6.2-20)$$

with

$$\varepsilon_{1ka} = (\omega_{ka} + B_{k1} \frac{\partial q_{k1}}{\partial f_a}) D_k - D_k (\omega_{ka} + B_{k1} \frac{\partial q_{k1}}{\partial f_a}) + D_k \omega_{1a} \quad (3.6.2-21)$$

In this analysis procedure, the derivative of the position vector equation with respect to the virtual displacement corresponds to:

$$\frac{\partial \underline{R}_p}{\partial} = [\frac{\partial D_k}{\partial} + D_k] A_{o1} \underline{r}_p + [I + D_k] \frac{\partial A_{o1}}{\partial} \underline{r}_1 \quad (3.6.2-22)$$

By using the following relationships:

$$\frac{\partial D_k}{\partial} = (\omega_k + B_{k1} \frac{\partial q_{k1}}{\partial}) D_k - D_k (\omega_k + B_{k1} \frac{\partial q_{k1}}{\partial}) \quad (3.6.2-23)$$

$$\frac{\partial A_{o1}}{\partial} = \omega_1 A_{o1} \quad (3.6.2-24)$$

equation (3.5.3-22) can be rewritten as:

$$\begin{aligned} \frac{\partial \underline{R}_p}{\partial} &= [\omega_1 + D_k + (D_k \omega_1 + (\omega_k + B_{k1} \frac{\partial q_{k1}}{\partial}) D_k - D_k (\omega_k + B_{k1} \frac{\partial q_{k1}}{\partial}))] A_{o1} \underline{r}_1 \\ &= \bar{\omega}_1(\) A_{o1} \underline{r}_1 \end{aligned} \quad (3.6.2-25)$$

where the new derivative operator $\bar{\omega}_1(\)$ corresponds to:

$$\bar{\omega}_1(\) = \omega_1 + D_k + (D_k \omega_1 + (\omega_k + \frac{\partial q_{k1}}{\partial}) D_k - D_k (\omega_k + \frac{\partial q_{k1}}{\partial})) \quad (3.6.2-26)$$

or

$$\bar{\omega}_1(\) = \omega_1 + D_k + \varepsilon_{1k} \quad (3.6.2-27)$$

with

$$\varepsilon_{1k} = (D_k \omega_1 + (\omega_k + B_{k1} \frac{\partial q_{k1}}{\partial}) D_k - D_k (\omega_k + B_{k1} \frac{\partial q_{k1}}{\partial})) \quad (3.6.2-28)$$

The velocity of the point P can now be written as:

$$\frac{d\bar{R}_p}{dt} = \left(\sum_{a=1}^{DOF} \bar{\omega}_{la} (\) \dot{f}_a + \bar{\omega}_l (\) \cdot \right) A_{ol} \bar{r}_l^p \quad (3.6.2-29)$$

b) Expression of the mass matrix

Introducing this relationship into the kinetic energy equation (3.3.1-2), the elements m_{ij} of the $(DOF+1) \times (DOF+1)$ real symmetric mass matrix $[M_\Delta]$ can be obtained by:

$$m_{ij} = \sum_{l=1}^{N_{li}} Tr [\bar{\omega}_{li} (\) A_{ol} J_l A_{ol}^T \bar{\omega}_{lj}^T (\)] \quad (3.6.2-30)$$

where L is the number of links in the system. Similarly, the last row (or last column) of the mass matrix will be given by:

$$m_{ii} = m_i = \sum_{l=1}^{N_{li}} Tr [\bar{\omega}_l (\) A_{ol} J_l A_{ol}^T \bar{\omega}_{li}^T (\)] \quad (3.6.2-31)$$

c) Derivation of the mass matrix

The differentiation of the mass matrix in Equation (3.6.2-31) can be expressed by:

$$\begin{aligned} \frac{\partial m_{ij}}{\partial f_a} &= \frac{\partial}{\partial f_a} \sum_{l=1}^{N_{li}} Tr [\bar{\omega}_l (\) A_{ol} J_l A_{ol}^T \bar{\omega}_{lj}^T (\)] \\ &= \sum_{l=1}^{N_{li}} Tr [\left(\frac{\partial \bar{\omega}_l (\)}{\partial f_a} A_{ol} + \bar{\omega}_l (\) \frac{\partial A_{ol}}{\partial f_a} \right) J_l A_{ol}^T \bar{\omega}_{lj}^T (\)] \\ &\quad + \sum_{l=1}^{N_{li}} Tr [\bar{\omega}_l (\) A_{ol} J_l \left(\frac{\partial A_{ol}^T}{\partial f_a} \bar{\omega}_{lj}^T (\) + A_{ol}^T \frac{\partial \bar{\omega}_{lj}^T (\)}{\partial f_a} \right)] \end{aligned} \quad (3.6.2-32)$$

By partial differentiating Equ. (3.6.2-19), we can get $\frac{\partial \bar{\omega}_{li} (\)}{\partial f_a}$, as:

$$\begin{aligned} \frac{\partial \bar{\omega}_{li} (\)}{\partial f_a} &= \frac{\partial \omega_{li}}{\partial f_a} + \frac{\partial \varepsilon_{lki}}{\partial f_a} \\ &= \gamma_{lia} + \frac{\partial \varepsilon_{lki}}{\partial f_a} \end{aligned} \quad (3.6.2-33)$$

where γ_{lia} can be found in Appendix B. In the same manner, we obtain by differentiating equation (3.6.2-27):

$$\begin{aligned} \frac{\partial \bar{\omega}_l(\)}{\partial f_a} &= \frac{\partial \omega_l}{\partial f_a} + \frac{\partial D_k}{\partial f_a} + \frac{\partial \varepsilon_{lk}}{\partial f_a} \\ &= \gamma_{1a} + (\omega_{ka} + B_{k1} \frac{\partial q_{k1}}{\partial f_a}) D_k - D_k (\omega_{ka} + B_{k1} \frac{\partial q_{k1}}{\partial f_a}) + \frac{\partial \varepsilon_{lk}}{\partial f_a} \end{aligned} \quad (3.6.2-34)$$

By introducing Equ. (3.6.2-33), (3.6.2-34) and (3.6.2-4) into Equ. (3.6.2-2), and taking into account that $\Delta=0$ in the considered real configuration, we can get:

$$\begin{aligned} \frac{\partial m_{ij}}{\partial f_a} &= \sum_{l=1}^{N_{li}} \text{Tr} \left[(\gamma_{1a} + (\omega_{ka} + B_{k1} \frac{\partial q_{k1}}{\partial f_a}) D_k - D_k (\omega_{ka} + \frac{\partial q_{k1}}{\partial f_a}) + \omega_l \omega_{la} + D_k \omega_{la}) A_{ol} J_1 A_{ol}^T \omega_{lj}^T \right] \\ &\quad + \sum_{l=1}^{N_{li}} \text{Tr} [(\omega_l + D_k) A_{ol} J_1 A_{ol}^T (\gamma_{1ja} + \omega_{lj} \omega_{la})^T] \end{aligned} \quad (3.6.2-35)$$

similarly,

$$\frac{\partial m_{ij}}{\partial} = \frac{\partial}{\partial} \sum_{l=1}^{N_{li}} \text{Tr} [\bar{\omega}_{li}(\) A_{ol} J_1 A_{ol}^T \bar{\omega}_{lj}^T(\)] \quad (3.6.2-36)$$

resulting in:

$$\begin{aligned} \frac{\partial m_{ij}}{\partial} &= \\ &\sum_{l=1}^{N_{li}} \text{Tr} \left[[\gamma_{1i} + D_k \omega_{li} + (\omega_{ki} + B_{k1} \frac{\partial q_{k1}}{\partial f_i}) D_k - D_k (\omega_{ki} + B_{k1} \frac{\partial q_{k1}}{\partial f_i}) + \omega_{li} \omega_l] A_{ol} J_1 A_{ol}^T \omega_{lj}^T \right] \\ &+ \sum_{l=1}^{N_{li}} \text{Tr} \left[\omega_{li} A_{ol} J_1 A_{ol}^T (\gamma_{1j} + D_k \omega_{lj} + (\omega_{kj} + \frac{\partial q_{k1}}{\partial f_i}) D_k - D_k (\omega_{kj} + \frac{\partial q_{k1}}{\partial f_i}) + \omega_{lj} \omega_l)^T \right] \end{aligned} \quad (3.6.2-37)$$

3.6.2.3 Expression of the static and dynamic parts of the contact force

After getting the new generalized masses and their derivatives with respect to the contact virtual displacement, we can use the principle of virtual work to calculate the normal contact forces F_{kn} . For the sake of simplicity, the force is divided into two parts; a quasi-static part $(F_{kn})_s$ and a dynamic part $(F_{kn})_d$:

$$F_{kn} = (F_{kn})_s + (F_{kn})_d \quad (3.6.2-38)$$

For the quasi-static part of the constraint force, let us consider the system at rest. The principle of virtual work applied on this position yields the following equation:

$$(F_{kn})_s * \sum_i F_{ai} * \delta s_{ai} + \sum_i F_{ci} * \delta s_{ci} = 0 \quad (3.6.2-39)$$

where

$$\sum_i F_{ai} * \delta s_{ai} = \text{work done by non-conservative forces acting on the system};$$

$$\sum_i F_{ci} * \delta s_{ci} = \text{work done by conservative forces.}$$

For a small virtual deformation Δ , δs_{ai} and δs_{ci} can be evaluated by the following first order approximation:

$$\delta s_{ai} = \frac{\partial s_{ai}}{\partial} * \quad \text{and} \quad \delta s_{ci} = \frac{\partial s_{ci}}{\partial} * \quad (3.6.2-40)$$

The quasi-static part of the contact force can therefore be evaluated by:

$$\begin{aligned} (F_{kn})_s &= -\sum_i F_{ai} * \frac{\partial s_{ai}}{\partial} - \sum_i F_{ci} * \frac{\partial s_{ci}}{\partial} \\ &= -F_a - F_c \end{aligned} \quad (3.6.2-41)$$

where

$$F_a = \sum_i F_{ai} \frac{\partial s_{ai}}{\partial} \quad (3.6.2-42)$$

and

$$F_c = \sum_i F_{ci} \frac{\partial s_{ci}}{\partial} \quad (3.6.2-43)$$

Combining Equations (3.6.2-38), (3.6.2-41) and (3.6.2-2), the inertia (dynamic) part of the contact force can be obtained by the following relationships:

$$(F_{kn})_d = \dot{P} - \frac{1}{2} \left\{ \begin{matrix} p \\ p \end{matrix} \right\}^T \left([M]^{-1} \left[\frac{\partial M}{\partial} \right] [M]^{-1} \right) \left\{ \begin{matrix} p \\ p \end{matrix} \right\} \quad (3.6.2-44)$$

If we come back to the definition of the momentum P :

$$P = \sum_{i=1}^{DOF} m_i \dot{f}_i + m \quad (3.6.2-45)$$

and take into account that, for the real system:

$$= \cdot \cdot \cdot = 0 \quad (3.6.2-46)$$

\dot{P} can be expressed as:

$$\dot{P} = \sum_{k=1}^{DOF} (\dot{m}_k) \dot{f}_k + \sum_{k=1}^{DOF} m_k \ddot{f}_k \quad (3.6.2-47)$$

By introducing the following relationship in Equ. (3.5.3-45):

$$\begin{Bmatrix} \underline{\underline{P}} \\ \underline{\underline{p}} \end{Bmatrix} = [M] \begin{Bmatrix} \dot{\underline{\underline{F}}} \\ \cdot \end{Bmatrix} \quad (3.6.2-48)$$

$$\ddot{\underline{\underline{m}}}_i = \sum_{i=1}^{DOF} \frac{\partial m_i}{\partial f_i} \dot{f}_i + \frac{\partial m_i}{\partial} \cdot = \sum_{i=1}^{DOF} \frac{\partial m_i}{\partial f_i} \dot{f}_i \quad (3.6.2-49)$$

we get the final following expression of the dynamic force:

$$(F_{kn})_d = \sum_{i=1}^{DOF} \sum_{j=1}^{DOF} \left(\frac{\partial m_i}{\partial f_j} \right) \dot{f}_i \dot{f}_j + \sum_{i=1}^{DOF} m_i \ddot{f}_i - \frac{1}{2} \begin{Bmatrix} \dot{\underline{\underline{f}}} \\ \cdot \end{Bmatrix}^T \left[\frac{\partial M}{\partial} \right] \begin{Bmatrix} \dot{\underline{\underline{f}}} \\ \cdot \end{Bmatrix} \quad (3.6.2-50)$$

3.6.3 Illustrative example of deletion/addition of a contact joint

The planar mechanical system shown in Fig. (3.6.3-1) is composed of a cam, which is a disk turning about an offset axis, and a translational flat-faced follower, maintained in contact with the cam by means of a spring. We will see that under certain circumstances, the contact force vanishes so that the contact between cam and follower is lost.

Fig. (3.6.3-2) and (3.6.3-3) show the evolution of the contact force and its components (static and dynamic parts) for two different rotation velocities of the cam, respectively 1.5 and 1.9 radians per second.

In the first case, the contact force is always greater than zero, so that the contact is always maintained.

On the contrary, with a rotation velocity of the cam equal to 1.9 radian/s, the dynamic part becomes largely negative so that the contact is lost.

Fig. (3.6.3-4) represents the motion of the follower versus the rotation angle of the cam. It can be seen that the displacement of the follower, during the contact loss, is larger for the second case.

Finally, figure 3.6.3-5 details the configuration of the system, for a rotation speed of 1.9 rad/sec, at different instants, the contact loss clearly appears for rotation angles of the cam going from 135 to 270 degrees.

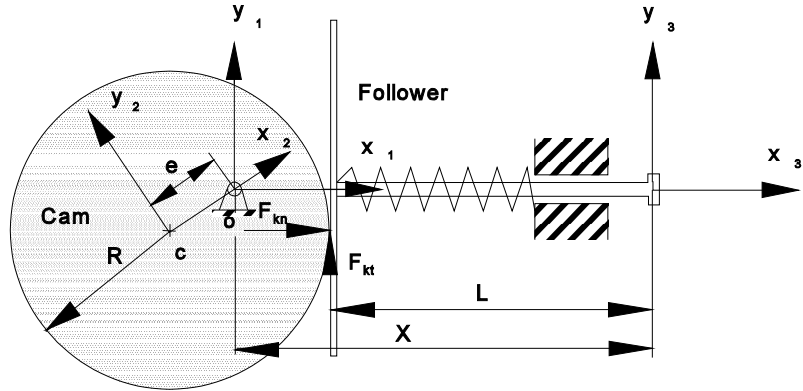


Fig. 3.6.3-1: Cam mechanism with flat-faced follower

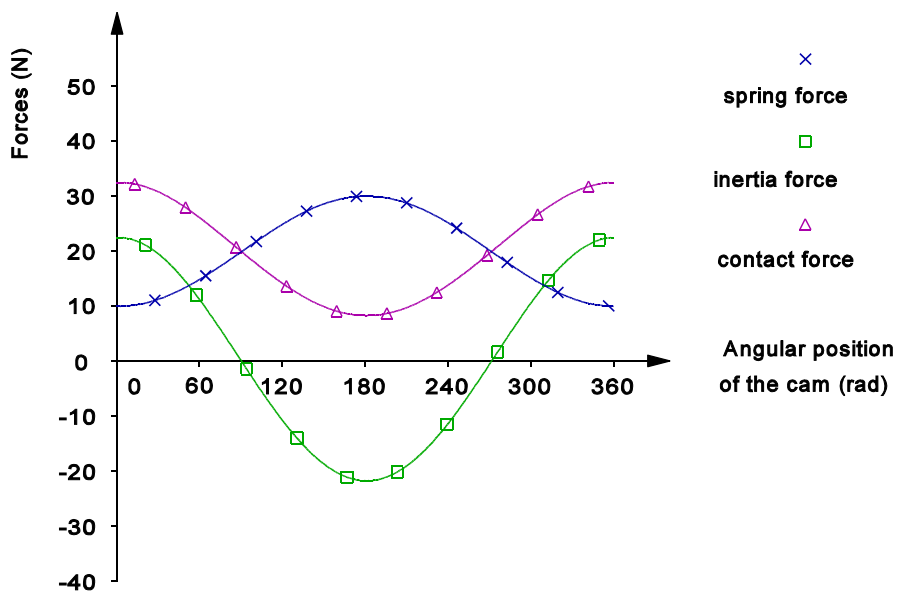


Fig. 3.6.3-2: Contact forces between cam and follower with a cam velocity of 1.5 rad/sec

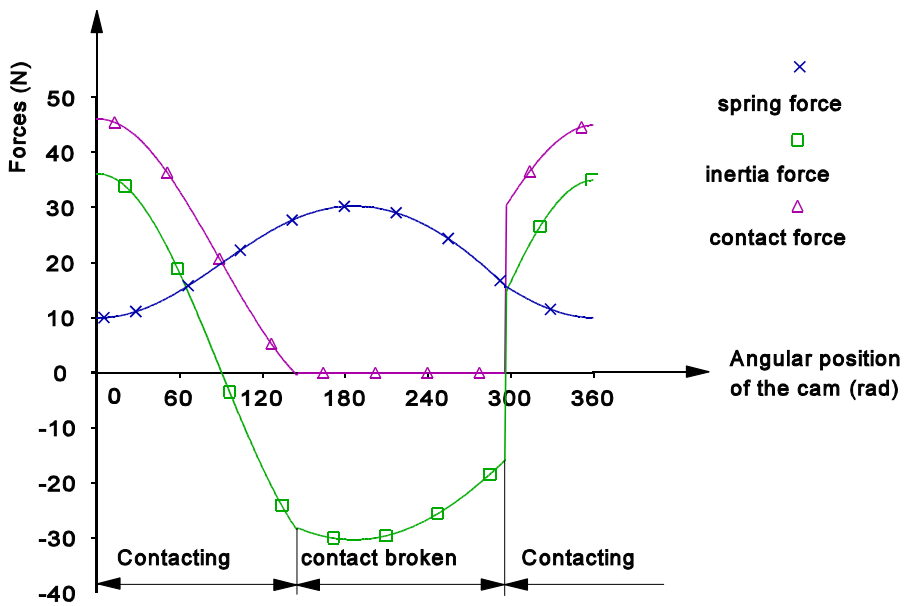


Fig. 3.6.3-3: Contact forces between cam and follower with a cam velocity of 1.9 rad/sec

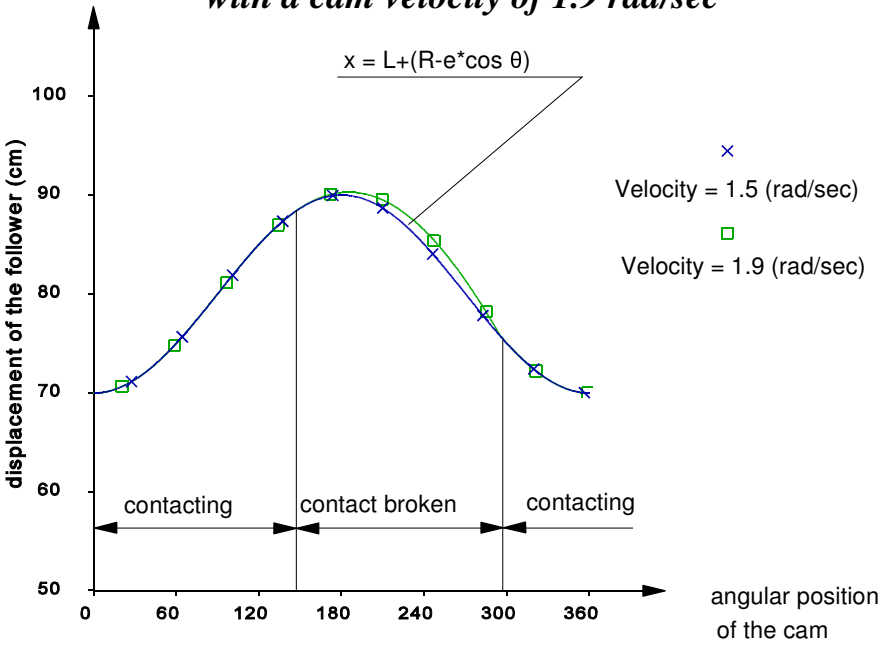
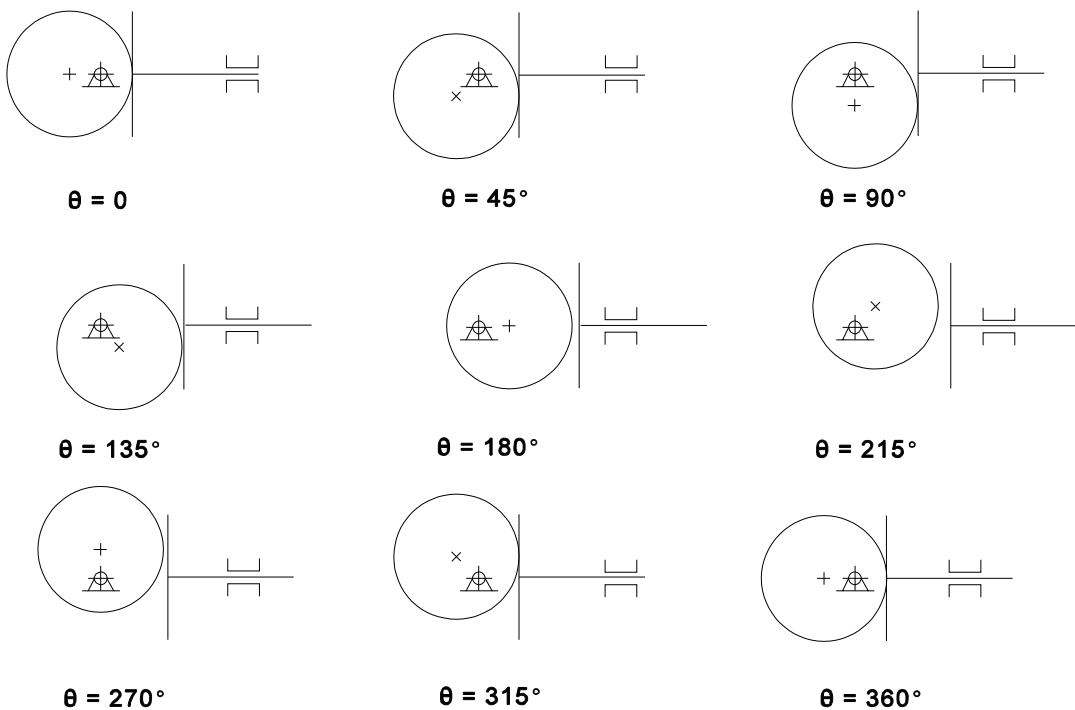


Fig. 3.6.3-4: Output motion of the cam mechanism at different velocities



*Fig. 3.6.3-5: Configuration of the cam-follower mechanism
(cam velocity = 1.9 rad/sec)*

3.7 Illustrative example: dynamics of a crank-slider connected to a four-bar linkage mechanism

Let's take the same illustrative example as in Section 2.6. The changes of the contact joints depend in practice on the dynamic behaviour of the mechanical system, concerning:

- 1) **the dynamic contact force:** when the contact force between bodies L4 and L5 equals zero, the contact will be broken and the real contact joint has to be changed into a virtual one.
- 2) **the impact between bodies L4 and L5.** If the impact due to interference is not a pure plastic impact (which means the restitution coefficient is different of zero), the virtual contact joint cannot be changed into a real one just after interference.

The dynamic simulation of the mechanism will be performed here to illustrate the monitoring of the changes of contact joints by means of the switching functions defined in the previous section. The physical parameters of the mechanism are the following ones:

$$\begin{aligned} m_2 = m_5 = m_7 &= 2.5 \text{ kg}, & m_3 = m_6 &= 5 \text{ kg}, & m_4 &= 1 \text{ kg}, \\ I_2 = 10^3 \text{ kgm}^2, & I_3 = I_6 = 20 \text{ kgm}^2, & I_5 = I_7 &= 15 \text{ kgm}^2, \\ \text{gravity acceleration, } g &= 9.81 \text{ m/sec}^2. \end{aligned}$$

a) Illustration of the changes of contact joints due to insufficient closing force

In the section 3.5 of the thesis, we have stated that the contact joint may be broken due to an insufficient contact force which is calculated by the application of the virtual displacement principle. Fig. 3.7-1 shows the different components of the calculated contact force in the contact joint C45 with the two static and dynamic contributions of the contact force. This analysis has been performed in case of an assumed plastic impact ($e=0$). When the rotation velocity of the crank equals 5 rad/sec (clockwise), the dynamic contact force is always larger than zero, which means that after the contact joint has been formed at time t_1 (here, the restitution coefficient is supposed to be zero), it always remains active during motion. From the Fig. 3.7-2, it can be seen that the action of the static force (static contribution) at the contact joint is larger than the negative action of the dynamic contribution, so that their composition (contact force) is larger than zero. Nevertheless, if the angular velocity ω increases to 8 rad/sec (clockwise), the negative action of the inertial forces becomes larger than the action of the gravity force. When it happens, the contact force vanishes and the contact joint will be broken. Fig. 3.7-2 shows that the contact is formed at time t_1 , is broken at time t_2 and is reformed again at time t_3 .

When the contact is active, the transition switching functions G_{T1} and G_{T2} pilot the change of contact element. Fig. 3.7-3 shows the total set of switching functions. The time t_1 and t_7 express the changes of contact joint due to interference (zero of G_{I1} switch). The times t_2 , t_3 , t_4 , t_6 , t_8 , and t_9 express the transition of the contacting elements of link L5 (zero of G_{I2} switch). The time t_5 shows the break of the contact joint due to the contact force (zero of G_{F1} switch). The resulting output motion of link L7 is shown in Fig. 3.7-4, which differs from the Fig. 2.6-4 by the break of the contact joint.

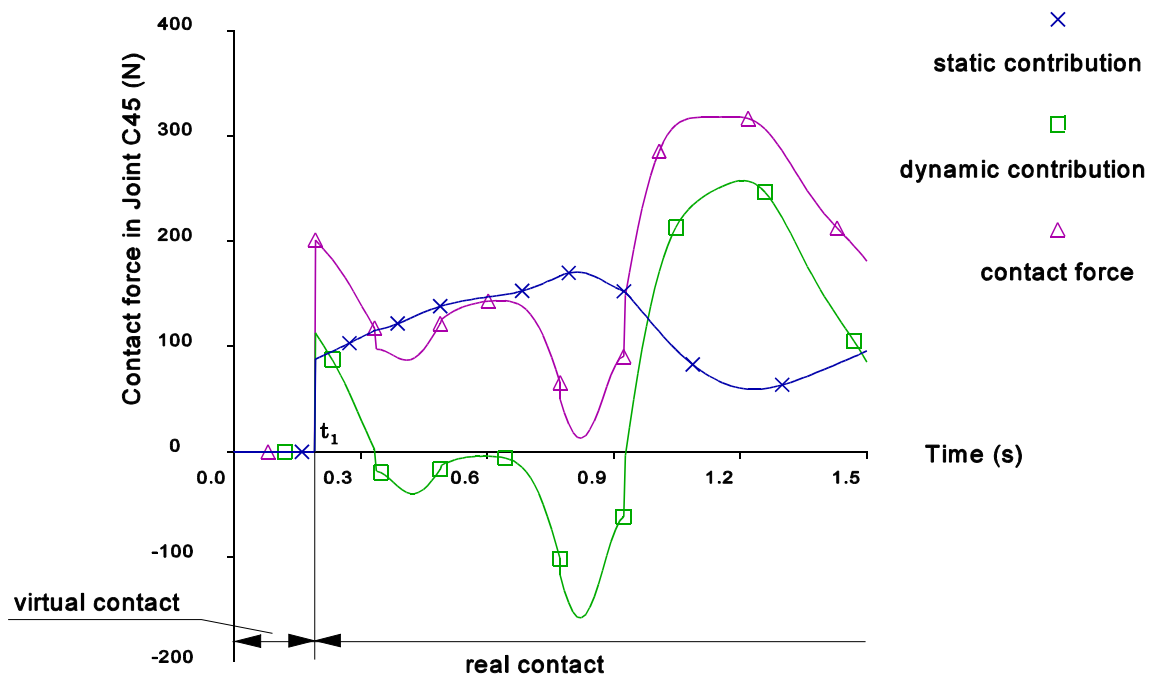


Fig. 3.7-1: Contact forces in the joint C45 when input speed, $\omega = -5 \text{ (rad/sec)}$

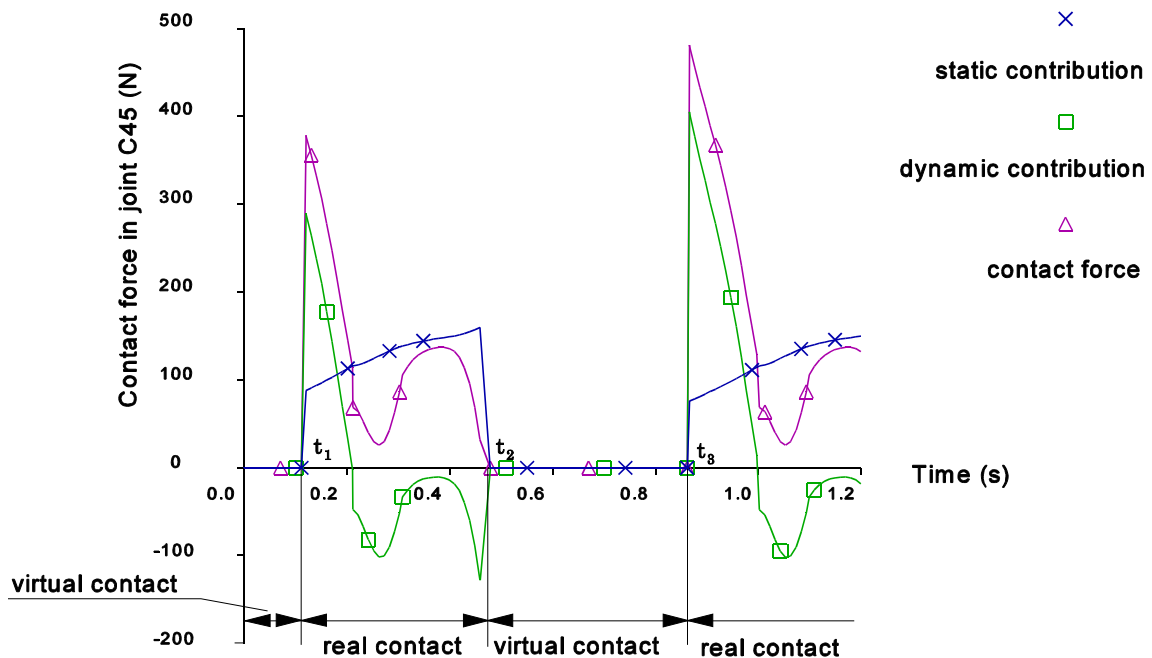
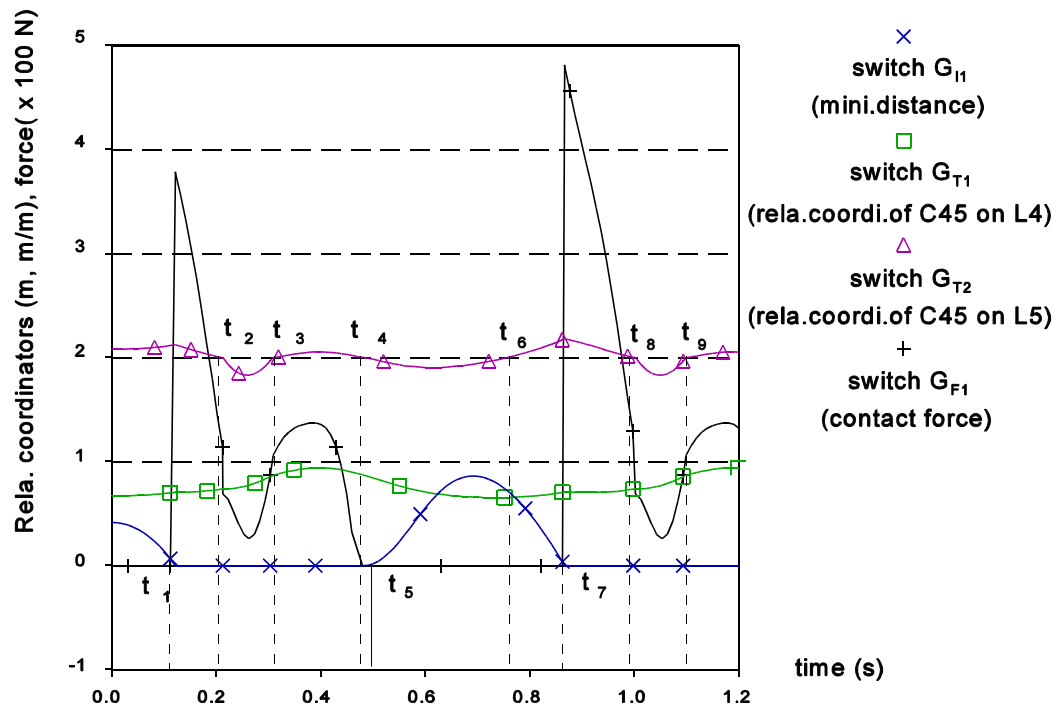
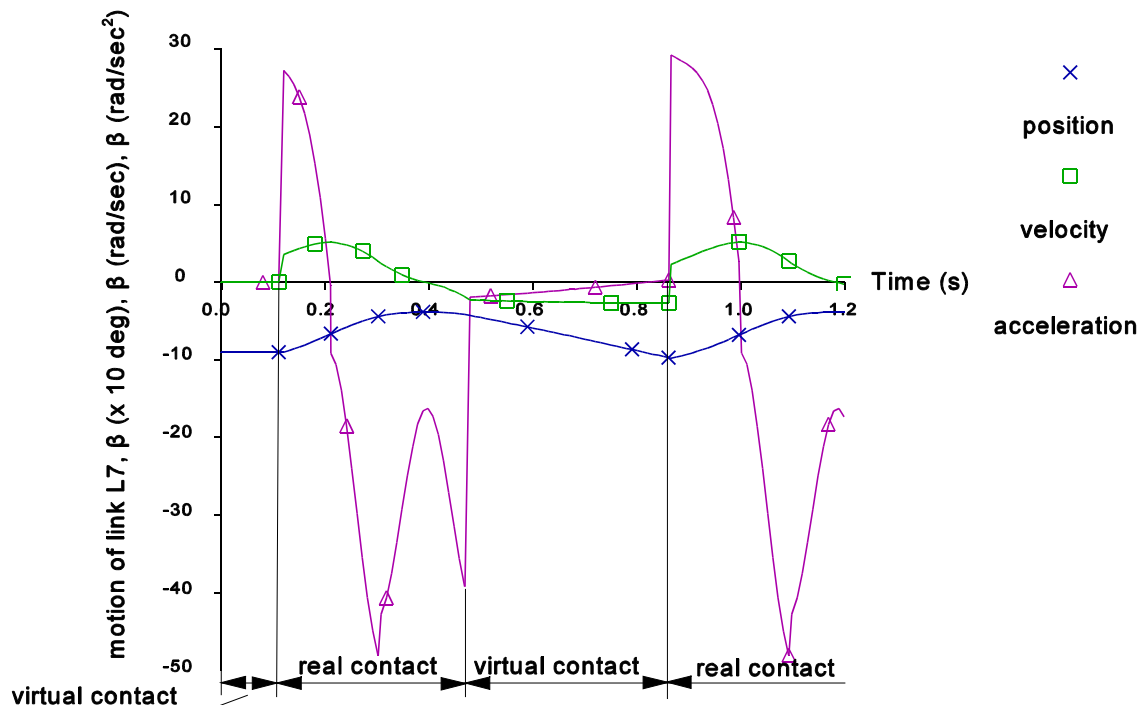


Fig. 3.7-2: Contact forces in the joint C45 mechanism when $\omega = -8 \text{ (rad/sec)}$



**Fig. 3.7-3: Switching functions, piloting the changes of the contact joints
($e=0, \omega=-8 \text{ rad/sec}$)**



**Fig. 3.7-4: Motion of L7: Dynamic simulation with
 $e=0$ and $\omega=-8 \text{ rad/sec}$**

The different phases of the simulation are listed in the following table 3.7-1.

Table 3.7-1: Different phases of the simulation for the mechanism of Fig. 2.6-1 ($e=0$)

discontinuous points	exact location(sec)	switch functions	physical meaning
t_1	0.1297	$G_{II}=0$	contact joint changes from virtual into real
t_2	0.2199	$G_{T2}=0$	contact surface changes from arc to point
t_3	0.3159	$G_{T2}=0$	contact surface changes from point to arc
t_4	0.4856	$G_{FI}=0$	contact joint changes from real into virtual
t_5	0.4951	$C_{T2}=0$	contact surface changes from arc to point
t_6	0.7557	$G_{T2}=0$	contact surface changes from point to arc
t_7	0.8702	$G_{II}=0$	contact joint changes from virtual into real
t_8	1.0053	$G_{T2}=0$	contact surface changes from arc to point
t_9	1.1009	$G_{T2}=0$	contact surface changes from point to arc

b) Changes of contact joints due to impact ($e \neq 0$)

A piecewise method is employed to analyse the velocity jumps due to impact. When the restitution coefficient does not equal zero, the contact joint is not formed just after interference. In practice, if the departing relative velocity is small (a conventional value of 10^{-3} m/s has been taken), the contact joint will be considered as formed. A restitution velocity switching function is used to trace the relative velocity just after impact. Fig. 3.7-5 shows the five switching functions used to detect the changes of contact joint. When the restitution coefficient does not equal zero ($e=0.2$, in this case), the contact joint is not directly formed at t_1 when the interference occurs (see the interference switch) because the relative velocity at that time does not equal zero (see the restitution velocity switch). After seven successive impacts, which are more and more closer each others, the contact will be considered as formed at t_2 , the relative velocity becoming less than the conventional tolerance 10^{-3} (see table 3.7-2).

Table 3.7-2: Departing velocities after impact

	impact time (sec)	departing velocity in C45(m/sec)
first impact	0.1297 (t_1)	1.4329
second impact	0.1864	0.2826

third impact	0.2027	0.0486
fourth impact	0.2070	0.0091
fifth impact	0.2083	0.0027
six impact	0.2085(t_2)	0.0007

The other switching points have the same meaning as in previous section. Fig. 3.7-6 shows the dynamic simulation results, which differs from fig. 3.7-4 owing to the non zero restitution coefficient. The different phases of the simulation are listed in table 3.7-3.

Table 3.7-3: Different phases of the simulation of the mechanism of Fig. 2.6-1 ($e=0.2$)

discontinuous points	exact location(sec)	switch functions	physical meaning
t_1	0.1297	$G_{II}=0$	interference between L4 and L5
t_2	0.2085	$G_{VI}=0$	contact joint changes from virtual into real
t_3	0.2202	$G_{T2}=0$	contact surface changes from arc to point
t_4	0.3161	$G_{T2}=0$	contact surface changes from point to arc
t_5	0.4861	$G_{FI}=0$	contact joint changes from real into virtual
t_6	0.4911	$C_{T2}=0$	contact surface changes from arc to point
t_7	0.7844	$G_{T2}=0$	contact surface changes from point to arc
t_8	0.8877	$G_{II}=0$	interference between L4 and L5
t_9	0.9912	$G_{VI}=0$	contact joint changes from virtual into real
t_{10}	1.0089	$G_{T2}=0$	contact surface changes from arc to point
t_{11}	1.1053	$G_{T2}=0$	contact surface changes from point to arc

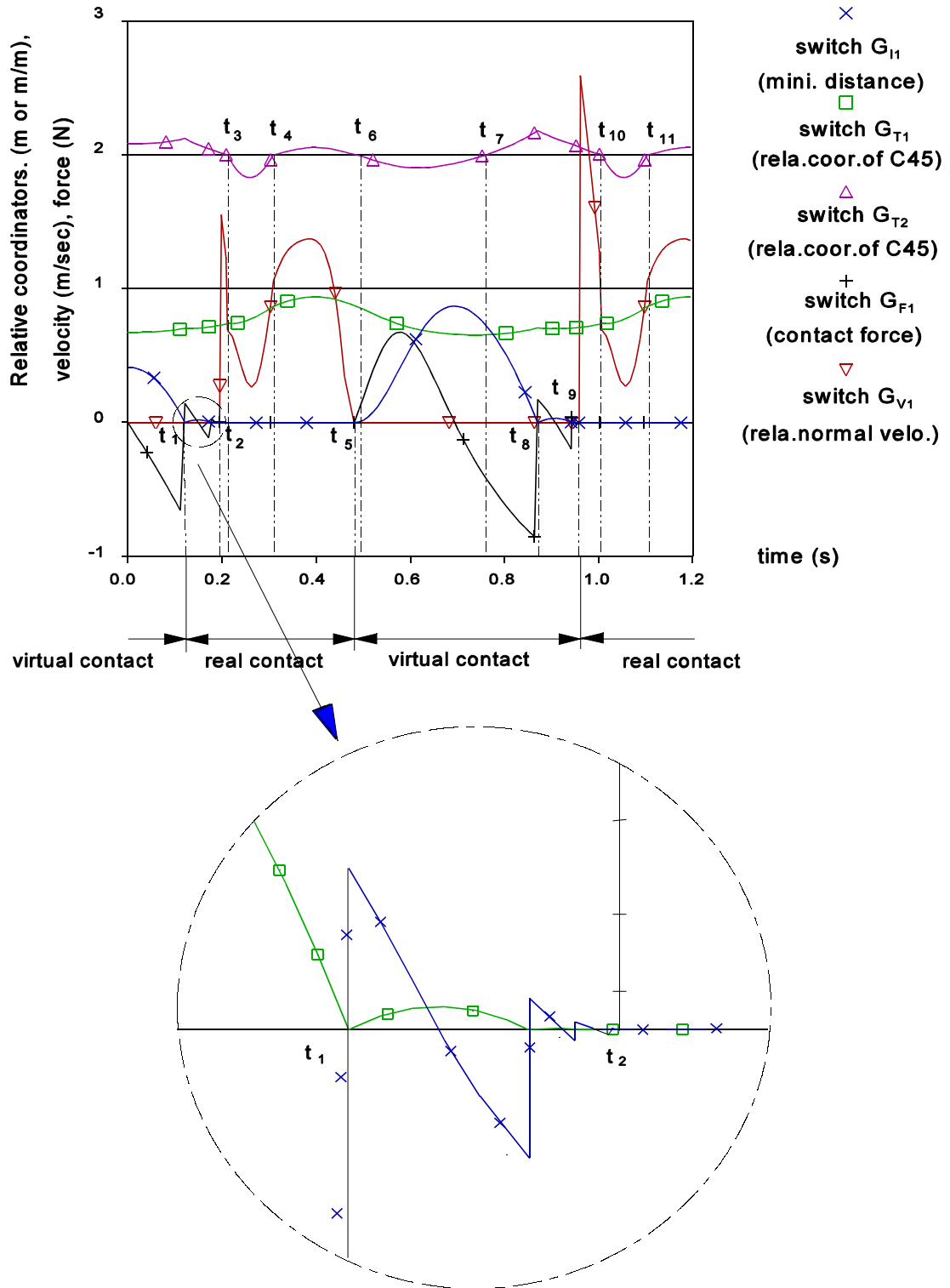


Fig. 3.7-5: Switching functions piloting the changes of the contact joint ($e=0.2, \omega=-8 \text{ rad/sec}$)

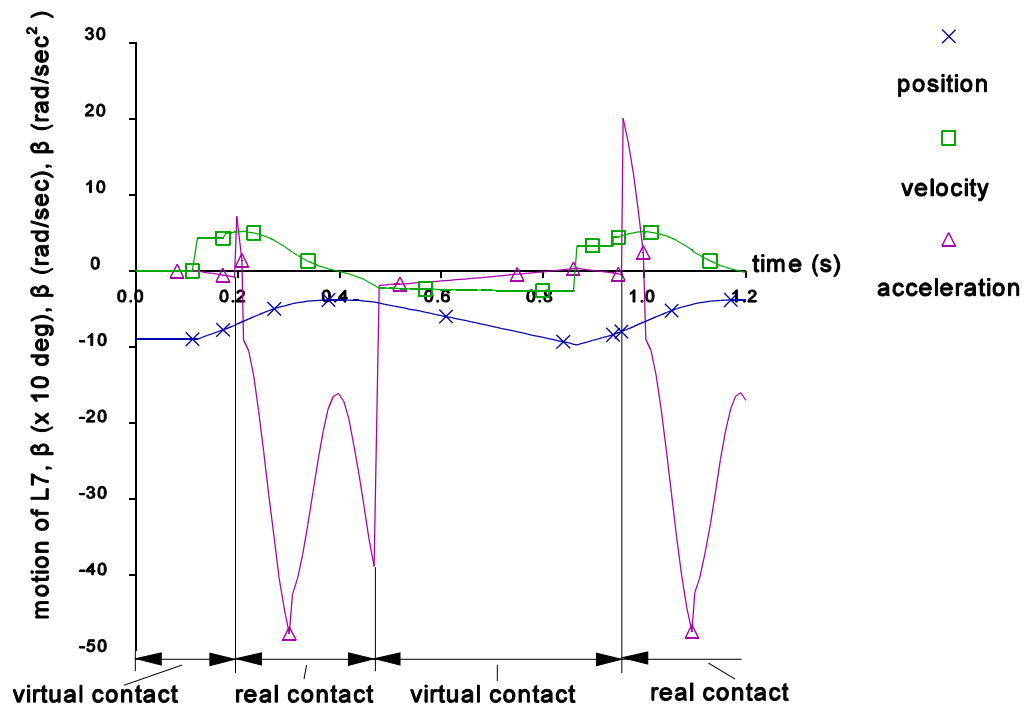


Fig. 3.7-6: motion of link 7 with $e=0.2$ and $\omega=-8 \text{ rad/sec}$

CHAPTER 4 - DESCRIPTION OF THE SOFTWARE AND EXAMPLES

4.1 Introduction

This chapter will first basically describe the ACDMC software using different procedures discussed in this thesis. The results obtained with three examples will then be presented. The first two examples are used to validate the simulation method. The last one illustrates an industrial application of mechanical systems with changing contact joints.

The first example is a simple cam-follower mechanism. The contact surface of the cam is formed by a set of continuous polynomials, so that the simulation results can be easily verified by the results obtained by ADAMS software (version 7.0) [49]. The second example is a cam-follower mechanism whose form is composed by a series of geometric elements. The simulation results will be confronted to a hand written explicit solution obtained at some particular positions. The last example is a sear-trigger mechanism of an automatic machine-gun.

4.2 Description of the ACDMC software

ACDMC stands for "Analyse Cinématique et Dynamique des Mécanismes avec liaisons de Contact" (kinematic and dynamic simulation of mechanisms with contact joints), which is an extension of ACMC (Analyse Cinématique des Mécanismes avec liaisons de Contact) developed in 1988 at the FPMs [50].

This software is a general purpose computer code suitable for the kinematic and dynamic simulation of mechanical systems containing rigid bodies, articular joints and changing contact joints. The contact surfaces consist of simple geometric elements, such as point, line segment, circle arc, circle and polynomials. It has been written in Turbo Pascal language (version 7.0) and approximately contains 300 procedures and functions. It is structured in the modular form illustrated in Fig. 4.2-1.

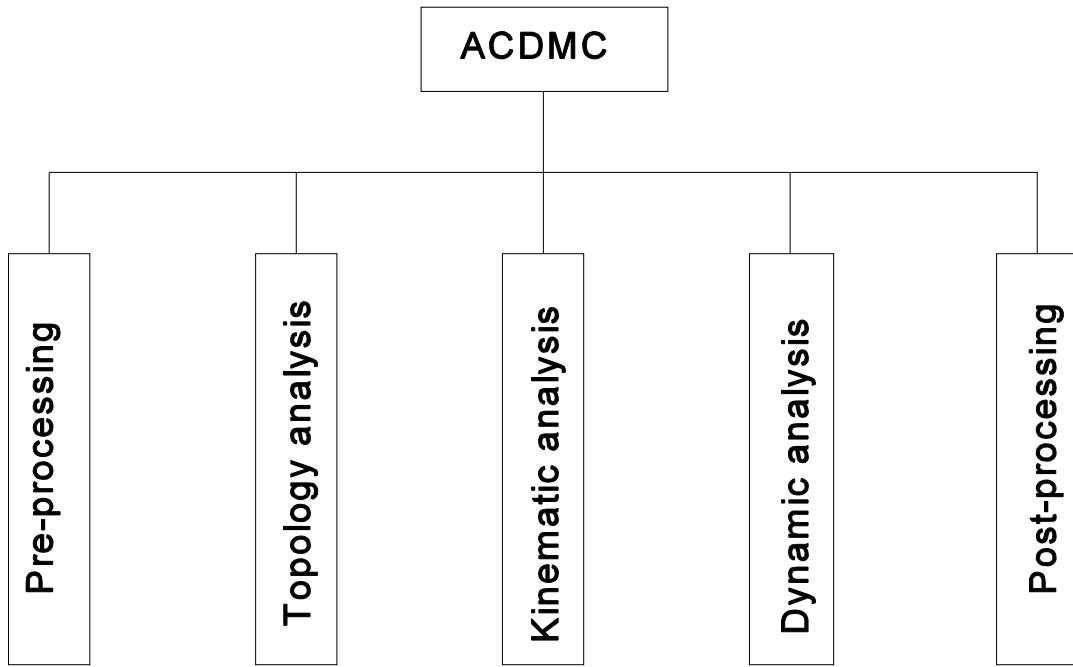


Fig. 4.2-1: Main functions of ACDMC software

The main functions of ACDMC software include the following action:

CREATE: interactive creation of the data file <name>.DYN to describe the mechanism,
INPUT: loading of an exit data file <name>.DYN.

TOPO: topology analysis
INITI: kinematic analysis and calculation of the initial position of the system,
DRIVE: definition of the independent variables (if wished by the user),
DYNA: dynamic simulation
ANIMA: animation of the mechanical system.

The principal options of the program are directly related to the material developed in the thesis.

The mechanical systems analysed with the ACDMC software are composed by rigid bodies interconnected by either classic or changing contact joints, and eventually subjected to the action of force elements like springs, dampers or external applied forces.

The inertial characteristics of the bodies, the local coordinates of the frames used to define the joints and the nature of the joints, are described in an input file (<name>.DYN), by means of a user- syntax based on self-explaining keywords (see Appendix D). The external effects, the force elements, the initial conditions and the simulation options are also defined in that style.

Concerning the contact joints, corresponding contact surfaces are given as a succession of graphic curves, chosen among five basic types: points, lines, arcs, circles and polynomials. The flowchart relative to an integration step in ACDMC is illustrated in Fig. (4.2-3).

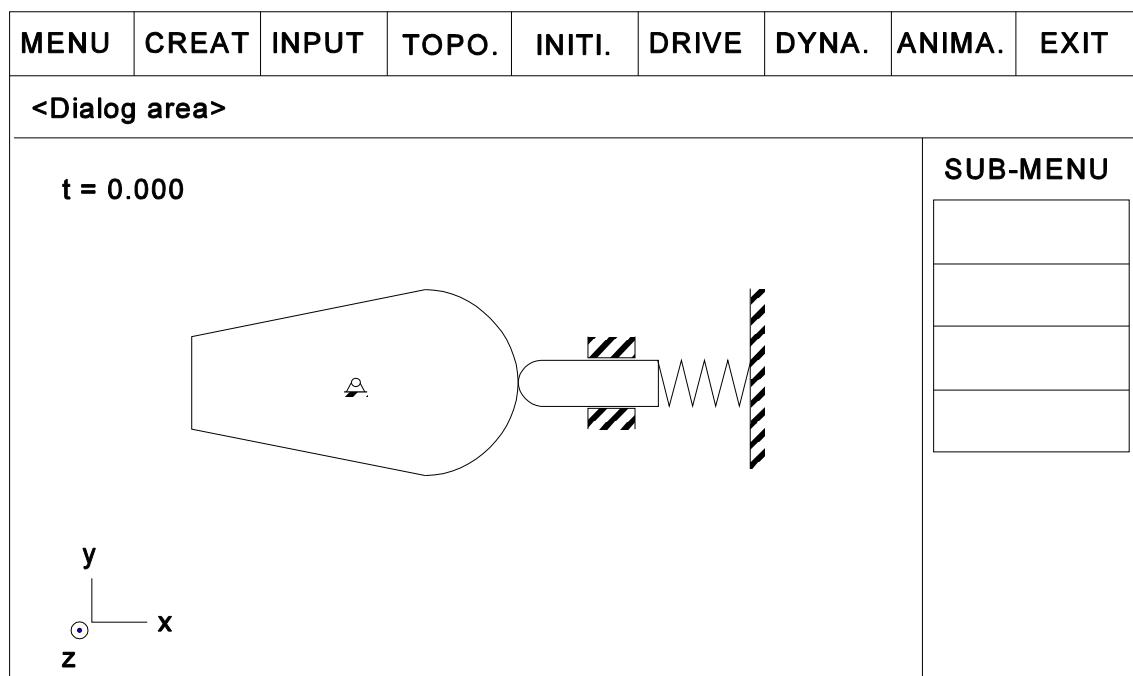


Fig. 4.2-2: Screen appearance of ACDMC software

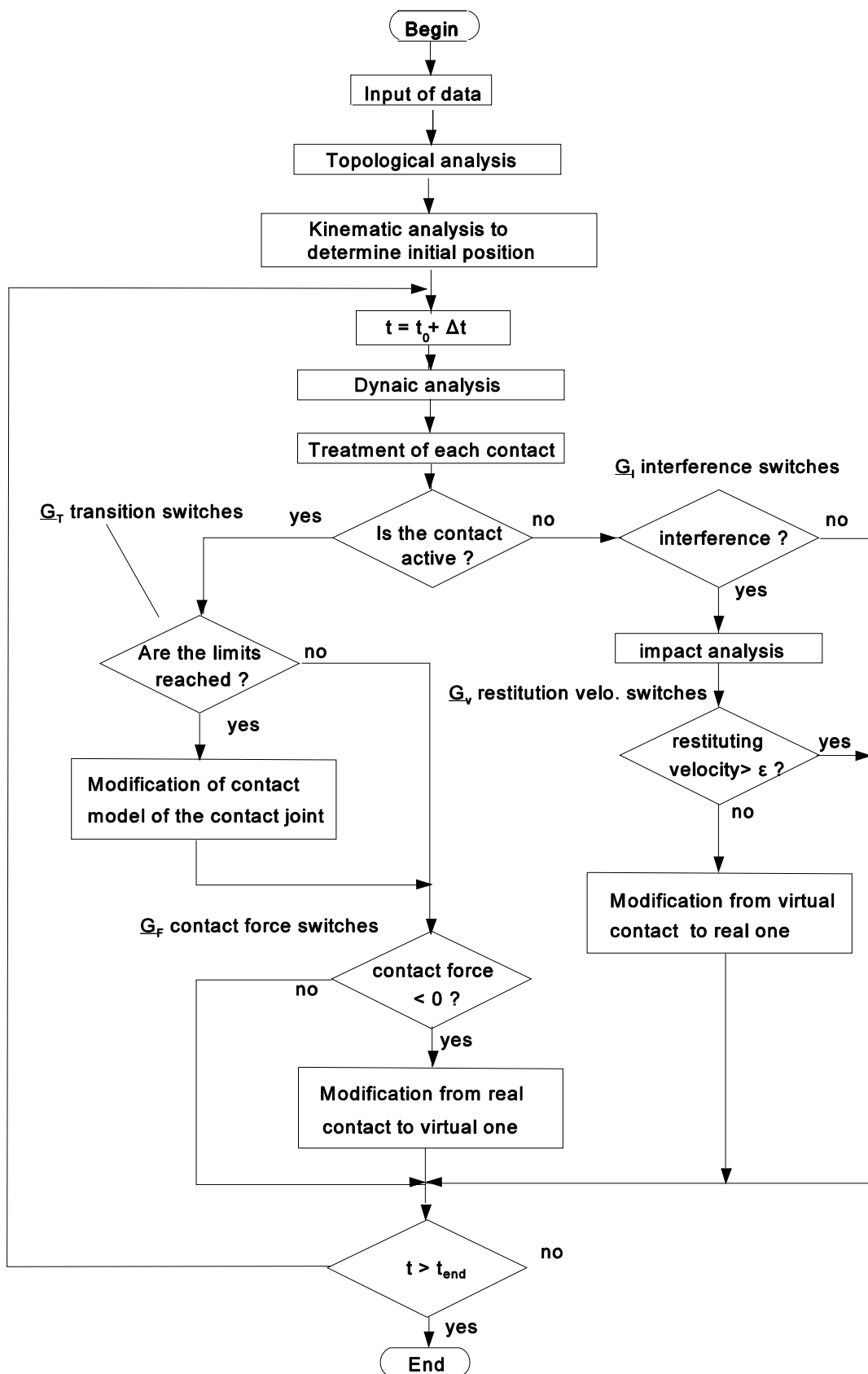


Fig. 4.2-3: flowchart of the ACDMC software

4.3 Simple cam-follower mechanism with a profile composed by a succession of polynomial curve lines

The dynamic behaviour of a cam-follower (see Fig. 4.3-1) is treated with the ACDMC software. The obtained results will be compared with those obtained by the well-known commercial ADAMS software (Automatic Dynamic Analysis of Mechanical Systems [49]). The appendix D shows the code used to describe the mechanism either with ACDMC or with ADAMS software.

The considered cam mechanism (Fig. 4.3-1) is composed by a translational follower and a cam whose shape is formed by a succession of polynomial curvilinear without discontinuities between each curve. A spring applies on the follower the necessary force to impose the contact. The contacting surface of the cam is formed by a series of polynomial curvilinear (see table 4.3-1). The main data are the following ones:

-- Dimension

$$r = 5 \text{ mm}, \quad L_1 = 45 \text{ mm}, \quad L_2 = 100 \text{ mm}, \quad L_3 = 150 \text{ mm}$$

$$\rho = (\text{see table 4.3-1}).$$

-- Inertial properties:

$$I_2 = 10^4 \text{ kg-mm} \quad m_3 = 0.5 \text{ kg}$$

-- Spring characteristics:

$$\text{stiffness} \quad k = 5 \text{ N/mm}$$

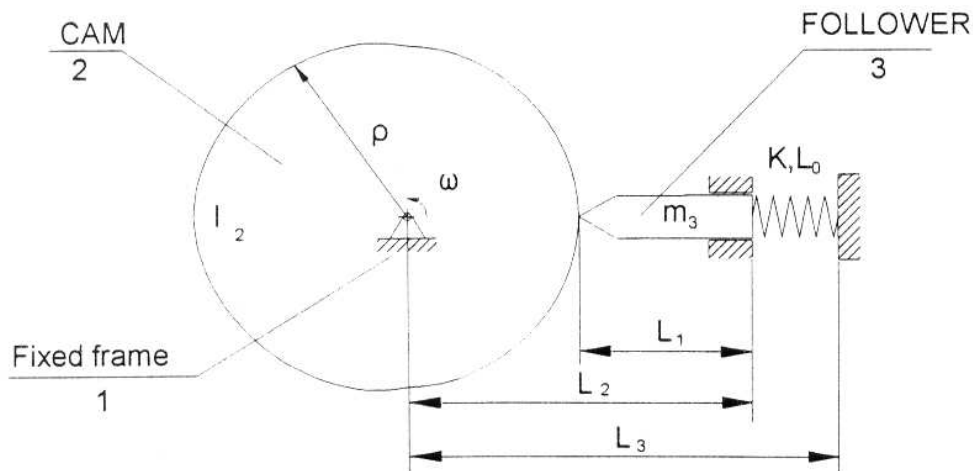


Fig. 4.3-1: Cam-follower mechanism

Natural length $L_0 = 100 \text{ mm}$.

-- Initial velocity of the cam:

$$\omega_0 = 5 \text{ (rad/sec)}$$

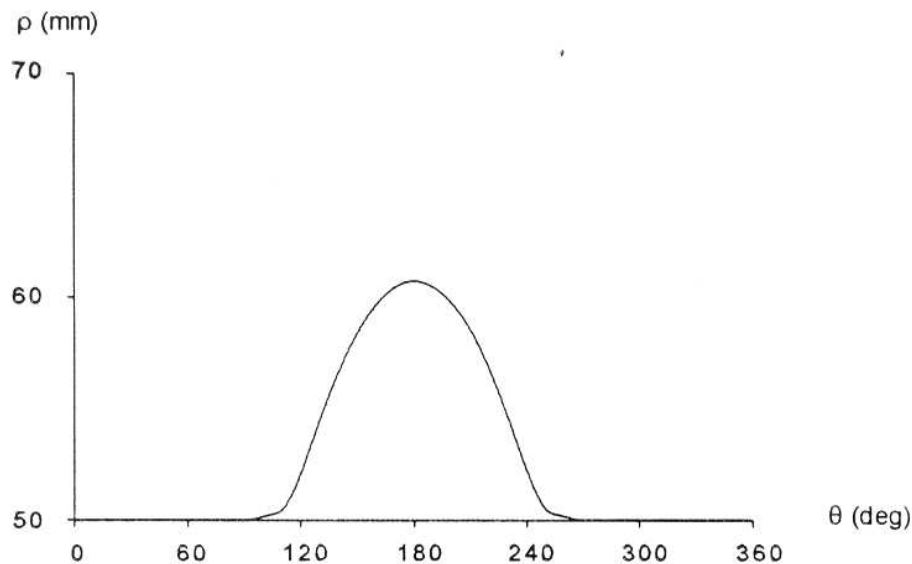


Fig. 4.3-2: Profile of the cam

The geometric characteristics of the cam profile are detailed in fig. 4.3-2 and table 4.3-1, in terms of polar coordinates*.

The time evolution of the displacement, velocity and acceleration of the follower are shown respectively on Fig. 4.3-3 to 4.3-5. The contact force is also given in Fig. 4.3-6.

In all figures, the results of ACDMC and ADAMS software show an excellent agreement.

* The details of this basic example have been received from Prof. M. Geradin, University of Liege, that we thank here.

Table 4.3-1: Polynomial function of the cam

$0^\circ < \theta < 90^\circ$	$\rho = \rho_0 = 50 \text{ (mm)}$
$90^\circ < \theta < 95^\circ$	$\rho = \rho_0 + 0.0008 * (\theta - 90^\circ)^3 - 0.00008 * (\theta - 90^\circ)^4$
$95^\circ < \theta < 105^\circ$	$\rho = \rho_0 - 0.05 + 0.02 * (\theta - 90^\circ)$
$105^\circ < \theta < 255^\circ$	$\rho = \rho_0 + 10.71475 - 14.0625 * \left(\frac{\theta - 180^\circ}{75}\right)^2 + 7.7344 * \left(\frac{\theta - 180^\circ}{75}\right)^{12} - 4.1367 * \left(\frac{\theta - 180^\circ}{75}\right)^1$
$255^\circ < \theta < 265^\circ$	$\rho = \rho_0 - 0.05 - 0.02 * (\theta - 270^\circ)$
$265^\circ < \theta < 270^\circ$	$\rho = \rho_0 - 0.0008 * (\theta - 270^\circ)^3 - 0.00008 * (\theta - 270^\circ)^4$
$270^\circ < \theta < 360^\circ$	$\rho = \rho_c$

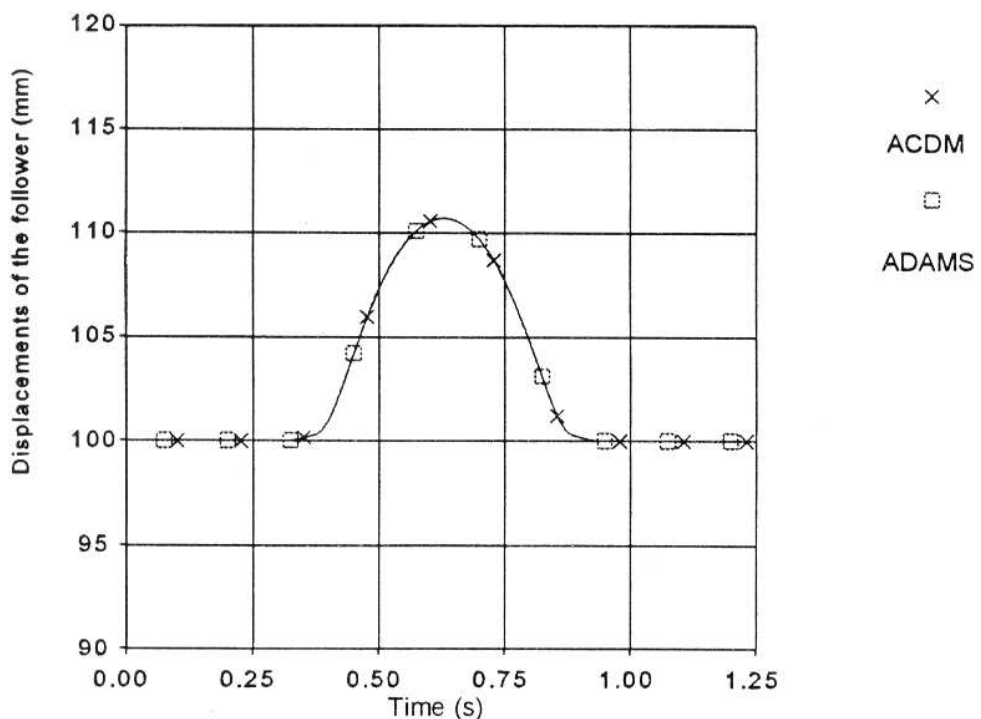


Fig. 4.3-3: Position analysis of the cam-follower mechanism of Fig. 4.3-1

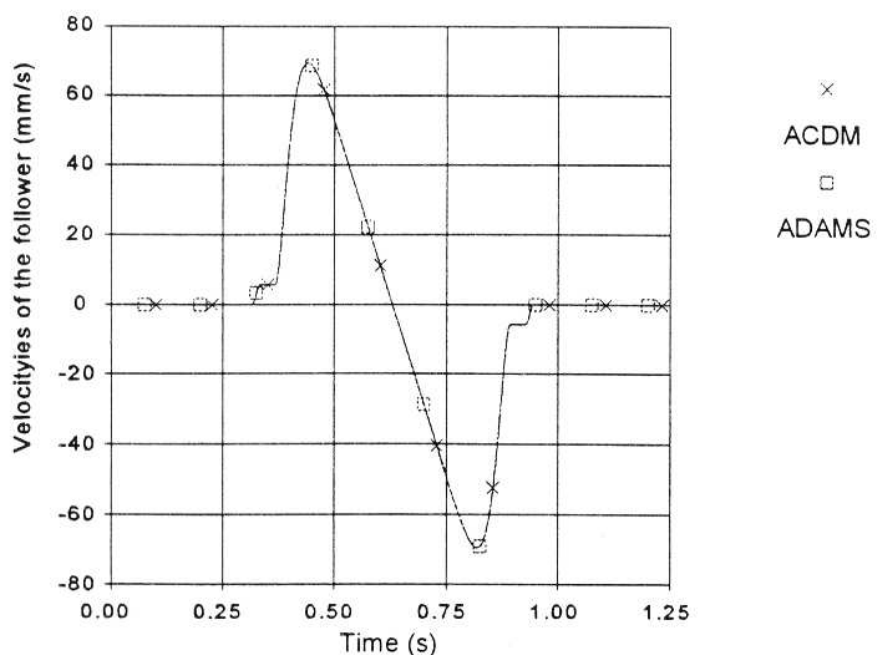


Fig. 4.3-4: Velocity analysis of the cam-follower mechanism of Fig. 4.3-1

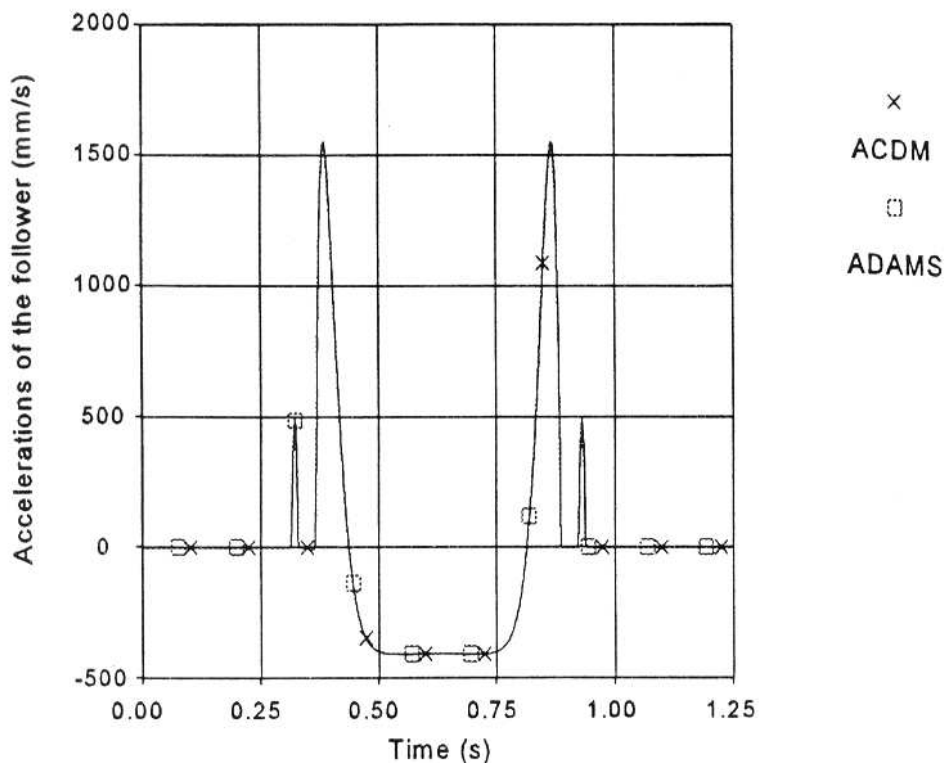


Fig. 4.3-5: Acceleration analysis of the cam-follower mechanism of Fig. 4.3-1

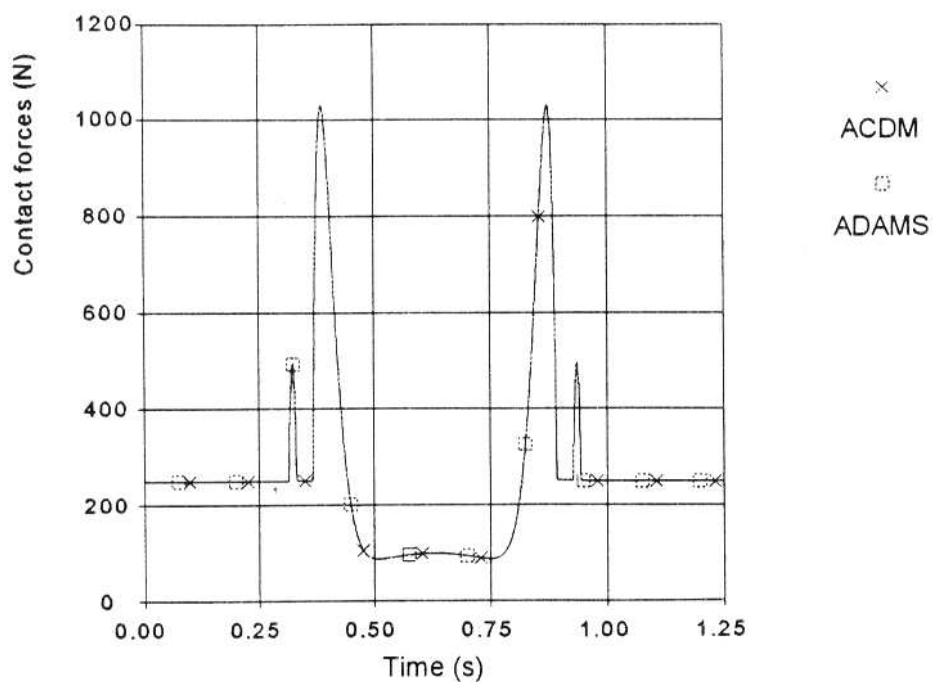
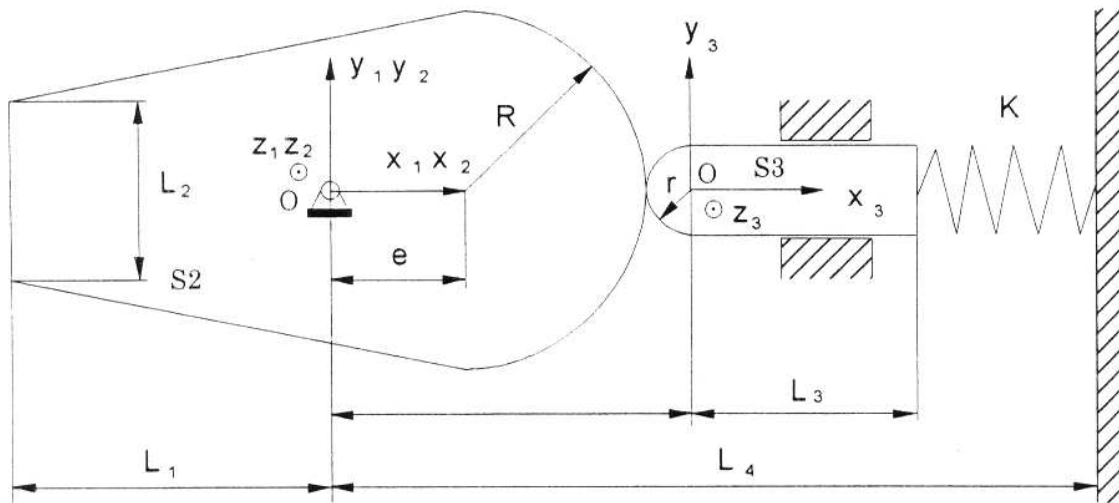


Fig. 4.3-6: Contact force analysis of the cam-follower mechanism of Fig. 4.3-1

4.4 Cam-follower mechanism with a profile composed by a series of geometric elements

A typical cam mechanism with a profile composed by a series of geometric elements is used, in order to validate the results obtained by the ADCMC software, by comparing them with an explicit handwritten solution at some particular instants. In order to trace the evolution of the contact, the surface of the cam is divided into the following basic elements (see Fig. 4.4-2): arc A-B, point B-C, line C-D, point D-E, line E-F, point F-G, line G-H, point H-I, arc I-A.



$$R = 20 \text{ cm}, \quad r = 5 \text{ cm}, \quad e = 15 \text{ cm}, \\ L_1 = 20 \text{ cm}, \quad L_2 = 35 \text{ cm}, \quad L_3 = 30 \text{ cm}, \quad L_4 = 90 \text{ cm}$$

Fig. 4.4-1: Cam-follower mechanism with a profile composed by a series of geometric elements

The main data describing this mechanism are listed below:

-- Dimension and geometric characteristics:

$$R = 20 \text{ cm}, \quad r = 5 \text{ cm}, \quad e = 15 \text{ cm}, \\ L_1 = 20 \text{ cm}, \quad L_2 = 35 \text{ cm}, \quad L_3 = 30 \text{ cm}, \quad L_4 = 90 \text{ cm}.$$

-- Inertial data:

$$m_3 = 0.15 \text{ kg}, \quad I_2 = 10^6 \text{ kg}\cdot\text{cm}^2.$$

-- Spring characteristics:

spring stiffness $k = 1.5 \text{ N/cm}$ or 0.35 N/cm ,
natural length $l_0 = 70 \text{ cm}$.

-- Initial angular velocity of a cam is assumed to be equal to:

$$\omega_1 = 0.5 \text{ (radian/s)}$$

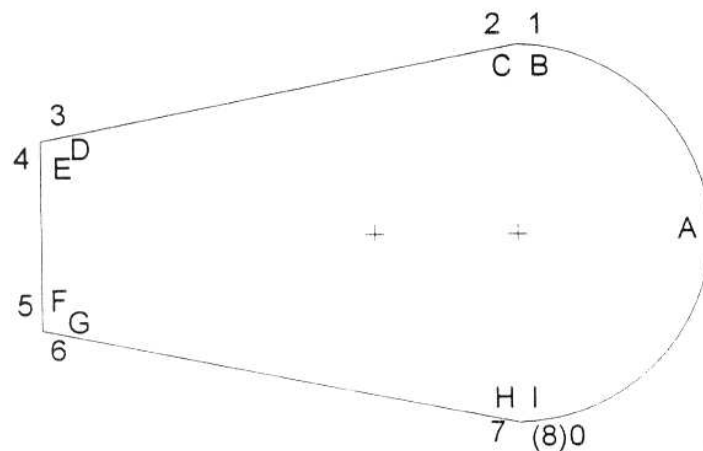


Fig. 4.4-2: Relative curvilinear coordinate and the mark of different contact elements for a cam with complex contact surfaces

The contact variables directly show the evolution during motion of the contacting point on the surface either of the cam or the follower (see Fig. 4.4-3).

The results presented in Fig. (4.4-4) to (4.4-7) show the evolution of the position, velocity and acceleration of the follower and the contact force between the cam and follower at different instants (with a stiffness constant = 1.5 N/cm). The contact force (Fig. 4.4-7) is in this case always positive, which means that the contact between cam and follower is always active.

In this example, the inertia of the cam has been voluntarily defined large, so that the rotation velocity of the cam can be considered as constant. In that case, it is possible to derive by hand a set of explicit motion equations, completely developed in appendix C, yielding results that can be confronted to the ones obtained by the ACDMC software at particular instants. The comparison is listed in table 4.4-1 where ρ and F_{CD} respectively refer to the radius of the cam at some specific contact points and the contact force between cam and follower. Only minor differences can be observed, due principally to the probable fluctuation in the cam velocity.

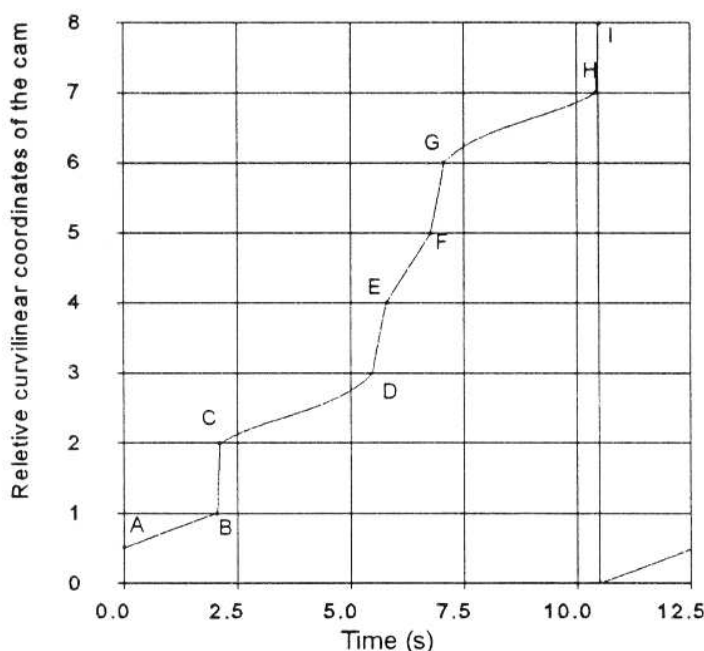


Fig. 4.4-3: Contacting position analysis of the cam-follower mechanism of Fig. 4.4-1 ($k=1.5\text{N/cm}$)

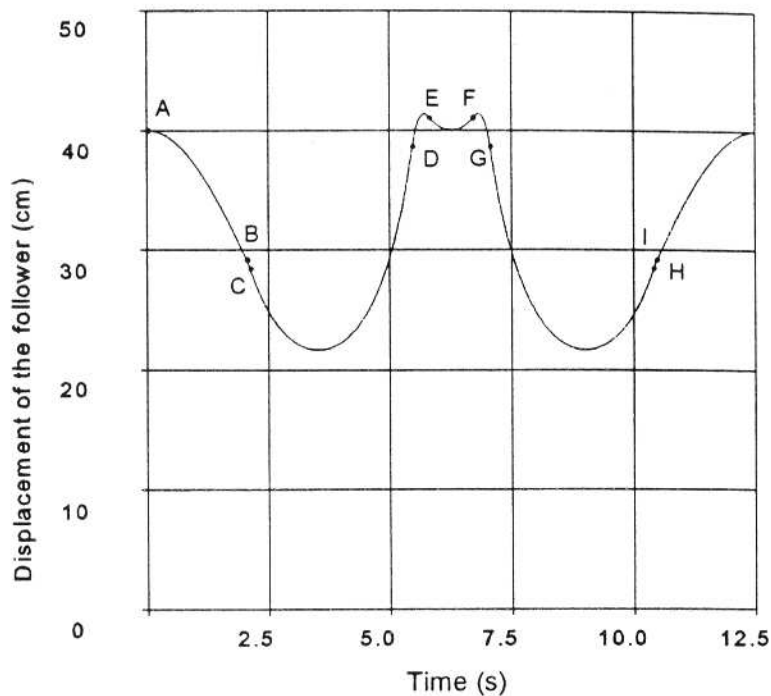


Fig. 4.4-4: Position analysis of the cam-follower mechanism of Fig. 4.4-1 ($k=1.5\text{N/cm}$)

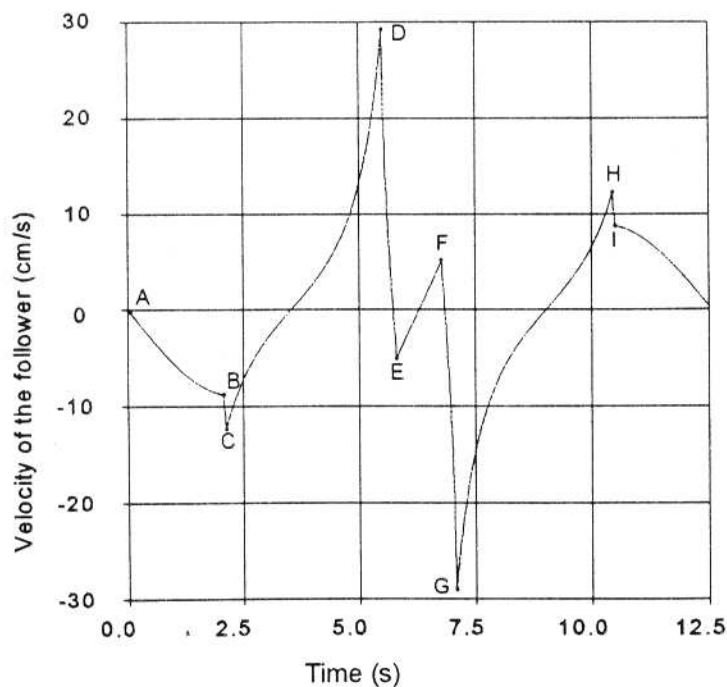


Fig. 4.4.5: Velocity analysis of a cam-follower mechanism of Fig. 4.4-1 ($k=1.5\text{N/cm}$)

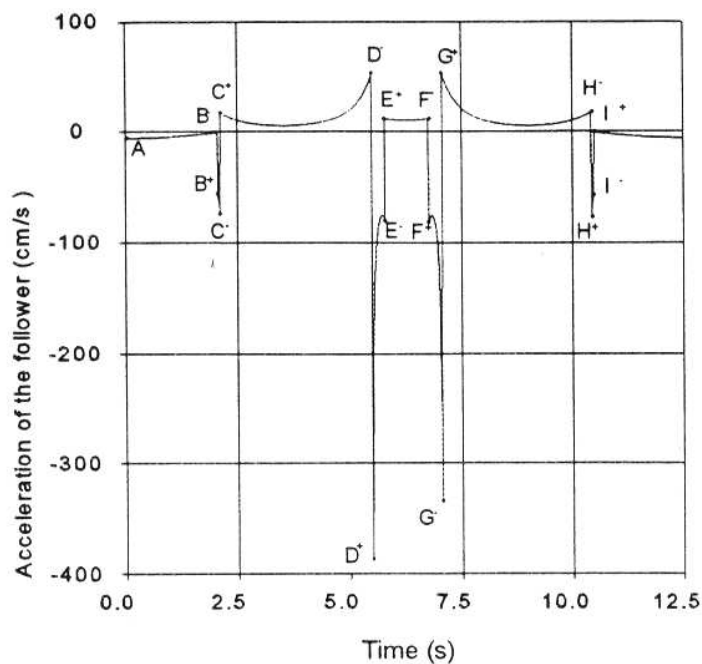


Fig. 4.4-6: Acceleration analysis of the cam-follower mechanism of Fig. 4.4-1 ($k=1.5 \text{ N/cm}$)

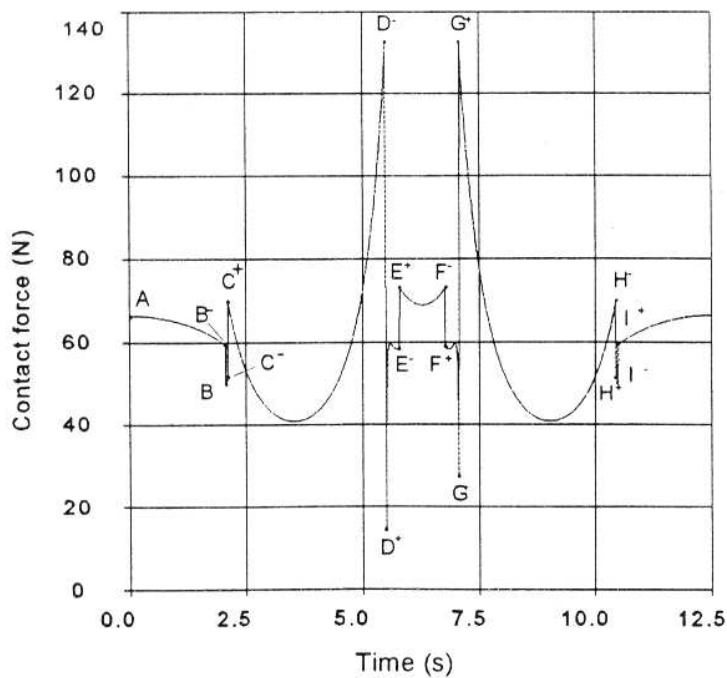


Fig. 4.4-7: Contact force evolution of the cam-follower mechanism of Fig. 4.4-1 ($k=1.5 \text{ N/cm}$)

Table 4.4-1: Comparison of simulation results

	ACDMC software	Explicit Equ.	Tolerance
ρ_A	40.0000	40.0000	0
$\dot{\rho}_A$	0.0000	0.0000	0
$\ddot{\rho}_A$	-6.0000	-6.0000	0
$(F_{CD})_A$	66.6000	66.6000	0
ρ_B	29.1525	29.1548	10^{-4}
$\dot{\rho}_B$	-8.7355	-8.7464	10^{-3}
$\ddot{\rho}_B$	-0.9797	-0.9430	10^{-1}
$\ddot{\rho}_B^+$	-55.2226	-54.8490	10^{-2}
$(F_{CD})_{B^-}$	59.3609	59.5817	10^{-2}
$(F_{CD})_{B^+}$	50.0971	50.1520	10^{-2}
ρ_c	28.5700	28.5779	10^{-4}
$\dot{\rho}_c$	-12.3133	-12.3019	10^{-3}
$\ddot{\rho}_c$	-73.1315	-74.1643	10^{-1}
$\ddot{\rho}_c^+$	17.7606	17.7050	10^{-2}
$(F_{CD})_{C^-}$	51.1256	51.7518	10^{-2}
$(F_{CD})_{C^+}$	69.9381	69.9251	10^{-2}

If the stiffness of the spring however decreases from $k=1.5\text{N/cm}$ to $k=0.35\text{ N/cm}$, the contact force will vanish and the contact between cam and follower will disappear momentarily (see Fig. 4.4-8). Fig. (4.4-9) shows the time evolution of the contact variables with this new stiffness value (dotted line relates to broken contact). The motion of the follower is also affected by the contact breaks and successive interferences, as shown in Fig. (4.4-10) - (4.4-13).

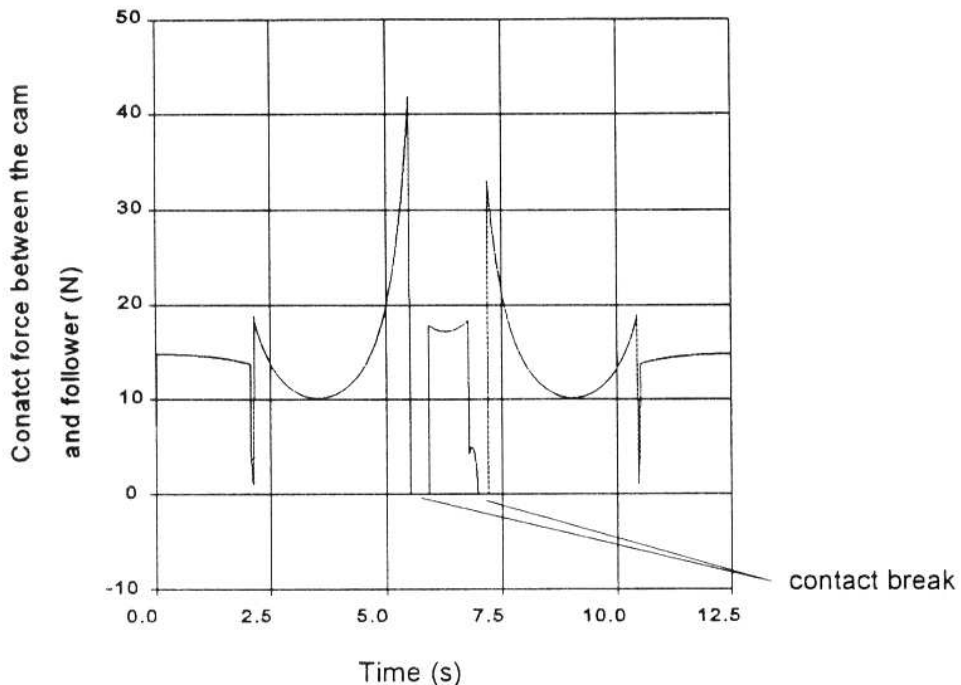


Fig. 4.4-8: Contact force evolution of the cam-follower mechanism of Fig. 4.4-1 ($k=0.35\text{N/cm}$)

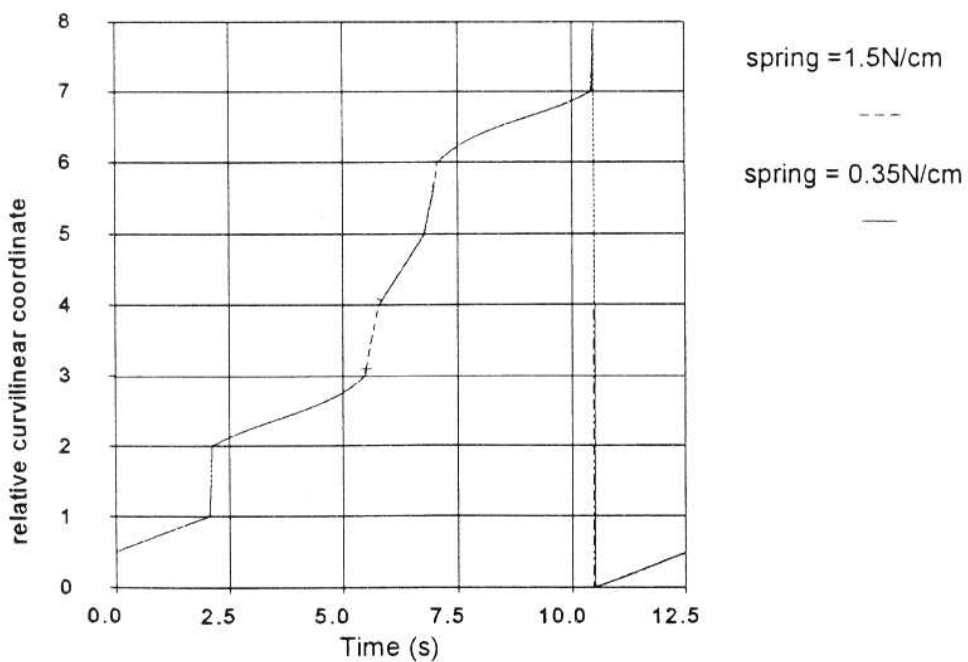


Fig. 4.4-9: Evolution of the follower position

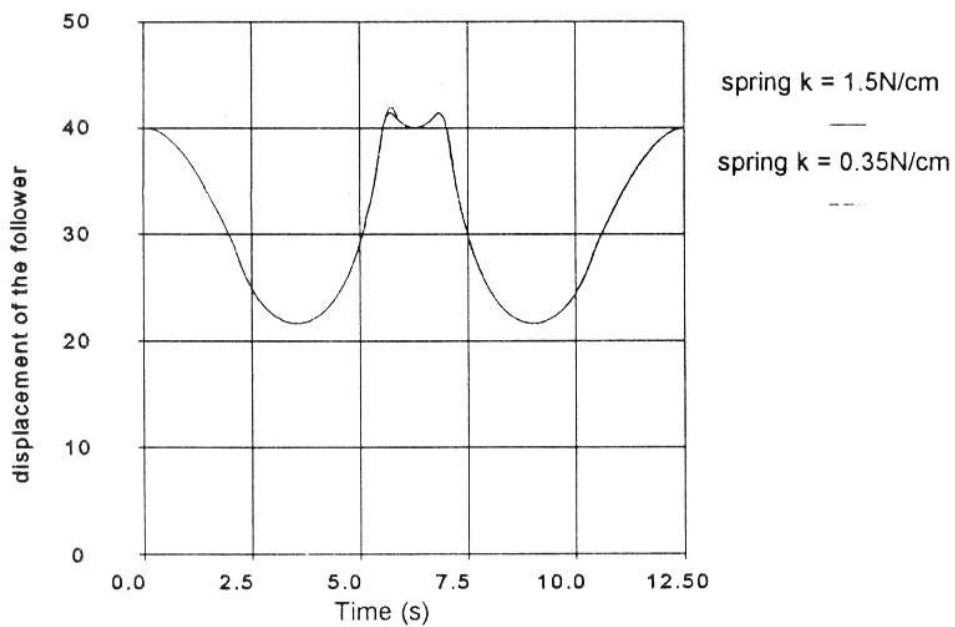


Fig. 4.4-10: Evolution of the follower position

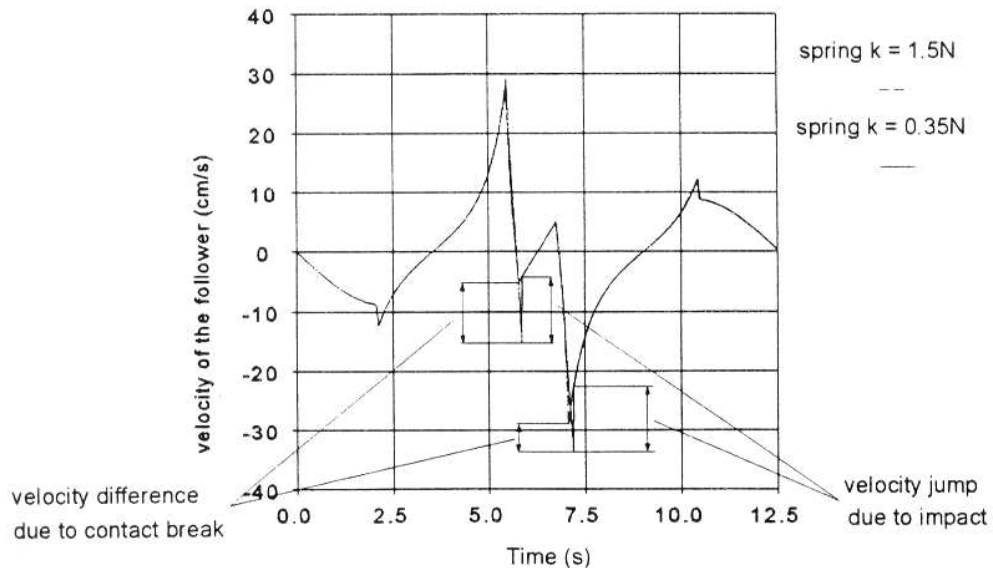


Fig. 4.4-11: Evolution of the follower velocity

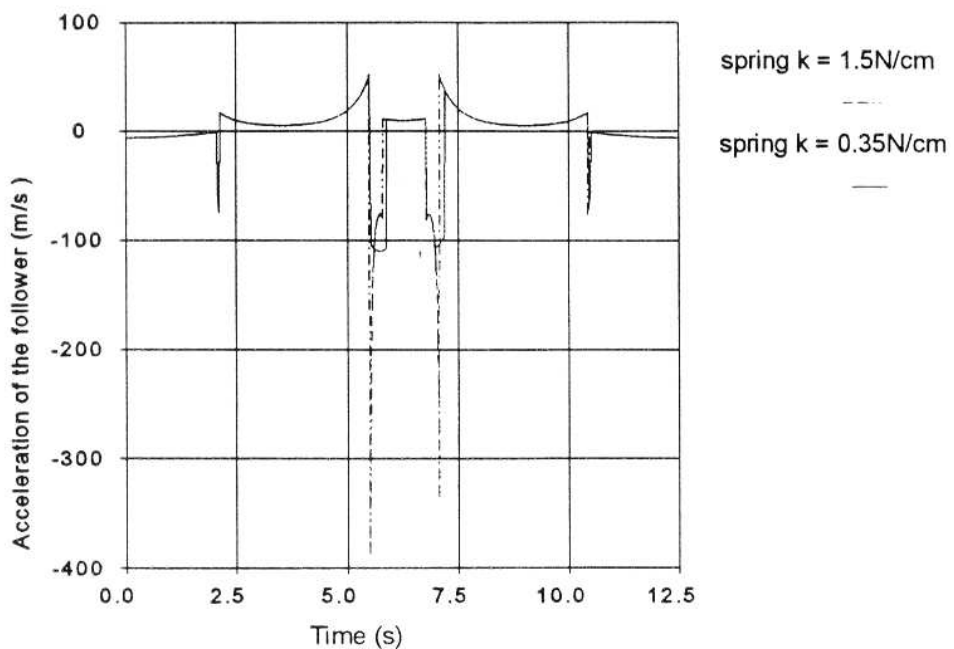


Fig. 4.4-12: Evolution of the follower acceleration

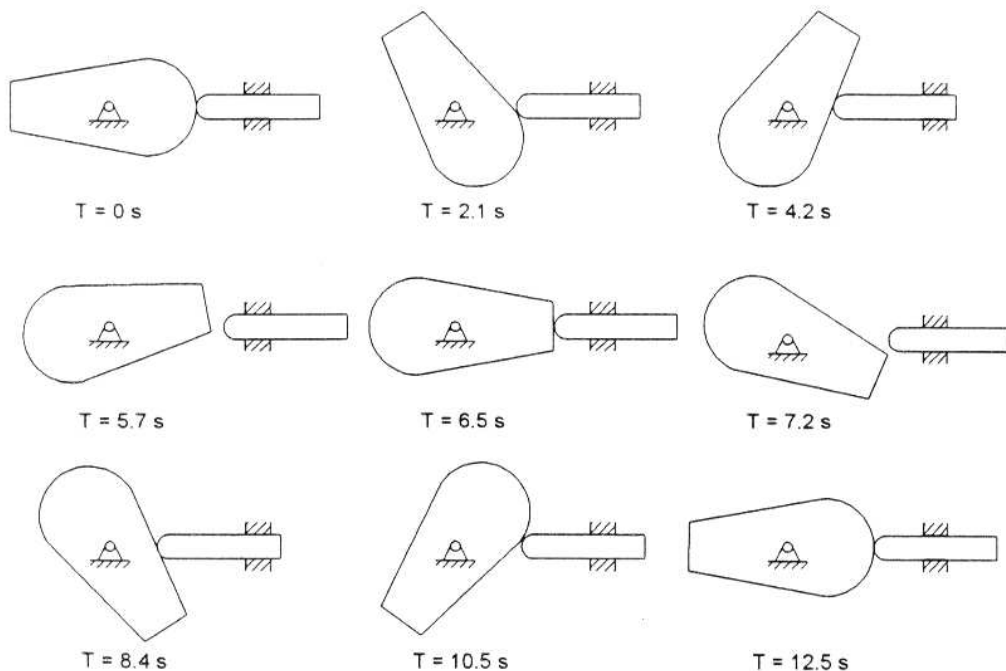


Fig. 4.4-13: Dynamic simulation of the cam-follower mechanism of Fig. 4.4-1 ($k=0.35\text{N/cm}$)

4.5 Trigger mechanism of an automatic machine-gun

The sear and trigger mechanism of an automatic machine-gun can be considered as a typical complex industrial example of a multibody system with changing contact joints. The purpose of this mechanism is to execute the different functions of the firing cycle.

The sear and trigger mechanism of a machine-gun considered in this thesis (Fig. 4.5-3) consists of six main components. The central part of this mechanism is the lower slide body L6, which can be animated of a translational motion along the DE axis, which has to be blocked in the stopping fire position, and to move freely in the automatic fire position. To ensure this blocking or deblocking, a series of cams and links which move with respect to the body trigger frame. The sear L2 can rotate about the A axis with respect to the body trigger L3, the tripping lever L4 about the B axis and the plunger tripping lever L5 about the C axis. These rotating bodies are drawn back to their positions by springs (not presented in Figure 4.5-3). Except the trigger, which is driven by an external force, all links are driven by an external couple.

When a couple acts on the trigger body L3, the trigger rotates and drives the sear L2 to deblock the lower slide body L6: the gun begins to fire. Meanwhile, the sear rotates down. The tripping lever blocks the sear due to the action of the spring, so that the lower slide body can move freely, being deblocked. This corresponds to the automatic fire stage. If the driving couple on the trigger body is suppressed, the sear rotates up due to the action of the spring. The lower slide body (L6) drives the tripping lever L4 to unblock the sear L2: the sear then locks the lower slide body and firing is stopped. Fig. (4.5-3), (4.5-4) and (4.5-5) illustrate the three basic different stages of the working cycle of the mechanism.

The topology analysis of the trigger mechanism has been presented in section 2.2. The contacts between bodies frequently change during operation. Some contact joints will appear at some time and disappear at another time, depending on the contact forces, and the interferences between the moving bodies. Taking advantage of the concept of virtual contact joints, the topology remains unchanged during motion. When a contact joint is broken, the contact joint is changed into a virtual one (expressed by dot line) and vice versa in case of interference, when a virtual loop is changed into a real one. Nine different forms of the topologies of the trigger mechanism are shown in Fig. 4.5-2, where dotted lines express the virtual loops. Fig. (4.5-7) illustrates the corresponding geometry of the trigger mechanism for each stage

These different stages are caused by the changes induced by five contact joints, C23 (between the sear and trigger body), C24 (between the sear and tripping lever), C26 (between the sear and lower slide body), C45 (between tripping lever and plunger tripping) and C65 (between lower slide body and plunger tripping lever). If a contact joint is active, the arc line (standing for the contact joint) is expressed by a solid line. Otherwise, it is expressed by a dot line. At stage 1, C26 has two contact points, which means the lower slide body is blocked (at a rest stage). In the same way, at stages 5, 6 and 7, the contact joint C24 has two contact points, which means the sear is blocked (at rest stages).

The data of this example have been obtained from the FN Company at Herstal.

An example of the simulation results concerning the contact joint C24 is illustrated in Fig. 4.5-9. This contact joint concerns curve elements of the sear and the tripping lever. Lines and arcs composing those curve elements and the associated relative coordinates are described in Fig. 4.5-8. The evolution during motion of the relative coordinates of the contact joint are shown in Fig. 4.5-9, the corresponding configuration being illustrated in Fig. 4.5-10.

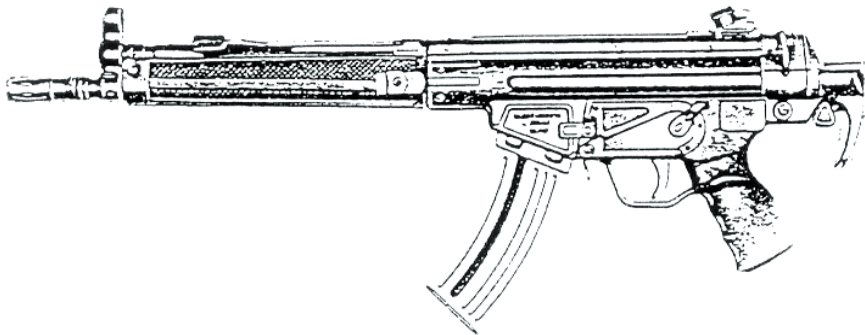
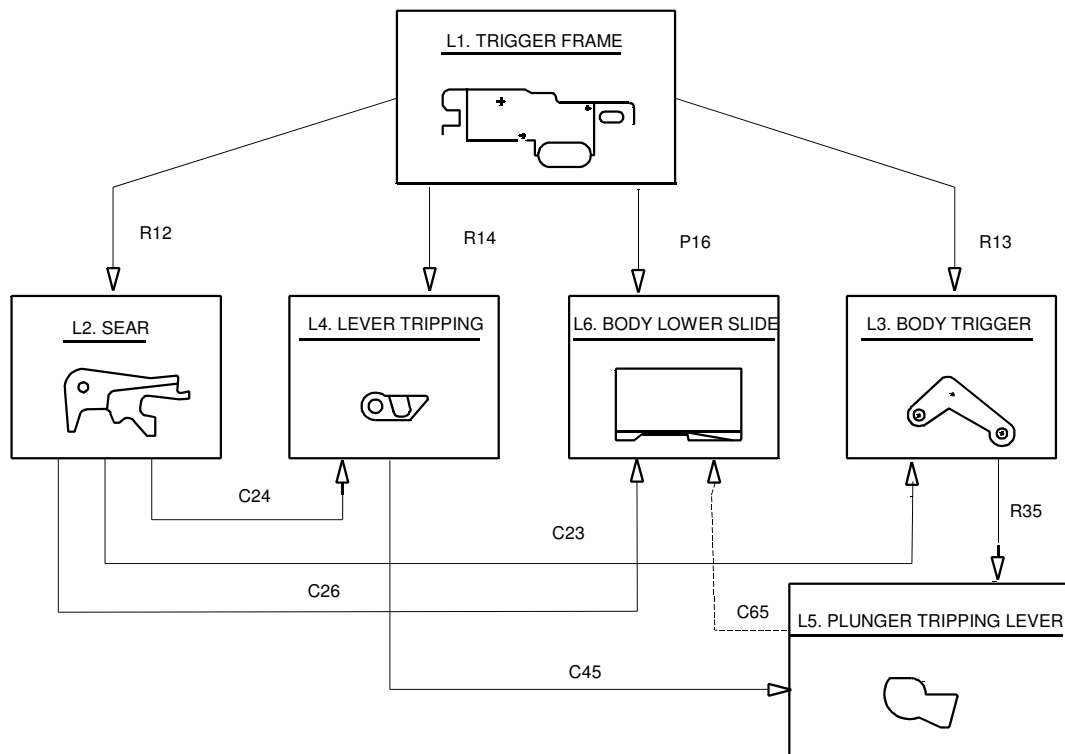
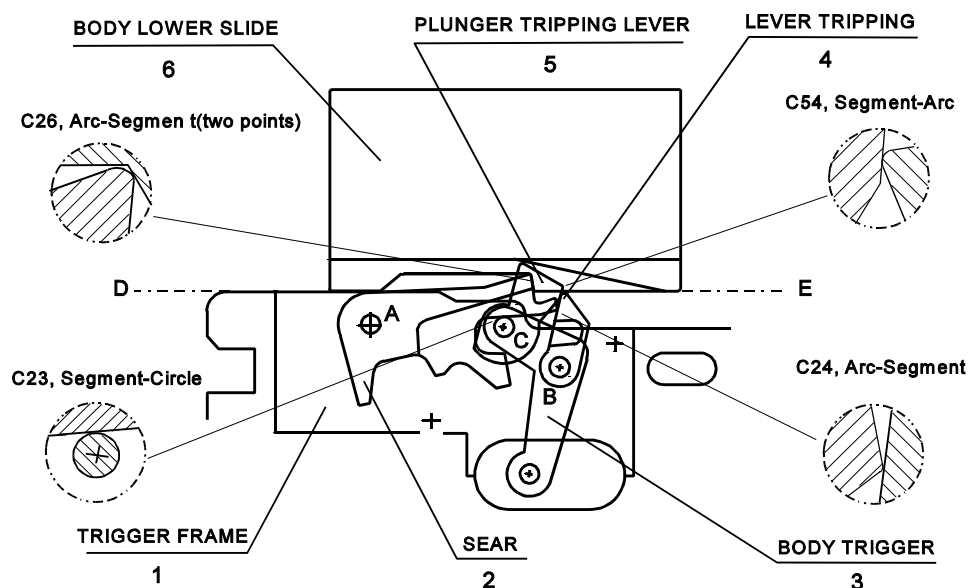


Fig. 4.5-1: An automatic machine-gun

*Fig. 4.5-2: Topology of the trigger mechanism**Fig. 4.5-3: Trigger mechanism: initial position - blocking stage*

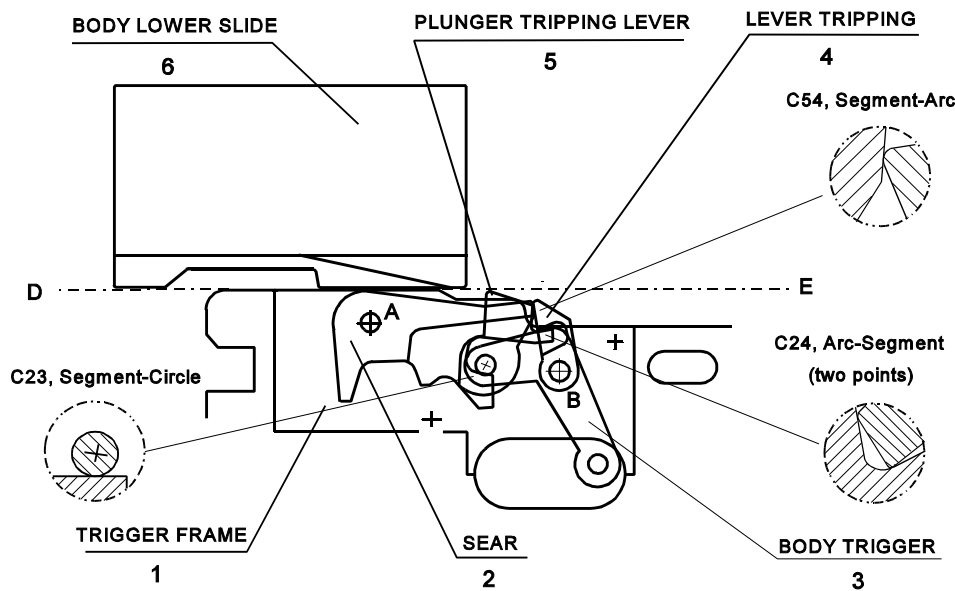


Fig. 4.5-4: Trigger mechanism: firing stage

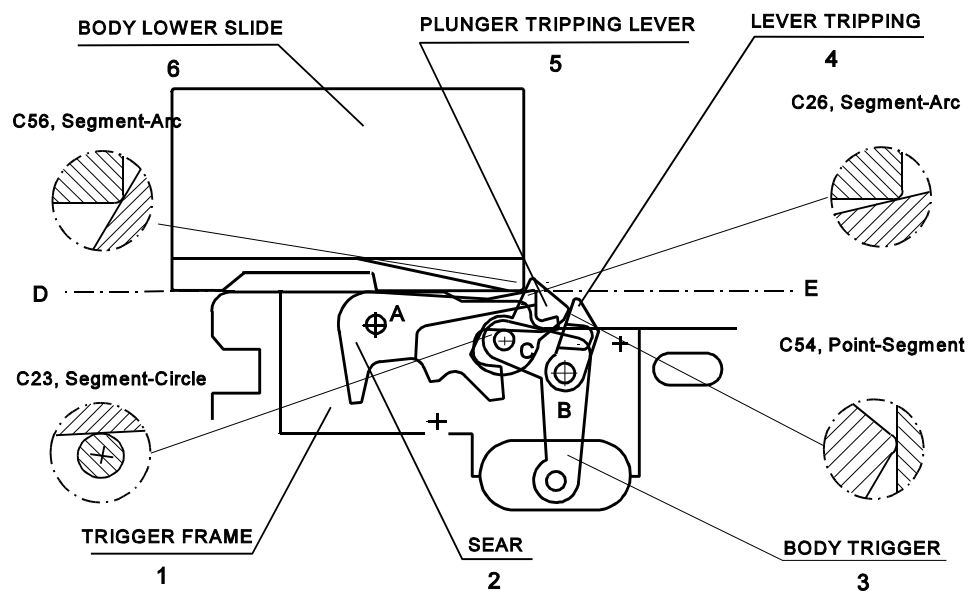


Fig. 4.5-5: Trigger mechanism: stopping stage

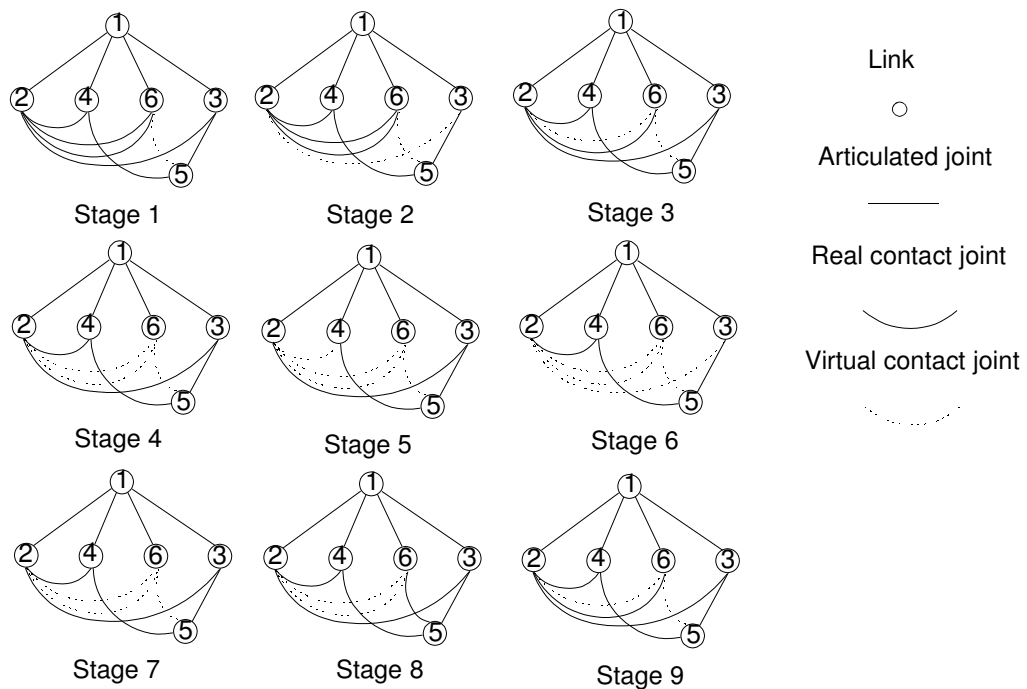


Fig. 4.5-6: Successive topologies of the trigger mechanism

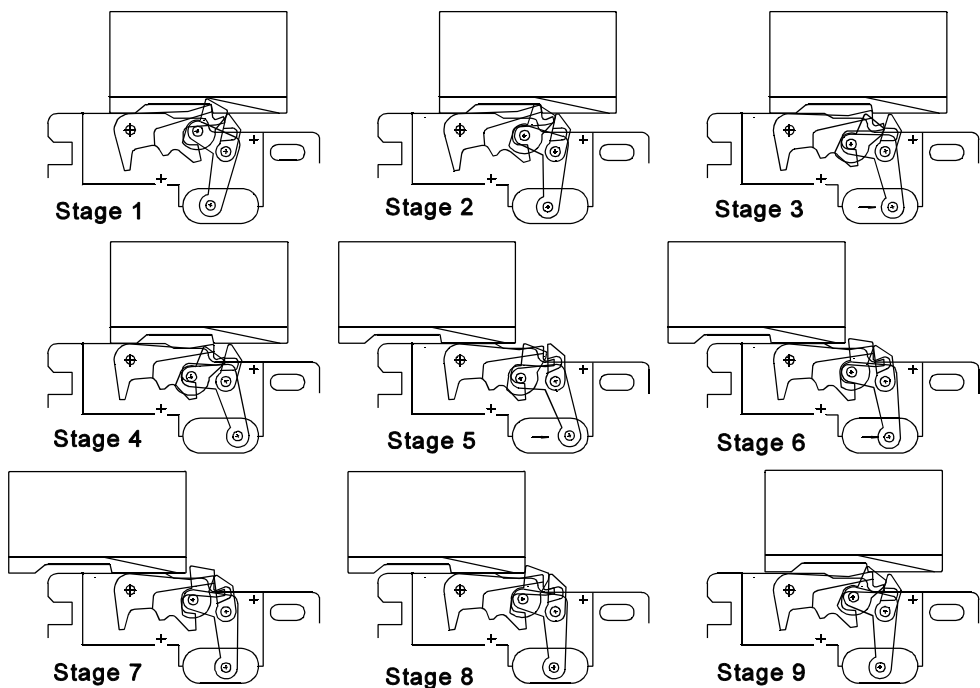


Fig. 4.5-7: Positions of the trigger mechanism for different successive topologies

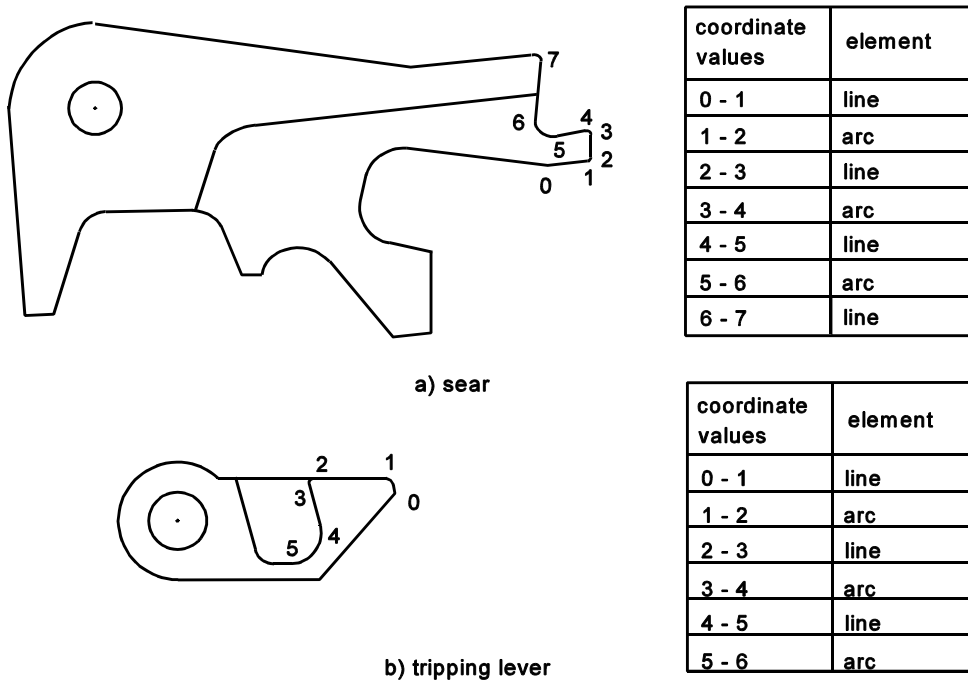


Fig. 4.5-8: Relative coordinates concerning the sear and tripping lever

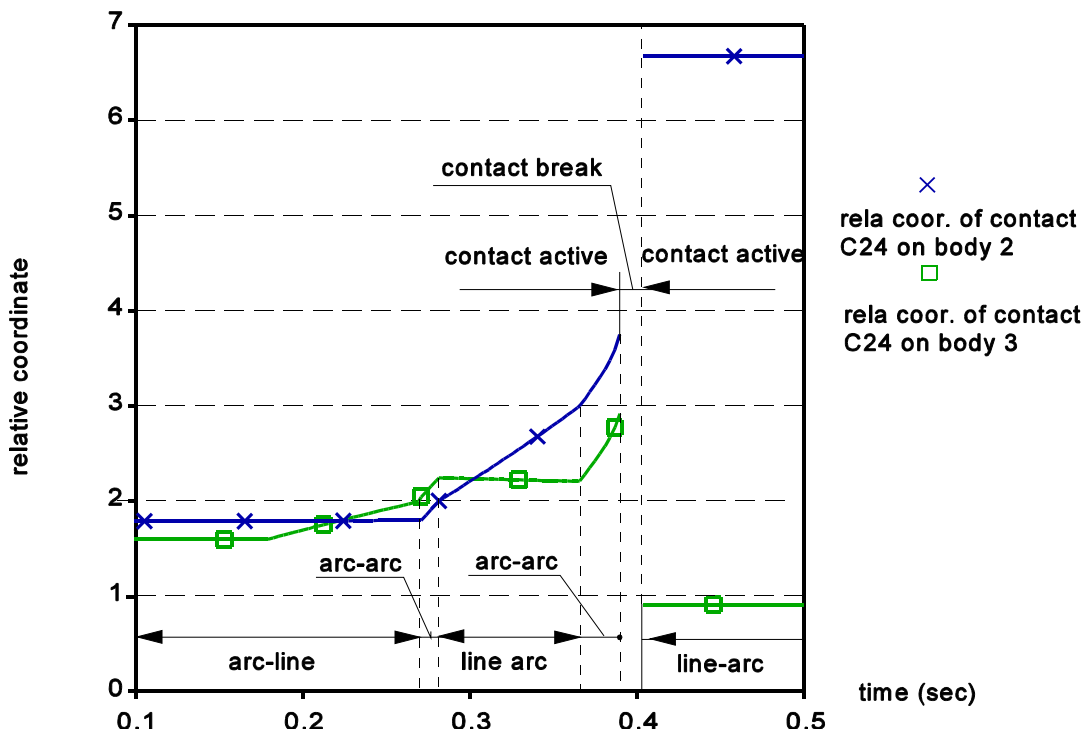


Fig. 4.5-9: Relative coordinates piloting the change of contact between the sear and tripping lever

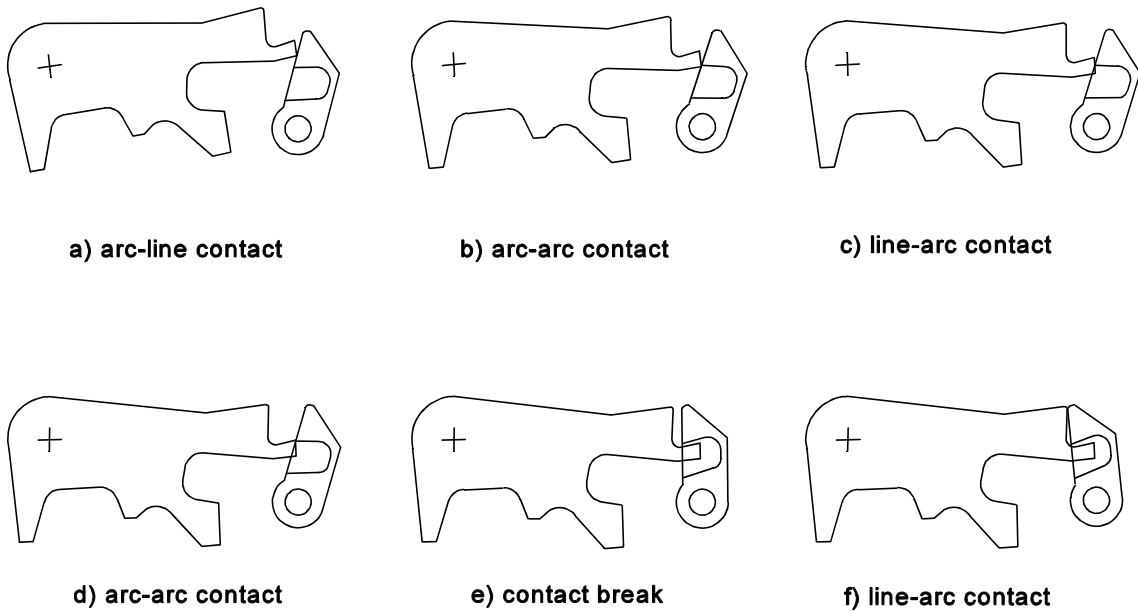


Fig. 4.5-10: Changes of contact model between the sear and tripping lever

Chapter 5 CONCLUSION

This thesis develops the principle of a unified approach for a computer-aided kinematic and dynamic simulation of mechanisms with changing contact joints. The considered particular contacting elements are formed by a series of juxtaposed simple geometric elements such as line segments, circle arcs, circles, points or curves with a polynomial profile.

Relative coordinates have been used to describe in a unified way the properties of either lower-pair or higher pair joints. An original set of relative coordinates have been associated to each contact joint: they are formed by an integer part associated to the current active contact element, the decimal part describing the exact location of the contact point.

The kinematic simulation is based on the use of a classical 4 x 4 transformation matrix concept. The closure of the loops detected by a topological analysis leads to the setting of the constraint equations at the basis of the kinematic behaviour.

The dynamic simulation is based on the Hamilton's formalism leading to the canonical equations of motion. A coordinate partitioning technique has been used to develop a minimal set of motion equations, integrated by a Runge-Kutta scheme.

The difficulty coming from the large number of potential contact and discontinuities induced by contact changes has been solved by the use of a set of switching functions; these ones are at the basis of the strategies developed to detect the modifications of constraints during motion, specially the transition between consecutive contact elements, the addition of constraints due to interferences between links and the break of constraints due to insufficient closing forces.

The computation of the contact forces has been made by the application of the principle of virtual displacements. Impact phenomena consecutive to interference phenomenon have been modelled either by a continuous or a piecewise method, this latter one being preferred in the particular context of the mechanisms considered in this thesis.

The use of virtual contact joints avoids to perform a new topological analysis, each time a contact appears or disappears: the deletion of an existing contact joint is reduced to the change from a 2-DOF active contact joint to a 3-DOF virtual contact joint.

Based on those choices, the ACDMC software has been developed and tested by analysing a series of basic mechanisms.

The main advantages consecutive to the different choices made in this thesis comes from the use of :

- relative coordinates, which allow a unified approach suitable either for lower-pair or contact joints,
- the aptitude of the relative coordinates defined for a contact joint to overcome:

- 1) the transition between consecutive elements(the integer part of an active contact joint coordinate is directly associated to the active curve element),
 - 2) the detection of interference, the third coordinate of a virtual contact joint is the distance between curves which can interfere and is thus directly associated to the occurrence of the interference.
- the concept of virtual contact joint which suppresses the need to successive topology analysis,
- a coherent dynamic formulation well adapted to an impact analysis by using a canonical formulation.

The developed strategy can be very useful to assist a designer to overcome the difficulties inherent to a tolerance analysis. The influence of shape and position modifications coming from manufacturing variations in relation to the nominal configurations can be estimated and be a real help when the designer must evaluate the necessary tolerances for an unaltered work cycle.

References

- [1] Artobolevsky I., Mechanisms in modern engineering design, vol. 1-4, MIR Publishers, Moscow 1979.
- [2] Arthur G. Erdman, "Modern Kinematics -- Developments in the Last Forty Years", John Wiley & Sons, Inc. 1993.
- [3] Wang Deming, C. Conti, P. Dehombreux and O. Verlinden, "A Computer-Aided Simulation Approach for Mechanisms with Intermittent Contact Joints", The Second International Conference on Computational Structures Technology", Athens, 1994.
- [4] Chakraborty J., Kinematics and geometry of planar and spatial cam mechanism, Ed. Wiley, New Dehli, India, 1979.
- [5] Werner Schiehlen, "Multibody Systems Hand Book", Springer-Verlag Berlin Heidelberg, 1990.
- [6] Leo Joskowicz, Elisha Sacks and Vijay Srinivasan, Kinematic Tolerance Analysis, Proc. of 3rd ACM symposium on Solid Modelling and Applications, Utash. ACM press, 1995.
- [7] Leo Joskowicz and Dorothy Neville, A representation language for mechanical behaviour, Artificial Intelligence in Engineering **10** (1996) 109-116.
- [8] Conti, C.; Corron, P. and Michotte, P.(1992), "A computer aided kinematic analysis system for mechanism design and computer simulation", Mech. Mach. Theory, Vol. 27, 1992, pp.563-574.
- [9] Dubowsky and etc., "Analytical and Experimental Study of the Prediction of Impacts in Planar Mechanical Systems With Clearances", Transactions of the ASME, Journal of Mechanisms, Transmissions, and Automation in Design, Vol. 106, December 1984.
- [10] Lee T. W. and Wang A. C. , "On the Dynamics of Intermittent Motion Mechanisms -Part 1, Dynamic Model and Response," Journal of Mechanisms, Transmission, and Automation in Design, Vol. 105, 1983, pp. 534-540.
- [11] F.Y. Chen, "Mechanics and Design of Cam Mechanisms", Library of Congress Cataloging in Publication Data, 1982.
- [12] Chang, C. W. and Shabana A. A., "Spatial Dynamics of Deformable Multibody Systems With Variable Kinematic Structure: Part 1 - Dynamic Model, Part 2 - Velocity Transformation", Trans. ASME, Journal of Mechanical Design, Vol 112, July 1990, pp. 153-167.
- [13] Crossley, F. R. E. And etc. "Computer Modelling of Systems with Intermittent Motion", Proceeding of the Fifth World Congress on Theory of Machines and Mechanisms-1979, Published by The American Society of Mechanical Engineers.
- [14] Winfrey, R.C., Anderson, R.V., and Gnilka, C.W., "Analysis of Elastic Machinery with Clearances", Trans. ASME, Journal of Engineering for Industry, Vol. 95, Aug. 1973, pp. 695-703.
- [15] Wehage, R.A., and Haug, E.J., "Dynamic Analysis of Mechanical Systems with Intermittent Motion", Trans. ASME, Journal of Mechanical Design, Vol. 104, No. 4, Oct. 1982, pp. 778-784.
- [16] Ehle, P. E., and Haug, E. J. "A Logical Function Method for Dynamic and Design Sensitivity Analysis of Mechanical systems with Intermittent motion", Trans. ASME Journal of Mechanical Design, Vol. 104, January 1982, pp. 90-100.
- [17] Ganter, M.A. and J.J.Uicker, Jr., "Dynamic Collision Detection Using Swept Solids",

- Trans. ASME, Journal of Mechanisms, Transmissions, and Automation in Design, Vol. 108, December, 1986, pp.549-555.
- [18] Gilmore, B. J. and Cipra, R. J., "Simulation of planar dynamic mechanical systems with changing topologies -part I: Characterization and Prediction of the Kinematic Constraint Changes, -Part II: Implementation Strategy and Simulation Results for Example Dynamic Systems", ASME, Journal of Mechanical Design, Vol. 113. 1991, pp.70-83.
- [19] Gilmore, B. J., "The Simulation of Mechanical Systems with a Changing Topology," Ph.D. Dissertation, Purdue University, August 1986.
- [20] Han, I.; Gilmore, B. J. and Ogot, M. M., "The incorporation of arc boundaries and stick/slip friction in a rule-based simulation algorithm for dynamic mechanical systems with changing topologies", ASME, J. of Mechanical Design, Vol. 115, 1993, pp. 432-434.
- [21] Han, I. and Gilmore B. J., " Multi-body Impact Motion with Friction-Analysis, Simulation, and Experimental Validation", Journal of Mechanical Design, Trans. ASME, Vol. 115, 1993, pp.412-422.
- [22] Charles L. Best and William G. Mclean, "Analytical Mechanics for Engineers -- Statics and Dynamics", International Textbook Company, Scranton Pennsylvania, 1965.
- [23] Meirovitch, L., "Methods of Analytical Dynamics, McGraw-Hill Book Company, 1970.
- [24] Goldsmith, W., Impact, the theory and physical Behaviour of colliding solids, Edward Arnold Ltd., 1960.
- [25] Hertz, H., Gesammelte Werke, Vol. 1, Leipzig, 1895, Chapter 5.
- [26] Kecs, W., and Teodorescu, P.P. "Applications of the Theory of Distributions in Mechanics", Abacus Press, Tunbridge Wells, Kent, England, 1974.
- [27] Ehle, P. E. and Haug, E. J., "A logical Function Method for Dynamic and Design Sensitivity Analysis of Mechanical Systems with Intermittent Motion", Trans. ASME Journal of Mechanical Design, Vol. 104, January 1982, pp. 90-100.
- [28] Huang, R.C., Haug, E.J., and Andrews, J.G. "Sensitivity Analysis of Large-Scale Mechanical Systems with Intermittent Motion", Technical Report, No. 83-10, The University of Iowa, College of Engineering, Jun 1983.
- [29] Khulief Y. A. and Shabana A. A., Dynamic Analysis of Constrained System of Rigid and Flexible Bodies with Intermittent Motion, Journal of Mechanisms, Transmissions, and Automation in Design, Trans. ASME, Vol. 108, 1986, pp. 38-45.
- [30] Khulief, Y. A., and Shabana, A. A., A continuous Force Model for the Impact Analysis of Flexible Multibody Systems," Mech. and Mach. Theory, Vol. 22, No. 3, 1987, pp. 213-224.
- [31] Haug, E. J. Wu. S-C and Yang S-M, "Dynamics of Mechanical System with Coulomb Friction, Stiction, Impact and Constraint Addition-Deletion", Mechanism and Machine Theory, Vol. 21, No. 5, pp. 401-406, 1986.
- [32] Wu S-C and Haug, E. J. "A Substructure Technique for Dynamics of Flexible Mechanical Systems of Flexible Mechanical Systems With Contact-Impact", Trans. ASME, Journal of Mechanical Design, Vol. 112, Sep. 1990, pp. 390-398.
- [33] Keller, J.B., Impact with Friction," ASME Journal of Applied Mechanics, Vol. 53, pp. 1-4. 1986.
- [34] Han, I. And Gilmore B. J. "Multi-body Impact Motion with Friction - Analysis, Simulation, and Experimental Validation", Trans. ASME, Journal of Mechanical Design, Vol. 115, Sep. 1993, pp. 412-422.

- [35] Wehage, R. A., "Generalized coordinate Partitioning in Dynamic Analysis of Mechanical Systems", Ph.D. dissertation, The University of Iowa, 1980.
- [36] Pereira, M. S. And Nikravesh, P. "Impact Dynamics of Multibody Systems with Frictional Contact Using Joint Coordinates and Canonical Equations of Motion", Computer Aided Analysis of Rigid and Flexible Mechanical Systems, NATO-advanced study Institute, pp. 505-525, 1993.
- [37] Lankarani, H. M., Canonical Impulse- Momentum Equations for Impact Analysis of Multibody Systems, Journal of Mechanical Design, Trans. ASME, Vol. 180, 1992, pp. 180-186.
- [38] Lankarani, H. M., Nikravesh, P. E., A Contact Force Model With Hysteresis Damping for Impact Analysis of Multibody Systems, Journal of Mechanical Design, Trans. ASME, Vol. 112, 1990, pp. 369-376.
- [39] Lankarani, H. M., "Canonical equation of motion and estimation of parameters in the analysis of impact problems", Ph.D. thesis, The University of Arizona, 1988.
- [40] Parviz E. Nikravesh, "Computer-Aided Analysis of Mechanical Systems", Prentice-Hall International, Inc., 1988.
- [41] "Dynamic analysis of mechanical system", Section 8.2 Graph Characterization of System Topology",
- [42] Branin, F.H., Jr., D.C. and transient analysis of Networks Using a Digital Computer, IRE Intern. Convent. Rec. , 1962, pp. 236-256.
- [43] Sheth, P. N., and J. J. Uicker, Jr., A Generalized Symbolic Notation for Mechanisms, Journal of Engineering for Industry, Trans. ASME, pp. 102-112, February, 1971.
- [44] Donald T. Greenwood, "Classical Dynamics", Prentice-Hall, INC., Englewood Cliffs, N.J., 1977.
- [45] Javier Garcid de Jalon and Eduardo Bayo, Kinematic and Dynamic Simulation of Multibody Systems, Springer-Verlag, New York, Inc. 1994.
- [46] Mani, N.K., Hang, E.J., and Atkinson, K.E., "Application of Singular Value Decomposition for Analysis of Mechanical System Dynamics", ASME J. of Mechanisms, Transmissions and Automation in Design, Vol. 107, 1985, pp 82-87.
- [47] Kim, S. S. And Vaderploeg, M.J., "A general and efficient method for dynamic analysis of mechanical systems using velocity transformation", ASME J. of Mechanisms, Transmissions and Automation in Design, Vol. 108, 1986, pp 176-182.
- [48] Ames, W.F. "Numerical Methods for Partial Differential Equations 2nd ed. New York: Academic Press, 1977.
- [49] Mauri Vesimaki and Sami Saarinen "ADAMS Basic Training", CSC - Tieteenlinen Laskenta by Centre for Scientific Computing, 1993.
- [50] Conti C., Dehombreux P., Verlinden O. and Datoussaid S., "ACIDYM, a modular software for computer-aided learning of kinematic and dynamic analysis of multibody systems", Advanced multibody systems dynamics: simulation and software Tools, Kluwer Academic Publishers, 1993, pp. 361-366.

Appendix A: Constraint transformation matrices and linear derivative operators

A.1 Lower-pair joints

In Section 2.3.3, we have derived the transformation matrices φ_k and its' linear derivative operators Q_{ki} for revolute and prismatic joints. Other lower-pair joints are described hereafter.

-- Screw joint

The conditions for a proper choice of the coordinate axes associated to a screw joint (see Fig. 2.3-1d in Section 2.3) are the following ones:

- a) the axes z_k^- and z_k^+ must be along the screw axis; their positive directions are identical but can be arbitrarily chosen,
- b) the $x_k^-y_k^-z_k^-$ and $x_k^+y_k^+z_k^+$ coordinate systems must be chosen such that there exists one position of the screw constraint for which the two coordinate systems are coincident.

There are two possible choices for the joint variable of a screw joint:

- first, the rotational motion, designated by θ_k , which is the angle measured from the positive x_k^- axis to the positive x_k^+ axis; this angle is considered as positive when measured counterclockwise about the positive z_k^-, z_k^+ axis,
- secondly, the translational motion, labelled by s_k , which is the distance from x_k^- to x_k^+ measured along z_k^-, z_k^+ ; this distance is considered as positive if it is in the same direction as z_k^-, z_k^+ .

Usually, the s_k is chosen as the independent variable of this 1-DOF joint:

$$q_{k1} = s_k = i * \theta_k \quad (\text{A.1-1})$$

where i is a kinematic constraint associated to the screw kinematics. The transformation matrix of the is expressed by:

$$\varphi(\underline{q}_k) = \begin{bmatrix} \cos \frac{2\pi q_{k1}}{i} & -\sin \frac{2\pi q_{k1}}{i} & 0 & 0 \\ \sin \frac{2\pi q_{k1}}{i} & \cos \frac{2\pi q_{k1}}{i} & 0 & 0 \\ 0 & 0 & 1 & q_{k1} \\ 0 & 0 & 0 & 0 \end{bmatrix} \quad (\text{A.1-2})$$

As it has been seen, the kinematics of a constrained mechanical system requires the derivatives of the constraint matrix with respect to the generalized coordinates. Since the derivative operation is a linear transformation, the same effects can be achieved by matrix Q_{k1} such that:

$$\frac{\partial \varphi_k}{\partial q_{k1}} = Q_{k1} \varphi_k \quad (\text{A.1-3})$$

and

$$Q_{k1} = \left(\frac{\partial \varphi_k}{\partial q_{k1}} \right) \varphi_k^{-1} \quad (\text{A.1-4})$$

The derivative operator matrix Q_{k1} for the screw joint is expressed by:

$$Q_{k1} = \begin{bmatrix} 0 & -\frac{2\pi}{q_{k1}} & 0 & 0 \\ \frac{2\pi}{q_{k1}} & 0 & 0 & 0 \\ 0 & 0 & 0 & 1 \\ 0 & 0 & 0 & 0 \end{bmatrix} \quad (\text{A.1-5})$$

-- Cylindric joint

The coordinate axes for a cylindric joint are chosen according to the same conventions as for a screw joint (see Fig. 2.3-1c in section 2.3). The variables θ_k and S_k are defined in the same way as for a screw joint. In the case of a cylindric joint, the parameter θ_k and S_k are not related, and both are chosen as independent variables:

$$\underline{q}_k = \begin{Bmatrix} q_{k1} \\ q_{k2} \end{Bmatrix} = \begin{Bmatrix} \theta_k \\ S_k \end{Bmatrix} \quad (\text{A.1-6})$$

The constraint matrix $\varphi_k(\underline{q}_k)$ is expressed by:

$$\varphi_k(\underline{q}_k) = \begin{bmatrix} \cos q_{k1} & -\sin q_{k1} & 0 & 0 \\ \sin q_{k1} & \cos q_{k1} & 0 & 0 \\ 0 & 0 & 1 & q_{k2} \\ 0 & 0 & 0 & 1 \end{bmatrix} \quad (\text{A.1-7})$$

The two derivative operator matrices, Q_{k1} and Q_{k2} , are given by:

$$Q_{k1} = \frac{\partial \varphi(\underline{q}_k)}{\partial q_{k1}} \varphi_k^{-1}(\underline{q}_k) = \begin{bmatrix} 0 & -1 & 0 & 0 \\ 1 & 0 & 0 & 0 \\ 0 & 0 & 0 & 0 \\ 0 & 0 & 0 & 0 \end{bmatrix} \quad (\text{A.1-8})$$

$$Q_{k2} = \frac{\partial \varphi(\underline{q}_k)}{\partial q_{k2}} \varphi_k^{-1}(\underline{q}_k) = \begin{bmatrix} 0 & 0 & 0 & 0 \\ 0 & 0 & 0 & 0 \\ 0 & 0 & 0 & 1 \\ 0 & 0 & 0 & 0 \end{bmatrix} \quad (\text{A.1-9})$$

-- Spheric joint

The spheric constraint allows three rotations about mutually orthogonal axes. The three Euler angles (Fig. 2.3-1e) are chosen as joint variables resulting in:

$$\underline{q}_k = \begin{bmatrix} q_{k1} \\ q_{k2} \\ q_{k3} \end{bmatrix} = \begin{bmatrix} \alpha_k \\ \beta_k \\ \gamma_k \end{bmatrix} \quad (\text{A.1-10})$$

In this figure, the Euler angles are defined in classical z,x,z order:

- a) beginning with the coordinate system x_k^-, y_k^-, z_k^- , a rotation about z_k^- by an angle α_k results in the "intermediate" coordinate system, with x_k^- aligning itself with the line of nodes,
- b) a rotation about the line of nodes by an angle β_k results in z_k^- shifting to z_k^+ ,
- c) finally, a rotation about z_k^+ axis an angle γ_k shifts the line of nodes axis to x_k^+ , thus defining the coordinate system x_k^+, y_k^+, z_k^+ .

The constraint matrix $\varphi_k(\underline{q}_k)$ is:

$$\varphi_k(\underline{q}_k) = \begin{bmatrix} cq_{k1}cq_{k3} - sq_{k1}cq_{k2}sq_{k3} & -cq_{k1}sq_{k3} - sq_{k1}cq_{k2}cq_{k3} & sq_{k1}sq_{k2} & 0 \\ sq_{k1}cq_{k3} + cq_{k1}cq_{k2}sq_{k3} & -sq_{k1}sq_{k3} + cq_{k1}cq_{k2}cq_{k3} & -cq_{k1}sq_{k2} & 0 \\ sq_{k2}sq_{k3} & sq_{k2}cq_{k3} & cq_{k2} & 0 \\ 0 & 0 & 0 & 1 \end{bmatrix} \quad (\text{A.1-11})$$

where

$$cq_i = \cos(q_i), sq_i = \sin(q_i) \quad i=1, 2, 3$$

The three corresponding derivative operators can be obtained by:

$$Q_{ki} = \frac{\partial \varphi(\underline{q}_k)}{\partial q_{ki}} \varphi_k^{-1}(\underline{q}_k) \quad i=1, 2, 3 \quad (\text{A.1-12})$$

leading to the following derivative matrices:

$$Q_{k1} = \begin{vmatrix} 0 & -1 & 0 & 0 \\ 1 & 0 & 0 & 0 \\ 0 & 0 & 0 & 0 \\ 0 & 0 & 0 & 0 \end{vmatrix} \quad (\text{A.1-13})$$

$$Q_{k2} = \begin{vmatrix} 0 & 0 & sq_{k1} & 0 \\ 0 & 0 & -cq_{k1} & 0 \\ -sq_{k1} & cq_{k1} & 0 & 0 \\ 0 & 0 & 0 & 0 \end{vmatrix} \quad (\text{A.1-14})$$

$$Q_{k3} = \begin{vmatrix} 0 & -cq_{k2} & -cq_{k1}sq_{k2} & 0 \\ cq_{k2} & 0 & -sq_{k2}cq_{k1} & 0 \\ cq_{k1}sq_{k2} & sq_{k2}cq_{k1} & 0 & 0 \\ 0 & 0 & 0 & 0 \end{vmatrix} \quad (\text{A.1-15})$$

-- Universal joint

The universal joint allows relative rotations about two mutually orthogonal axes (see Fig. (2.3-1f)). The following conditions are imposed to derive the constraint matrix.

- a) The origins of the x_k^-, y_k^-, z_k^- coordinate frame attached to link i and the x_k^+, y_k^+, z_k^+ coordinate frame attached to link j must be coincident.
- b) The axes z_k^- and z_k^+ must be respectively directed along each axis of rotation of the universal joint.

The universal joint variables are:

$$\underline{q}_k = \begin{Bmatrix} q_{k1} \\ q_{k2} \end{Bmatrix} = \begin{Bmatrix} \theta_{k1} \\ \theta_{k2} \end{Bmatrix} \quad (\text{A.1-16})$$

leading to the following universal joint matrix:

$$\varphi_k(\underline{q}_k) = \begin{vmatrix} cq_{k1}cq_{k2} & -cq_{k1}sq_{k2} & sq_{k1} & 0 \\ sq_{k1}cq_{k2} & -sq_{k1}sq_{k2} & -cq_{k1} & 0 \\ sq_{k2} & cq_{k2} & 0 & 0 \\ 0 & 0 & 0 & 1 \end{vmatrix} \quad (\text{A.1-17})$$

where,

$$cq_i = \cos(q_i), \quad sq_i = \sin(q_i) \quad i=1, 2$$

The two derivative operator matrices are found to be:

$$Q_{k1} = \begin{vmatrix} 0 & -1 & 0 & 0 \\ 1 & 0 & 0 & 0 \\ 0 & 0 & 0 & 0 \\ 0 & 0 & 0 & 0 \end{vmatrix} \quad (\text{A.1-18})$$

$$Q_{k2} = \begin{vmatrix} 0 & 0 & -cq_{k1} & 0 \\ 0 & 0 & -sq_{k1} & 0 \\ cq_{k1} & sq_{k1} & 0 & 0 \\ 0 & 0 & 0 & 0 \end{vmatrix} \quad (\text{A.1-19})$$

-- Planar joint

A planar joint allows two relative translations along orthogonal axes and a relative rotation about the axis perpendicular to the plane of the translational axes. The following conditions are imposed to derive the constraint matrix:

- a) The x_k^- , y_k^- , and x_k^+ , y_k^+ planes must coincide with the two planar surfaces.
- b) The z_k^- and z_k^+ axes must both be directed on the same side of this common plane.

The three pair variables are the two translation coordinates, S_{k1} and S_{k2} , and the rotation coordinate θ_k :

$$\underline{q}_k = \begin{Bmatrix} q_{k1} \\ q_{k2} \\ q_{k3} \end{Bmatrix} = \begin{Bmatrix} \theta_k \\ S_{k1} \\ S_{k2} \end{Bmatrix} \quad (\text{A.1-20})$$

The constraint matrix is:

$$\varphi_k(\underline{q}_k) = \begin{vmatrix} cq_{k1} & -sq_{k1} & 0 & q_{k2} \\ sq_{k1} & cq_{k1} & 0 & q_{k3} \\ 0 & 0 & 1 & 0 \\ 0 & 0 & 0 & 1 \end{vmatrix} \quad (\text{A.1-21})$$

The following derivative operator matrices can be found:

$$Q_{k1} = \begin{Bmatrix} 0 & -1 & 0 & S_{k2} \\ 1 & 0 & 0 & -S_{k3} \\ 0 & 0 & 0 & 0 \\ 0 & 0 & 0 & 0 \end{Bmatrix} \quad (\text{A.1-22})$$

$$Q_{k2} = \begin{bmatrix} 0 & 0 & 0 & 1 \\ 0 & 0 & 0 & 0 \\ 0 & 0 & 0 & 0 \\ 0 & 0 & 0 & 0 \end{bmatrix} \quad (\text{A.1-23})$$

$$Q_{k3} = \begin{bmatrix} 0 & 0 & 0 & 0 \\ 0 & 0 & 0 & 1 \\ 0 & 0 & 0 & 0 \\ 0 & 0 & 0 & 0 \end{bmatrix} \quad (\text{A.1-24})$$

-- Pure rolling joint

The assumptions on the placement of the two coordinate frames are:

- a) the z_k^- and z_k^+ axes lie along the respective axes of the two gears,
- b) the $x_k^-y_k^-$ and $x_k^+y_k^+$ axes all lie in the common plane of the two gears,
- c) the common perpendicular directed from z_k^- to z_k^+ is designated by t_k ,
- d) there is one position for the gear pair such that the positive x_k^- and x_k^+ axes are both directed along the positive direction t_k .

Since the pure roll constraint has a single degree of freedom, either q_1 or q_2 may be selected as the constraint variable, due to the ratio i existing between the two parameters.

$$i = \frac{q_1}{q_2} = \frac{R_2}{R_1} \quad (\text{A.1-25})$$

The following constraint matrix can be derived:

$$\varphi_k(\underline{q}_k) = \begin{Bmatrix} \cos(1+i)q_{k1} & -\sin(1+i)q_{k1} & 0 & (1+i)R_1 \sin q_{k1} \\ \sin(1+i)q_{k1} & \cos(1+i)q_{k1} & 0 & (1+i)R_1 \cos q_{k1} \\ 0 & 0 & 1 & 0 \\ 0 & 0 & 0 & 1 \end{Bmatrix} \quad (\text{A.1-26})$$

The derivative operator matrix Q_{k1} is given by:

$$Q_{k1} = \begin{bmatrix} 0 & -(1+i) & 0 & i(1+i) \sin q_{k1} \\ (1+i) & 0 & 0 & -i(1+i) \cos q_{k1} (1+i) \\ 0 & 0 & 0 & 0 \\ 0 & 0 & 0 & 0 \end{bmatrix} \quad (\text{A.1-27})$$

A.2 Contact joints

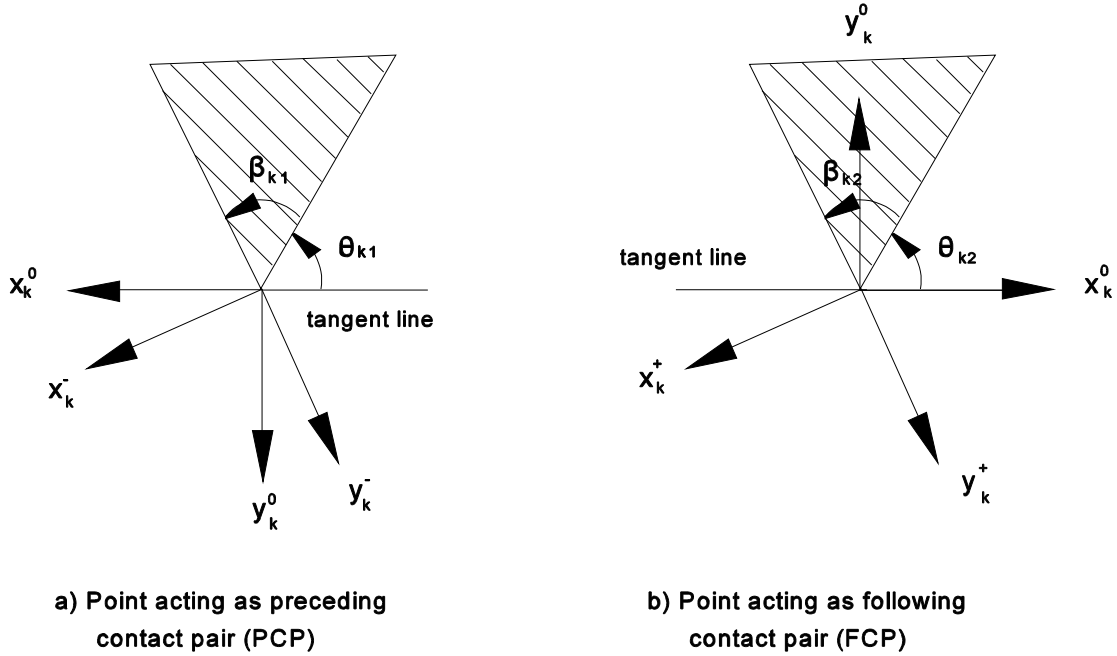


Fig. A.2-1: Point as a contacting element

-- Point element

Any contact joint can be divided into two parts: a preceding (PCP) and following contact pair (FCP). When a point element is used as a preceding contacting surface, the transformation from an arc coordinate frame to the intermediate frame, $x_k^-, y_k^-, z_k^- \Rightarrow x_k^0, y_k^0, z_k^0$, can be considered as a planar x-y rotation $(\theta_{k1} + \beta_{k1}) - 90^\circ$ about the z_k axis, leading to:

$$\varphi_{kp}(q_{k1}) = \varphi_{kp}(\theta_{k1}) = \begin{bmatrix} \sin(\theta_{k1} + \beta_{k1}) & \cos(\theta_{k1} + \beta_{k1}) & 0 & 0 \\ -\cos(\theta_{k1} + \beta_{k1}) & \sin(\theta_{k1} + \beta_{k1}) & 0 & 0 \\ 0 & 0 & 1 & 0 \\ 0 & 0 & 0 & 1 \end{bmatrix} \quad (\text{A.2-1})$$

where θ_{k1} can be expressed in function of the relative curvilinear coordinate q_{k1} by:

$$\theta_{k1} = (q_{k1} - i_{k1} + 1)(180 - \beta_{k1}) \quad (\text{A.2-2})$$

The derivation of this transformation matrix yields:

$$\frac{\partial \varphi_{kp}}{\partial q_{k1}} = -\frac{\partial \varphi_{kp}}{\partial \theta_{k1}} \beta_{k1} = -\begin{vmatrix} \cos(\theta_{k1} + \beta_{k1}) & -\sin(\theta_{j1} + \beta_{k1}) & 0 & 0 \\ \sin(\theta_{k1} + \beta_{k1}) & \cos(\theta_{k1} + \beta_{k1}) & 0 & 0 \\ 0 & 0 & 0 & 0 \\ 0 & 0 & 0 & 0 \end{vmatrix} \beta_{k1} \quad (\text{A.2-3})$$

and its inversion:

$$\varphi_{kp}^{-1} = \begin{vmatrix} \sin(\theta_{k1} + \beta_{k1}) & -\cos(\theta_{k1} + \beta_{k1}) & 0 & 0 \\ \cos(\theta_{k1} + \beta_{k1}) & \sin(\theta_{k1} + \beta_{k1}) & 0 & 0 \\ 0 & 0 & 1 & 0 \\ 0 & 0 & 0 & 1 \end{vmatrix} \quad (\text{A.2-4})$$

The corresponding derivative matrix is expressed by:

$$Q_{k1} = \frac{\partial \varphi_{kp}}{\partial q_{k1}} \varphi_{kp}^{-1} = \begin{vmatrix} 0 & 1 & 0 & 0 \\ -1 & 0 & 0 & 0 \\ 0 & 0 & 0 & 0 \\ 0 & 0 & 0 & 0 \end{vmatrix} \beta_{k1} \quad (\text{A.2-5})$$

When a point element acts as a following contacting surface, the transformation from the intermediate frame to the joint coordinate frame, $x_k^0, y_k^0, z_k^0 \Rightarrow x_k^+, y_k^+, z_k^+$, can be considered as a planar x-y rotation of $(\theta_{k1} + \beta_{k1}) + 90^\circ$ about the z_k axis, leading to:

$$\varphi_{kf}(q_{k2}) = \varphi_{kf}(\theta_{k2}) = \begin{vmatrix} -\sin(\theta_{k2} + \beta_{k2}) & \cos(\theta_{k2} + \beta_{k2}) & 0 & 0 \\ -\cos(\theta_{k2} + \beta_{k2}) & -\sin(\theta_{k2} + \beta_{k2}) & 0 & 0 \\ 0 & 0 & 1 & 0 \\ 0 & 0 & 0 & 1 \end{vmatrix} \quad (\text{A.2-6})$$

where θ_{k2} expressed in function of the relative curvilinear coordinate q_{k2} gives:

$$\theta_{k2} = (q_{k2} - i_{k2} + 1) * (180 - \beta_{k2}) \quad (\text{A.2-7})$$

The derivative operator matrix is found to be:

$$Q_{k2} = \varphi_{kp}(q_{k1}) Q'_{k2} \varphi_{kp}^{-1}(q_{k1}) \quad (\text{A.2-8})$$

with

$$Q'_{k2} = \frac{\partial \varphi_{kf}}{\partial q_{k2}} \varphi_{kf}^{-1} = \begin{vmatrix} 0 & -1 & 0 & 0 \\ 1 & 0 & 0 & 0 \\ 0 & 0 & 0 & 0 \\ 0 & 0 & 0 & 0 \end{vmatrix} \beta_{k2} \quad (\text{A.2-9})$$

-- Circle contact element

When a circle element is used as a preceding contacting surface, the transformation from a circle coordinate frame to the intermediate frame, $x_k^-, y_k^-, z_k^- \Rightarrow x_k^0, y_k^0, z_k^0$, can be considered as a planar x-y rotation of θ_{k1} about z_k , leads to:

$$\varphi_{kp}(q_{k1}) = \varphi_{kp}(\theta_{k1}) = \begin{bmatrix} \cos(\theta_{k1}) & -\sin(\theta_{k1}) & 0 & -R_{k1}\cos(\theta_{k1}) \\ \sin(\theta_{k1}) & \cos(\theta_{k1}) & 0 & R_{k1}\sin(\theta_{k1}) \\ 0 & 0 & 1 & 0 \\ 0 & 0 & 0 & 1 \end{bmatrix} \quad (\text{A.2-10})$$

where, θ_{k1} can be expressed by relative curvilinear coordinate q_{k1} ,

$$\theta_{k1} = q_{k1} * 360 \quad (\text{A.2-11})$$

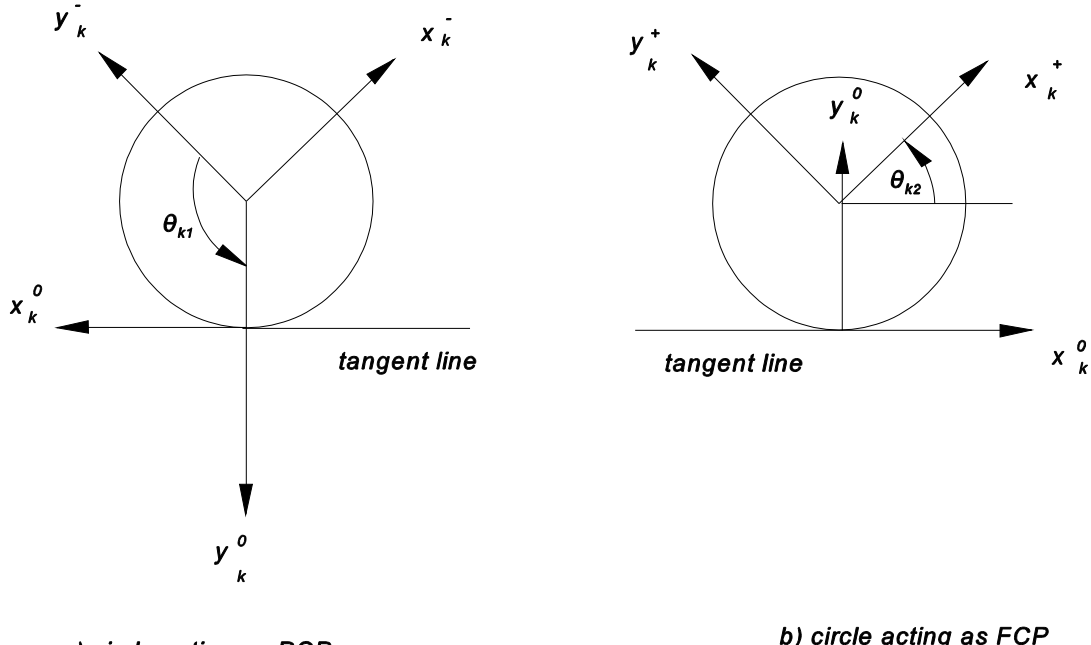


Fig. A.2-2: Circle as a contact element

The corresponding derivative matrix is then expressed by:

$$Q_{k1} = \begin{bmatrix} 0 & -1 & 0 & 0 \\ 1 & 0 & 0 & 0 \\ 0 & 0 & 0 & 0 \\ 0 & 0 & 0 & 0 \end{bmatrix} 2\pi \quad (\text{A.2-12})$$

When a circle element acts as a following contacting surface, the transformation from the intermediate frame to the circle coordinate frame, $x_k^0, y_k^0, z_k^0 \Rightarrow x_k^+, y_k^+, z_k^+$. can be considered as a planar x-y rotating 180- θ_{k2} about z_k , leads to: leads to the following transform matrix is

$$\varphi_{kf}(q_{k2}) = \varphi_{kf}(\theta_{k2}) = \begin{bmatrix} -\cos(\theta_{k2}) & -\sin(\theta_{k2}) & 0 & 0 \\ \sin(\theta_{k2}) & -\cos(\theta_{k2}) & 0 & R_{k2} \\ 0 & 0 & 1 & 0 \\ 0 & 0 & 0 & 1 \end{bmatrix} \quad (\text{A.2-13})$$

where θ_{k2} is expressed by relative curvilinear coordinate q_{k2} ,

$$\theta_{k2} = q_{k2} * 360 \quad (\text{A.2-14})$$

The derivative operator matrix is found to be:

$$Q_{k2} = \varphi_{kp}(q_{k1}) Q'_{k2} \varphi_{kp}^{-1}(q_{k1}) \quad (\text{A.2-15})$$

with

$$Q'_{k2} = \frac{\partial \varphi_{kf}}{\partial q_{kf}} \varphi_{k2}^{-1} = \begin{bmatrix} 0 & -1 & 0 & 0 \\ 1 & 0 & 0 & 0 \\ 0 & 0 & 0 & 0 \\ 0 & 0 & 0 & 0 \end{bmatrix} 2\pi \quad (\text{A.2-16})$$

Appendix B: Generalized mass matrix and it's derivatives

In order to derive the generalized mass matrix and it's partial differentiation, we recall here the motion equations:

$$\dot{\underline{f}} = [\underline{M}]^{-1} \underline{p} \quad (\text{B-1})$$

$$\dot{\underline{p}} = \underline{F}_a + \underline{F}_c - \frac{1}{2} \underline{p}^T ([\underline{M}]^{-1} [\frac{\partial \underline{M}}{\partial \underline{f}}] [\underline{M}]^{-1]) \underline{p} \quad (\text{B-2})$$

where the elements of the mass matrix $[\underline{M}]$ are expressed by:

$$m_{ij} = \sum_{k=1}^L \text{Tr} [\omega_{ki} A_{ok} J_k A_{ok}^T \omega_{kj}^T] \quad (\text{B-3})$$

and the differentiation of the mass matrix with respect to the generalized coordinates f_a can be computed from the general term:

$$\begin{aligned} \frac{\partial m_{ji}}{\partial f_{ka}} &= \sum_{k=1}^L \text{Tr} [(\frac{\partial \omega_{ki}}{\partial f_{ka}} A_{oi} + \omega_{ki} \frac{\partial A_{ok}}{\partial q_{ka}}) J_k A_{ok}^T \omega_{kj}^T] \\ &+ \sum_{k=1}^L \text{Tr} [\omega_{ki} A_{ok} J_k ((\frac{\partial A_{ok}}{\partial f_{ka}})^T \omega_{kj}^T + A_{ok}^T (\frac{\partial \omega_{kj}}{\partial f_{ka}})^T)] \end{aligned} \quad (\text{B-4})$$

From Equ. (3.3.2-7), the generalized velocity parameter matrix ω_{kb} is expressed by:

$$\omega_{ki} = \sum_{a=1}^n \Lambda_{ka} k_{ai} \quad (\text{B-5})$$

It can also be expressed in function of the joint variables q_{ji} . From the definition of the influence coefficient matrix $[K]$ and taking into account Equ. (2.2.4-25), the following equations can be obtained:

$$K_{ab} = \frac{\partial q_a'}{\partial f_b} \quad (\text{B-6})$$

and

$$\sum_{a=1}^n \Lambda_{ka} \partial q_a' = \sum_{j=1}^{k-1} \sum_{i=1}^{t_j} B_{ji} \partial q_{ji} \quad (\text{B-7})$$

So the Equ. (B-5) can be rewritten as:

$$\omega_{kb} = \sum_{j=1}^{k-1} \sum_{i=1}^{t_j} B_{ji} \frac{\partial q_{ji}}{\partial f_b} . \quad (\text{B-8})$$

From Equ. (2.2.4-13),

$$\frac{\partial A_{ok}}{\partial f_a} = \sum_{j=1}^{k-1} \sum_{i=1}^{t_j} B_{ji} \frac{\partial q_{ji}}{\partial f_a} A_{ok} = \omega_{ka} A_{ok} \quad (\text{B-9})$$

Equ. (B-4) can be rewritten as

$$\begin{aligned} \frac{\partial m_{ji}}{\partial f_a} &= \sum_{k=1}^L \operatorname{Tr} [(\gamma_{ki} + \omega_{ki} \omega_{ka}) A_{ok} J_k A_{ok}^T \omega_{kj}^T] \\ &+ \sum_{k=1}^L \operatorname{Tr} [\omega_{ki} A_{ok} J_k A_{ok}^T (\omega_{ka}^T \omega_{kj}^T + \gamma_{kj}^T)] \end{aligned} \quad (\text{B-10})$$

where

$$\gamma_{kba} = \frac{\partial \omega_{kb}}{\partial f_a} = \sum_{j=1}^{k-1} \sum_{i=1}^{t_j} \left(\frac{\partial B_{ji}}{\partial f_a} \frac{\partial q_{ji}}{\partial f_b} + B_{ji} \frac{\partial^2 q_{ji}}{\partial f_b \partial f_a} \right) \quad (\text{B-11})$$

The term $\frac{\partial B_{ji}}{\partial f_a}$ can be obtained by differentiating Equ. (2.2.4-14)

$$\begin{aligned} \frac{\partial B_{ji}}{\partial f_a} &= \frac{\partial}{\partial f_a} (A_{oj} T_{jj} Q_{ji} T_{jj}^{-1} A_{oj}^{-1}) \\ &= \frac{\partial A_{oj}}{\partial f_a} T_{jj} Q_{ji} T_{jj}^{-1} A_{oj}^{-1} + A_{oj} T_{jj} \frac{\partial Q_{ji}}{\partial f_a} T_{jj}^{-1} A_{oj}^{-1} + A_{oj} T_{jj} Q_{ji} T_{jj}^{-1} \frac{\partial A_{oj}^{-1}}{\partial f_a} \end{aligned} \quad (\text{B-12})$$

As $A_{oj} A_{oj}^{-1} = I$, one has:

$$\frac{\partial A_{ok}}{\partial f_a} A_{ok}^{-1} + A_{ok} \frac{\partial A_{ok}^{-1}}{\partial f_a} = 0 \quad (\text{B-13})$$

and

$$\frac{\partial A_{ok}^{-1}}{\partial f_a} = -A_{ok}^{-1} \frac{\partial A_{ok}}{\partial f_a} A_{ok}^{-1} \quad (\text{B-14})$$

From Equ. (B-9), the equation can be rewritten as

$$\frac{\partial A_{ok}^{-1}}{\partial f_a} = -A_{ok}^{-1} \omega_{ka} \quad (\text{B-15})$$

Submitting Equ. (B-9) into Equ. (B-15), one obtains:

$$\frac{\partial B_{ji}}{\partial f_a} = \omega_{ja} B_{ji} + R_{jia} - B_{ji} \omega_{ja} \quad (B-16)$$

where R_{jia} is the second derivative operator of a joint.

$$R_{jia} = A_{oj} T_{jj} \frac{\partial Q_{ji}}{\partial f_a} T_{jj}^{-1} A_{oj}^{-1} \quad (B-17)$$

Second partial derivatives of constraint variables with respect to independent generalized coordinates in Equ. (B-11) can be obtained by differentiating twice the constraints with respect to the independent constraint variables, f_a and f_b :

$$[\sum_{i=1}^{t_1} B_{1i} \frac{\partial^2 q_{1i}}{\partial f_a \partial f_b} + \sum_{i=1}^{t_2} B_{2i} \frac{\partial^2 q_{2i}}{\partial f_a \partial f_b} + \dots + \sum_{i=1}^{t_n} B_{ni} \frac{\partial^2 q_{ni}}{\partial f_a \partial f_b}]_1 + [C(a, b)]_1 = [0] \quad (B-18)$$

The matrix $[C(a, b)]_1$ is obtained from the previous derived equations:

$$\begin{aligned} [C(a, b)]_1 &= \sum_{j=1}^n \sum_{i=1}^{t_j} \frac{\partial B_{ji}}{\partial f_b} \frac{\partial q_{ji}}{\partial f_a} \\ &= \sum_{j=1}^m \sum_{i=1}^{t_j} [\omega_{jb} B_{ji} - B_{ji} \omega_{jb} + \sum_{c=1}^{t_i} R_{jic}] \frac{\partial q_{ji}}{\partial f_a} \end{aligned} \quad (B-16)$$

Equ. (B-18) is a set of linear algebraic equations, which can be formulated by the same procedure outlined in section 2.2.4-b.

Appendix C: Position, velocity, acceleration and static analysis of a cam-follower mechanism

The cam-follower mechanism of Fig. 4.4-1 can be solved by hand by expressing the set of explicit kinematic and dynamic equations at different stages of the motion. The central inertia moment I_2 of the cam has been voluntarily considered as large in order to keep the angular velocity constant during motion. The comparison between results obtained by the ACDMC software with those obtained "by hand" is made considering the kinematic behaviour (position, velocity, acceleration) and the calculation of the contact force, respectively in the AB, BC, and CD parts of the cam.

C.1 A-B segment, "arc-arc" contact

C.1.1 Position analysis

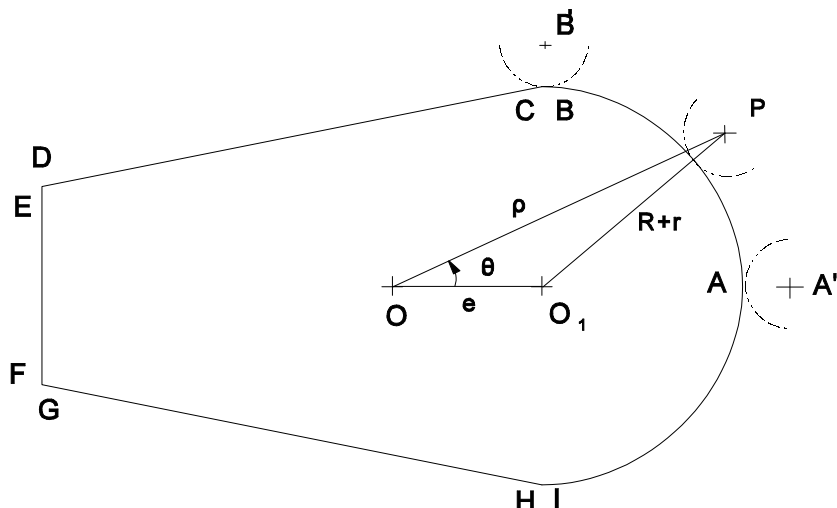


Fig. C.1-1: Cam-follower mechanism with an "arc-arc" contact joint

From Fig. (C.1-1), considering the triangle $O-O_1-P$, the geometric constraint equation in the part "A-B" of the cam, can be expressed by:

$$(\rho - e * \cos\theta)^2 + (e * \sin\theta)^2 = (R+r)^2 \quad (\text{C.1-1})$$

or

$$\rho = \sqrt{(R+r)^2 - (\sin\theta)^2} + e * \cos\theta \quad (C.1-2)$$

At point A,

$$\theta_A = 0, \quad t_A = 0, \quad \rho_A = R+r+e = 40 \text{ (cm)}, \quad (C.1-3)$$

At point B, the angular parameter can be obtained by following geometric relationship,

$$\theta_{B1} = \operatorname{tg}^{-1}\left(\frac{R+r}{e}\right) = 59.0362^\circ, \quad t_B = 2.0608 \text{ (s)} \quad (C.1-4)$$

leading to:

$$\rho_{B1} = \sqrt{(R+r)^2 - (e * \sin\theta_{B1})^2} + e * \cos\theta_{B1} = 29.1548 \text{ (cm)} \quad (C.1-5)$$

C.1.2 Velocity analysis

Differentiating the geometric constraint equation, the following velocity constraint equation is obtained in the part A-B of the cam:

$$2(\rho - e \cos\theta)(\dot{\rho} + e \omega \sin\theta) + e^2 \omega \sin 2\theta = 0 \quad (C.1-6)$$

or

$$\dot{\rho} = \frac{e^2 \omega \sin 2\theta}{2(\rho - e \cos\theta)} - e \sin\theta \omega \quad (C.1-7)$$

At point A,

$$\dot{\rho}_A = 0 \quad (C.1-8)$$

At point B,

$$\dot{\rho}_{B1} = -\left(\frac{e^2 \sin\theta_{B1}}{2(\rho_{B1} - e \cos\theta_{B1})} + e \sin\theta_{B1}\right) * \omega_2 = -8.7464 \text{ (cm/sec)} \quad (C.1-9)$$

C.1.3 Acceleration analysis

Differentiating the velocity constraint equation, the following acceleration equation is obtained in the part A-B of the cam:

$$\ddot{\rho} = -\frac{e^2 \omega}{2} \left(\frac{\cos 2\theta * 2\omega(\rho - e \cos\theta) - \sin 2\theta(\dot{\rho} + e \omega \sin\theta)}{\rho - e \cos\theta} \right) - e \omega^2 \cos\theta \quad (C.1-10)$$

At point A,

$$\ddot{\rho}_A = \frac{e^2 * \omega_2}{2} * \frac{2 * \omega_2 * (\rho_{A1} - e)}{(\rho_{A1} - e)^2} - e * \omega_2^2 = -6 \text{ (cm/sec}^2) \quad (C.1-11)$$

At point B, because the acceleration is not continuous at point B, we will use B^- to associate the point B to the part "A-B" of the cam and B^+ to describe the point B associated with the element "B-C". One has:

$$\ddot{\rho}_{B^-} = -\frac{e^2 \omega_2^2}{2} \left(\frac{\cos 2\theta_B * 2\omega_2 (\rho_B - e \cos \theta_B) - \sin 2\theta_B (\dot{\rho}_B + e \omega_2 \sin \theta_B)}{(\rho_B - e \cos \theta_B)^2} \right)$$

$$-e \omega_2^2 \cos \theta_B = -0.9430 \text{ (cm/sec}^2\text{)} \quad (\text{C.1-12})$$

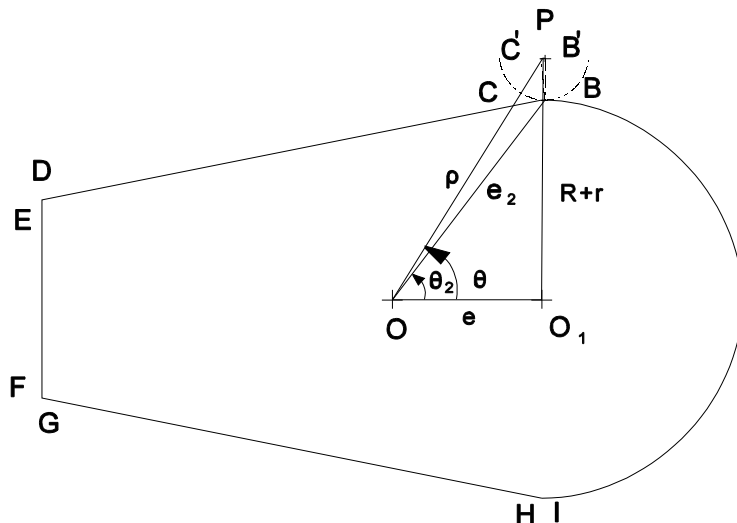


Fig. C.2-1: Cam-follower mechanism with an "arc-point" contact joint

C.2 Element B-C, "point-arc" contact

C.2.1 Position analysis

From Fig. (C.2-1), considering the triangle O, O_1, P , the geometric constraint equation in the element "B-C" can be expressed by:

$$(\rho - e_2 \cos(\theta - \theta_2))^2 + (e_2 \sin(\theta - \theta_2))^2 = r^2 \quad (\text{C.2-1})$$

where:

$$e_2 = \sqrt{e^2 + R^2} = 25 \text{ (cm)} \quad (\text{C.2-2})$$

$$\theta_2 = \operatorname{tg}^{-1}\left(\frac{R}{e}\right) = 53.1301^\circ \quad (\text{C.2-3})$$

This equation can be rewritten as:

$$\rho = \sqrt{r^2 - (e_2 \sin(\theta - \theta_2))^2 + e_2 \cos(\theta - \theta_2)} \quad (\text{C.2-4})$$

At point C, the angular value can be obtained by following geometric relationship:

$$\theta_c = \operatorname{arctg}\left(\frac{e - r \sin \alpha_{CD}}{R + r \cos \alpha_{CD}}\right) \quad (\text{C.2-5})$$

where:

$$\alpha_{CD} = \operatorname{tg}^{-1}\left(\frac{R - l_2/2}{l_1 + e}\right) = 11.3099^\circ \quad (\text{C.2-6})$$

leading to:

$$\theta_c = 60.6221^\circ \text{ and } \rho_c = 28.5779 \text{ (cm)} \quad (\text{C.2-7})$$

C.2.2 Velocity analysis

The differentiation of the geometric constraint equation provides the following velocity in part "B-C" of the cam:

$$2(\rho - e_2 \cos(\theta - \theta_2))(\dot{\rho} - e_2 \omega \sin(\theta - \theta_2)) + e_2^2 \omega \sin(2(\theta - \theta_2)) = 0 \quad (\text{C.2-8})$$

or:

$$\dot{\rho} = -\frac{e_2^2 \omega \sin(2(\theta - \theta_2))}{2(\rho - e_2 \cos(\theta - \theta_2))} - e_2 \omega \sin(\theta - \theta_2) \quad (\text{C.2-9})$$

At point C:

$$\dot{\rho}_c = \frac{e_2^2 \omega \sin(2(\theta_c - \theta_2))}{2(\rho - e_2 \cos(\theta_c - \theta_2))} - e_2 \omega \sin(\theta_c - \theta_2) = -12.3019 \text{ (cm/sec)} \quad (\text{C.2-10})$$

C.2.3 Acceleration analysis

The differentiation of the velocity constraint equation again gives the acceleration in the part "B-C" of the cam:

$$\ddot{\rho} = -\frac{e_2^2 \omega}{2} \left(\frac{2\omega \cos 2(\theta - \theta_2)(\rho - e_2 \cos(\theta - \theta_2)) - \sin 2(\theta - \theta_2)(\dot{\rho} + e_2 \omega \sin(\theta - \theta_2))}{(\rho - e_2 \cos(\theta - \theta_2))^2} \right)$$

$$-e_2 \omega^2 \cos(\theta - \theta_2) \quad (C.2-11)$$

At point B⁺

$$\ddot{\rho}_{B^+} = -54.849 \text{ (cm/sec}^2\text{)} \quad (C.2-12)$$

At point C⁻

$$\ddot{\rho}_{C^-} = -74.1643 \text{ (cm/sec}^2\text{)} \quad (C.2-13)$$

C.3 Element C-D, "arc-line" contact

C.3.1 Position analysis

From the Fig. (C.3-1), the equation of line C-D can be written as

$$y = k(x - x_0) + y_0 \quad (C.3-1)$$

where

$$x_0 = x_D' = -L_1 - r * \sin \alpha = -35.9806 \text{ (cm)} \quad (C.3-2)$$

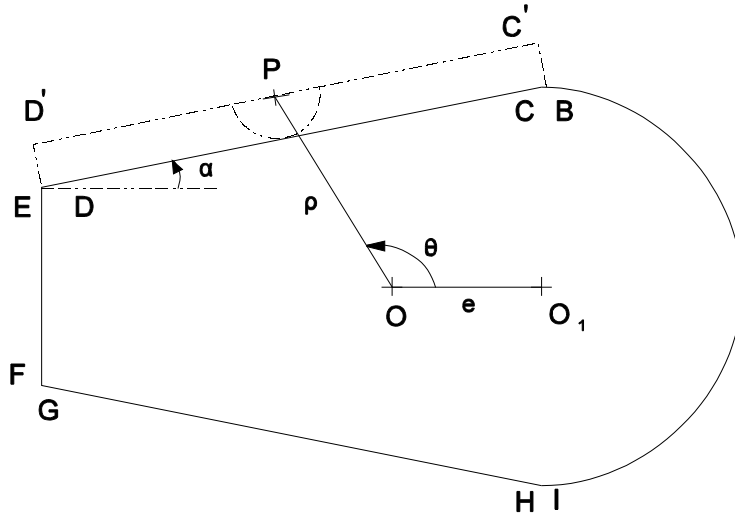


Fig. C.3-1: Cam-follower mechanism with an "arc-line" contact joint

$$Y_0 = Y_{D'} = L_2 / 2 + r * \cos \alpha = 14.9029 \text{ (cm)} \quad (\text{C.3-3})$$

and

$$k = t g \alpha_{CD} = \frac{R - L_2 / 2}{L_1 + e} = 0.2 \quad (\text{C.3-4})$$

leading to:

$$y = 0.2(x + 35.9806) + 14.9029 \quad (\text{C.3-5})$$

Defining:

$$x = \rho \cos \theta, \quad y = \rho \sin \theta \quad (\text{C.3-6})$$

the geometric constraint equation can be written as:

$$\rho = \frac{22.0990}{\sin \theta - 0.2 \cos \theta} \quad (\text{C.3-7})$$

C.3.2 Velocity analysis

Differentiating the geometric constraint equation, the velocity of the part "C-D" is obtained.

$$\dot{\phi} = -\frac{22.099}{(Sin\theta - 0.2Cos\theta)^2} (Cos\theta + 0.2Sin\theta)\dot{\theta} \quad (\text{C.3-8})$$

At the point C⁺:

$$\dot{\phi}_{c^+} = \rho_{c^-} = -12.3019 \text{ (cm/sec)}$$

C.3.2 Acceleration Analysis

The differentiation of the velocity equation provides the acceleration in part "C-D" of the cam:

$$\ddot{\phi} = 22.099 \left(\frac{(Cos\theta + 0.2Sin\theta)^2}{(Sin\theta - 0.2Cos\theta)^3} + \frac{1}{Sin\theta - 0.2Cos\theta} \right) \dot{\theta}^2 \quad (\text{C.3-9})$$

At the point C⁺:

$$\ddot{\phi}_{c^+} = 17.7050 \text{ (cm/sec}^2\text{)} \quad (\text{C.3-10})$$

C.4 Contact force analysis

The contact force between the cam and the follower consists of two parts: a static force caused by the spring action and a dynamic force caused by the inertial effects. Considering the body 3 shown in Fig. (4.4-1), the Newton's second law of motion is expressed by:

$$F_{CD} * Cos\varphi - F_s = m * \ddot{\phi} \quad (\text{C.4-1})$$

or

$$F_{CD} = \frac{m * \ddot{\phi} + k * (l_0 + \rho + l_3 - l_4)}{Cos\varphi} \quad (\text{C.4-2})$$

At point A:

$$\varphi_A = 0 \quad (\text{C.4-3})$$

and

$$(F_{CD})_A = \frac{m * \ddot{\phi}_A + k * (l_0 + \rho_A + l_3 - l_4)}{Cos\varphi_A} = 66.6 \text{ (N)} \quad (\text{C.4-4})$$

At point B:

$$\varphi_B = arctg \left(\frac{e * sin\theta_B}{\rho_B - e * cos\theta_B} \right) = 30.9637^\circ \quad (\text{C.4-5})$$

The acceleration is not continuous at point B; we will therefore distinguish point B⁻ on the segment A-B and point B⁺ on the segment B-C:

At point B⁻,

$$(F_{CD})_{B^-} = \frac{m * \ddot{\rho}_B + k * (l_0 + \rho_B + l_3 - l_4)}{\cos \varphi_B} = 59.5817 \text{ (N)} \quad (\text{C.4-6})$$

At point B⁺,

$$(F_{CD})_{B^+} = \frac{m * \ddot{\rho}_B + k * (l_0 + \rho_B + l_3 - l_4)}{\cos \varphi_B} = 50.1520 \text{ (N)} \quad (\text{C.4-7})$$

At point C:

$$\varphi_C = 90^\circ - \theta_C - \alpha_{CD} = 40.6878^\circ \quad (\text{C.4-8})$$

At point C⁻,

$$(F_{CD})_{C^-} = \frac{m * \ddot{\rho}_C + k * (l_0 + \rho_C + l_3 - l_4)}{\cos \varphi_C} = 51.7518 \text{ (N)} \quad (\text{C.4-9})$$

At point C⁺,

$$(F_{CD})_{C^+} = \frac{m * \ddot{\rho}_C + k * (l_0 + \rho_C + l_3 - l_4)}{\cos \varphi_C} = 69.9251 \text{ (N)} \quad (\text{C.4-10})$$

The comparison of those results has been listed in Table 4.4-1 in section 4.4.

Appendix D Structure of the data used by ACDMC software and examples of input files

In the section, first the data file of ACDMC will be described, then two data code files of examples used in Chapter 4 are listed, finaly a data code file od ADAMS is appended.

D.1 Description of the data code file of ACDMC softerware

1) Mechanism part: (data about the mechanism)

Entity: mech
Name: name of the mechanism (input)
Gravity: gravity parameter (input)
Time: duration time of simulation (input)
Step: integration step size (input)
State: state of the simulation process (such as, pre-processing phase, topology analysis, kinematic analysis, dynamic analysis, post-processing)(output)

2) Link part: (data about links)

Entity: link
Name: name of the link (input)
Aro: transformation matrix between a conventional local frame attached to the link and the inertial fram (usually, the two frames are same)(input)
Mass: inertial matrix (see Equ. 3.3.2-11)(input)

3) Surface part: (data about joint surfaces)

Entity: surf
Name: name of the surface(frame)(input)
Type: type of the joint (input)

If the frame is used to define an articular joint, then

Shape: transformation matrix between the conventional local frame of the link and the frame associated to the joint.(see section 2.3)(input)

if the frame is used to define a contact joint, then

Normal vector: normal vector used to describe the curve line of the contact surface (input)

Type of contact curve: type of curve (point, seg, arc, circle, poly)(input)

(for a point element)

The data of the point element is determined by preceding element and following element. Nothing is input for the element.

(for an arc element)

Centre: position of the centre point of the arc (input)

Pinit: starting point of the arc (input)

Pend: end point of the arc (input)

Concave or convex: input the property of the curve line (concave or convex)(input)
(for a line segment)

Pinit: starting point of the line segment (input)

Pend: end point of the line segment (input)

(for a circle element)

Centre: centre of the circle (input)

Radial: radius of the circle (input)

Pinit: starting of the circle (attention, the start point must be on the circle)(input)

Concave or convex: property (concave or convex)(input)

(for a polynomial element)

Num: number of terms in the polynomial function (input)

Coeffi: coefficients in the polynomial function (input)

Order: order of all terms of the polynomial function (input)

Ao: initial polar coordinate (input)

Ro: initial polar coordinate (input)

Origi: original point of the polar coordinate (input)

Concave or convex: property (concave or convex) of the curve line (input)

4) Pair part: (data about joint pairs)

Entity: pair

Name: name of the pair (input)

Pinlink: name of the link associated with the input pair (input)

Pinsurf: name of the input pair (input)

Poutlink: name of the link associated with the output pair (input)

Poutsurf: name of the output pair (input)

Type: type of pair (input)

5) Ocli part: (data about the motion parameters of links)

Entity: ocli

Name: name of the link (input)

Solid: name of the model used to describe the 3D shape of the link (input)

Fixed: state of the link (true or false)(input)

6) Ocpa part: (data about the motion parameters of joints)

Entity: ocpa

Name: name of ocpa(usually it is same as the name of the joint)(input)

Joint: name of the joint (input)

Force: external force applied on the joint (input)

Stiff: stiffness of the spring applied on the joint (input)

Length: initial length of the spring applied on the joint (input)

Inlink: name of link on which a input pair of the joint is located)(input)

Outlink: name of link on which a output pair of the joint is located)(input)

Initial:position: initial position of the joint variables (input)

Initial velocity: initial velocity of the joint variables (input)

Independent variable: indicated which joint variable are as independent coordinate
(input)

If the joint is a contact joint, then

Active contact: contact state (true or false)(input and output)

Re: restitution coefficient (input)

7) Topology part: (data about the topology)

Entity: loop

Name: the order number of loops (output)

State: the property of the loop (open or closed) (output)

Num: the number of the joint in the loop (output)

RECLLOOP: input the direction of the joint, it is same of the direction of the loop
(True or false) (output)

D.2 Data code file of the ACDMC system for example of the section 4.3

```

ENTITY      : MACH
NAME        : example_2
GRAVITY    : 0.0000
TIME        : 13.0000
STEP        : 1.0000E-0002
STADE       : Post-proceeding

ENTITY      : LINK
NAME        : cam2_1
AR0
 1.0000000000 0.0000000000 0.0000000000 0.0000000000
 0.0000000000 1.0000000000 0.0000000000 0.0000000000
 0.0000000000 0.0000000000 1.0000000000 0.0000000000
MASS
 0.0000000000 0.0000000000 0.0000000000 0.0000000000
 0.0000000000 0.0000000000 0.0000000000 0.0000000000
 0.0000000000 0.0000000000 0.0000000000 0.0000000000
 0.0000000000 0.0000000000 0.0000000000 0.0000000000

ENTITY      : SURF
NAME        : 12
TYPE        : REPERE
SHAPE
 1.0000000000 0.0000000000 0.0000000000 0.0000000000
 0.0000000000 1.0000000000 0.0000000000 0.0000000000
 0.0000000000 0.0000000000 1.0000000000 0.0000000000

ENTITY      : SURF
NAME        : 13
TYPE        : REPERE
SHAPE
 0.0000000000 0.0000000000 1.0000000000 0.0000000000
 1.0000000000 0.0000000000 0.0000000000 0.0000000000
 0.0000000000 1.0000000000 0.0000000000 0.0000000000

ENTITY      : LINK
NAME        : cam2_2
AR0
 1.0000000000 0.0000000000 0.0000000000 0.0000000000
 0.0000000000 1.0000000000 0.0000000000 0.0000000000
 0.0000000000 0.0000000000 1.0000000000 0.0000000000
MASS
1000.0000000000 0.0000000000 0.0000000000 0.0000000000

```

```

0.0000000000 0.0000000000 0.0000000000 0.0000000000
0.0000000000 0.0000000000 0.0000000000 0.0000000000
0.0000000000 0.0000000000 0.0000000000 5.0000000000

ENTITY      : SURF
NAME        : 21
TYPE OF SURFACE : REPERE
SHAPE
1.0000000000 0.0000000000 0.0000000000 0.0000000000
0.0000000000 1.0000000000 0.0000000000 0.0000000000
0.0000000000 0.0000000000 1.0000000000 0.0000000000

ENTITY      : SURF
NAME        : 23
TYPE OF SURFACE : COURBE
NORMAL VECTOR : 0.0000000000 0.0000000000 1.0000000000
TYPE OF CURVE : ARC
CENTRE       : 0.0000000000 0.0000000000 0.0000000000
PINIT        : 54.9346068000 0.0000000000 0.0000000000
PEND         : 0.0000000000 54.9346068000 0.0000000000
CONCAVE OR CONVEX : CONVEX
FIN : NO
TYPE OF CURVE : POLY
NUM          : 3
COEFFI       : 54.93460680  0.0008000 -0.00008000
ORDER        : 0 3 4
Ao           : 0
Ro           : 1
Original     : 0.0000000000 0.0000000000 0.0000000000
CONCAVE OU CONVEXE : CONVEXE
FIN          : NON
TYPE OF CURVE : POLYLN
NUM          : 2
COEFFI       : 54.88460680  0.02000000
ORDER        : 0 1
Ao           : 5
Ro           : 1
CENTRE       : 0.0000000000 0.0000000000 0.0000000000
CONCAVE OU CONVEX : CONVEX
FIN          : NO
TYPE OF CURVE : POLYLN
NUM          : 4
COEFFI       : 65.6493560 -14.06250000  7.73437500 -4.13671880
ORDER        : 0 2 12 16
Ao           : -75
Ro           : 1
Ko           : 75
CENTRE       : 0.0000000000 0.0000000000 0.0000000000
CONCAVE OU CONVEX : CONVEX
FIN          : NO
TYPE OF CURVE : POLYLN
NUM          : 2
COEFFI       : 54.88460680 -0.02000000
ORDER        : 0 1
Ao           : -15
Ro           : 1
Ko           : 1
CENTRE       : 0.0000000000 0.0000000000 0.0000000000
CONCAVE OU CONVEX : CONVEX
FIN          : NON
TYPE OF CURVE : POLYLN
NUM          : 3
COEFFI       : 54.93460680 -0.00080000 -0.00008000
ORDER        : 0 3 4
Ao           : -5
Ro           : 1
CENTRE       : 0.0000000000 0.0000000000 0.0000000000
CONCAVE OU CONVEX : CONVEX
FIN          : NO
PARTIE DE COURBE : ARC

```

```

CENTRE      : 0.0000000000 0.0000000000 0.0000000000
CONCAVE OU CONVEX : CONVEX
FIN         : YES

ENTITY      : LINK
NAME        : cam2_3
ARO
  1.0000000000 0.0000000000 0.0000000000 0.0000000000
  0.0000000000 1.0000000000 0.0000000000 0.0000000000
  0.0000000000 0.0000000000 1.0000000000 0.0000000000
MASS
  0.0000000000 0.0000000000 0.0000000000 0.0000000000
  0.0000000000 0.0000000000 0.0000000000 0.0000000000
  0.0000000000 0.0000000000 0.0000000000 0.0000000000
  0.0000000000 0.0000000000 0.0000000000 0.1500000000

ENTITY      : SURF
NAEE        : 32
TYPE DE SURFACE : COURBE
NORMAL VECTOR : 0.0000000000 0.0000000000 1.0000000000
TYPE OF CURVE: ARC
CENTRE      : 0.0000000000 0.0000000000 0.0000000000
PINIT       : 0.0000000000 5.0000000000 0.0000000000
PEND        : 0.0000000000 -5.0000000000 0.0000000000
CONCAVE OU CONVEX : CONVEX
FIN         : YES

ENTITY      : SURF
NAME        : 31
TYPE OF SURFACE : REPERE
SHAPE
  0.0000000000 0.0000000000 1.0000000000 0.0000000000
  1.0000000000 0.0000000000 0.0000000000 0.0000000000
  0.0000000000 1.0000000000 0.0000000000 0.0000000000

ENTITY      : PAIR
NAME        : 1
PINLINK    : cam2_1
PINSURF    : 12
POUTLINK   : cam2_2
POUTSURF   : 21
TYPEPAIR   : ROTOIDE

ENTITY      : PAIR
NOM         : 2
PINLINK    : cam2_2
PINSURF    : 23
POUTLINK   : cam2_3
POUTSURF   : 32
TYPEPAIR   : CONTACT

ENTITE     : PAIR
NAME        : 3
PINLINK    : cam2_1
PINSURF    : 13
POUTLINK   : cam2_3
POUTSURF   : 31
TYPEPAIR   : PRISMATIQUE

ENTITY      : OCLI
NAME        : cam2_1
SOLIDE     : cam2_1
FIXED      : TRUE

ENTITE     : OCLI
NOM         : cam2_2
SOLIDE     : cam2_2
FIXED      : FALSE

ENTITY      : OCLI

```

```

NAME      : cam2_3
SOLIDE    : cam2_3
FIXED     : FALSE

ENTITY    : OCPA
NAME      : 1
JOINT     : 1
FORCE     : 0.00000000000000E+0000
STIFF     : 0.00000000000000E+0000
LENGTH    : 0.00000000000000E+0000
LINK OF INPUT PAIR : cam2_1
LINK OF OUTPUT PAIR : cam2_2
INITIAL POSITION:
 0.0000000000 0.0000000000 0.0000000000 0.0000000000 0.0000000000 0.0000000000
INITIAL VELOCITY:
-50.00000000 0.0000000000 0.0000000000 0.0000000000 0.0000000000 0.0000000000
ARMOTOR[1] : TRUE
ARMOTOR[2] : FALSE
ARMOTOR[3] : FALSE
ARMOTOR[4] : FALSE
ARMOTOR[5] : FALSE
ARMOTOR[6] : FALSE

ENTITY    : OCPA
NAME      : 2
JOINT     : 2
FORCE     : 0.00000000000000E+0000
STIFF     : 0.00000000000000E+0000
LENGTH    : 0.00000000000000E+0000
LINK OF INPUT PAIR : cam2_1
LINK OF OUTPUT PAIR : cam2_2
INITIAL POSITION:
 0.5000000000 0.5000000000 0.0000000000 0.0000000000 0.0000000000 0.0000000000
ARVELVAR :
 0.0000000000 0.0000000000 0.0000000000 0.0000000000 0.0000000000 0.0000000000
ARMOTOR[1] : FALSE
ARMOTOR[2] : FALSE
ARMOTOR[3] : FALSE
ARMOTOR[4] : FALSE
ARMOTOR[5] : FALSE
ARMOTOR[6] : FALSE
CONTACT ACTIF : TRUE
Restitution : 0

ENTITY    : OCPA
NAME      : 3
JOINT     : 3
FORCE     : 0.00000000000000E+0000
STIFF     : -1.00000000000000E+0002
LENGTH    : 0.00000000000000E+0000
LINK OF INPUT PAIR : cam2_1
LINK OF OUTPUT PAIR : cam2_2
INITIAL POSITION:
 59.93450600 0.0000000000 0.0000000000 0.0000000000 0.0000000000 0.0000000000
INITIAL VELOCITY :
 0.0000000000 0.0000000000 0.0000000000 0.0000000000 0.0000000000 0.0000000000
ARMOTOR[1] : FALSE
ARMOTOR[2] : FALSE
ARMOTOR[3] : FALSE
ARMOTOR[4] : FALSE
ARMOTOR[5] : FALSE
ARMOTOR[6] : FALSE

ENTITY    : LOOP
NAME      : 1
CHAIN     : CLOSED
NUMPAIR   : 3
RECLOOP   : TRUE
1
RECLOOP   : TRUE

```

```

2
RECLOOP  : FALSE
3

```

D.3 Date code file of ACDMC for the example in section 4.4

```

ENTITY      : MACH
NAME        : exampl2
GRAVITY    : 0.0000
TIME        : 13.0000
STEP        : 1.0000E-0002
STADE       : SIMULATION

ENTITY      : LINK
NAME        : cam2_3
ARO
 1.0000000000 0.0000000000 0.0000000000 0.0000000000
 0.0000000000 1.0000000000 0.0000000000 0.0000000000
 0.0000000000 0.0000000000 1.0000000000 0.0000000000
MASS
 0.0000000000 0.0000000000 0.0000000000 0.0000000000
 0.0000000000 0.0000000000 0.0000000000 0.0000000000
 0.0000000000 0.0000000000 0.0000000000 0.0000000000
 0.0000000000 0.0000000000 0.0000000000 0.5000000000

ENTITY      : SURF
NAME        : 31
TYPE DE SURFACE : REPERE
SHAPE
 0.0000000000 0.0000000000 1.0000000000 0.0000000000
 1.0000000000 0.0000000000 0.0000000000 0.0000000000
 0.0000000000 1.0000000000 0.0000000000 0.0000000000

ENTITY      : SURF
NAME        : 32
TYPE        : COURBE
NORMAL VECTOR : 0.0000000000 0.0000000000 1.0000000000
TYPE OF CURVE : ARC
CENTRE     : 0.0000000000 0.0000000000 0.0000000000
PINIT      : 0.0000000000 5.0000000000 0.0000000000
PEND       : 0.0000000000 -5.0000000000 0.0000000000
CONCAVE OU CONVEX : CONVEX
FIN         : YES

ENTITY      : LINK
NAME        : cam2_2
ARO
 1.0000000000 0.0000000000 0.0000000000 0.0000000000
 0.0000000000 1.0000000000 0.0000000000 0.0000000000
 0.0000000000 0.0000000000 1.0000000000 0.0000000000
MASS
9800.0000000000 0.0000000000 0.0000000000 0.0000000000
 0.0000000000 0.0000000000 0.0000000000 0.0000000000
 0.0000000000 0.0000000000 0.0000000000 0.0000000000
 0.0000000000 0.0000000000 0.0000000000 0.0500000000

ENTITY      : SURF
NAME        : 23
TYPE        : COURBE
NORMAL VECTOR : 0.0000000000 0.0000000000 1.0000000000
TYPE OF CURVE : ARC
CENTRE     : 15.0000000000 0.0000000000 0.0000000000
PINIT      : 15.0000000000 -20.0000000000 0.0000000000
PEND       : 15.0000000000 20.0000000000 0.0000000000
CONCAVE OR CONVEX : CONVEX
FIN         : NO
PARTIE DE COURBE : POINT
FIN         : NO
TYPE OF CURVE : SEGMENT

```

```

PEND      : -35.0000000000 10.0000000000 0.0000000000
FIN       : NO
TYPE OF CURVE : POINT
FIN       : NO
TYPE OF CURVE : SEGMENT
PEND      : -35.0000000000 -10.0000000000 0.0000000000
FIN       : NO
TYPE OF CURVE : POINT
FIN       : NO
TYPE OF CURVE : SEGMENT
PEND      : 15.0000000000 -20.0000000000 0.0000000000
FIN       : NO
TYPE OF CURVE : POINT
FIN       : YES

ENTITY    : SURF
NAME      : 21
TYPE DE SURFACE : REPERE
SHAPE
 1.0000000000 0.0000000000 0.0000000000 0.0000000000
 0.0000000000 1.0000000000 0.0000000000 0.0000000000
 0.0000000000 0.0000000000 1.0000000000 0.0000000000

ENTITY    : LINK
NAME      : cam2_1
ARO
 1.0000000000 0.0000000000 0.0000000000 0.0000000000
 0.0000000000 1.0000000000 0.0000000000 0.0000000000
 0.0000000000 0.0000000000 1.0000000000 0.0000000000
MASS
 0.0000000000 0.0000000000 0.0000000000 0.0000000000
 0.0000000000 0.0000000000 0.0000000000 0.0000000000
 0.0000000000 0.0000000000 0.0000000000 0.0000000000
 0.0000000000 0.0000000000 0.0000000000 0.0000000000

ENTITY    : SURF
NAME      : 13
TYPE DE SURFACE : REPERE
SHAPE
 0.0000000000 0.0000000000 1.0000000000 0.0000000000
 1.0000000000 0.0000000000 0.0000000000 0.0000000000
 0.0000000000 1.0000000000 0.0000000000 0.0000000000

ENTITY    : SURF
NAME      : 12
TYPE DE SURFACE : REPERE
SHAPE
 1.0000000000 0.0000000000 0.0000000000 0.0000000000
 0.0000000000 1.0000000000 0.0000000000 0.0000000000
 0.0000000000 0.0000000000 1.0000000000 0.0000000000

ENTITY    : PAIR
NAME      : 3
PINLINK  : cam2_1
PINSURF   : 13
POUTLINK  : cam2_3
POUTSURF  : 31
TYPEPAIR   : PRISMATIQUE

ENTITY    : PAIR
NAME      : 2
PINLINK  : cam2_2
PINSURF   : 23
POUTLINK  : cam2_3
POUTSURF  : 32
TYPEPAIR   : CONTACT

ENTITE   : PAIR
NAME      : 1
PINLINK  : cam2_1

```

```

PINSURF      : 12
POUTLINK     : cam2_2
POUTSURF     : 21
TYPEPAIR     : ROTOIDE

ENTITY       : OCLI
NAME         : cam2_3
SOLIDE       : cam2_3
FIXED        : FALSE

ENTITY       : OCLI
NAME         : cam2_2
SOLIDE       : cam2_2
FIXED        : FALSE

ENTITY       : OCLI
NAME         : cam2_1
SOLIDE       : cam2_1
FIXED        : TRUE

ENTITY       : OCPA
NAME         : 3
JOINT        : 3
FORCE        : 0.00000000000000E+0000
STIFF        : 0.00000000000000E+0000
LENGTH       : 0.00000000000000E+0000
LINK OF INPUT PAIR   : cam2_1
LINK OF OUTPUT PAIR : cam2_3
INITIAL POSITION:
40.00000000 0.00000000 0.00000000 0.00000000 0.00000000 0.00000000
INITIAL VELOCITY:
0.00000000 0.00000000 0.00000000 0.00000000 0.00000000 0.00000000
INITIAL VELOCITY:
0.00000000 0.00000000 0.00000000 0.00000000 0.00000000 0.00000000
ARMOTOR[1]   : FALSE
ARMOTOR[2]   : FALSE
ARMOTOR[3]   : FALSE
ARMOTOR[4]   : FALSE
ARMOTOR[5]   : FALSE
ARMOTOR[6]   : FALSE

ENTITY       : OCPA
NAME         : 2
LIAISON      : 2
FORCE        : 0.00000000000000E+0000
STIFF        : 0.00000000000000E+0000
LENGTH       : 0.00000000000000E+0000
LINK OF INPUT PAIR   : cam2_2
LINK OF OUTPUT PAIR : cam2_3
INITIAL POSITION:
0.50000000 0.50000000 0.00000000 0.00000000 0.00000000 0.00000000
INITIAL VELOCITY :
0.00000000 0.00000000 0.00000000 0.00000000 0.00000000 0.00000000
LISTE LAST : FALSE
LISTE PROX LAST : FALSE
ARMOTOR[1]   : FALSE
ARMOTOR[2]   : FALSE
ARMOTOR[3]   : FALSE
ARMOTOR[4]   : FALSE
ARMOTOR[5]   : FALSE
ARMOTOR[6]   : FALSE
CONTACT ACTIF : TRUE
Restitution   : 0

ENTITY       : OCPA
NAME         : 1
JOINT        : 1
FORCE        : 0.00000000000000E+0000

```

```

STIFF           : 0.000000000000000E+0000
LENGTH         : 0.000000000000000E+0000
LINK OF INPUT PAIR : cam2_1
LINK OF OUTPUT PAIR : cam2_2
INITIAL POSITION:
  0.0000000  0.0000000  0.0000000  0.0000000  0.0000000  0.0000000
INITIAL POSITION:
 -0.5000000  0.0000000  0.0000000  0.0000000  0.0000000  0.0000000
ARMOTOR[1] :    TRUE
ARMOTOR[2] :   FALSE
ARMOTOR[3] :   FALSE
ARMOTOR[4] :   FALSE
ARMOTOR[5] :   FALSE
ARMOTOR[6] :   FALSE

ENTITY      : LOOP
NAME        : 1
CHAIN       : CLOSED
NUMPAIR    : 3
RECLOOP    : TRUE
1
RECLOOP    : TRUE
2
RECLOOP    : FALSE
3

```

D.4 Data code file of the ADAMS system for example of section 4.3

```

*****PART MODULES*****
PART - (01) GROUND
PART/01,GROUND
MARKER/01
  PART - (02) CAM
PART/02, MASS=200, CM=02
, IP=20000,20000,40000
, QG=0,0,0
, WZ=5
, EXACT=X
MARKER/02, QP=0,0,0
!     REQUESTS
!REQUEST/01, DISPLACEMENT, I=02, J=01
!, COMMENT=CAM CG DISPLACEMENT
  GRAPHICS
GRAPHICS/01, CURVE, CID=01, CRM=02, SEG=200
  PART - (03) FOLLOWER
PART/03, MASS=0.5, CM=04
, IP=10,10,10
, QG=100,0,0,0
, EXACT=X
MARKER/04, QP=0,0,0
  REQUESTS
REQUEST/02, DISPLACEMENT, I=04, J=01
, COMMENT=FOLLOWER CG DISPLACEMENT
REQUEST/03, VELOCITY, I=04, J=01
. COMMENT=FOLLOWER CG VELOCITY
REQUEST/04, ACCELERATION, I=04, J=01
, COMMENT=FOLLOWER CG ACCELERATION
  GRAPHICS
GRAPHICS/02, CURVE, CID=02, CRM=04, SEG=200
*****CONSTRAINT MODULES*****
JOINT/01, REVOLUTE, I=07, J=08
MARKER/07, PART=01, QP= 0,0,0
MARKER/08, PART=02, QP= 0,0,0
!REQUEST/05, FORCE, I=07, J=08
!, COMMENT=CAM JOINT CG FORCE
CVCV/01, ICURVE=01, JCURVE=02, IFLOAT=9, IRM=10, JFLOAT=11, JRM=12
, IDISP=0,0,0, JDISP=-100,0,0
CURVE/01, CLOSED, MATRIX=01, CURVE_POINTS

```

```
CURVE/02, OPEN, MATRIX=02, CURVE_POINTS
MATRIX/01, FULL = RORDER, ROWS=361, COLUMNS=3,
, VALUES=50.0,0
, 4.9992384758E+01, 8.7262032186E-01,0
, 4.9969541351E+01, 1.7449748351E+00,0
, 4.9931476738E+01, 2.6167978121E+00,0
, 4.9878202513E+01, 3.4878236872E+00,0
, 4.9809734904E+01, 4.3577871374E+00,0
.....
, the data cab be obtained by equations inthe table 4.3-1,
.....
, 4.9384417030E+01,-7.8217232519E+00,0
, 4.9513403437E+01,-6.9586550478E+00,0
, 4.9627307582E+01,-6.0934671702E+00,0
, 4.9726094768E+01,-5.2264231632E+00,0
, 4.9809734904E+01,-4.3577871374E+00,0
, 4.9878202513E+01,-3.4878236871E+00,0
, 4.9931476738E+01,-2.6167978122E+00,0
, 4.9969541351E+01,-1.7449748351E+00,0
, 4.9992384758E+01,-8.7262032202E-01,0
, 5.0000000000E+01, 0.0000000000E+00,0
MATRIX/02, FULL = RORDER, ROWS=5, COLUMNS=3,
, VALUES=-45,-5,0
,-48.535,-3.535, 0.0
,-50, 0.0, 0.0
,-48.535, 3.535, 0.0
,-45, 5.0, 0.0
MARKER/9, FLOATING, PART=02
MARKER/11, FLOATING, PART=03
MARKER/10, PART=02, QP=0.0,0
MARKER/12, PART=03, QP=0.0,0
REQUEST/06, FORCE, I=11, J=9
, COMMENT=CAM CONTACT CG FORCE
JOINT/2, TRANSLATIONAL, I=13, J=14
MARKER/13, PART=01, QP=0.0,0, REULER=-90D,-90D,0D
MARKER/14, PART=03, QP=0.0,0, REULER=-90D,-90D,0D
*****FORCE MODULES*****
springdamper/1, I=15, J=16, TRANSLATION, k=15, L=100
MARKER/15, PART=01, QP=150,0,0
MARKER/16, PART=03, QP=0,0,0
*****SOLUTION, EXECUTION, AND OUTPUT PARAMENTER*****  
*****  
OUTPUT/ GRSAVE, REQSAVE  
RESULTS/  
  
END
```